Universidade Federal de Pernambuco
Centro de Ciências Exatas e da Natureza
Programa de Pós-Graduação em Física

Tiago Teixeira Saraiva

Extended Ginzburg-Landau Theory and Spatial Scales of Band Condensates

Recife
2018

Tiago Teixeira Saraiva

Extended Ginzburg-Landau Theory and Spatial Scales of Band Condensates

Tese apresentada ao Programa de Pós-Graduação em Física do Departamento de Física da Universidade Federal de Pernambuco como parte dos requisitos para obtenção do título de Doutor em Física.

Área de concentração: Física Teórica e Computacional - Supercondutividade.

Supervisor: Prof. Dr. Arkady Shanenko

Co-supervisor: Prof. Dr. Clécio C. de Souza Silva

Recife

2018

Catalogação na fonte
Bibliotecária Arabelly Ascoli CRB4-2068

S243e Saraiva, Tiago Teixeira
Extended Ginzburg-Landau theory and spatial scales of band condensates / Tiago Teixeira Saraiva. – 2018.
132 f.: il., fig., tab.

Orientador: Arkady Shanenko
Tese (Doutorado) – Universidade Federal de Pernambuco. CCEN. Física. Recife, 2018.
Inclui referências e apêndices.

1. Supercondutores. 2. Multibandas. 3. Comprimento de coerência. 4. Domínio intertipo. I. Shanenko, Arkady (orientador). II. Título.

530.1 CDD (22. ed.) UFPE-FQ 2019-51

TIAGO TEIXEIRA SARAIVA

EXTENDED GINZBURG-LANDAU THEORY AND SPATIAL SCALES OF BAND CONDENSATES

Tese apresentada ao Programa de Pós-Graduação em Física da Universidade Federal de Pernambuco, como requisito parcial para a obtenção do título de Doutor em Física.

Aprovada em: 08/05/2018.

BANCA EXAMINADORA

_____

Prof. Dr. Arkady Shanenko
Orientador
Universidade Federal de Pernambuco

_____

Profª Drª Azadeh Mohammadi
Examinadora Interna
Universidade Federal de Pernambuco

_____

Prof. Dr. Andrey Chaves
Examinador Externo
Universidade Federal do Ceará

_____

Prof. Dr. Mauro Melchiades Doria
Examinador Externo
Universidade Federal do Rio de Janeiro

PARTICIPAÇÃO VIA VIDEOCONFERÊNCIA

_____

Prof. Dr. Alexei Vagov
Examinador Externo
Bayreuth University

To Álamo, Isabel and Dion,
the lights of my life.

ACKNOWLEDGEMENTS

I thank my family for all the emotional, financial support and encouragement they have given me throughout my life. My parents, Álamo and Isabel and my brother, Dion, uncles and aunts, grandparents, cousins, are, in fact, a continuous source of hope and joy that I could always count on when I went through Crato, my hometown.

I also thank, for all the support and happy moments, friends Arthur Parente, Samuel, Arthur and Matheus Costa, Guilherme Magalhães, Marcel Moura, Thiago Sobral, Felipe Filgueira, Lucas Fantini, Moacyr Lobo, Kainã Terto, Florentino Silva, Paulo Guerra , André Amado and Azadeh Mohammadi, Raoni Moreira, Francisco, Leonardo Dornelles, Natália Alves, among many others. I would also like to thank my girlfriend Natalia Martín for showing me so much beauty in the world beyond physics and for teaching me so much about life.

I thank my advisor Arkady Shanenko for all the wisdom and opportunity to meet and be part of the Russian school of physics, which has contributed so much to the development of physics. I also thank Clécio de Souza Silva and Albino Aguiar for accompanying me since the beginning of my walk through the physics department of UFPE. In fact, there is not enough room to thank everyone who helped me. It is very important to recognize the contribution of the department's staff, especially Alexsandra Melo.

Agradeço à minha família por todo o suporte emocional, financeiro e todo o encorajamento que me deram durante toda minha vida. Meus pais, Álamo e Isabel e meu irmão, Dion, tios e tias, avós, primos, esses são, de fato, uma fonte contínua de esperança e alegria que, embora tenha me afastado um pouco durante a realização desse projeto, pude contar sempre que passei pelo Crato, minha cidade natal.

Agradeço também, por todo o apoio e aos momentos felizes, aos amigos Arthur Parente, Samuel, Arthur e Matheus Costa, Guilherme Magalhães, Marcel Moura, Thiago Sobral, Felipe Filgueira, Lucas Fantini, Moacyr Lobo, Kainã Terto, Florentino Silva, Paulo Guerra, André Amado e Azadeh Mohammadi, Raoni Moreira, Francisco, Leonardo Dornelles, Natália Alves, entre tantos outros. Gostaria de agradecer também à minha namorada Natalia Martin por ter me mostrado tanta beleza no mundo além da Física e por tanto me ensinar sobre a vida.

Agradeço ao meu orientador Arkady Shanenko por toda a sabedoria e pela oportunidade de conhecer e fazer parte da escola russa de física, que tanto contribuiu ao desenvolvimento da física. Agradeço também a Clécio de Souza Silva e a Albino Aguiar por me acompanharem desde o começo da minha caminhada pelo departamento

de física da UFPE. De fato, não há espaço suficiente para a agradecer a todos os que contribuíram para que o meu curso de doutorado se realizasse. É muito importante reconhecer a contribuição dos funcionários do departamento, especialemte, Alexsandra Melo.

"If you put water into a cup, it becomes the cup. You put water into a bottle and it becomes the bottle. You put it in a teapot, it becomes the teapot. Now, water can flow or it can crash. Be water, my friend."

(Bruce Lee, 1971)

ABSTRACT

The Thesis is focused on superconducting phenomena that can not be captured by the standard Ginzburg-Landau (GL) theory. Furthermore, the phenomena of interest can hardly be investigated in necessary detail by means of the full microscopic formalism, due to abnormal technical difficulties. This is why the present study is performed within the extended GL formalism (SHANENKO et al., 2011; VAGOV et al., 2012) that goes to one order beyond the GL theory in the perturbation expansion of the microscopic equations over the proximity to T_c but can still be analytically solved in many physically important cases. One of those phenomena is the formation of a finite intertype domain (AUER; ULLMAIER, 1973; BRANDT; DAS, 2011; VAGOV et al., 2016) in the phase diagram between standard superconductivity types I and II, where the superconducting magnetic response cannot be classified in the conventional terms. First evidences of such a domain date back to 1960's but little was known about effects of the anisotropy on its formation. This point has been clarified in the present Thesis. It has been recently demonstrated (VAGOV et al., 2016) that the intertype domain is expanded in the presence of multiple bands (multi-band superconductors) with different spatial scales. Important competition between band length scales arises from nonlocal effects beyond the standard GL approach (SARAIVA et al., 2017). It has been demonstrated in the Thesis that a notable deviation between the coherent scales of different band condensates can appear even far beyond the regime of nearly decoupled bands. This allows for a deeper insight on how the band length scales depend on microscopic parameters and will certainly be appealing to experimentalists, as the conclusions are relevant for the spatial distribution of the superconducting condensate in the vortex core of multi-band materials and their possible intertype magnetic response.

Keywords: Superconductivity. Multiband Superconductors. Healing lengths. Intertype domain. Bogomolny Point.

RESUMO

Esta tese está focada em fenômenos que não podem ser capturados pela teoria de Ginzburg-Landau (GL) padrão. Por outro lado, esses dificilmente podem ser investigados em tal nível de detalhe pela teoria microscópica devido a dificuldades técnicas. Portanto, o presente trabalho é realizado no âmbito do formalismo de Ginzburg-Landau Estendido (SHANENKO et al., 2011; VAGOV et al., 2012), que vai até uma ordem além da teoria GL na expansão perturbativa das equações microscópicas na vizinhança da temperatura crítica mas que ainda pode ser resolvido analiticamente em muitos casos importantes fisicamente. Um desses fenômenos é a formação de um domínio intertipo (AUER; ULLMAIER, 1973; BRANDT; DAS, 2011; VAGOV et al., 2016), no diagrama de fases, entre os tipos I e II, onde a resposta magnética do supercondutor não pode ser classificada nos termos convencionais. As primeiras evidências de tal domínio aconteceram nos anos 60 mas muito pouco se sabia sobre os efeitos da anisotropia na sua formação. Esse ponto foi clarificado nessa tese. Recentemente, foi demonstrado (VAGOV et al., 2016) que o domínio intertipo é expandido na presença de múltiplas bandas supercondutoras (supercondutores multi-bandas) com escalas espaciais diferentes. Uma competição importante entre as escalas de comprimento dessas bandas é gerada por efeitos não-locais além do modelo GL padrão (SARAIVA et al., 2017). Nessa tese também foi demonstrado que uma diferença notável entre as comprimentos de coerência dos condensados de bandas diferentes podem aparecer mesmo muito além do regime de acoplamento fraco entre bandas. Isso possibilitou um entendimento mais profundo de como as escalas de comprimento dependem dos parâmetros microscópicos e certamente serão de interesse experimental, um vez que as conclusões são relevantes no que tange à distribuição espacial do condensado supercondutor no núcleo dos vórtices em materiais multi-bandas e suas possíveis reposta magnética intertipo.

Palavras-chave: Supercondutividade. Supercondutores multibandas. Comprimento de coerência. Domínio intertipo. ponto de Bogomolny.

LIST OF FIGURES

CONTENTS

1 INTRODUCTION

Not like Homer would I write,
Not like Dante if I might,
Not like Shakespeare at his best,
Not like Goethe or the rest,
Like myself, however small,
Like myself, or not at all.

William Allingham -
Blackberries

Chapter Contents

In this chapter we present historically and conceptually this young, about one century old, beautiful area of condensed matter physics called *superconductivity*. The historical presentation contains the most important experiments which contributed fundamentally in the understanding of the phenomenology. In the theoretical revision, some of the early phenomenological theories are shown up to the very last steps for construction of the microscopic theory of superconductivity.

1.1 The Discovery of Superconductivity

In the end of the 19th and beginning of the 20th centuries many scientists in Europe and around the globe pursued the lowest limit of temperature reachable in nature. Among them was Heike Kamerlingh-Onnes, who devoted himself to studying this problem not merely as a race for the absolute zero temperature but specially because extremely cold systems might present new and exciting physical phenomena.

Onnes wrote his doctoral thesis on the van der Waals law of the corresponding states, which involved measuring thermodynamic quantities of gases at the critical point (which in gases generally happens at low temperatures) and this was his initial interest when he began his activities after being appointed professor in experimental physics at the Leiden University (Netherlands) in 1882. At that time, the final element of the "race" was believed to be Hydrogen (~20K), the lightest element, which had been liquefied by J. Dewar (inventor of the Dewar flasks) in 1889. But with the discovery of Helium on earth, Onnes could make his first major contribution to science by establishing the liquefying temperature of 5.2K (the lowest known at that time), even lower than Hydrogen. After this deed, Onnes was for some years the only scientist capable of studying the properties of materials at such low temperatures (OUBOTER, 1987) (people called the Leiden University "coldest place on earth") because of the unique experimental apparatus in his possession. Along the years he had the idea of improving the experimental apparatus with the possibility of measuring physical properties of metals at liquid Hydrogen or Helium thermal bath, which was an extremely important experiment at that time for the physics community in order to confirm the limits of thermodynamic laws. As sketched in Fig. 1, Lord Kelvin considered that resistivity should be infinite because

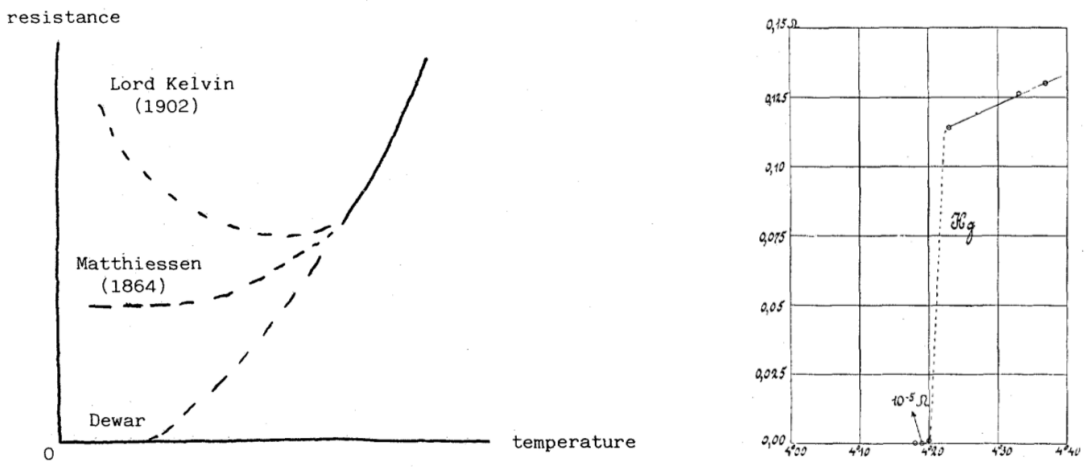

Figure 1 – On the left, sketches for different theoretical proposals for the physical behaviour of the resistivity of metals in the limit of extremely low temperatures. On the right, the original plot of the measurements performed by K. Onnes and collaborators in 1908.

electrons would "freeze" and become incapable of being conducted, while Matthiessen considered that should be a minimum disorder in the system which prohibited the electrons of being in this frozen state imposing a finite value for the resistivity when $T \rightarrow 0$. Dewar, on the other hand, extrapolated the experimental results obtained using liquid Hydrogen and proposed that the resistivity should go smoothly to zero at lower temperatures.

Aided by C. Dorsman and G. Holst, Onnes was able to do an experiment to measure the electric resistance of Mercury at extremely low temperatures in a liquid Helium thermal bath. They noticed that the resistivity dropped abruptly to zero at the temperature of 4.2K. This discontinuity in the resistivity curve was against any expectation. Then, in 1908, Onnes published the discovery of a new state of matter called "supraconductors" (which he latter changed to superconductors[1]) which granted him the Nobel Prize of Physics in 1913 "for his investigations on the properties of matter at low temperatures which led, inter alia, to the production of liquid helium".

Another key feature of superconductors was discovered in the 30s by Meissner and Ochsenfeld. They measured the magnetization of a superconductor under an applied magnetic field and found that it was completely expelled from the sample (up to a critical field), the so-called Meissner effect. In other words, superconductors are perfect diamagnetic materials. The magnetic behavior of superconductors is a key feature to differ this class of materials from perfect conductors, i.e. materials with infinite conductivity. It is well known that perfect conductors have null electric field inside and thus, by the Faraday's law, the magnetic field must be constant inside these materials. In the case of superconductors, the magnetic field must be constant and null (a phenomenon that was understood decades after the discovery of superconductivity). As shown in Fig. 2, in the process of *field cooling* (where one applies magnetic field in the sample and then starts to refrigerate it bellow T_c), the behaviour of a superconductor is different from a perfect conductor because the field is expelled from the sample, instead of staying constant. By superposition, the summation of the external field applied originally in Fig. 2 a) and the field generated by the magnetization of the superconductor shown in Fig. 2 c), results in the field configuration shown in Fig. 2 b). The Meissner effect can be a very effective tool for determining the presence of the superconducting state, once the original way by K. Ohnes involved applying currents which may induce vortex dynamics in the system causing heating and lowering the critical temperature.

Unfortunately, the physical explanation for this phenomenon has not been given before Onnes death once the quantum theory was not well developed at that time and the concept of macroscopic quantum behavior was not applied to this problem until

[1] Another contribution by Onnes was coining the term *Enthalpy* to indicate the function $E + PV$ in the context of thermodynamics, which was called the Gibbs function at that time (HOWARD, 2002).

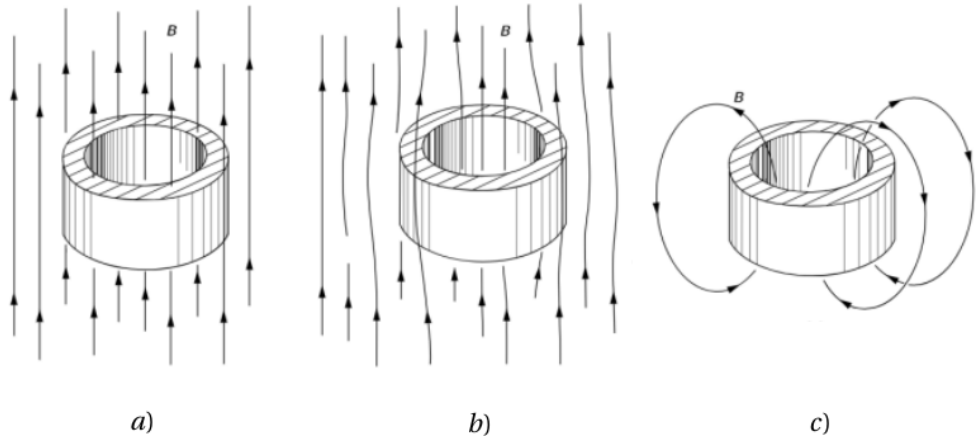

Figure 2 – a) Applied magnetic field lines on a superconducting cylinder for $T > T_c$. b) When $T < T_c$, the magnetic field is expelled from the sample, part of it gets trapped inside the cavity and part outside. c) Sketch of the magnetic field lines created by the magnetization of the superconductor in order to screen the applied field. Figure taken from Ref. (FEYNMAN; LEIGHTON; SANDS, 2011).

the 50s. The comprehension of the superconducting state and other condensates is still being developed even after more than 100 years after its discovery.

1.2 Early Theories

The first major success towards explaining the phenomenology of superconductors was given by the brothers Fritz and Heinz London. In their studies, they developed an equation which described magnetic field in superconductors by improving the Drude model. The derivation presented here is not the one originally derived but involves more deep concepts related to their line of thinking. Considering that the ground state of a superconducting system presents zero average canonical momentum[2] $\langle \vec{p}_c \rangle$, one gets

$$\langle \vec{p}_c \rangle = m \langle \vec{v} \rangle + \frac{Q}{c} \vec{A} = 0, \tag{1.1}$$

where m and Q are the mass and the charge of the superconducting charge carriers, left as incognitos. Originally, the single electronic charge and mass were used in the equation above because, at that time, it was not known that the mechanism of superconductivity involved pairs of electrons, the Cooper pairs, which was later demonstrated within the microscopic theory. Then, one can derive a proportionality relation between the density of current of superconducting electrons $\vec{j}_s = n_s Q \langle \vec{v} \rangle$, and the vector potential $\vec{A}$:

$$\vec{j}_s = -\frac{n_s Q^2}{mc} \vec{A}, \tag{1.2}$$

[2] A theorem derived by Bloch, which was never published.

where n_s is the density of superconducting electrons, also called the superfluid density. Eq. 1.2 is a key equation in superconductivity and can be used to derive the set of equations ruling the electrodynamics of superconductors[3], e.g. by taking the curl on both sides,

$$\vec{E} = \partial_t(\Lambda \vec{j_s}) \tag{1.3}$$

$$\vec{h} = -c\vec{\nabla} \times \left(\Lambda \vec{j_s}\right) \tag{1.4}$$

where, $\Lambda = \frac{m}{n_s Q^2}$. Note that London brothers decided to neglect the term involving the gradient of the scalar potential in Eq. (1.3) because comparison with experimental values for the relaxation time of the electric charge density showed negligible values (LONDON, 1950; HIRSCH, 2004). Also, by applying $\vec{\nabla} \times \vec{h} = \frac{4\pi}{c}\vec{j_s}$ (accordingly, the Ampère-Maxwell equation is applied in the quasi-static regime), it is possible to derive an equation solely for the magnetic field

$$\nabla^2 \vec{h} = \frac{1}{\lambda_L^2}\vec{h} \tag{1.5}$$

where

$$\lambda_L^2 = \frac{mc^2}{4\pi n_s Q^2}. \tag{1.6}$$

For instance, let us consider an ideal infinite superconductor occupying a half-space, say $x > 0$ in Cartesian coordinate system. This is a simple model for systems where the size of the sample is much bigger than λ_L. If one applies a constant magnetic field $\vec{H} = H\hat{k}$, then the field configuration must have translational symmetry along the y and z directions and then Eq. (1.5) becomes

$$\frac{d^2h}{dx^2} = \frac{1}{\lambda_L^2}h \tag{1.7}$$

The solution to this equation can be generally expressed as a linear combination of two exponentials but, obviously, the magnetic field must be finite throughout the entire sample and one must neglect the diverging contribution. Also, the magnetic field immediately before the interface must me equal to the applied field and thus the solution becomes

$$\vec{h}(x) = H\exp(-x/\lambda_L)\hat{k} \tag{1.8}$$

This typical decaying length of the magnetic field in the superconducting sample, highlighted in Fig. 3, is called the London penetration depth and is very important in the study of superconductors as will be seen later. Note that it is not possible to determine the charge of the quasi-particles of superconductivity by applying experimental values for λ_L because it is independent of how many particles compose the quasi-particles involved in the mechanism of superconductivity (double mass, double charge and half density would not change λ_L or Λ).

[3] In this notation, the local magnetic induction is $\vec{h}$.

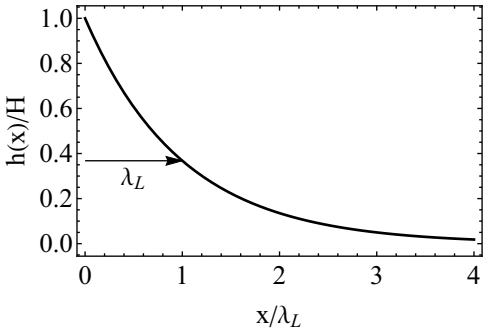

Figure 3 – Plot of the magnetic field configuration as a function of the distance from a vacuum-superconductor interface in an idealized system of an infinite superconductor occupying half the space, e.g. for $x > 0$.

London brothers were the first who assumed that the superfluid properties of He^4 are related to the Bose-Einstein condensation (which was later formally justified by N. Bogolyubov). Also, in this line of thought, they linked Eq. (1.5) with the equation for a time-independent field $\phi(\vec{x})$ representing the wave function of a spin-0 particle

$$\nabla^2\phi - \frac{m^2c^2}{\hbar^2}\phi = 0, \tag{1.9}$$

where the the length plays the role of mass. As a matter of fact, this screening length was inspiration for the Higgs mechanism for explaining the mass of elementary particles. At that time, brothers London could not explain this proposal or produce any important consequence from it and therefore the scientific community did not pay much attention to it, but actually they were pioneers in introducing the idea of a *condensate*, i.e. the collective behavior of many particles in a single quantum state could be represented by a *macroscopic wave function*.

Another typical length in superconductors was proposed by A. Pippard when he generalized Eq. (1.2) in its non-local form (PIPPARD, 1953) based on the Chamber's generalization of the Ohm's law (TINKHAM, 1996)

$$\vec{j}_s(\vec{r}) = \frac{4\pi}{c\lambda^2}\vec{A} \rightarrow \frac{3}{\lambda^2 c\xi_0}\int d\vec{r}' \frac{\vec{R}[\vec{R}\cdot\vec{A}(\vec{r}')]\exp(-R/\xi_0)}{R^4}, \tag{1.10}$$

where $\vec{R} = \vec{r} - \vec{r}'$ and ξ_0 is a new length. In this formulation, the superconducting current at the point $\vec{r}$ depends on the vector potential in a sphere of radius ξ_0. Pippard estimated this characteristic length by using the uncertainty principle. By assuming that only electrons with energy within an interval kT_c from the Fermi level contribute, the uncertainty in the momentum must be around $\Delta p \approx \frac{kT_c}{k_F}$, where v_F is the Fermi velocity and $k = 1.38 \times 10^{-23}$ is the Boltzman constant. This leads to a characteristic length

$$\xi_0 = a_p \frac{\hbar v_F}{kT_c}, \tag{1.11}$$

where a_p is a numerical factor which was determined experimentally to be close to 0.15 in tin and aluminium (later this value was determined by using the microscopic theory of superconductivity $a_p \approx 0.18$).

In 1937 L. Landau formulated a theory of broad application in order to describe systems in the vicinity of a second order phase transition (LANDAU, 1937). Among these was superconductivity because the specific heat of a superconductor has a discontinuity at the critical temperature which means it is a second order phase transition. The initial difficulty was to define the order parameter of the system, the quantity which should be zero above the critical temperature and non-zero bellow it, representing the disordered and ordered phases respectively. It is worth remembering the passionate presentation (in my opinion) of the subject done by A. Abrikosov, Nobel laureate in 2003, one of the most important students of Landau and great contributor to the field of superconductivity.

> "In 1950, Vitalii Ginzburg and Lev Landau published their famous paper on the theory of superconductivity. The approach was based on the general theory of the second order phase transitions proposed by Landau in 1937. There Landau introduced the main variable, the so called 'order parameter' which was finite below the transition and zero above it. Different phase transitions had different order parameters, and whereas it was evident for, e. g., the ferromagnetic transition, namely, the spontaneous magnetization, it was far less evident for the superconducting transition. Ginzburg and Landau had a stroke of genius, when they chose, as the order parameter some sort of wave function. At that time nobody knew about Cooper pairs, and about their Bose condensate, where all particles become coherent, i. e. described by the same wave function. This assumption was the basis of the new theory, which managed to solve the main contradiction of the old theory by Fritz and Heinz London, namely, the positive surface energy. Besides it made many useful predictions, such as the critical magnetic field of thin films, the critical current in thin wires etc."
>
> A. A. Abrikosov - Nobel Prize Lecture, 2003

According to Ginzburg and Landau, one must expand the free energy of the system in powers series of the order parameter, where the odd terms are neglected in favour of the phase symmetry

$$\mathfrak{F}_s(\Psi) = \mathfrak{F}_n + \alpha|\Psi|^2 + \frac{\beta}{2}|\Psi|^4 + \ldots \tag{1.12}$$

The free energy related to others thermodynamic variables is represented by the function $\mathfrak{F}_N$ and will be treated as a temperature-independent constant because it is assumed

that the other quantities are well behaved close to the transition. Then one must consider the superconducting case to happen when the part related to the transition is negative:

$$\Delta\mathfrak{F} = \mathfrak{F}_s - \mathfrak{F}_N < 0, \tag{1.13}$$

which means that the superconducting state is energetically more favourable than the normal state. The series is truncated up to the fourth power by the assumption that the order parameter is small in the vicinity of T_c and the coefficients α and β appearing in the expansion must be such that the theory will reproduce the character of most phase transitions: $\alpha(T) = a\tau$ and $\beta = b$ (historically it is defined that $a < 0$ and $b > 0$), where $\tau = 1 - T/T_c$. Thus if $T > T_c$ there is only one energy minimum of the free-energy functional, $\Psi = 0$, and if $T < T_c$ (note that α becomes negative) the system has a non trivial solution $\Psi_\infty = \sqrt{|a|\tau/b}$, as is shown in Fig. 4. This spontaneous break down of the symmetry can be found in magnetic systems, structural phase transitions in solids and even in particle theory serving as basis for the Higgs mechanism.

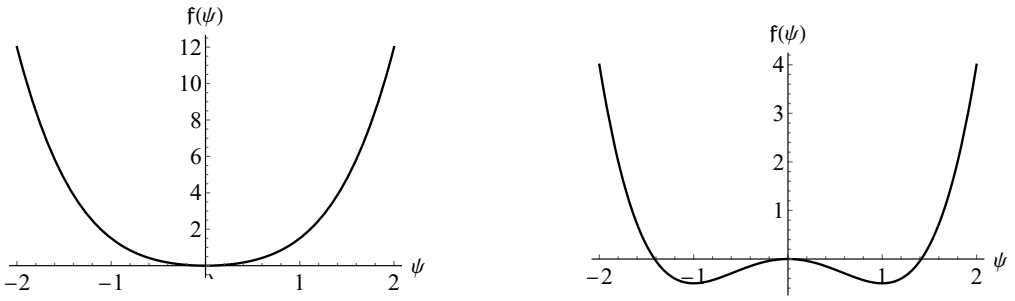

Figure 4 – Plots of the free energy density (in units of $a^2\tau^2/2b$) in dimensionless form. On the left, the case for $T > T_c$ and on the right, for $T < T_c$.

Then, for systems with spatial inhomogeneities it is included the simplest scalar term involving the gradient of the order parameter $|\vec{\nabla}\Psi|^2$. These inhomogeneities may arise from many sources, such as interfaces with different materials (resulting in different boundary conditions), applied electro-magnetic fields, sample imperfections etc. The case with electric fields involves dynamical problems in superconductors but this is out of the scope of this thesis. In the case of systems with applied magnetic fields, one must account for the vector potential through the minimum coupling ($\vec{\nabla} \to \vec{D} = \vec{\nabla} - i\frac{Q}{\hbar c}\vec{A}$) besides the common term of the magnetic energy[4]. Note that the order parameter must gain a phase factor of $\frac{Q}{\hbar c}\chi$ when performing a gauge change of $\vec{\nabla}\chi$ in order to have gauge invariance. Finally, the free energy functional becomes

$$\Delta\mathfrak{F}[\Psi, \Psi^*, \vec{A}] = \int d^3x\, \mathfrak{f}_s(\Psi, \Psi^*, \vec{A}) = \int d^3x \left[a\tau|\Psi|^2 + \frac{b}{2}|\psi|^4 + \mathcal{K}|\vec{D}\Psi|^2 + \frac{1}{8\pi}(\vec{\nabla}\times\vec{A})^2 \right]. \tag{1.14}$$

[4] This was the step needed in order to construct the energy functional for superconductors. It is not trivial why the order parameter has to be considered a complex number in superconductors.

From this functional, one can derive the thermodynamic critical field of the system by considering the energy necessary to take the system from the uniform solution ($|\Psi_\infty|^2 = |a|\tau/b$) at zero field to the normal state:

$$\mathfrak{F}_s - \mathfrak{F}_n = -\frac{(a\tau)^2}{2b} = -\frac{1}{8\pi}H_c^2 \Rightarrow H_c^2 = \frac{4\pi a^2\tau^2}{b} \tag{1.15}$$

This is the critical field of the Meissner state, where the magnetic field penetrates the superconductor only up to a certain typical length that will be shown to be λ_L. The set of parameters a, b and $\mathcal{K}$ are phenomenological and must be determined in order to match experimental results and within the framework of a microscopic theory where it was possible to derive analytic expressions for them in terms of microscopic parameters.

The condition of minimum energy allows the use of the Euler-Lagrange equations for the free energy density

$$\frac{\partial \mathfrak{f}_s}{\partial q} - \sum_i \partial_i \frac{\partial \mathfrak{f}_s}{\partial(\partial_i q)} = 0, \tag{1.16}$$

where q stands for Ψ and the components of $\vec{A}$. The result is the GL equations:

$$a\tau\Psi + b|\Psi|^2\Psi - \mathcal{K}\vec{D}^2\Psi = 0, \tag{1.17}$$

$$\frac{1}{4\pi}\vec{\nabla}\times\vec{\nabla}\times\vec{A} = -\mathcal{K}\frac{iQ}{\hbar c}\left(\Psi^*\vec{D}\Psi - \Psi\vec{D}^*\Psi^*\right). \tag{1.18}$$

These are called the equation for the order parameter and for the vector potential, respectively, although they are a set of coupled non-linear equations. They can be analytically solved in some regimes of approximation and it is possible to derive typical lengths for the order parameter and for the vector potential.

Consider the system without magnetic field but still with inhomogeneities, i.e. the gradient term is still present in Eq. (1.17). The order parameter is expressed in dimensionless units $\psi = \Psi/\Psi_\infty$, where Ψ_∞ is the solution for the uniform case. As previously done with the London equation, let us consider the superconducting sample occupying the half-space, say $x > 0$, but in this case the material beside the superconductor prevents the formation of the condensate in the boundary, e.g. magnetic materials or highly impure materials. By assuming symmetry in the y and z directions, the equation for the order parameter becomes

$$\psi - |\psi|^2\psi + \xi^2\frac{d^2\psi}{dx^2} = 0. \tag{1.19}$$

The analytic solution for this equation plotted in Fig. 5 is

$$\psi(x) = \tanh(x/\sqrt{2}\xi). \tag{1.20}$$

where the characteristic length

$$\xi^2 = \frac{\mathcal{K}}{|a|\tau} \tag{1.21}$$

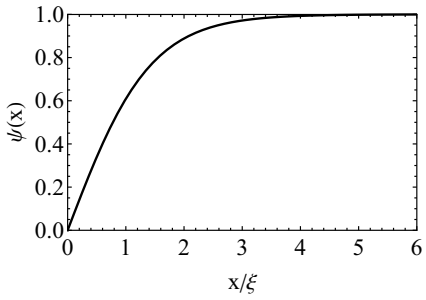

Figure 5 – Plot of the order parameter in the case of an interface with a material that prevents the formation of the superconducting condensate in the boundary in situations where ξ is much smaller than the dimensions of the sample.

is called the *coherence length*. In systems where spatial variations of the order parameter can be neglected, i.e. the coherence length is much smaller than the London penetration length, Ψ can be taken as the uniform solution $\Psi_\infty^2 = |a|\tau/b$. In this case, Eq. (1.18) is reduced to the London equation, Eq. (1.2),

$$\frac{c}{4\pi}\vec{\nabla}\times\vec{\nabla}\times\vec{A} = \vec{j_s} = -2\frac{\mathcal{K}Q^2}{\hbar^2 c}|\Psi_\infty|^2\vec{A} \tag{1.22}$$

with the penetration depth of the magnetic field

$$\lambda^2 = \frac{b\hbar^2c^2}{8\pi|a|\tau\mathcal{K}Q^2}. \tag{1.23}$$

Assuming that Ψ can be interpreted as a wave function, $|\Psi|^2$ gives the local density of superconducting particles. Then, for the uniform solution this density reads $n_s = |\Psi_\infty|^2 = |a|\tau/b$. Also, $|\vec{D}\Psi|^2$ works as a kinetic term and thus one can define $\mathcal{K} = \hbar^2/2m$, where instead of $\mathcal{K}$, the phenomenologic quantity is the mass of the particles involved m. With such assumptions, London theory is exactly recovered. This is the so-called *London limit* of the GL equations. Note that the GL theory not only introduced another characteristic length of superconductors, the coherence length, but has also provided their temperature scaling $\xi,\ \lambda \sim \tau^{-1/2}$ in the vicinity of the critical temperature.

Both interface problems examined so far are limiting cases of a more general picture where ξ and λ may be comparable. Consider, again assuming yz symmetry, the situation where the magnetic field is so strong that it destroys the superconducting state for $x \leq 0$ and, as the order parameter recovers from zero to its maximum value, the magnetic field tends to zero, for $x > 0$. In this case, it will be applied the constraint that the magnetic field is fixed at $H = H_c$, while only the magnetic induction h may vary. This can be done through a Legendre transformation, where one obtains the Gibbs free energy from the Helmholtz free energy by adding the term $-hH_c/4\pi$ to f_s. Thus we calculate the energy difference per unit area for that particular configuration, the

so-called surface energy

$$\begin{aligned}\sigma_{sn} &= \int_{-\infty}^{\infty} dx\,(\mathfrak{g}_{sH} - \mathfrak{g}_{s0}) = \int_{-\infty}^{\infty} dx\left(\mathfrak{f}_{sH} - \frac{hH_c}{4\pi} - \mathfrak{f}_{s0}\right) \\ &= \int_{-\infty}^{\infty} dx\left[\alpha|\Psi|^2 + \frac{\beta}{2}|\Psi|^4 + \mathcal{K}|\vec{D}\Psi|^2 + \frac{(h-H_c)^2}{8\pi}\right] \\ &= \int_{-\infty}^{\infty} dx\left[-\frac{\beta}{4}|\Psi|^4 + \frac{(h-H_c)^2}{8\pi}\right] \end{aligned} \tag{1.24}$$

where, after integrating by parts the kinetic term and neglecting the surface term, we have used Eq. (1.17) in order to obtain the last line. As can be seen, σ_{sn} can be either positive or negative whether the order parameter of field contributions have larger absolute value, respectively. By solving numerically the GL equations it was demonstrated that if the GL parameter

$$\kappa = \frac{\lambda}{\xi} \tag{1.25}$$

is larger than $\kappa_0 = 1/\sqrt{2}$, then σ_{sn} becomes negative and, otherwise, positive. In other words, this parameter determines whether the domain-wall solution is energetically favourable over the trivial solution $\Psi = 0$ and $h = H_c$.

As can be seen in Fig. 6, there is a region with length $\sim |\xi - \lambda|$ where either the

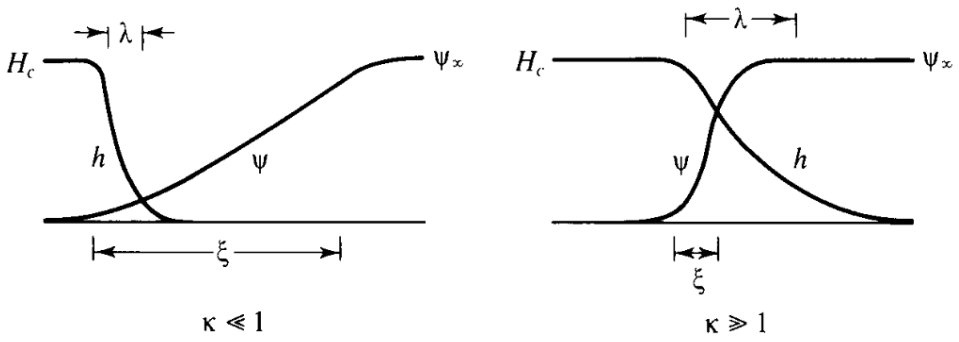

Figure 6 – On the left, deep type I behaviour ($\kappa \ll 1$). On the right, deep type II behaviour ($\kappa \gg 1$). Figure taken from Ref. (TINKHAM, 1996)

condensate or the magnetic field part will contribute more to σ_{sn}.

In 1957, Alexei Abrikosov published the vortex lattice solution for the Ginzburg-Landau equations motivated by magnetization measurements of thin films by Lev Schubnikov et al. (ABRIKOSOV, 1957b; ABRIKOSOV, 1957a). This was a new breakthrough in the field because nobody expected vortices in superconductors[5]. Abrikosov considered axially symmetric solutions of the GL equations in the limit of high magnetic

[5] Even Landau was against the idea of vortices in superconductors once he believed that the high stray fields energy would not favor vortices. Only after the works of R. Feynman on vortices in superfluids he agreed with the publication.

fields, where the order parameter becomes diminished, and therefore its influence over the vector potential can be neglected together with the cubic term. By doing so, the first GL equation is reduced to

$$-\vec{D}^2\Psi = \frac{1}{\xi^2}\Psi. \tag{1.26}$$

When considering that the plane of the film is the xy plane, and choosing the vector potential of the constant field as $\vec{A} = Hx\hat{j}$, the equation for the order parameter becomes

$$-\left(\vec{\nabla} - i\frac{Q}{\hbar c}Hx\hat{j}\right)^2\Psi = -\left(\nabla^2 - 2i\frac{Q}{\hbar c}Hx\partial_y - \frac{Q^2}{\hbar^2c^2}H^2x^2\right)\Psi = \frac{1}{\xi^2}\Psi. \tag{1.27}$$

With the ansatz $\Psi(x,y) = \exp(iky)\rho(x)$, one obtains the equation for the quantum harmonic oscillator

$$\rho'' - \left(k - \frac{Q}{\hbar c}Hx\right)^2\rho = -\frac{1}{\xi^2}\rho. \tag{1.28}$$

Therefore, the minimum energy is known and it provides the highest field

$$H_{c2} = -\frac{\hbar c}{Q\xi^2}, \tag{1.29}$$

which is nucleation field of the vortex phase (note that $H_{c2} \sim \tau$) and the eigenfunctions can be linearly combined in order to produce solutions with periodic zeros, or a vortex lattice, such as

$$\psi(x,y) = \sum_{n=-\infty}^{\infty} C_n \exp(ik_n y)\exp\left[-\frac{1}{\xi^2}\left(x - \frac{k_n\xi^2}{H/H_{c2}}\right)^2\right], \tag{1.30}$$

where C_n and k_n are defined accordingly to the symmetry of the vortex lattice. The lowest energy configuration was initially believed to be the square lattice but latter it was demonstrated to be the triangular by analysis of the Free energy (KLEINER; ROTH; AUTLER, 1964) and experimentally confirmed by Bitter decoration technique (TRÄUBLE; ESSMANN, 1968), which results in the plot of Fig. 7. Abrikosov discovered this new superconducting state and initiated the traditional classification that distinguishes *type-I* and *type-II* superconductors. More specifically, the first type, with $\kappa < \kappa_0$, only present the Meissner phase and exhibits a first order phase transition to the normal phase at H_c while the second kind, with $\kappa > \kappa_0$, shows second order phase transitions at H_{c1} (the field where the first vortex penetrates the sample) and at H_{c2} also allows the vortex state, as shown in Fig. 8.

1.3 The Microscopic Theory of Superconductivity

Although these early theories led to many predictions which were experimentally confirmed, they were not developed on a microscopic basis and could not provide the true explanation for the phenomenon of superconductivity. These early theories and

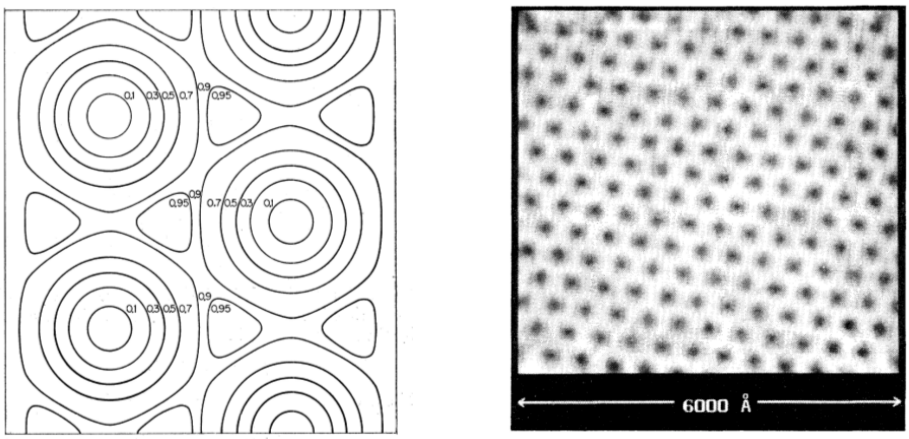

Figure 7 – On the left, square modulus of the order parameter for the triangular vortex lattice solution from Ref. (KLEINER; ROTH; AUTLER, 1964). The figure on the right is the Scanning-Tunnelling-Microscopy results for $NbSe_2$ at 1.8K from Ref. (HESS et al., 1989).

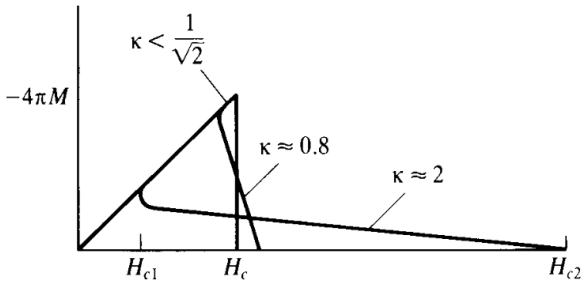

Figure 8 – Comparison between magnetization curves with the same value of thermodynamic critical field H_c but with different values of κ. For clarity, H_{c2} is only marked for the curve with highest κ. Figure taken from Ref. (TINKHAM, 1996).

experiments showed that it was reasonable to assume that this phenomenon could not arise from classical physics, i.e. it is a macroscopic manifestation of quantum mechanics. The initial idea of pairing of electrons as the mechanism of superconductivity was introduced in 1946 by R. Ogg Jr (OGG, 1946). Inspired by the phenomenology of liquid Helium, where the bosonic nature of He^4 produces a higher critical temperature than its fermionic isotope, He^3, he proposed a mechanism for obtaining superconductors with higher T_c when instead of having single electrons, they would be in a paired state. In essence, the pairing of electrons produces states with spin 0 and 1 which could enable at least subset of the quasi-particles to condense in the single quantum pair state similar to the Bose-Einstein condensation. This step was very important towards developing a microscopic theory for the phenomenon although he could not explain the attractive interaction between these electrons or produce any accurate prediction about the critical temperature of the superconductors. In 1950, H. Frölich proposed the interaction

which is now generally believed to give rise to superconductivity (FRÖHLICH, 1950). He suggested that the attractive interaction of the conducting electrons arises from the interaction with the ions of the crystalline lattice. In fact this phonon-mediated mechanism was experimentally confirmed in the same year with the discovery of the *isotope effect* (MAXWELL, 1950; REYNOLDS et al., 1950), i.e. the critical temperature and field are proportional to the inverse square root of the atomic mass for isotopes of the same element. By using the *jellium* model, in which the solid is approximated by a fluid of electrons and point ions, Bardeen and Pines (BARDEEN; PINES, 1955; PINES, 1958) were able to derive an analytic expression for the effective Fourier components of the electron-electron interaction which could become negative. The first contribution, which is positive-definite, accounted the dielectric (repulsive) response from the conduction electrons, and the second accounted the phonon mediated interaction, which is of the same order of the first contribution and therefore could result in negative matrix elements for the interaction (GENNES, 1999). From these considerations, it became evident how the pairing process could occur and very good arguments towards the condensation of the pairs (effective bosons) were produced by Schafroth (SCHAFROTH, 1955).

One of the last conceptual steps towards establishing a consistent microscopic theory of superconductivity, done by L. Cooper, was to show that the bound state of two electrons in the case of an arbitrarily small attractive force becomes energetically favourable in the presence of the Fermi sea of conducting electrons (COOPER, 1956). Based on the ideas of Frölich and Bardeen and Pines, he was able to produce a very simplified model for the interaction potential between two electrons:

$$V(\vec{k},\vec{k}') = \frac{1}{\Omega}\int d^3r V(\vec{r}) e^{-i(\vec{k}-\vec{k}')\cdot\vec{r}} = \begin{cases} -V/\Omega, & \text{if } \frac{\hbar^2k^2}{2m_e}, \frac{\hbar^2k'^2}{2m_e} \leq E_F + \hbar\omega_c \\ 0, & \text{otherwise.} \end{cases} \tag{1.31}$$

In this expression, V is a constant and Ω is the sample volume, also ω_c is a frequency of the order of the Debye frequency, ω_D, the limiting frequency of the phonon spectrum. The solution of the Schrödinger equation for the electron pair in the presence of the Fermi sea will have very low contribution from states much bellow the Fermi energy, once the density of states is much more pronounced from the Fermi level above. In other words, the Fourier transform produces integrals which will approximated as

$$\int \frac{d^3k}{(2\pi)^3} \to \int N(\xi_k)d\xi_k \approx N(0)\int_{-\hbar\omega_D}^{\hbar\omega_D} d\xi_k, \tag{1.32}$$

where $\xi_k = \frac{\hbar^2k^2}{2m_e} - \mu$ is the single-electron energy measured from the Fermi level and $N(0)$ is the density of states at the Fermi level. The energy of this paired state is

$$E \approx -2\hbar\omega_D \exp\left[-2/N(0)V\right] \tag{1.33}$$

which means that the energy of the bound pair of electrons is always smaller than the dissociated case, no matter how weak is the interaction constant V.

This was a prelude to the Nobel prize award publication by J. Bardeen, L. Cooper and J. Schrieffer (BCS) in 1957 where they explained the existence of the superconducting state from first principles (BARDEEN; COOPER; SCHRIEFFER, 1957). By considering that the number of particles is so large that the occupancy of each state $\vec{k}$ depends solely on the average occupancy of the other states (the Hartree self-consistent field), BCS could express the superconducting ground state as

$$|\psi_G\rangle = \prod_{\vec{k}=\vec{k}_1 \ldots \vec{k}_M} (u_{\vec{k}} + v_{\vec{k}} c^{\dagger}_{\vec{k}\uparrow} c^{\dagger}_{-\vec{k}\downarrow})|\phi_0\rangle \tag{1.34}$$

where the summation occurs over all M $\vec{k}$ values present in the band, $c^{\dagger}_{\vec{k}\uparrow}$ is the creation operator for an electron with wave number $\vec{k}$, $|u_{\vec{k}}|^2 + |v_{\vec{k}}|^2 = 1$ and $|\phi_0\rangle$ is the vacuum state with no particles. It is easy to show that $|v_{\vec{k}}|^2$ is the probability of the state $(\vec{k}\uparrow, -\vec{k}\downarrow)$ to be occupied and that $|\psi_G\rangle$ is not an eigenstate of the number operator if all $u_{\vec{k}}$ and $v_{\vec{k}}$ are finite. In this case, the number of particles is not fixed and instead one has the mean number of particles $\bar{N}$ fixed but with small variation from this value for real materials. As for the Hamiltonian, the interaction part was significantly simplified by neglecting terms which involved electrons not paired as $(\vec{k}\uparrow, -\vec{k}\downarrow)$, more specifically the only important diagrams are shown in Fig. 9. The so-called pairing (or reduced) Hamiltonian is

$$H_{\mathrm{BCS}} = \sum_{\vec{k}\sigma} \epsilon_{\vec{k}} c^{\dagger}_{\vec{k}\sigma} c_{\vec{k}\sigma}, + \frac{1}{2} \sum_{\vec{k}\vec{l}} V_{\vec{k}\vec{l}} c^{\dagger}_{\vec{k}\uparrow} c^{\dagger}_{-\vec{k}\downarrow} \langle c_{-\vec{l}\downarrow} c_{\vec{l}\uparrow} \rangle + h.c. \tag{1.35}$$

where $\sigma = \uparrow, \downarrow$ and the average $\langle \ldots \rangle$ is calculated with $|\psi_G\rangle$. In the next chapter, it will be demonstrated how the Ginzburg-Landau phenomenological theories of superconductivity are derived from the microscopic theory.

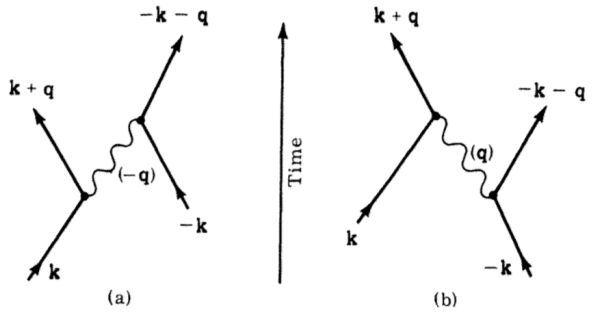

Figure 9 – Sketch of the attractive interaction between two electrons through a phonon in the BCS model. Figure taken from Ref. (TINKHAM, 1996).

2 THEORETICAL METHODS

> "Almost no one comes down here unless of course there is a problem. That's how it is with people: nobody cares how it works as long as it works. I like it down here."
>
> Counselor Hamann - *The Matrix Reloaded*

Chapter Contents

In this chapter the works of L. P. Gor'kov published during the late 1950s are discussed. With quantum field theory methods it was possible to prove that the Bardeen, Cooper and Schriefer (BCS) theory results in Ginzburg-Landau (GL) equations. Also, the experimental deviations from the BCS theory are reviewed that lead to important generalizations of the model to the state of the art developments in the field of multi-band superconductors. In particular, the extended GL (EGL) formalism is derived and its main theoretical achievements are discussed.

2.1 Gor'kov Derivation of Ginzburg-Landau Theory

In the late 1950's the works of L. P. Gor'kov (GOR'KOV, 1958; GOR'KOV, 1959) have established a direct connection between the BCS approach and the GL theory. By using the BCS-Bogolibov Hamiltonian, i.e., the Hamiltonian formulation of the BCS model by Bogoliubov and his coauthors, Gor'kov has applied standard methods of quantum field theory (ABRIKOSOV; DZYALOSHINSKI; GOR'KOV, 1965) to derive the GL equations. The core of this derivation relies on the assumption that the excitation gap can be identified as the order parameter of the system. As will be seen later, this is, in a sense, misleading for compounds with more than one superconducting band (multi-band superconductors).

The Hamiltonian operator $\mathcal{H}_{BCS}$ includes the usual kinetic part absorbing the chemical potential in such a way that only the averaged number of particles is controlled (the grand canonical formalism). The interaction part is the second term shown in Eq. 2.1. Other terms related to the interaction between particles, i.e., the Hartree and Fock contributions, are accounted as constants and hidden in the chemical potential μ, once they do not have a specific reason to vary significantly when crossing T_c.

$$\mathcal{H}_{\text{BCS}} = \sum_{\sigma} \int d^D x \psi^{\dagger}_{\sigma}(\vec{x}) \mathcal{T}_x \psi_{\sigma}(\vec{x}) + \int d^D x \left[\psi^{\dagger}_{\uparrow}(\vec{x}) \psi^{\dagger}_{\downarrow}(\vec{x}) \Delta(\vec{x}) + \Delta^*(\vec{x}) \psi_{\downarrow}(\vec{x}) \psi_{\uparrow}(\vec{x}) \right] \tag{2.1}$$

where $\mathcal{T}_x$ is the single-electron kinetic energy operator

$$\mathcal{T}_x \equiv -\frac{\hbar^2}{2m_e} \left(\vec{\nabla} - i \frac{e}{\hbar c} \vec{A} \right)^2 - \mu \tag{2.2}$$

and the energy gap is

$$\Delta(\vec{x}) = g \left\langle \psi_{\uparrow}(\vec{x}) \psi_{\downarrow}(\vec{x}) \right\rangle . \tag{2.3}$$

The equations of motion can be derived once it is stated that the field operators obey fermionic commutation rules

$$\left\{ \psi_{\sigma}(\vec{x}), \psi^{\dagger}_{\sigma'}(\vec{x}') \right\} = \delta_{\sigma,\sigma'} \delta(\vec{x} - \vec{x}'), \tag{2.4}$$

$$\{ \psi_{\sigma}(\vec{x}), \psi_{\sigma'}(\vec{x}') \} = 0 \tag{2.5}$$

and, in order to work with finite temperatures, it will be defined temperature Heisenberg field-operators

$$\psi_{\sigma}(\vec{x}, t) = \exp(\mathcal{H}_{BCS} t/\hbar)\ \psi_{\sigma}(\vec{x})\ \exp(-\mathcal{H}_{BCS} t/\hbar), \tag{2.6}$$

$$\overline{\psi}_{\sigma}(\vec{x}, t) = \exp(\mathcal{H}_{BCS} t/\hbar)\ \psi^{\dagger}_{\sigma}(\vec{x})\ \exp(-\mathcal{H}_{BCS} t/\hbar). \tag{2.7}$$

Their equations of motion are derived, as described explicitly at appendix A, by using the commutators of these operators with $\mathcal{H}_{BCS}$

$$-\hbar \partial_t \psi_{\uparrow}(\vec{x}, t) = \left[\psi_{\uparrow}(\vec{x}, t), \mathcal{H}_{BCS} \right] = \mathcal{T}_x \psi_{\uparrow}(\vec{x}, t) + \Delta(\vec{x}) \overline{\psi}_{\downarrow}(\vec{x}, t), \tag{2.8}$$

$$-\hbar \partial_t \overline{\psi}_{\downarrow}(\vec{x}, t) = \left[\overline{\psi}_{\downarrow}(\vec{x}, t), \mathcal{H}_{BCS} \right] = -\mathcal{T}^*_x \overline{\psi}_{\downarrow}(\vec{x}, t) + \Delta^*(\vec{x}) \psi_{\uparrow}(\vec{x}, t). \tag{2.9}$$

or, in the matrix form,

$$-\hbar\partial_t \begin{pmatrix} \psi_\uparrow(\vec{x},t) \\ \overline{\psi}_\downarrow(\vec{x},t) \end{pmatrix} = \begin{pmatrix} \mathcal{T}_x & \Delta(\vec{x}) \\ \Delta^*(\vec{x}) & -\mathcal{T}_x^* \end{pmatrix} \begin{pmatrix} \psi_\uparrow(\vec{x},t) \\ \overline{\psi}_\downarrow(\vec{x},t) \end{pmatrix}. \tag{2.10}$$

From these equations, one can derive the equations of motion for the corresponding Green functions, as described explicitly at appendix A:

$$\begin{aligned} -\hbar\partial_t \mathcal{G}(\vec{x},t;\vec{x}',t') &= \partial_t \left\langle T_t \psi_\uparrow(\vec{x},t)\overline{\psi}_\uparrow(\vec{x}',t')\right\rangle \\ &= \delta(t-t')\delta(\vec{x}-\vec{x}') + \mathcal{T}_x \mathcal{G}(\vec{x},t;\vec{x}',t') + \Delta(\vec{x})\overline{\mathcal{F}}(\vec{x},t;\vec{x}',t'), \qquad (2.11) \\ -\hbar\partial_t \overline{\mathcal{F}}(\vec{x},t;\vec{x}',t') &= \partial_t \left\langle T_t \overline{\psi}_\downarrow(\vec{x},t)\overline{\psi}_\uparrow(\vec{x}',t')\right\rangle \\ &= \Delta^*(\vec{x})\mathcal{G}(\vec{x},t;\vec{x}',t') - \mathcal{T}_x^* \overline{\mathcal{F}}(\vec{x},t;\vec{x}',t'), \qquad (2.12) \\ -\hbar\partial_t \overline{\mathcal{G}}(\vec{x},t;\vec{x}',t') &= \partial_t \left\langle T_t \overline{\psi}_\downarrow(\vec{x},t)\psi_\downarrow(\vec{x}',t')\right\rangle \\ &= \delta(t-t')\delta(\vec{x}-\vec{x}') + \Delta^*(\vec{x})\mathcal{F}(\vec{x},t;\vec{x}',t') - \mathcal{T}_x^* \overline{\mathcal{G}}(\vec{x},t;\vec{x}',t'), \qquad (2.13) \\ -\hbar\partial_t \mathcal{F}(\vec{x},t;\vec{x}',t') &= \partial_t \left\langle T_t \psi_\uparrow(\vec{x},t)\psi_\downarrow(\vec{x}',t')\right\rangle \\ &= \mathcal{T}_x^* \mathcal{F}(\vec{x},t;\vec{x}',t') - \Delta(\vec{x})\overline{\mathcal{F}}(\vec{x},t;\vec{x}',t'), \qquad (2.14) \end{aligned}$$

where T_t is the time-ordering operator. Note that there are no δ functions in the equations of motion for $\mathcal{F}$ and $\overline{\mathcal{F}}$, thus they are called *anomalous Green functions*. Also, we can use the following matrix notations[1]

$$G(\vec{x},t;\vec{x}',t') = \begin{pmatrix} \mathcal{G}(\vec{x},t;\vec{x}',t') & \mathcal{F}(\vec{x},t;\vec{x}',t') \\ \overline{\mathcal{F}}(\vec{x},t;\vec{x}',t') & \overline{\mathcal{G}}(\vec{x},t;\vec{x}',t') \end{pmatrix}, \tag{2.15}$$

$$\check{1} = \begin{pmatrix} 1 & 0 \\ 0 & 1 \end{pmatrix}, \tag{2.16}$$

$$\mathcal{H}_{BdG} = \begin{pmatrix} \mathcal{T}_x & \Delta(\vec{x}) \\ \Delta^*(\vec{x}) & -\mathcal{T}_x^* \end{pmatrix}, \tag{2.17}$$

in order to condense all the equations for the Green functions to the matrix form given by

$$-\hbar\partial_t G(\vec{x},t;\vec{x}',t') = \delta(t-t')\delta(\vec{x}-\vec{x}')\check{1} + \mathcal{H}_{BdG}G(\vec{x},t;\vec{x}',t'). \tag{2.18}$$

It is well-known that for the sake of the trace convergence the applicability domain of the above definitions of the Green functions is restricted to the interval $-\beta\hbar < t - t' < \beta\hbar$. In this interval the Green functions are anti-periodic in $t - t'$. Considering, as an example, the case of the Green function

$$\mathcal{G}(\vec{x},t;\vec{x}',t') = -\frac{1}{\hbar}\left\langle T_t \psi_\uparrow(\vec{x},t)\overline{\psi}_\uparrow(\vec{x}',t')\right\rangle, \tag{2.19}$$

[1] The label BdG at the Hamiltonian matrix refers to the Bogoliubov-de Gennes Hamiltonian appearing in the matrix equation involving the Green functions.

we first write it as a function of $\eta \equiv t - t'$ (this comes from the fact that the Hamiltonian operator does not depend explicitly on time). Then defining the *advanced*, $\mathcal{G}^{>}(\vec{x}, \vec{x}', \eta)$, and *retarded*, $\mathcal{G}^{<}(\vec{x}, \vec{x}', \eta)$, Green functions

$$\mathcal{G}(\vec{x}, t; \vec{x}', t') = -\frac{1}{\hbar} \begin{cases} \left\langle \psi_\uparrow(\vec{x}, \eta) \overline{\psi}_\downarrow(\vec{x}', 0') \right\rangle = \mathcal{G}^{>}(\vec{x}, \vec{x}', \eta), & \text{if } \eta{>}0 \\ -\left\langle \overline{\psi}_\downarrow(\vec{x}', 0') \psi_\uparrow(\vec{x}, \eta) \right\rangle = \mathcal{G}^{<}(\vec{x}, \vec{x}', \eta), & \text{if } \eta{<}0 \end{cases} \tag{2.20}$$

one derives the following relation:

$$\begin{aligned} \mathcal{G}^{>}(\vec{x}, \vec{x}', \eta) &= -\left\langle \exp(-\beta\mathcal{H}) \exp(\mathcal{H}\eta) \psi_\uparrow(\vec{x}) \exp(-\mathcal{H}\eta) \psi_\downarrow^\dagger(\vec{x}') \right\rangle = \\ &= -\left\langle \exp\left[(\eta - \beta)\mathcal{H}\right] \psi_\uparrow(\vec{x}) \exp\left[-(\eta - \beta)\mathcal{H}\right] \exp(-\beta\mathcal{H}) \psi_\downarrow^\dagger(\vec{x}') \right\rangle = \\ &= -\left\langle \exp(-\beta\mathcal{H}) \psi_\downarrow^\dagger(\vec{x}') \exp\left[(\eta - \beta)\mathcal{H}\right] \psi_\uparrow(\vec{x}) \exp\left[-(\eta - \beta)\mathcal{H}\right] \right\rangle = \\ &= \left\langle \overline{\psi}_\downarrow(\vec{x}', 0) \psi_\uparrow(\vec{x}, \eta - \beta) \right\rangle = -\mathcal{G}^{<}(\vec{x}, \vec{x}', \eta - \beta). \end{aligned} \tag{2.21}$$

Now, to invoke the time Fourier transform and so significantly simplify our treatment, we assume that the Green functions are defined for $-\infty < t - t' < \infty$ and anti-periodic, following the above expression. In the interval $-\beta\hbar < t - t' < \beta\hbar$ this construction coincides with the original formulation. In order to do this, one must change the delta-function $\delta(t - t')$ in Eq. (2.18) by its anti-periodic generalization:

$$\delta(t - t') \to \sum_{n=-\infty}^{\infty} \delta(t - t' + n\beta\hbar)(-1)^n, \tag{2.22}$$

as represented in Fig. 10. The only consequence of this replacement is an appearance

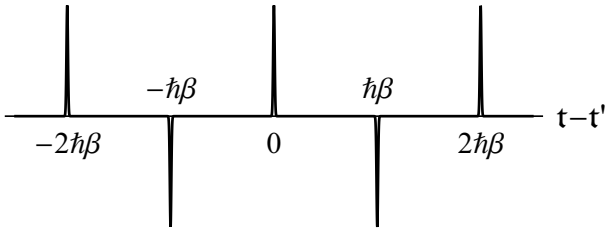

Figure 10 – Sketch of the periodic sum of δ functions introduced in Eq. (2.18) in order to make the Green functions periodic in the interval $2\beta\hbar$.

of discontinuities at $t - t' = \pm\beta\hbar, \pm 2\beta\hbar, \ldots$ that can in no way influence the physical behavior at $-\beta\hbar < t - t' < \beta\hbar$. The Fourier components of the reconstructed Green functions $\mathcal{Y} = \left\{\mathcal{G}, \overline{\mathcal{G}}, \mathcal{F}, \overline{\mathcal{F}}\right\}$ are given by

$$\mathcal{Y}(\vec{x}, t; \vec{x}', t') \equiv \frac{1}{\beta\hbar} \sum_{n=-\infty}^{\infty} \exp\left(-i\omega_n \eta\right) \mathcal{Y}_\omega(\vec{x}, \vec{x}'), \tag{2.23}$$

$$\mathcal{Y}_\omega(\vec{x}, \vec{x}') \equiv \frac{1}{2} \int_{-\hbar\beta}^{\hbar\beta} d\eta \, \exp\left(i\omega_n \eta\right) \mathcal{Y}(\vec{x}, \tau; \vec{x}', \tau') \tag{2.24}$$

where $\omega_n = \pi(2n+1)/\beta\hbar$ are the fermionic Matsubara frequencies. Using these Fourier components, the Gor'kov-Nambu equation

$$-\hbar\partial_t G(\vec{x},t;\vec{x}',t') = \sum_{n=-\infty}^{\infty} \delta(t-t'+n\beta\hbar)(-1)^n \delta(\vec{x}-\vec{x}')\check{1} + \mathcal{H}_{BdG} G(\vec{x},t;\vec{x}',t') \quad (2.25)$$

can be rearranged. When introducing

$$G_\omega(\vec{x},\vec{x}') \equiv \begin{pmatrix} \mathcal{G}_\omega(\vec{x},\vec{x}') & \mathcal{F}_\omega(\vec{x},\vec{x}') \\ \overline{\mathcal{F}}_\omega(\vec{x},\vec{x}') & \overline{\mathcal{G}}_\omega(\vec{x},\vec{x}') \end{pmatrix}, \quad (2.26)$$

the left-hand side of Eq. (2.25) becomes

$$-\hbar\partial_t \left[\frac{1}{\beta\hbar}\sum_{n=-\infty}^{\infty} \exp\left[-i\omega_n(t-t')\right] G_\omega(\vec{x},\vec{x}')\right] = \frac{1}{\beta\hbar}\sum_{n=-\infty}^{\infty} (i\hbar\omega_n)\exp\left[-i\omega_n(t-t')\right] G_\omega(\vec{x},\vec{x}'), \quad (2.27)$$

and the Fourier transform of the summation of δ functions is[2]

$$\begin{aligned} &\frac{1}{2}\int_{-\hbar\beta}^{\hbar\beta} d\eta\ \exp\left(-i\omega_{n'}\eta\right) \sum_{n=-\infty}^{\infty} \delta(\eta+n\beta\hbar)(-1)^n = \\ &= \frac{1}{2}\int_{-\hbar\beta}^{\hbar\beta} d\eta\ \exp\left(-i\omega_{n'}\eta\right)\left(-\delta(\eta-\beta\hbar)+\delta(\eta)-\delta(\eta+\beta\hbar)\right] = \\ &= \frac{1}{2}\left\{-\frac{1}{2}\exp[-i\pi(2n'+1)]+1-\frac{1}{2}\exp[i\pi(2n'+1)]\right\} = \frac{1}{2}(\frac{1}{2}+1+\frac{1}{2}) = 1 \end{aligned} \quad (2.28)$$

As the $\mathcal{H}_{BdG}$ operator only depends on the spacial variables, the last term is simply reduced to

$$\begin{aligned} \mathcal{H}_{BdG} G(\vec{x},t;\vec{x}',t') &= \mathcal{H}_{BdG}\frac{1}{\beta\hbar}\sum_{n=-\infty}^{\infty} \exp\left(-i\omega_n\eta\right) G_\omega(\vec{x},\vec{x}') = \\ &= \frac{1}{\beta\hbar}\sum_{n=-\infty}^{\infty} \exp\left(-i\omega_n\eta\right) \mathcal{H}_{BdG} G_\omega(\vec{x},\vec{x}') \end{aligned} \quad (2.29)$$

Finally, the Gor'kov-Nambu equation for the Fourier transforms of the Green functions reads

$$i\hbar\omega G_\omega(\vec{x},\vec{x}') = \delta(\vec{x}-\vec{x}')\check{1} + \mathcal{H}_{BdG} G_\omega(\vec{x},\vec{x}'). \quad (2.30)$$

or, explicitly,

$$i\hbar\omega \begin{pmatrix} \mathcal{G}_\omega(\vec{x},\vec{x}') & \mathcal{F}_\omega(\vec{x},\vec{x}') \\ \overline{\mathcal{F}}_\omega(\vec{x},\vec{x}') & \overline{\mathcal{G}}_\omega(\vec{x},\vec{x}') \end{pmatrix} = \delta(\vec{x}-\vec{x}') \begin{pmatrix} 1 & 0 \\ 0 & 1 \end{pmatrix} + \begin{pmatrix} \mathcal{T}_x & \Delta(\vec{x}) \\ \Delta^*(\vec{x}) & -\mathcal{T}_x^* \end{pmatrix} \begin{pmatrix} \mathcal{G}_\omega(\vec{x},\vec{x}') & \mathcal{F}_\omega(\vec{x},\vec{x}') \\ \overline{\mathcal{F}}_\omega(\vec{x},\vec{x}') & \overline{\mathcal{G}}_\omega(\vec{x},\vec{x}') \end{pmatrix} \quad (2.31)$$

[2] Actually, the normalization constants appearing in front of the Fourier transform and its inverse are defined such that this terms results one.

In order to solve these equations, it is convenient to introduce new operators in the Hilbert space defined as

$$\langle \vec{x} \,|\hat{\mathcal{Y}}_\omega\, |\vec{x}'\rangle = \mathcal{Y}_\omega(\vec{x},\vec{x}') \rightarrow \check{G}_\omega = \begin{pmatrix} \hat{\mathcal{G}}_\omega & \hat{\mathcal{F}}_\omega \\ \hat{\bar{\mathcal{F}}}_\omega & \hat{\bar{\mathcal{G}}}_\omega \end{pmatrix} \tag{2.32}$$

and

$$\langle \vec{x} \,|\hat{\mathcal{T}}\, |\vec{x}'\rangle = \delta(\vec{x}-\vec{x}')\mathcal{T}_{x'}, \tag{2.33}$$

$$\langle \vec{x} \,|\hat{\Delta}\, |\vec{x}'\rangle = \delta(\vec{x}-\vec{x}')\Delta(\vec{x}'). \tag{2.34}$$

Also, as the $\mathcal{H}_{BdG}$ operator can be expressed as the sum of the kinetic and interaction (condensate) contributions

$$\check{\mathcal{T}} = \begin{pmatrix} \hat{\mathcal{T}} & 0 \\ 0 & -\hat{\mathcal{T}}^* \end{pmatrix}, \tag{2.35}$$

$$\check{\Delta} = \begin{pmatrix} 0 & \hat{\Delta} \\ \hat{\Delta}^* & 0 \end{pmatrix}, \tag{2.36}$$

Eq. (2.30) results in

$$\begin{aligned} -i\hbar\omega_n \langle \vec{x} \,|\check{G}_\omega\, |\vec{x}'\rangle &= \delta(\vec{x}-\vec{x}')\check{1} + \mathcal{H}_{BdG}G_\omega(\vec{x},\vec{x}') = \\ &= \langle \vec{x}\, |\vec{x}'\rangle \check{1} + \int d\vec{x}'' \langle \vec{x} \,|(\check{\mathcal{T}}+\check{\Delta})\, |\vec{x}''\rangle \langle \vec{x}'' \,|\check{G}_\omega\, |\vec{x}'\rangle = \\ &= \langle \vec{x}\, |\vec{x}'\rangle \check{1} + \langle \vec{x} \,|(\check{\mathcal{T}}+\check{\Delta})\check{G}_\omega\, |\vec{x}'\rangle \end{aligned} \tag{2.37}$$

By using the completeness relation of the Hilbert space, one obtains the Gor'kov-Nambu equations in the operator form

$$\left(i\hbar\omega_n - \check{\mathcal{T}}\right)\check{G}_\omega = \check{1} + \check{\Delta}\check{G}_\omega. \tag{2.38}$$

In the normal state, i.e., in the absence of condensed pairs, $\hat{\Delta} = 0$, the normal or unperturbed Green function operator can be constructed as

$$\left(i\hbar\omega_n - \check{\mathcal{T}}\right)\check{G}^{(0)}_\omega = \check{1} \Rightarrow \left(i\hbar\omega_n - \check{\mathcal{T}}\right) = \left[\check{G}^{(0)}_\omega\right]^{-1}. \tag{2.39}$$

In the explicit form Eq. (2.39) writes

$$\begin{cases} (i\hbar\omega_n - \hat{\mathcal{T}}\,)\hat{\mathcal{G}}^{(0)}_\omega = 1, \\ (i\hbar\omega_n + \hat{\mathcal{T}}^*)\hat{\bar{\mathcal{F}}}^{(0)}_\omega = 0, \\ (i\hbar\omega_n - \hat{\mathcal{T}}\,)\hat{\mathcal{F}}^{(0)}_\omega = 0, \\ (i\hbar\omega_n + \hat{\mathcal{T}}^*)\hat{\bar{\mathcal{G}}}^{(0)}_\omega = 1, \end{cases} \Rightarrow \begin{cases} \hat{\mathcal{G}}^{(0)}_\omega = (i\hbar\omega_n - \hat{\mathcal{T}}\,)^{-1}, \\ \hat{\bar{\mathcal{G}}}^{(0)}_\omega = (i\hbar\omega_n + \hat{\mathcal{T}}^*\,)^{-1}, \\ \hat{\bar{\mathcal{F}}}^{(0)}_\omega = \hat{\mathcal{F}}^{(0)}_\omega = 0. \end{cases} \tag{2.40}$$

The next step is to multiply Eq. (2.39) on the left by the inverse of the normal Green function. This yields

$$\left[\check{G}^{(0)}_\omega\right]^{-1}\check{G}_\omega = \check{1} + \check{\Delta}\check{G}_\omega \Rightarrow \check{G}_\omega = \check{G}^{(0)}_\omega + \check{G}^{(0)}_\omega\check{\Delta}\check{G}_\omega, \tag{2.41}$$

which is the representation of the Gor'kov-Nambu formalism in the form of the matrix Dyson equation. By invoking iterations, one obtains

$$\check{G}_\omega = \check{G}^{(0)}_\omega + \check{G}^{(0)}_\omega \check{\Delta} \check{G}^{(0)}_\omega + \check{G}^{(0)}_\omega \check{\Delta} \check{G}^{(0)}_\omega \check{\Delta} \check{G}^{(0)}_\omega + \dots . \tag{2.42}$$

To construct the self-consistency equation for the superconducting gap, one needs to extract the equation for the anomalous Green function. In its explicit form Eq. (2.41) is given by

$$\begin{pmatrix} \hat{\mathcal{G}}_\omega & \hat{\mathcal{F}}_\omega \\ \hat{\bar{\mathcal{F}}}_\omega & \hat{\bar{\mathcal{G}}}_\omega \end{pmatrix} = \begin{pmatrix} \hat{\mathcal{G}}^{(0)}_\omega & 0 \\ 0 & \hat{\bar{\mathcal{G}}}^{(0)}_\omega \end{pmatrix} + \begin{pmatrix} \hat{\mathcal{G}}^{(0)}_\omega & 0 \\ 0 & \hat{\bar{\mathcal{G}}}^{(0)}_\omega \end{pmatrix} \begin{pmatrix} 0 & \hat{\Delta} \\ \hat{\Delta}^* & 0 \end{pmatrix} \begin{pmatrix} \hat{\mathcal{G}}_\omega & \hat{\mathcal{F}}_\omega \\ \hat{\bar{\mathcal{F}}}_\omega & \hat{\bar{\mathcal{G}}}_\omega \end{pmatrix}, \tag{2.43}$$

and one finds

$$\begin{cases} \hat{\bar{\mathcal{G}}}_\omega = \hat{\bar{\mathcal{G}}}^{(0)}_\omega + \hat{\bar{\mathcal{G}}}^{(0)}_\omega \hat{\Delta}^* \hat{\mathcal{F}}_\omega \\ \hat{\mathcal{F}}_\omega = \hat{\mathcal{G}}^{(0)}_\omega \hat{\Delta} \hat{\bar{\mathcal{G}}}_\omega \end{cases} \Rightarrow \begin{cases} \hat{\bar{\mathcal{G}}}_\omega = \hat{\bar{\mathcal{G}}}^{(0)}_\omega + \hat{\bar{\mathcal{G}}}^{(0)}_\omega \hat{\Delta}^* \left[\hat{\mathcal{G}}^{(0)}_\omega \hat{\Delta} \hat{\bar{\mathcal{G}}}_\omega \right] \\ \hat{\mathcal{F}}_\omega = \hat{\mathcal{G}}^{(0)}_\omega \hat{\Delta} \hat{\bar{\mathcal{G}}}_\omega \end{cases} \tag{2.44}$$

Iterations lead to

$$\hat{\mathcal{F}}_\omega = \hat{\mathcal{G}}^{(0)}_\omega \hat{\Delta} \hat{\bar{\mathcal{G}}}^{(0)}_\omega + \hat{\mathcal{G}}^{(0)}_\omega \hat{\Delta} \hat{\bar{\mathcal{G}}}^{(0)}_\omega \hat{\Delta}^* \hat{\mathcal{G}}^{(0)}_\omega \hat{\Delta} \hat{\bar{\mathcal{G}}}^{(0)}_\omega + \dots . \tag{2.45}$$

Given Eq. (2.14), there is an important relation between the energy gap and the anomalous Green function:

$$\begin{aligned} \Delta(\vec{x}) &= \langle \psi_\downarrow(\vec{x}) \psi_\uparrow(\vec{x}) \rangle = -g\hbar \lim_{\vec{x}' \to \vec{x}} \lim_{\eta \to 0^+} \mathcal{F}(\vec{x}, t, \vec{x}', t') \\ &= -g\hbar \lim_{\vec{x}' \to \vec{x}} \lim_{\eta \to 0^+} \frac{1}{\beta\hbar} \sum_\omega \exp(-i\omega\eta) \mathcal{F}_\omega(\vec{x}, \vec{x}') = -gT \lim_{\vec{x}' \to \vec{x}} \lim_{\eta \to 0^+} \sum_\omega \exp(-i\omega\eta) \mathcal{F}_\omega(\vec{x}, \vec{x}'). \end{aligned} \tag{2.46}$$

Using the completeness relation, i.e., by inserting identity operators $\hat{1} = \int dy \, |\vec{y}\rangle \langle \vec{y}|$ in Eq. (2.45), one obtains the self-consistency equation whose right-hand-side is expanded in powers of the order parameter (gap function), i.e.

$$\begin{aligned} \Delta(\vec{x}) = &\int d^3y K_a(\vec{x}, \vec{y}) \Delta(\vec{y}) + \int \left(\prod_{i=1}^{3} d^3 y_i \right) K_b(\vec{x}, \vec{y}_1, \vec{y}_2, \vec{y}_3) \Delta(\vec{y}_1) \Delta^*(\vec{y}_2) \Delta(\vec{y}_3) + \\ &+ \int \left(\prod_{i=1}^{5} d^3 y_i \right) K_c(\vec{x}, \vec{y}_1, \vec{y}_2, \vec{y}_3, \vec{y}_4, \vec{y}_5) \Delta(\vec{y}_1) \Delta^*(\vec{y}_2) \Delta(\vec{y}_3) \Delta^*(\vec{y}_4) \Delta(\vec{y}_5) + \dots , \end{aligned} \tag{2.47}$$

wherein the integral kernels are written as

$$K_a(\vec{x}, \vec{y}) = -gT \lim_{\eta \to 0^+} \sum_\omega \exp(-i\omega\eta) \mathcal{G}^{(0)}_\omega(\vec{x}, \vec{y}) \bar{\mathcal{G}}^{(0)}_\omega(\vec{y}, \vec{x}), \tag{2.48}$$

$$K_b(\vec{x}, \vec{y}_1, \vec{y}_2, \vec{y}_3) = -gT \lim_{\eta \to 0^+} \sum_\omega \mathcal{G}^{(0)}_\omega(\vec{x}, \vec{y}_1) \bar{\mathcal{G}}^{(0)}_\omega(\vec{y}_1, \vec{y}_2) \mathcal{G}^{(0)}_\omega(\vec{y}_2, \vec{y}_3) \mathcal{G}^{(0)}_\omega(\vec{y}_3, \vec{x}), \tag{2.49}$$

$$K_c(\vec{x}, \vec{y}_1, \vec{y}_5) = -gT \lim_{\eta \to 0^+} \sum_\omega \mathcal{G}^{(0)}_\omega(\vec{x}, \vec{y}_1) \bar{\mathcal{G}}^{(0)}_\omega(\vec{y}_1, \vec{y}_2) \dots \bar{\mathcal{G}}^{(0)}_\omega(\vec{y}_3, \vec{y}_4) \mathcal{G}^{(0)}_\omega(\vec{y}_4, \vec{y}_5) \mathcal{G}^{(0)}_\omega(\vec{y}_5, \vec{x}) \tag{2.50}$$

In order to obtain the GL equations, one must truncate the infinite series in powers of the gap in Eq. (2.47), keeping only the first and third powers (the well-known Gor'kov truncation). To obtain the EGL formalism, it is of importance to include the fifth-power term.

In the absence of magnetic fields, for the unperturbed or normal-metal Green function one gets

$$\begin{aligned}
\mathcal{G}_{\omega}^{(0)}(\vec{x},\vec{x}') &= \langle \vec{x} \,|(i\hbar\omega_n - \hat{\mathcal{T}}\,)^{-1}\,|\vec{x}'\rangle = \\
&= \int \frac{d^3k}{(2\pi)^3}\frac{d^3k'}{(2\pi)^3}\left\langle \vec{x}|\vec{k}\right\rangle\left\langle \vec{k}\,|(i\hbar\omega_n - \hat{\mathcal{T}}\,)^{-1}\,|\vec{k}'\right\rangle\left\langle \vec{k}'|\vec{x}'\right\rangle = \\
&= \int \frac{d^3k}{(2\pi)^3}\frac{d^3k'}{(2\pi)^3}\exp(i\vec{k}\cdot\vec{x})\frac{1}{i\hbar\omega_n - \xi_k}(2\pi)^3\delta(\vec{k}-\vec{k}')\exp(-i\vec{k}'\cdot\vec{x}') = \\
&= \int \frac{d^3k}{(2\pi)^3}\frac{\exp[i\vec{k}\cdot(\vec{x}-\vec{x}')]}{i\hbar\omega_n - \xi_k}, \qquad (2.51)
\end{aligned}$$

where ξ_k is the single-particle dispersion. For a spherically symmetric Fermi surface and in the parabolic band approximation we have

$$\xi_k = \frac{\hbar^2k^2}{2m_e} - \mu. \qquad (2.52)$$

For the standard deep-band approximation[3], one can determine the unperturbed Green function as

$$\begin{aligned}
\mathcal{G}_{\omega}^{(0)}(\vec{x},\vec{x}') &= \int \frac{d^3k}{(2\pi)^3}\frac{\exp\left[i\vec{k}\cdot(\vec{x}-\vec{x}')\right]}{i\hbar\omega - \xi_k} \\
&= \int_0^{\infty} k^2\frac{dk}{(2\pi)^3}\int_0^{2\pi}d\varphi\int_{-1}^{1}d(\cos\theta)\frac{\exp\left(ik|\vec{x}-\vec{x}'|\cos\theta\right)}{i\hbar\omega - \xi_k} \\
&= \int_0^{\infty} k^2\frac{dk}{(2\pi)^2}\frac{1}{i\hbar\omega - \xi_k}\frac{\exp(ikz)-\exp(-ikz)}{ikz} \\
&= -\frac{m_e}{i\hbar^2(2\pi)^2 z}\int_{-\mu}^{\infty}d\xi\frac{\exp\left[i\left(k_F+\frac{\xi}{\hbar v_F}\right)z\right]-\exp\left[-i\left(k_F+\frac{\xi}{\hbar v_F}\right)z\right]}{\xi - i\hbar\omega} \qquad (2.53)
\end{aligned}$$

where $z = |\vec{z}| = |\vec{x}-\vec{x}'|$. The last integral can be calculated performing the analytic extension of ξ to the complex plane. As sketched in Fig. 11, the first contour is used for calculating the left term inside the integral and the second contour for the right term. By doing so, if the pole lays above the horizontal axis, $\omega > 0$, the left term is the only

[3] In the deep-band regime, one can approximate $\xi_k = \frac{\hbar^2k^2}{2m_e} - \frac{\hbar^2k_F^2}{2m_e} = \frac{\hbar^2}{2m_e}(k-k_f)(k+k_F) \approx \frac{\hbar^2k_F}{m_e}(k-k_F) = \hbar v_F(k-k_F)$ once the energy gap is much smaller than the chemical potential (the Fermi energy) and thus only momenta very close to the Fermi level contribute. The limit of integration is taken so that $\mu \to \infty$.

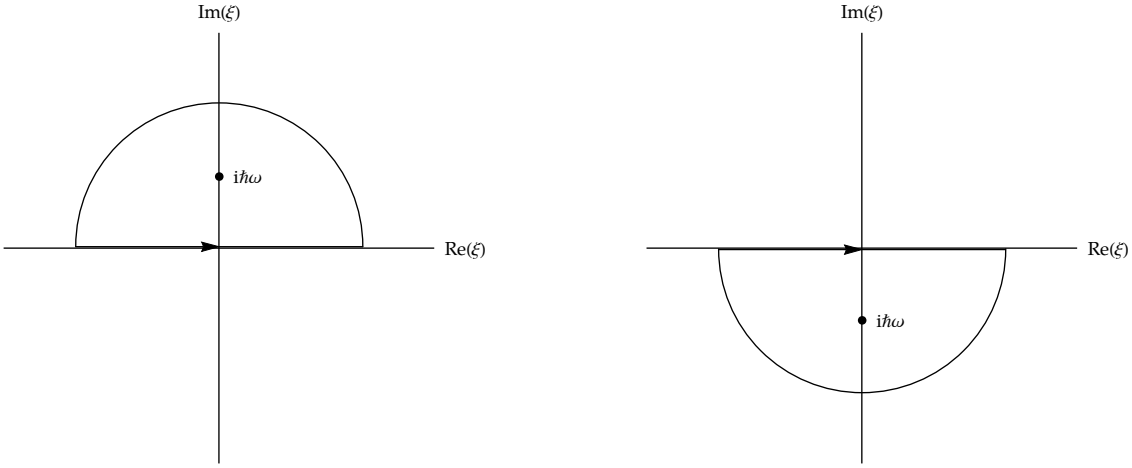

Figure 11 – Sketches of the contours of integration (straight lines joined to semi-circumferences) used to calculate Eq. (2.53).

non-zero and vice-versa. The final result is

$$\mathcal{G}_{\omega}^{(0)}(\vec{x},\vec{x}') = -\frac{\pi N(0)}{k_F z}\exp\left[i\mathrm{sgn}(\omega)k_F z - \frac{|\omega|}{v_F}z\right], \tag{2.54}$$

where $N(0) = \frac{m_e k_F}{2\pi^2\hbar^2}$ is the density of states at the Fermi surface. Following similar steps, one also finds

$$\overline{\mathcal{G}}_{\omega}^{(0)}(\vec{x},\vec{x}') = \int \frac{d^3k}{(2\pi)^3}\frac{\exp[i\vec{k}\cdot(\vec{x}-\vec{x}')]}{i\hbar\omega_n + \xi_k} = -\mathcal{G}_{-\omega}^{(0)}(\vec{x},\vec{x}'). \tag{2.55}$$

It is important to note that the characteristic length of the exponential decay of the unperturbed Green functions, $\frac{v_F}{|\omega_0|} \propto \frac{\hbar v_F}{T} = \frac{\hbar v_F}{T_c}\left[1+\tau+\mathcal{O}(\tau^2)\right]$, which is fundamental in order to get the partial-differential-equation structure of the GL and EGL theories. This is the typical length of the correlation between two electrons, in agreement to what was estimated by Pippard in Eq. (1.11), as shown in the Introduction. Also, very close to the critical temperature, the typical spatial lengths of the order parameter and vector potential are much larger than this length, once $\xi, \lambda \sim \tau^{-1/2}$.

In the presence of magnetic fields, one must include the vector potential in the Green functions and, in turn, in the self-consistency equation. The original derivation by Gor'kov incorporates the magnetic-field effects via a phase factor (also known as the Peierls substitution) in the Green function, i.e.,

$$\mathcal{G}_{B\omega}^{(0)}(\vec{x},\vec{x}') = \mathrm{e}^{i\Phi(\vec{x},\vec{x}')}\mathcal{G}_{\omega}^{(0)}(\vec{x},\vec{x}'). \tag{2.56}$$

From the equation for the normal Green function one obtains

$$\vec{\nabla}_x\Phi(\vec{x},\vec{x}') = \frac{e}{\hbar c}\vec{A}(\vec{x}), \tag{2.57}$$

which can be cast in the semi-classical approximation

$$\Phi(\vec{x},\vec{x}') \approx \frac{e}{\hbar c}\vec{A}(\vec{x}')\cdot(\vec{x}-\vec{x}'). \tag{2.58}$$

Equation (2.58) is related to the Green function approximation, the path integral derivation of the Green function in the presence of a magnetic field is presented in detail in Ref. (VAGOV et al., 2012), Appendix B.

Considering that the system is immediately below the critical temperature, the gap becomes small enough in order to keep only the first power of the order parameter in the self-consistency equation. As the characteristic lengths diverge when approaching T_c, the gap can be considered as a constant. Thus Eq. (2.47) becomes

$$\Delta = \int d^3 z K_a(\vec{z})\Delta \Rightarrow I_{a1} = \int d^3 z K_a(\vec{z}) = gN(0)\ln\left(\frac{2e^{\gamma}\hbar\omega_c}{\pi T_c}\right) = 1. \tag{2.59}$$

I_{a1} is the integral considered in detail in appendix A. The calculation of I_{a1} is performed so that to abandon the well-known ultraviolet divergence by introducing the cut-off energy $\hbar\omega_c$, which is identified with the Debye energy when the superconductivity is mediated by phonons. Also, note that the result of the integral was expanded in $\tau = 1 - T/T_c$ and the series was truncated to the leading order. This expression provides the equation for T_c in terms of the microscopic parameters of the superconductor

$$T_c = \frac{2e^{\gamma}}{\pi}\hbar\omega_c e^{-1/gN(0)} \approx 1.14\hbar\omega_c e^{-1/gN(0)} \tag{2.60}$$

and it is in agreement with the first estimate by Cooper, in Eq. (1.33).

In order to obtain the relevant gap equation, one must consider Eq. 2.47 beyond the approximation resulting in the calculation of T_c. First, one needs to incorporate the third powers of the order parameter in Eq. (2.47). Second, considering that the typical length of the spatial variations of the gap become much larger than the typical spatial length of the integral kernels, it is reasonable to expand the gap in the Taylor series around point $\vec{x}$ as (expansion in terms of the order-parameter spatial gradients)

$$\Delta(\vec{x}') \approx \Delta(\vec{x}) + (\vec{z}\cdot\vec{\nabla})\Delta(\vec{x}) + \frac{(\vec{z}\cdot\vec{\nabla})^2}{2}\Delta(\vec{x}) \tag{2.61}$$

where, recall, $\vec{z} = \vec{x} - \vec{x}'$. Finally, as the typical length of the spatial variations of the vector potential is also much larger than the characteristic lengths of the integral kernels in the self-consistency equation, we can take

$$\mathrm{e}^{i\Phi(\vec{z})} \approx 1 + i\frac{e}{\hbar c}\vec{z}\cdot\vec{A}(\vec{x}), \tag{2.62}$$

Now we have all the ingredients at our disposal in order to obtain the GL equation from Eq. (2.47).

The spherical symmetry of the Green function significantly simplifies the gradient expansion (2.61). Indeed, the first-order gradient term $(\vec{z}\cdot\vec{\nabla})$ and the crossed contributions in the second-order gradient term $z_i z_j \partial_i \partial_j$ (with $i \neq j$) do not contribute to Eq. (2.61). Thus only the gradient terms such as $z_i^2 \partial_i^2$ are to be considered and, in this case, for

each squared spatial coordinate we can use the replacement $z_i^2 \to z^2/3$. Finally, the gap expansion yields

$$\Delta(\vec{x}) = \int d^3z K_a(\vec{z})\Delta(\vec{x}) + \frac{1}{6}\int d^3z K_a(\vec{z}) z^2 \vec{D}^2\Delta(\vec{x}) + \int \left(\prod_{i=1}^{3} d^3y_i\right) K_b(\vec{x}, \vec{y}_1, \vec{y}_2, \vec{y}_3)|\Delta(\vec{x})|^2\Delta(\vec{x}). \quad (2.63)$$

where[4] $\vec{D} = \vec{\nabla} - i\frac{2e}{\hbar c}\vec{A}$, the so-called gauge invariant derivative. Note that the double charge appearing from the product of two Green functions confirms that the charge carriers in superconductors are made of two electrons. Furthermore, after canceling the term in the left hand side with the leading order term in τ resulting from the first integral on the right, one obtains the GL equation [recovering Eq. (1.17)]

$$a\tau\Delta + b|\Delta|^2\Delta - \mathcal{K}\vec{D}^2\Delta = 0, \quad (2.64)$$

where

$$a = gN(0), \qquad b = gN(0)\frac{7\zeta(3)}{8\pi^2 T_c^2}, \qquad \mathcal{K} = gN(0)\frac{7\zeta(3)}{48\pi^2 T_c^2}\hbar^2 v_F^2. \quad (2.65)$$

Notice that, for the sake of the illustration, we have adopted the superconducting system in the so-called clean limit.

In order to obtain the GL equation for the current, Gor'kov has employed the linear response to the magnetic field (GOR'KOV, 1959; FETTER; WALECKA, 2003):

$$\vec{j}(\vec{x}) = \lim_{t-t'\to 0}\lim_{\vec{x}'\to\vec{x}}\left[\frac{i\hbar e}{m}(\vec{\nabla}_x - \vec{\nabla}_{x'})\overline{\mathcal{G}}(\vec{x}, t; \vec{x}', t') - \frac{2e^2}{mc}\vec{A}(\vec{x})\overline{\mathcal{G}}(\vec{x}, t; \vec{x}', t')\right], \quad (2.66)$$

where the expression for $\overline{\mathcal{G}}$ must be accounted up to the leading correction $\delta\overline{\mathcal{G}}_\omega$ given by

$$\overline{\mathcal{G}}_\omega(\vec{x}, \vec{x}') = \overline{\mathcal{G}}^{(0)}_{B\omega}(\vec{x}, \vec{x}') + \delta\overline{\mathcal{G}}_{B\omega}(\vec{x}, \vec{x}'), \quad (2.67)$$

$$\delta\overline{\mathcal{G}}_\omega(\vec{x}, \vec{x}') = \hbar^{-2}\int d^3y d^3z \overline{\mathcal{G}}^{(0)}_{B\omega}(\vec{x}, \vec{y})\mathcal{G}^{(0)}_{B\omega}(\vec{y}, \vec{z})\overline{\mathcal{G}}^{(0)}_{B\omega}(\vec{z}, \vec{x}')\Delta^*(\vec{y})\Delta(\vec{z}). \quad (2.68)$$

The contribution of $\overline{\mathcal{G}}^{(0)}_{B\omega}(\vec{x}, \vec{x}')$ to $\vec{j}(\vec{x})$ is zero, considering the linear expansion in the Pierls factor in Eq. (2.62), i.e.

$$\lim_{\vec{x}\to\vec{x}'}\frac{ie\hbar}{m}(\vec{\nabla}_x - \vec{\nabla}_{x'})\overline{\mathcal{G}}^{(0)}_{B\omega}(\vec{x}, \vec{x}') = \frac{2e^2}{mc}\vec{A}(\vec{x})\overline{\mathcal{G}}^{(0)}_{B\omega}(\vec{x}, \vec{x}). \quad (2.69)$$

[4] To be clear, the expression for the kernels K_a and K_b in this equation are in terms of the Greens functions in the absence of magnetic field, once its effect was accounted with the $e^{i\Phi}$ term, which produced the gauge invariant derivative.

So the current is reduced to

$$\begin{aligned}\vec{j}(\vec{x}) &= \frac{ieT}{m}\sum_n\left[(\vec{\nabla}_x-\vec{\nabla}_{x'})\delta\overline{\mathcal{G}}^{(0)}_\omega(\vec{x},\vec{x}')\right]_{\vec{x}'\to\vec{x}} - \frac{2e^2T}{mc\hbar}\vec{A}(\vec{x})\sum_n\delta\overline{\mathcal{G}}^{(0)}_\omega(\vec{x},\vec{x}')\\ &= \frac{ieT}{mi\hbar^2}\sum_n\int d^3y d^3z\Delta(\vec{y})\Delta^*(\vec{z})e^{i\Phi(\vec{y},\vec{z})}\mathcal{G}^{(0)}_\omega(\vec{y},\vec{z})\left\{e^{i\Phi(\vec{z},\vec{x}')}\mathcal{G}^{(0)}_{-\omega}(\vec{z},\vec{x}')\vec{\nabla}_x\left[e^{i\Phi(\vec{y},\vec{x})}\mathcal{G}^{(0)}_{-\omega}(\vec{y},\vec{x})\right]\right.\\ &\quad\left.-e^{i\Phi(\vec{y},\vec{x})}\mathcal{G}^{(0)}_{-\omega}(\vec{y},\vec{x})\vec{\nabla}_{x'}\left[e^{i\Phi(\vec{x}',\vec{z})}\mathcal{G}^{(0)}_{-\omega}(\vec{x}',\vec{z})\right]\right\} - \frac{2e^2T}{mc\hbar}\vec{A}(\vec{x})\sum_n\delta\overline{\mathcal{G}}^{(0)}_{B,\omega}(\vec{x},\vec{x}').\end{aligned} \tag{2.70}$$

Note that this expression is written in terms of $\mathcal{G}^{(0)}_\omega$ due to Eq. (2.55). Also, due to the limit $t-t'\to 0$, the exponential factors from the Fourier transforms. By using Eq. (2.62), can further simplify the above relation as

$$\begin{aligned}\vec{j}(\vec{x}) &= \frac{eT}{mi\hbar^2}\sum_n\int d^3y d^3z\mathcal{G}^{(0)}_\omega(\vec{y},\vec{z})\left[\mathcal{G}^{(0)}_\omega(x,\vec{z})\vec{\nabla}_x\mathcal{G}^{(0)}_\omega(\vec{y},\vec{x})-\mathcal{G}^{(0)}_\omega(\vec{y},\vec{x})\vec{\nabla}_x\mathcal{G}^{(0)}_\omega(\vec{x},\vec{z})\right]\\ &\quad\times\left[|\Delta(\vec{x})|^2-\frac{2ie}{\hbar c}|\Delta(\vec{x})|^2\vec{A}(\vec{x})\cdot(\vec{z}-\vec{y})+\Delta^*(\vec{x})(\vec{y}-\vec{x})\cdot\vec{\nabla}\Delta(\vec{x})+\Delta(\vec{x})(\vec{z}-\vec{x})\cdot\vec{\nabla}\Delta^*(\vec{x})\right].\end{aligned} \tag{2.71}$$

In the presence of the spherical symmetry one finally gets

$$\begin{aligned}\vec{j}(\vec{x}) &= \frac{eT}{mi\hbar^2}\sum_n\int d^3y d^3z\mathcal{G}^{(0)}_\omega(\vec{y},\vec{z})\left[\mathcal{G}^{(0)}_\omega(\vec{x},\vec{z})\vec{\nabla}_x\mathcal{G}^{(0)}_\omega(\vec{y},\vec{x})-\mathcal{G}^{(0)}_\omega(\vec{y},\vec{x})\vec{\nabla}_x\mathcal{G}^{(0)}_\omega(\vec{x},\vec{z})\right]\\ &\quad\times\left[-\frac{2ie}{\hbar c}|\Delta(\vec{x})|^2\vec{A}(\vec{x})\cdot(\vec{z}-\vec{y})+\Delta^*(\vec{x})\vec{y}\cdot\vec{\nabla}\Delta(\vec{x})+\Delta(\vec{x})\vec{z}\cdot\vec{\nabla}\Delta^*(\vec{x})\right]=\\ &= gN(0)\frac{7\zeta(3)\hbar^2v_F^2}{16\pi^2T_c^2}\left[\Delta^*(\vec{x})\vec{D}\Delta(\vec{x})-\Delta(\vec{x})\vec{D}^*\Delta^*(\vec{x})\right].\end{aligned} \tag{2.72}$$

2.2 The Need for Generalizations of the BCS and GL Theories

In spite of the success of the BCS and GL theories in describing most phenomena in superconductors, eventually, some deviations started to be reported in experimental papers. For example, Ref. (BOORSE, 1959) is one of the first reports compiling experimental results from many groups and comparing them with the BCS predictions. The author suggested that the discrepancies were due to anisotropy of the superconducting gap and the BCS theory should be generalized, once there were no anisotropic effects in the initial formulation. The anisotropy was readily detected by ultrasonic attenuation experiments, where it was possible to have access to specific regions (in different directions) of the Fermi surface (remember that this surface was initially treated as spherically symmetric) (MORSE; OLSEN; GAVENDA, 1959). Even though the BCS theory seemed to need a generalization, at that time it was known the anisotropic version of the

GL theory, derived by Ginzburg in 1952 (before the BCS theory), which in principle was derived to explain these phenomena (for example, anisotropy of the critical field, H_{c2}). But only after the generalization by Gor'kov and Melik-Barkhudarov (GOR'KOV; MELIK-BARKHUDAROV, 1964) of the derivation of the GL theory from the microscopic theory for systems with anisotropic Fermi surfaces it was possible to understand how this anisotropy should be considered in the microscopically consistent manner. In 1964, Tilley et al. (TILLEY; GURP; BERGHOUT, 1964) proposed that the anisotropy in the critical field, which they had found in Nb samples, would substantiate the anisotropic GL theory derived by Gor'kov. However, in 1967 Hohenberg and Wherthamer (HOHENBERG; WERTHAMER, 1967) has noticed that from the microscopic theory one can prove that the mass tensor appearing in the GL theory for materials with cubic structure such as Nb should be proportional to the identity matrix and therefore one should go to higher order contributions in the gap expansion, increasing non-local effects in the results. In other words, in case of such simple structures one needed to extend the GL theory in order to explain the anisotropy in the experimental results.

Another important issue related to the applicability of the BCS and GL approaches, dates back to 1959 when the group of M. Tinkham performed measurements of far infrared photon absorption in superconductors in order to measure the superconducting energy gap. Instead of finding a smooth curve followed by an abrupt drop of the number of reflected photons with energies around the gap, they found a non-trivial structure (RICHARDS; TINKHAM, 1960; GINSBERG; RICHARDS; TINKHAM, 1959). Even though the authors suggested that this might be also due to anisotropy, their results motivated theorists from another group to provide another view on this subject. Suhl et al. (SUHL; MATTHIAS; WALKER, 1959) proposed that this behavior might be due to the interaction of multiple condensates in a single compound, i.e., multiple gaps, which could be a reason for the non-trivial structure of the absorption curve with distinguished peaks. They justified the appearance of multiple condensates in a single material with the formation of different bands of conducting electrons from different atomic orbitals, which is the case of the transition metals (orbitals s and d and possibly s and p). Therefore, in their seminal paper, Suhl et al. proposed a generalization of the BCS Hamiltonian to the case of an arbitrary number, N, of the superconducting condensates (investigated in a more detail the case with $N = 2$):

$$\mathcal{H} = \sum_{i=1}^{N} \sum_{\vec{k}\sigma} \epsilon_{i,k} a^{\dagger}_{i,k\sigma} a_{i,k\sigma} - \frac{1}{2} \sum_{i,j=1}^{N} V_{ij} \sum_{\vec{k}\vec{k}'} a_{i,k\uparrow} a^{\dagger}_{i,-k\downarrow} a^{\dagger}_{j,-k'\downarrow} a_{j,k'\uparrow}, \tag{2.73}$$

where ϵ_{ik} is the single-electron dispersion corresponding to band i and V_{ij} is the averaged interaction energy between electrons in band i and electrons in band j.

The subsequent series of articles, that is discussed below in this section, have resulted in the formalism which is the basis of the results of the present thesis. The

discovery of a superconductor with the relatively high critical temperature $T_c = 39$K, i.e., magnesium diborade (NAGAMATSU et al., 2001), started the flourishing of theoretical and experimental studies about non-cuprates with high T_c at an impressive rate (for a review about the articles following the next year after the discovery of MgB_2, see Ref. (BUZEA; YAMASHITA, 2001)). Furthermore, MgB_2 has been shown to present more than one superconducting gap (KARAPETROV et al., 2001; BOUQUET et al., 2001a; GIUBILEO et al., 2001; LIU; MAZIN; KORTUS, 2001; IAVARONE et al., 2002). An extensive study of its microscopic properties (BUD'KO et al., 2001; GOLUBOV et al., 2002; MAZIN; ANTROPOV, 2003) appeared soon after the discovery of its multiband nature, together with some proposals for generalizing the GL theory for this case (BOUQUET et al., 2001b; ASKERZADE; GENCER; GüçLü, 2002; KONSIN; SORKIN, 2004), mostly based on the assumption of a multi-component order parameter. Eventually, many surprising effects (some of them could not be explained through the traditional physical picture) started to be reported, such as single-vortices presenting absence of rotational symmetry (PECHENIK et al., 2002), long-range attraction between vortices (BABAEV; SPEIGHT, 2005), vortex clusters (MOSHCHALKOV et al., 2009). In 2011, Kogan and Shmalian criticized (KOGAN; SCHMALIAN, 2011) the so-called multi-component GL models e.g. Ref's. (ASKERZADE; GENCER; GüçLü, 2002; BABAEV; SPEIGHT, 2005), by showing that the coupling terms used were inconsistent with the microscopic theory and produced equal gap profiles in the scope of the GL theory. Unfortunately, the microscopic theory presents many technical difficulties in order to effectively investigate so complicated gap profiles such as vortex lattices. This issue of obtaining a simpler theory which could produce an effective picture about these new phenomena reported in multi-band superconductors contributed to the development of an extension of the GL theory, discussed in the next section.

2.3 The Extended Ginzburg-Landau Formalism

By using the Suhl-Mathias-Walker Hamiltonian (SUHL; MATTHIAS; WALKER, 1959) given by Eq. 2.73, the leading corrections to the GL theory have been derived in Ref. (SHANENKO et al., 2011; VAGOV et al., 2012) in order to be able to capture the difference between the spatial profiles of the band-dependent gaps in multi-band superconductors. Let us consider the Hamiltonian for a system with N overlapping bands in terms of the field operators, i.e.,

$$\mathcal{H} = \sum_{i=1}^{N} \int \mathrm{d}^3x \left[\sum_{\sigma} \psi^{\dagger}_{i\sigma}(\vec{x}) T_i(\vec{x}) \psi_{i\sigma}(\vec{x}) + \psi^{\dagger}_{i\uparrow}(\vec{x}) \psi^{\dagger}_{i\downarrow}(\vec{x}) \Delta_i(\vec{x}) + h.c. \right] \tag{2.74}$$

where $\mathcal{T}_x$ is the band-dependent single-electron energy operator (it is band-dependent, $i = 1, 2, 3...N$, due to the effective electronic mass m_i and the chemical potential measured

from the edge of the band μ_i)

$$\mathcal{T}_x \equiv -\frac{\hbar^2}{2m_i}\left(\vec{\nabla} - i\frac{e}{\hbar c}\vec{A}\right)^2 - \mu_i, \tag{2.75}$$

and the superconducting band-gap $\Delta_i(\vec{x})$ is defined as

$$\Delta_i(\vec{x}) = \sum_j g_{ij}\left\langle \psi_{j\uparrow}(\vec{x})\psi_{j\downarrow}(\vec{x})\right\rangle \tag{2.76}$$

As will be seen below, in this case, the band-gap function $\Delta_i(\vec{x})$ is not the true Landau order parameter of the system. Using these definitions, one can follow the Gor'kov recipe described previously. The equations of motion for the field operators in the Heisenberg picture are given by

$$-\hbar\partial_{\mathrm{t}}\begin{pmatrix} \psi_{i\uparrow}(\vec{x},\mathrm{t}) \\ \overline{\psi}_{i\downarrow}(\vec{x},\mathrm{t}) \end{pmatrix} = \begin{pmatrix} T_{ix} & \Delta_i(\vec{x}) \\ \Delta_i(\vec{x})^* & -T^*_{ix} \end{pmatrix}\begin{pmatrix} \psi_{i\uparrow}(\vec{x},\mathrm{t}) \\ \overline{\psi}_{i\downarrow}(\vec{x},\mathrm{t}) \end{pmatrix}, \tag{2.77}$$

Introducing the band-dependent Green functions

$$\mathcal{G}_i(\vec{x}\mathrm{t},\vec{x}'\mathrm{t}') = -\frac{1}{\hbar}\left\langle T_{\mathrm{t}}\psi_{i\uparrow}(\vec{x},\mathrm{t})\overline{\psi}_{i\uparrow}(\vec{x}',\mathrm{t}')\right\rangle, \tag{2.78}$$

$$\overline{\mathcal{F}}_i(\vec{x}\mathrm{t},\vec{x}'\mathrm{t}') = -\frac{1}{\hbar}\left\langle T_{\mathrm{t}}\overline{\psi}_{i\downarrow}(\vec{x},\mathrm{t})\overline{\psi}_{i\uparrow}(\vec{x}',\mathrm{t}')\right\rangle, \tag{2.79}$$

$$\overline{\mathcal{G}}_i(\vec{x}\mathrm{t},\vec{x}'\mathrm{t}') = -\frac{1}{\hbar}\left\langle T_{\mathrm{t}}\overline{\psi}_{i\downarrow}(\vec{x},\mathrm{t})\psi_{i\downarrow}(\vec{x}',\mathrm{t}')\right\rangle, \tag{2.80}$$

$$\mathcal{F}_i(\vec{x}\mathrm{t},\vec{x}'\mathrm{t}') = -\frac{1}{\hbar}\left\langle T_{\mathrm{t}}\psi_{i\downarrow}(\vec{x},\mathrm{t})\psi_{i\downarrow}(\vec{x}',\mathrm{t}')\right\rangle, \tag{2.81}$$

one can obtain their equations of motion (for the Fourier transforms represented as operators in the Hilbert space and in matrix form)

$$\check{G}_{i\omega} = \check{G}^{(0)}_{i\omega} + \check{G}^{(0)}_{i\omega}\check{\Delta}_i\check{G}_{i\omega}. \tag{2.82}$$

2.3.1 Systems in the absence of magnetic fields

In the absence of magnetic fields, the unperturbed Green functions for each band i are

$$\mathcal{G}^{(0)}_{i\omega}(\vec{x},\vec{x}') = \int \frac{d^3k}{(2\pi)^3}\frac{\exp[i\vec{k}\cdot(\vec{x}-\vec{x}')]}{i\hbar\omega_n - \xi_{ik}} = -\overline{\mathcal{G}}^{(0)}_{i,-\omega}(\vec{x},\vec{x}') \tag{2.83}$$

$$\mathcal{F}^{(0)}_{i\omega}(\vec{x},\vec{x}') = \overline{\mathcal{F}}^{(0)}_{i\omega}(\vec{x},\vec{x}') = 0 \tag{2.84}$$

where $\xi_{i\omega}$ is the band-dependent single-particle dispersion. Then, by using the relation

$$-gT\lim_{\vec{x}'\to\vec{x}}\lim_{\eta\to 0^+}\sum_\omega \exp(-i\omega\eta)\mathcal{F}_{i\omega}(\vec{x},\vec{x}') = \left\langle \psi_{i\uparrow}(\vec{x})\psi_{i\downarrow}(\vec{x})\right\rangle, \tag{2.85}$$

the expansions for the anomalous Green functions in coordinate space become

$$\langle\psi_{i\uparrow}(\vec{x})\psi_{i\downarrow}(\vec{x})\rangle = \int \mathrm{d}\vec{y}K_{ia}(\vec{x},\vec{y})\Delta_i(\vec{y}) + \int\prod_{j=1}^{3}\mathrm{d}\vec{y}_j K_{ib}\left(\vec{x},\{\vec{y}\}_3\right)\Delta_i(\vec{y}_1)\Delta_i^*(\vec{y}_2)\Delta_i(\vec{y}_3)+$$
$$+\int\prod_{j=1}^{5}\mathrm{d}\vec{y}_j K_{ic}\left(\vec{x},\{\vec{y}\}_5\right)\Delta_i(\vec{y}_1)\Delta_i^*(\vec{y}_2)\Delta_i(\vec{y}_3)\Delta_i^*(\vec{y}_4)\Delta_i(\vec{y}_5)+\ldots \tag{2.86}$$

where the band-dependent kernels read

$$K_{ia}(\vec{x},\vec{y}) = -gT\lim_{\eta\to 0^+}\sum_{\omega}\exp(-i\omega\eta)\mathcal{G}^{(0)}_{i\omega}(\vec{x},\vec{y})\overline{\mathcal{G}}^{(0)}_{i\omega}(\vec{y},\vec{x}), \tag{2.87}$$

$$K_{ib}\left(\vec{x},\{\vec{y}\}_3\right) = -gT\lim_{\eta\to 0^+}\sum_{\omega}\exp(-i\omega\eta)\mathcal{G}^{(0)}_{i\omega}(\vec{x},\vec{y}_1)\overline{\mathcal{G}}^{(0)}_{i\omega}(\vec{y}_1,\vec{y}_2)\ldots\overline{\mathcal{G}}^{(0)}_{i\omega}(\vec{y}_3,\vec{x}), \tag{2.88}$$

$$K_{ic}\left(\vec{x},\{\vec{y}\}_5\right) = -gT\lim_{\eta\to 0^+}\sum_{\omega}\exp(-i\omega\eta)\mathcal{G}^{(0)}_{i\omega}(\vec{x},\vec{y}_1)\overline{\mathcal{G}}^{(0)}_{i\omega}(\vec{y}_1,\vec{y}_2)\ldots\mathcal{G}^{(0)}_{i\omega}(\vec{y}_4,\vec{y}_5)\overline{\mathcal{G}}^{(0)}_{i\omega}(\vec{y}_5,\vec{x}). \tag{2.89}$$

The series in Eq. (2.86) is truncated so that to include the fifth power of the corresponding superconducting gap function, which makes it possible to get the next-to-leading order contributions to the band-dependent gaps. Also, the gaps inside integrals are expanded in the Taylor series (again, we define $\vec{z} = \vec{y} - \vec{x}$)

$$\Delta_i(\vec{y}) = \Delta_i(\vec{z}+\vec{x}) = \sum_{n=0}^{\infty}\frac{\left(\vec{z}\cdot\vec{\nabla}\right)^n}{n!}\Delta_i(\vec{x}). \tag{2.90}$$

Finally the relevant quantities are expanded in small deviation from the critical temperature $\tau = 1 - T/T_c$ such as:

$$\Delta_i(\vec{y}) = \tau^{1/2}\sum_{n=0}^{\infty}\tau^n\Delta_i^{(n)}(\vec{x}), \tag{2.91}$$

in order to correctly select the terms of the same order of magnitude in the self-consistency equation. Furthermore, as one has $\xi \sim \tau^{-1/2}$, then any spatial gradient is proportional to $\tau^{1/2}$, i.e., $\nabla \propto \tau^{1/2}$. The self-consistency (matrix) equation taken in order $\tau^{1/2}$ gives the equation for T_c; when selecting the terms of order $\tau^{3/2}$, one recovers the GL theory; and finally, selecting the terms of order $\tau^{5/2}$, one obtains the leading correction to the GL theory. The GL theory taken together with its leading correction is the EGL formalism. Based on these considerations, it is clear that one should consider the Taylor expansion of the gaps, i.e. Eq. (2.90), up to the fourth order derivatives for the gaps inside the integrals involving K_{ia}, up to the second order inside the integrals involving K_{ib} and just the leading term inside the integral involving K_{ic}. Due to the spherical symmetry

of the kernels, some odd-order terms of these expansions can be neglected, which is shown in detail in Appendix A and, after performing the relevant integrations, the matrix self-consistency equation (before expanding in τ) becomes

$$\sum_j \gamma_{ij}\Delta_j = a_{i1}\Delta_i + a_{i2}\nabla^2\Delta_i + a_{i3}\nabla^2(\nabla^2\Delta_i) - b_{i1}\Delta_i|\Delta_i|^2 \\ - b_{i2}\left[2\Delta_i|\vec{\nabla}\Delta_i|^2 + 3\Delta_i^*(\vec{\nabla}\Delta_i)^2\Delta_i^2\nabla^2\Delta_i^* + 4|\Delta_i|^2\nabla^2\Delta_i\right] + c_i|\Delta_i|^4\Delta_i \quad (2.92)$$

where

$$a_{i1} = N_i(0)\ln\left(\frac{2e^\Gamma\hbar\omega_c}{\pi T}\right), \qquad b_{i1} = N_i(0)\frac{7\zeta(3)}{8\pi^2T^2}, \quad (2.93)$$

$$a_{i2} = \frac{b_{i1}}{6}\hbar^2v_i^2, \qquad b_{i2} = N_i(0)\frac{\hbar^2v_F^2}{9}\frac{93\zeta(5)}{128\pi^4T^4}, \quad (2.94)$$

$$a_{i3} = N_i(0)\frac{\hbar^4v_i^4}{30}\frac{93\zeta(5)}{128\pi^4T^4}, \qquad c_{i1} = N_i(0)\frac{93\zeta(5)}{128\pi^4T^4}. \quad (2.95)$$

and $N_i(0)$ is the density of states at the Fermi level at band i.

In order to get the correct mathematical structures, it is convenient to rescale the band-dependent gaps and the spatial coordinates as

$$\tau^{1/2}\Delta_i^{(n)} \to \Delta_i^{(n)} \quad (2.96)$$

$$\vec{x} \to \tau^{-1/2}\vec{x}. \quad (2.97)$$

Finally, after matching the terms of the same order in τ and invoking the τ-expansion of the relevant coefficients as

$$a_{i1} = A_i - a_i\left[\tau + \frac{\tau^2}{2} + O(\tau^3)\right], \ A_i = N_i(0)\ln\left(\frac{2e^\Gamma\hbar\omega_c}{\pi T_c}\right), \ a_i = -N_i(0) \quad (2.98)$$

$$a_{i2} = \mathcal{K}_i[1 + 2\tau + O(\tau^2)], \ \mathcal{K}_i = \frac{b_i}{6}\hbar^2v_i^2 \quad (2.99)$$

$$a_{i3} = \mathcal{Q}_i[1 + O(\tau)], \quad \mathcal{Q}_i = N_i(0)\frac{\hbar^4v_i^4}{30}\frac{93\zeta(5)}{128\pi^4T_c^4} \quad (2.100)$$

$$b_{i1} = b_i[1 + 2\tau + O(\tau^2)], \quad b_i = N_i(0)\frac{7\zeta(3)}{8\pi^2T_c^2} \quad (2.101)$$

$$b_{i2} = \mathcal{L}_i[1 + O(\tau)], \quad \mathcal{L}_i = N_i(0)\frac{\hbar^2v_i^2}{9}\frac{93\zeta(5)}{128\pi^4T_c^4} \quad (2.102)$$

$$c_{i1} = c_i[1 + O(\tau)], \quad c_i = N_i(0)\frac{93\zeta(5)}{128\pi^4T_c^4}, \quad (2.103)$$

one obtains the following set of coupled equations involving the contributions of orders

$\tau^{1/2}$, $\tau^{3/2}$ and $\tau^{5/2}$

$$\sum_j L_{ij}\Delta_j^{(0)} = 0, \tag{2.104}$$

$$\sum_j L_{ij}\Delta_j^{(1)} = -a_i\Delta_i^{(0)} - b_i|\Delta_i^{(0)}|^2\Delta_i^{(0)} + \mathcal{K}_i\vec{\nabla}^2\Delta_i^{(0)}, \tag{2.105}$$

$$\sum_j L_{ij}\Delta_j^{(2)} = -a_i\Delta_i^{(1)} - b_i\left(2\Delta_i^{(1)}|\Delta_i^{(0)}|^2 + \Delta_i^{*(1)}\Delta_i^{(0)2}\right) + \mathcal{K}_i\vec{\nabla}\Delta_i^{(1)} - F_i\left(\Delta_i^{(0)}\right), \tag{2.106}$$

respectively. Here[5]

$$L_{ij} = \gamma_{ij} - \mathcal{A}_i\delta_{ij} \tag{2.107}$$

and

$$\begin{aligned} F_i\left(\Delta_i^{(0)}\right) = &-\frac{a_i}{2}\Delta_i^{(0)} + 2\mathcal{K}_i\vec{\nabla}^2\Delta_i^{(0)} + \mathcal{Q}_i\vec{\nabla}^2(\vec{\nabla}^2\Delta_i^{(0)}) - 2b_i|\Delta_i^{(0)}|^2\Delta_i^{(0)} \\ &- \mathcal{L}_i\left[2\Delta_i^{(0)}|\vec{\nabla}\Delta_i^{(0)}|^2 + 3\Delta_i^{*(0)}(\vec{\nabla}\Delta_i^{(0)})^2 + \Delta_i^{2(0)}\vec{\nabla}^2\Delta_i^{*(0)} + 4|\Delta_i^{(0)}|^2\vec{\nabla}^2\Delta_i^{(0)}\right] \\ &+ c_i|\Delta_i^{(0)}|^4\Delta_i^{(0)}. \end{aligned} \tag{2.108}$$

It is possible to prove that the spatial profiles of the band superconducting condensates in multi-band superconductors are proportional to one another in the leading-order in τ, i.e., within the GL theory. For example, in the two-band case Eq. (2.104) yields

$$\det(L) = (\gamma_{11} - \mathcal{A}_1)(\gamma_{22} - \mathcal{A}_2) - \gamma_{12}^2 = 0 \tag{2.109}$$

in the case of a non-trivial solution for $\vec{\Delta}^{(0)}$. This gives the equation for T_c. Given the set of microscopic parameters ω_c, N_i and g_{ij}, it is possible to get

$$\begin{aligned} \frac{T_c}{\hbar\omega_c} = \frac{2e^\gamma}{\pi}\exp\Bigg\{ &-\frac{g_{11}N_1(0) + g_{22}N_2(0)}{2N_1(0)N_2(0)\left(g_{11}g_{22} - g_{12}^2\right)} \\ &\times\left[1 - \sqrt{1 - 2N_1(0)N_2(0)\frac{g_{11}g_{22} - g_{12}^2}{g_{11}N_1(0) + g_{22}N_2(0)}}\right]\Bigg\}, \end{aligned} \tag{2.110}$$

exactly the expression firstly derived by Suhl et al. (SUHL; MATTHIAS; WALKER, 1959) from Eq. (2.73) via the Bogoliubov-Valatin transformation. The matrix L has two eigenvalues (λ_1 and λ_2) and the two corresponding eigenvectors ($\vec{\eta}_1$ and $\vec{\eta}_2$). At least one of these eigenvalues must be zero, say λ_1, in order to assure Eq. (2.109). Therefore, the gap vector must be proportional to the eigenvector associated with the zero eigenvalue, i.e.,

$$\vec{\Delta}^{(0)} = \Psi(\vec{x})\vec{\eta}_1. \tag{2.111}$$

[5] Notice that δ_{ij} is the Kronecker symbol. Note that L_{ij} is a symmetric matrix, once g_{ij} is symmetric and so is $\mathcal{A}_i\delta_{ij}$.

According to this expression, both gaps must have the same spatial profile up to a proportionality factor given by the entries of $\vec{\eta}_1$ (SHANENKO et al., 2011), in agreement with the results by Kogan and Schmalian (KOGAN; SCHMALIAN, 2011). The function $\Psi(\vec{x})$ can be considered as the *true Landau order parameter* of the system, which is the reason why the vector $\vec{\Delta}$ is being called gap vector, instead of the order parameter vector.

The next step is to substitute this expression for $\vec{\Delta}^{(0)}$ in Eq. (2.105), and then the leading corrections to the gaps can be obtained by calculating $\vec{\Delta}^{(1)}$ from Eq. (2.106). The procedure of analytically calculating this leading correction within the EGL formalism will be considered in chapter 4.

2.3.2 Systems in the presence of magnetic field: superconductivity between standard types

Although the Abrikosov's division between types I and II of superconductivity was very important in order to stablish a basic picture to interpret very complex phenomena in superconductors, the state of the art publications in the subject show the need of a wider way of approach. It is long known that the order parameter in type-I materials with $\kappa \approx 1/\sqrt{2}$ may present stable phases in which magnetic field penetrating the sample in domains much wider than the London penetration length (KRÄGELOH, 1969; KRÄGELOH, ; ESSMANN, 1971; PROZOROV, 2007). In such cases the system may present a plethora of patterns, not only the Meissner and Abrikosov's lattice phases and the magnetic response exhibits a discontinuity at the first critical field, as shown in Fig. 12. The EGL formalism has also elucidated the situation of the classification of

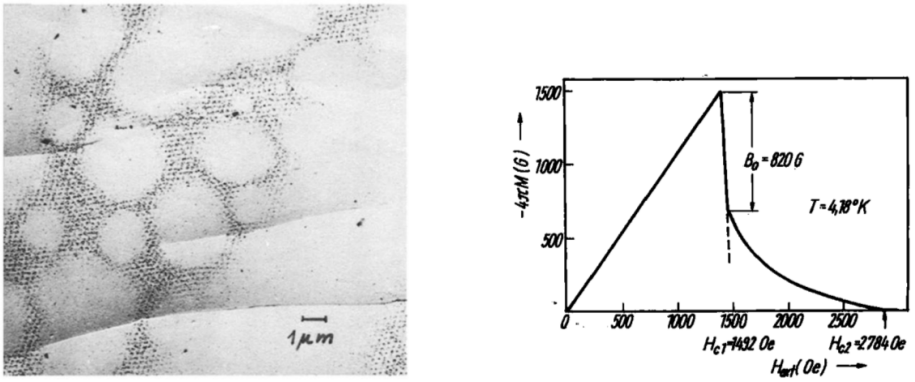

Figure 12 – On the left, the magnetic field profiles from a Pb-1.89 wt.% Tl sample in a field of 329 Oe at 1.25K from Ref. (KRÄGELOH, 1969). On the right, the magnetization curve as function of the external field for Niobium single-crystal at 4.18K from Ref. (KUMPF, 1971).

the superconductivity types in single- and multi-band superconducting systems. In 2016, Vagov et al (VAGOV et al., 2016). considered the case of single- and two-band

superconductors under the effect of applied magnetic fields in the vicinity of $\kappa \approx 1/\sqrt{2}$. This work has brought another physical picture for the unusual phenomena observed in multi-band compounds by considering the Bogomolnyi self-duality into the EGL equations in order to describe the so-called *intertype* domain between the standard types I and II in the (κ, T) plane which can be significantly expanded in two-band (and more generally, in multi-band) superconductors. One should note that the intertype domain cannot be captured by the standard GL theory as non-local effects beyond the GL domain should be taken into account.

In the presence of a magnetic field, the vector potential and the magnetic field must also be expanded in powers of τ similarly to the gaps, i.e.,

$$\vec{\Delta} = \tau^{1/2}\left(\vec{\Delta}^{(0)} + \tau\vec{\Delta}^{(1)} + ...\right) \tag{2.112}$$

$$\vec{A} = \tau^{1/2}\left(\vec{\mathfrak{A}} + \tau\vec{\mathfrak{a}} + ...\right) \tag{2.113}$$

$$\vec{B} = \tau\left(\vec{\mathfrak{B}} + \tau\vec{\mathfrak{b}} + ...\right) \tag{2.114}$$

Invoking this expansion, the authors of Ref. (VAGOV et al., 2016) derived the equations for the gaps and magnetic field (in the leading and next-to-leading orders in τ) by minimizing the free energy density ($\mathfrak{F}_s = \int \mathfrak{f}_s d^3x$) constructed by the standard methods of quantum field theory (VAGOV et al., 2016; POPOV, 1987). Following the analysis of Ref. (VAGOV et al., 2016), after matching the terms of the same order in τ one finds that the EGL free energy density becomes

$$\mathfrak{f}_s = \tau^2\left(\tau^{-1}\mathfrak{f}^{(-1)} + \mathfrak{f}^{(0)} + \tau\mathfrak{f}^{(0)} + ...\right), \tag{2.115}$$

and the terms of this expansion are given by[6]

$$\mathfrak{f}^{(-1)} = \left\langle\vec{\Delta}^{(0)}|L|\vec{\Delta}^{(0)}\right\rangle, \tag{2.116}$$

$$\mathfrak{f}^{(0)} = \frac{\vec{\mathfrak{B}}^2}{8\pi} + \left(\left\langle\vec{\Delta}^{(0)}|L|\vec{\Delta}^{(1)}\right\rangle + c.c.\right) + \sum_n\left[a_n|\Delta_n^{(0)}|^2 + \frac{b_n}{2}|\Delta^{(0)}|^4 + \mathcal{K}_n|\mathfrak{D}\Delta_n^{(0)}|^2\right], \tag{2.117}$$

$$\mathfrak{f}^{(1)} = \frac{\vec{\mathfrak{B}}\cdot\vec{\mathfrak{b}}}{2\pi} + \left(\left\langle\vec{\Delta}^{(0)}|L|\vec{\Delta}^{(2)}\right\rangle + c.c.\right) + \left\langle\vec{\Delta}^{(1)}|L|\vec{\Delta}^{(1)}\right\rangle + \sum_n\left(\mathfrak{f}_{n,1}^{(1)} + \mathfrak{f}_{n,2}^{(1)}\right), \tag{2.118}$$

$$\begin{aligned}\mathfrak{f}_{n,1}^{(1)} = {} & \frac{a_n}{2}|\Delta_n^{(0)}|^2 + 2\mathcal{K}_n|\vec{\mathfrak{D}}\Delta_n^{(0)}|^2 + \frac{b_n}{36}\frac{e^2\hbar^2}{m^2c^2}\vec{\mathfrak{B}}^2|\Delta_n^{(0)}|^2 + b_n|\Delta_n^{(0)}|^4 \\ & - Q_n\left\{|\vec{\mathfrak{D}}^2\Delta_n^{(0)}|^2 + \frac{1}{3}(\vec{i}_n\cdot\vec{\nabla}\times\vec{\mathfrak{B}}) + \frac{4e^2}{\hbar^2c^2}\vec{\mathfrak{B}}^2|\Delta_n^{(0)}|^2\right\} \\ & - \frac{\mathcal{L}_n}{2}\left\{8|\Delta_n^{(0)}|^2|\mathfrak{D}\Delta_n^{(0)}|^2 + \left[\Delta_n^{(0)2}\left(\mathfrak{D}^*\Delta_n^{*(0)}\right)^2 + c.c.\right]\right\},\end{aligned} \tag{2.119}$$

$$\mathfrak{f}_{n,2}^{(1)} = \left(a_n + b_n|\Delta_n^{(0)}|^2\right)\left(\Delta_n^{*(0)}\Delta_n^{(1)} + c.c.\right) + \mathcal{K}_n\left[\left(\vec{\mathfrak{D}}\Delta_n^{(0)}\cdot\vec{\mathfrak{D}}^*\Delta_n^{*(1)} + c.c.\right) - (\vec{\mathfrak{a}}\cdot\vec{i}_n)\right] \tag{2.120}$$

[6] Here, $\langle ...\rangle$ denotes the scalar (inner) product in the band space.

$\vec{\mathfrak{D}} = \vec{\nabla} - i\frac{2e}{\hbar c}\vec{\mathfrak{A}}$ is the gauge-invariant derivative with the leading order contribution of the vector potential and $\vec{i}_n = i\frac{2e}{\hbar c}\left(\Delta_n^{(0)}\mathfrak{D}^*\vec{\Delta}_n^{*(0)} - \Delta_n^{*(0)}\mathfrak{D}\vec{\Delta}_n^{(0)}\right)$ is the supercurrent density contribution of band n. From this functional, it is possible to derive the Gibbs free energy that is used in the criterion of the interchange between types I and II. For illustration, let us here consider the switching between types I and II in the isotropic single-band case, which can be the basis for our further consideration in chapter 3.

By invoking the following Legendre transformation[7]

$$\mathfrak{G}_s = \int \mathfrak{g}_s d^3x, \qquad \mathfrak{g}_s = \mathfrak{f}_s + \frac{H_c^2}{8\pi} - \frac{H_c B}{4\pi}, \tag{2.121}$$

one is able to calculate the Gibbs free energy functional, taken at the thermodynamic critical field and measured from the normal state Gibbs free energy, as a series in τ with the coefficients dependent on κ. Then, the nucleation of a non-uniform condensate/field configuration can be investigated on the basis of the criterion $\mathfrak{G}_s(\kappa, T) = 0$. Using this criterion for various non-uniform configurations (e.g., for the single vortex solution, the domain wall between the normal and superconducting state, etc.), it is possible to find the corresponding value of κ above which a non-uniform pattern (representing the well-known mixed state) becomes stable. For instance, considering the dimensionless units

$$\vec{x} \to \lambda_L\sqrt{2}\vec{x}, \quad \vec{\mathfrak{A}} \to \frac{H_c^{(0)}\lambda_L}{\kappa}\vec{\mathfrak{A}}, \quad \vec{\mathfrak{B}} \to \frac{H_c^{(0)}}{\sqrt{2}\kappa}\vec{\mathfrak{B}}, \quad \Delta^{(0)} \to \Psi_\infty\Psi, \tag{2.122}$$

$$\vec{i} \to \frac{H_c^{(0)}}{4\pi\mathcal{K}\lambda_L}\vec{i}, \quad \mathfrak{f}_s \to \frac{H_c^{(0)2}}{4\pi}\mathfrak{f}_s, \quad \mathfrak{g}_s \to \frac{H_c^{(0)2}}{4\pi}\mathfrak{g}_s, \quad \mathfrak{G}_s \to \frac{H_c^{(0)2}(\sqrt{2}\lambda_L)^3}{4\pi}\mathfrak{G}_s, \tag{2.123}$$

the Gibbs free energy difference becomes

$$\mathfrak{g}_s = \tau^2\left(\mathfrak{g}_s^{(0)} + \tau\mathfrak{g}_s^{(1)} + ...\right), \tag{2.124}$$

$$\mathfrak{g}_s^{(0)} = \frac{1}{2}\left(\frac{|\vec{\mathfrak{B}}|}{\sqrt{2}\kappa} - 1\right)^2 + \frac{1}{\sqrt{2}\kappa^2}|\vec{\mathfrak{D}}\Psi|^2 - |\Psi|^2 + \frac{1}{4}|\Psi|^4, \tag{2.125}$$

$$\begin{aligned}\mathfrak{g}_s^{(1)} = {} & \left(\frac{|\vec{\mathfrak{B}}|}{\sqrt{2}\kappa} - 1\right)\left(\frac{1}{2} + \frac{ac}{3b^2}\right) - \frac{|\Psi|^2}{2} + |\Psi|^4 + \frac{|\vec{\mathfrak{D}}\Psi|^2}{\kappa^2} + \frac{1}{4\kappa^4}\frac{a\mathcal{Q}}{\mathcal{K}^2}\left\{|\vec{\mathfrak{D}}^2\Psi|^2 + \frac{1}{3}(\vec{\nabla}\times\vec{\mathfrak{B}})^2\right. \\ & \left. + \vec{\mathfrak{B}}^2|\Psi|^2\right\} + \frac{1}{4\kappa^2}\frac{a\mathcal{L}}{b\mathcal{K}}\left\{8|\Psi|^2|\vec{\mathfrak{D}}\Psi|^2 + [\Psi^2(\vec{\mathfrak{D}}^*\Psi^*)^2 + c.c]\right\} + \frac{ac}{3b^2}|\Psi|^6.\end{aligned} \tag{2.126}$$

With this expression, it is possible to determine the boundaries between types I and II in the (κ, T) plane by expanding $\mathfrak{G}_s$ around $\kappa_0 = 1/\sqrt{2}$

$$\mathfrak{G}_s = \tau^2\left(\mathfrak{G}_s^{(0)} + \frac{d\mathfrak{G}_s^{(0)}}{d\kappa}\Big|_{\kappa=\kappa_0}\delta\kappa + \tau\mathfrak{G}^{(1)} + ...\right) \tag{2.127}$$

[7] Note that critical field H_c used in this expression must be expanded in τ. The leading order contribution calculated in chapter 1 is $H_c^{(0)} = \sqrt{\frac{4\pi a^2}{b}}$ and the leading correction is easily found to be $H_c^{(1)} = -\left(\frac{1}{2} + \frac{ac}{3b^2}\right)H_c^{(0)}$ from Eq. (2.126).

where $\delta\kappa = \kappa - \kappa_0$. The term $d\mathfrak{G}_s^{(0)}/d\kappa$ has contributions from the explicit appearance of κ and its implicit appearance from the derivatives $d\Psi/d\kappa$ and $d\vec{\mathfrak{A}}/d\kappa$. Notice, that the implicit contributions are zero because they are proportional to $\delta\mathfrak{G}_s^{(0)}/\delta\Psi$ and $\delta\mathfrak{g}_s^{(0)}/\delta\vec{\mathfrak{A}}$, which are zero in the equilibrium, see Ref. (VAGOV et al., 2016). At $\kappa = \kappa_0$, a solution to the GL equations can be obtained by using the Bogomolnyi self-duality equations

$$(\partial_y + i\partial_x)\Psi = (\vec{\mathfrak{A}}_x - i\vec{\mathfrak{A}})\Psi, \tag{2.128}$$

$$|\vec{\mathfrak{B}}| = 1 - |\Psi|^2, \tag{2.129}$$

that are useful to simplify the integrals in $\mathfrak{G}_s$. Then, the Gibbs free energy difference becomes

$$\mathfrak{G}_s = \tau^2\left\{-\sqrt{2}\mathcal{I}\,\delta\kappa + \tau\left[\left(1 - \frac{ac}{3b^2} + 2\frac{a\mathcal{Q}}{\mathcal{K}^2}\right)\mathcal{I} + \left(2\frac{a\mathcal{L}}{b\mathcal{K}} - \frac{ac}{3b^2} - \frac{5}{3}\frac{a\mathcal{Q}}{\mathcal{K}^2}\right)\mathcal{J}\right] + \ldots\right\} \tag{2.130}$$

where

$$\mathcal{I} = \int |\Psi|^2(1-|\Psi|^2)d^3x, \qquad \mathcal{J} = \int |\Psi|^4(1-|\Psi|^2)d^3x \tag{2.131}$$

are the only two quantities dependent on the the order parameter at $\kappa = \kappa_0$. Note that $\mathfrak{G}_s^{(0)}$ is zero, a manifestation of the degeneracy at the Bogomolnyi point.

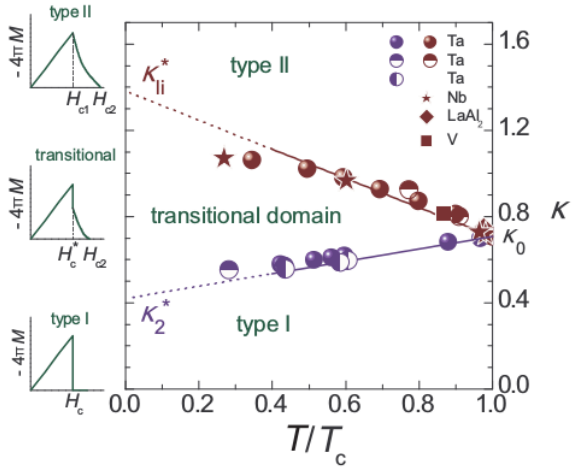

Figure 13 – Phase diagram of superconductivity types in the (κ, T) plane derived from the EGL formalism and comparison with experimental data, see Ref. (VAGOV et al., 2016). The curves marked by κ_{li}^* and κ_2^* correspond to κ_u and κ_l defined by Eqs. (2.133) and (2.134), respectively.

By using the criterion of the nucleation of a particular nonuniform configuration, i.e., $\mathfrak{G}_s(\kappa, T) = 0$, one employs Eq. (2.130) to find the boundary between types I and II, i.e., for type I only the Meissner phase is realized while the nonuniform (the mixed state) configuration becomes stable in type II. The criterion yields

$$\kappa^* = \kappa_0\left\{1 + \tau\left[1 - \frac{ac}{3b^2} + 2\frac{a\mathcal{Q}}{\mathcal{K}^2} + \frac{\mathcal{J}}{\mathcal{I}}\left(2\frac{a\mathcal{L}}{b\mathcal{K}} - \frac{ac}{b^2} - \frac{5}{3}\frac{a\mathcal{Q}}{\mathcal{K}^2}\right)\right]\right\}. \tag{2.132}$$

The ratios of material parameters in this expression are independent of the material, the only term to be calculated is $\mathcal{J}/\mathcal{I}$ for a given configuration. It is of importance that the use of different nonuniform condensate/field configurations in the nucleation criterion results in different boundaries between types I and II. Only for $T \to T_c$ this difference disappears and one arrives at the standard classification: type I is below κ_0 while type II is above κ_0. Below T_c one gets a finite *transitional domain* between types I and II (below it is also referred to as *intertype domain*), see Fig. 13. The upper (max) and lower (min) boundaries of this domain in the isotropic single-band superconductors are material-independent

$$\kappa_{max} = \kappa_0(1 + 0.95\tau), \tag{2.133}$$

$$\kappa_{min} = \kappa_0(1 - 0.407\tau). \tag{2.134}$$

Notice in the presence of multiple contributing bands the intertype domain is not material-independent any more, see Ref. (VAGOV et al., 2016).

3 THE BOGOMOLNY POINT IN ANISOTROPIC SUPERCONDUCTORS

"Messing up with the system never felt so good."

Tom Morello - 2010

Chapter Contents

In this chapter a scaling approach is applied to prove an equivalence between the classifications of the superconductivity types in anisotropic and isotropic superconductors. This scaling approach, applied here to the extended Ginzburg-Landau (EGL) formalism, is similar to previous schemes adopted for the Ginzburg-Landau (GL) equations in single-band superconductors. The objective of the investigation in this chapter is to generalize the consideration of the intertype (IT) domain in isotropic single-band superconductors in Ref. (VAGOV et al., 2016) to the case of a system with a single but anisotropic Fermi Surface, for which the GL parameter $\kappa = \lambda/\xi$ becomes more subtle to determine.

3.1 Anisotropic Hamiltonian and scaling scheme

As mentioned in the previous chapter, the problem of anisotropic superconductors may demand some generalizations to the Bardeen, Cooper and Schriefer (BCS) model. Essentially, anisotropy in superconductors refers to direction-dependent electronic propagation and magnetic response. Comparing theory and experiment in this case can become complicated, because the controlling parameters in the fabrication of the sample such as purity, granularity, doping, etc. are of importance. Also, it is important to note that some anisotropic superconductors are layered, where the Lawrence-Doniach model is more adequate (LAWRENCE; DONIACH,) but this case is beyond our consideration.

In the derivation of the GL theory for anisotropic superconductors Gor'kov and Melik-Barkhudarov did not specify the Hamiltonian operator, i.e., their results are valid in the most general case (GOR'KOV; MELIK-BARKHUDAROV, 1964). Here, as we are interested in the IT domain and needs to go beyond the standard GL formalism, we restrict ourselves to modeling the anisotropy by introducing the kinetic energy operator with the direction-dependent electronic masses m_j such as

$$\mathcal{T} = -\sum_{j=1}^{3} \frac{\hbar^2}{2m_j}\left(\partial_j - i\frac{e}{\hbar c}A_j\right)^2 - \mu. \tag{3.1}$$

The domain of integration of the unperturbed Green function

$$\mathcal{G}_{\omega}^{(0)}(\vec{x},\vec{x}') = \int \frac{d^3k}{(2\pi)^3}\frac{\exp[i\,\vec{k}\cdot(\vec{x}-\vec{x}')]}{i\hbar\omega - \xi_k} \tag{3.2}$$

is the elliptic Fermi surface and the dispersion relation takes the form

$$\xi_k = \sum_{j=1}^{3}\frac{\hbar^2}{2m_j}k_j^2 - \mu. \tag{3.3}$$

In this case, one can use a simple scaling method to isotropize the Hamiltonian by finding proper scaling factors α_i for the spatial coordinates, the particle momentum projections, and the vector potential and magnetic field components[1]

$$\tilde{x}_i = \frac{1}{\sqrt{\alpha_i}}x_i, \quad \tilde{k}_i = \sqrt{\alpha_i}k_i, \quad \tilde{A}_i = \sqrt{\alpha_i}A_i, \quad \tilde{B}_i = \frac{1}{\sqrt{\alpha_i}}B_i, \tag{3.4}$$

which results in a unique electronic mass M for each direction

$$\mathcal{T} = -\sum_{i=1}^{3}\frac{\hbar^2}{2M}\left(\tilde{\partial}_j - i\frac{e}{\hbar c}\tilde{A}_i\right)^2 - \mu \tag{3.5}$$

[1] The notation adopted in this chapter is such that scaled vectors have a tilde instead of arrow $\vec{v} \to \tilde{v}$ and the nth entry of the scaled vector is $\tilde{v}_n$. Also, $\tilde{\partial}_n$ corresponds to the partial derivative with respect to the nth coordinate $\partial/\partial\tilde{x}_n$.

and does not induce alteration in the elements of volume after this variable change as

$$\alpha_i m_i = \alpha_j m_j = M \quad (\forall\, i, j), \tag{3.6}$$

$$\prod_{i=1}^{3} \sqrt{\alpha_i} = 1. \tag{3.7}$$

The single-particle dispersion becomes direction independent so that the Fermi surface is spherically symmetric. The (unique) real solution to this system of equations is (KLEMM; CLEM, 1980)

$$\alpha_i = \frac{M}{m_i}, \quad M = \sqrt[3]{m_x m_y m_z}. \tag{3.8}$$

Note that the Maxwell equation $\tilde{\nabla} \cdot \tilde{B} = 0$ and the relation $\tilde{B} = \tilde{\nabla} \times \tilde{A}$ remain valid in this new scheme. In our consideration the magnetic field is chosen to be directed along one of the principle crystalline axes, in order to avoid unnecessary extra rotations in the system of coordinates (KLEMM; CLEM, 1980) and to simplify the results. For instance, let us consider the GL equations for the bulk system and $\vec{H} = H\hat{z}$, where $\hat{z}$ the unit vector in the positive z direction. By using the isotropic equations and performing the inverse scaling transformation defined by Eq. (3.4), one derives the following set of equations:

$$a\Delta^{(0)} + b|\Delta^{(0)}|^2\Delta^{(0)} - \left(\mathcal{K}_x \mathcal{D}_x^2 + \mathcal{K}_y \mathcal{D}_y^2\right)\Delta^{(0)} = 0, \tag{3.9}$$

$$\partial_y B = 4\pi \mathcal{K}_x \alpha_z i \frac{2e}{\hbar c}\left(\Delta_0 \mathcal{D}_x^* \Delta_0^* - \Delta_0^* \mathcal{D}_x \Delta_0\right), \tag{3.10}$$

$$\partial_x B = -4\pi \mathcal{K}_y \alpha_z i \frac{2e}{\hbar c}\left(\Delta_0 \mathcal{D}_y^* \Delta_0^* - \Delta_0^* \mathcal{D}_y \Delta_0\right). \tag{3.11}$$

In this case, $a = -N(0)$, $b = N(0)\frac{7\zeta(3)}{8\pi^2 T_c^2}$ and $\mathcal{K}_j = \frac{b}{6}\hbar^2 v_j^2$. From this set of equations one extracts the characteristic lengths

$$\xi_j^{(z)} = \sqrt{\frac{\mathcal{K}_j}{|a|}}, \quad \lambda_j^{(z)} = \sqrt{\frac{\hbar^2 c^2 b,}{32\pi^2 e^2 \mathcal{K}_j \alpha_z |a|}} \tag{3.12}$$

where $j = x,\ y$ and the superscript z reflects the field direction. With these expressions, one can derive different GL parameters $\kappa_j = \lambda_j/\xi_j$ and the fact that one has different κ_x and κ_y might leave an impression that the GL parameter is not unique and, consequently, the unambiguous definition of the corresponding superconductivity type cannot be performed. However, the GL parameter $k^{(z)}$ is to be established from the coefficients of the effective isotropic GL theory. Indeed, using the coefficients of the scaled GL theory, one obtains that the relevant GL parameter is given by the harmonic average

$$\kappa^{(z)} = \sqrt{\kappa_x \kappa_y}. \tag{3.13}$$

3.2 The Bogomolny line and the intertype domain

The fact that the anisotropic GL theory (here with the fixed direction of the magnetic field along one of the principal crystalline axes) can be reduced to the isotropic theory and has the uniquely defined GL parameter, Eq. (3.13), has an important physical consequence that has not been explicitly noted so far: an anisotropic GL theory allows only for the two standard superconductivity types I and II. The relevant GL parameter, that corresponds to the field direction (z above) or on the chosen plane (x - y plane above), is controlled by the two direction-dependent κ_x and κ_y parameters so that its critical value κ_0 is in fact the critical curve in the (κ_x, κ_y) plane given by the relation $\kappa_x\kappa_y = \kappa_0^2 = 1/2$. Below and above this curve we have, respectively, type I and type II, see Fig. 14.

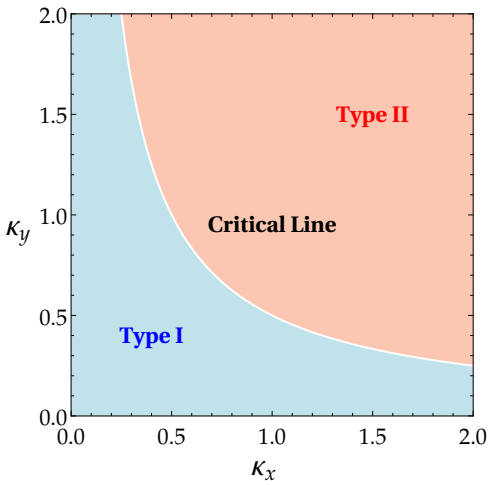

Figure 14 – Classification of the superconductivity types illustrated in the (κ_x, κ_y) plane. Types I and II correspond to blue and red regions, respectively. The white curve represents the critical regime $\kappa_x\kappa_y = \kappa_0^2 = 1/2$.

Keeping the link to the isotropic theory, we recall that the critical curve $\kappa_x\kappa_y = \kappa_0^2$ separates types I and II only for $T \to T_c$. Below T_c, as has been mentioned in chapter 2, the finite IT (transitional) domain appears in the phase diagram between types I and II. Once the scaling scheme is applied to the Hamiltonian, one can expect that the scaling works to any order in the τ-expansion of the microscopic equations. So, the τ expansion for the critical GL parameter of the isotropic system

$$\kappa^* = \kappa_0 \left\{1 + \tau \left[1 - \frac{ac}{3b^2} + 2\frac{aQ}{\mathcal{K}^2} + \frac{\mathcal{J}}{\mathcal{I}}\left(2\frac{a\mathcal{L}}{b\mathcal{K}} - \frac{ac}{b^2} - \frac{5}{3}\frac{aQ}{\mathcal{K}^2}\right)\right]\right\}. \tag{3.14}$$

can be applied for the anisotropic case beyond the standard GL approach. Hence, the upper boundaries of the IT domain in the anisotropic case are simply extracted from Eqs. (2.133) and (2.134). In this sense the IT domain appears to be not affected by the anisotropy. In the (κ_x, κ_y) plane any critical parameter given by Eq. (3.14) becomes the

critical curve determined by $\kappa^* = \sqrt{\kappa_x \kappa_y}$. Thus, we have two curves that define the upper and lower boundaries of the IT domain in the (κ_x, κ_y) plane, as illustrated in Fig. 15.

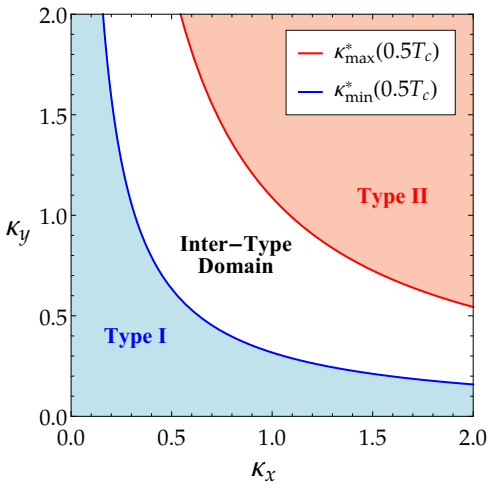

Figure 15 – Classification of superconducting types in the (κ_x, κ_y) diagram for $T = 0.5T_c$. Type I and II correspond to blue and red regions, respectively. The white region corresponds to the IT domain, i.e. it is expected that the system presents neither type-I or type-II behavior.

Notice that the present analysis of the intertype behavior is in agreement with experimental results reported previously for TaN alloys (WEBER; SPORNA; SEIDL, 1978; MOSER; SEIDL; WEBER, 1982; SAUERZOPF et al., 1987). In the experiments discussed in Refs. (WEBER; SPORNA; SEIDL, 1978; MOSER; SEIDL; WEBER, 1982; SAUERZOPF et al., 1987), the authors studied the superconducting magnetic response at various amplitudes and inclinations of the magnetic field and at various temperatures near the boundary between type I and the IT domain. In addition, the GL parameter of the system of interest was varied in these experiments by nitrogen doping.

It is important to note that the IT regime is referred to as the type II/1 in Refs. (WEBER; SPORNA; SEIDL, 1978; MOSER; SEIDL; WEBER, 1982; SAUERZOPF et al., 1987). The type II/1 concept assumes that single-flux quantum (Abrikosov) vortices play a role of elementary entities (“particles") of the mixed state in both IT and type-II superconductors, while relatively weak vortex interactions help to arrange these “elementary particles" in a particular form of the Abrikosov lattice. Within this picture all differences between the magnetic properties of IT and type-II superconductors can be explained only in terms of the change in the vortex interaction which becomes attractive at long ranges in the intertype regime. Acknowledging this similarity, the name “type-II/1" has been coined for IT superconductors, while type II is referred to as “type-II/2". Recently it has been demonstrated that the IT physics is not simply reduced to attractive single-quantum vortices. Indeed, multi-quantum vortices and

vortex clusters are of importance near the boundary between the IT and type I regimes, see Ref. (VAGOV et al., 2016).

This boundary is derived from the measurements of the magnetization. The IT response reveals itself in a first-order transition between the Meissner and mixed states, seen as an abrupt drop in the magnetization. In type-I superconductors this drop is down to zero, i.e., the mixed state disappears and we obtain the first-order transition from the Meissner state to the normal one. As seen in Fig 16, the superconductivity type of the superconducting sample depends on the orientation of the applied magnetic field with respect to the crystal principal directions. Strikingly, there is a situation when

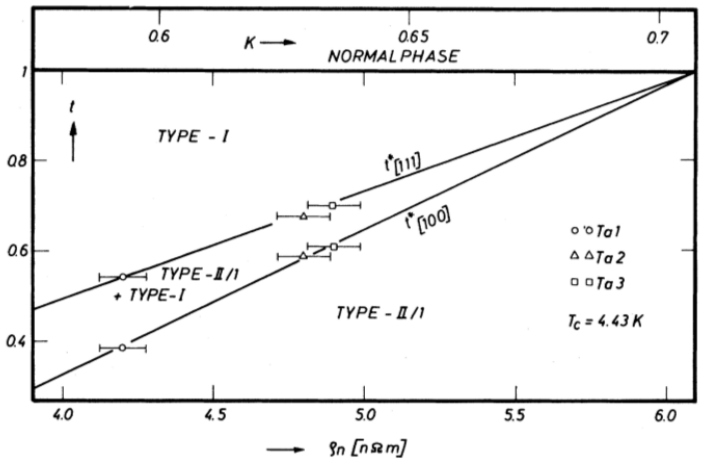

Figure 16 – Phase diagram of superconducting types from Ref. (WEBER; SPORNA; SEIDL, 1978) in which they report different temperature dependence of the lower boundary of the IT domain (full lines) depending on the orientation of the magnetic field. The resistivity at the normal state ρ_n is translated into a value of κ by the Gor'kov-Goodman formula.

the superconducting magnetic response is of type I for one direction of the magnetic field while it is of type-II/1 (i.e., IT) for another direction. This is in agreement with our findings as the effective GL parameter for the z direction is $\kappa^{(z)} = \sqrt{\kappa_x \kappa_y}$ while, say, for the x direction we have a completely different value $\kappa^{(x)} = \sqrt{\kappa_y \kappa_z}$. The unexpected dependence of the superconductivity type on the direction of the applied magnetic field found in Ref. (WEBER; SPORNA; SEIDL, 1978) has not been explained previously.

4 GAP HEALING-LENGTHS WITHIN THE EGL THEORY

"I was driving it by a kind of instinct, only I was in a different dimension."

Ayrton Senna - 1993

Chapter Contents

An analytic solution for a spatially uniform distribution of a two-band condensate is investigated within the extended Ginzburg-Landau (EGL) formalism in this chapter. With this solution, it is possible to calculate the leading corrections in $\tau = 1 - T/T_c$ to the Ginzburg-Landau (GL) coherence length in single- and two-band superconductors. The leading correction is material-independent in the case of a single-band system, while it is strongly dependent on the relevant material parameters in the two-band case. In the two-band case we investigate the deviation between the band-dependent leading corrections to the GL length and find that the spatial characteristic lengths of the different band condensates can be notably different far beyond the regime of nearly decoupled bands, contrary to the common expectation. We also discuss a possible relation of this difference between the band coherent lengthscales to anomalous vortex distributions found in MgB_2.

4.1 Analytic solution of the EGL equation for single-band superconductors

Consider the single-band case of the EGL equations, (2.105) and (2.106), in the absence of magnetic fields

$$a\Delta^{(0)} + b|\Delta^{(0)}|^2\Delta^{(0)} - \mathcal{K}\nabla^2\Delta^{(0)} = 0, \tag{4.1}$$

$$a\Delta^{(1)} + b\left[2\Delta^{(1)}|\Delta^{(0)}|^2 + \Delta^{*(1)}\left(\Delta^{(0)}\right)^2\right] - \mathcal{K}\nabla^2\Delta^{(1)} = F\left(\Delta^{(0)}\right), \tag{4.2}$$

$$\begin{aligned} F\left(\Delta^{(0)}\right) = {} & \frac{a}{2}\Delta^{(0)} + 2\mathcal{K}\nabla^2\Delta^{(0)} + \mathcal{Q}\nabla^2\left(\nabla^2\Delta^{(0)}\right) - 2b|\Delta^{(0)}|^2\Delta^{(0)} \\ & - \mathcal{L}\left[2\Delta^{(0)}|\vec{\nabla}\Delta^{(0)}|^2 + 3\Delta^{*(0)}\left(\vec{\nabla}\Delta^{(0)}\right)^2 + \left(\Delta^{(0)}\right)^2\nabla^2\Delta^{*(0)} + 4|\Delta^{(0)}|^2\nabla^2\Delta^{(0)}\right] \\ & + c|\Delta^{(0)}|^4\Delta^{(0)} \end{aligned} \tag{4.3}$$

The constant or uniform solutions of the EGL formalism can be easily found by neglecting derivatives

$$\Delta^{(0)} = \sqrt{-\frac{a}{b}} = \Psi_\infty, \tag{4.4}$$

$$\Delta^{(1)} = -\left(\frac{3}{4} + \frac{ac}{2b^2}\right)\Psi_\infty \Rightarrow \frac{\Delta^{(1)}}{\Psi_\infty} = -\left(\frac{3}{4} - \frac{\alpha}{2}\right) \approx -0.068987, \tag{4.5}$$

where $\alpha = -ac/b^2 = \frac{93\zeta(5)}{98\zeta(3)^2} \approx 0.681$ is a numeric constant recurrent in the following calculations. As seen, the uniform solution for $\Delta^{(1)}$ is easily expressed in units of Ψ_∞ and then the coefficients from the τ expansion for Δ are expressed in dimensionless units

$$\psi(\vec{x}) = \frac{\Delta^{(0)}(\vec{x})}{\Psi_\infty}, \qquad \varphi(\vec{x}) = \frac{\Delta^{(1)}(\vec{x})}{\Psi_\infty}. \tag{4.6}$$

As seen, the GL equation provides the characteristic length scale of the gap in the leading order $\xi_{GL} = \sqrt{-\mathcal{K}/a}$. After redefining distances in units of ξ_{GL}, one obtains the EGL equations in dimensionless units:

$$\psi - \psi^3 + \nabla^2\psi = 0, \tag{4.7}$$

$$(1 - 2|\psi|^2)\varphi - \psi^2\varphi^* + \nabla^2\varphi = \tilde{F}(\psi) \tag{4.8}$$

where

$$\begin{aligned} \tilde{F}(\psi) = {} & -\frac{1}{2}\psi - 2\nabla^2\psi + \frac{a\mathcal{Q}}{\mathcal{K}^2}\nabla^2(\nabla^2\psi) + 2|\psi|^2\psi \\ & - \frac{a\mathcal{L}}{b\mathcal{K}}\left[2\psi|\nabla\psi|^2 + 3\psi^*(\nabla\psi)^2 + \psi^2\nabla^2\psi^* + 4|\psi|^2\nabla^2\psi\right] + \frac{ac}{b^2}|\psi|^4\psi. \end{aligned} \tag{4.9}$$

Eq. (4.8) can be simplified by considering ψ and φ real functions (once the systems does not involve magnetic field) and also the function $\tilde{F}$ can be manipulated by

eliminating all the terms involving $\nabla^2\psi$ by using equation (4.7)

$$\tilde{F}(\psi) = \left(\frac{3}{2} + \frac{a\mathcal{Q}}{\mathcal{K}^2}\right)\psi + \left(5\frac{a\mathcal{L}}{b\mathcal{K}} - 4\frac{a\mathcal{Q}}{\mathcal{K}^2}\right)|\psi|^2\psi \tag{4.10}$$

$$+ \left(\frac{ac}{b^2} + 3\frac{a\mathcal{Q}}{\mathcal{K}^2} - 5\frac{a\mathcal{L}}{b\mathcal{K}}\right)|\psi|^4\psi + \left(6\frac{a\mathcal{Q}}{\mathcal{K}^2} - 5\frac{a\mathcal{L}}{b\mathcal{K}}\right)\psi(\nabla\psi)^2, \tag{4.11}$$

while all the ratios between auxiliary parameters can be written in terms of α

$$\frac{ac}{b^2} = -\alpha, \qquad \frac{a\mathcal{Q}}{\mathcal{K}^2} = -\frac{6}{5}\alpha, \qquad \frac{a\mathcal{L}}{b\mathcal{K}} = \frac{2}{3}\alpha. \tag{4.12}$$

Finally the EGL equation acquires the form

$$(1 - 3\psi^2)\varphi + \nabla^2\varphi = A\psi + B\psi^3 + C\psi^5 + D\psi(\nabla\psi)^2 \tag{4.13}$$

where de coefficients above are

$$A = \frac{3}{2} - \frac{6}{5}\alpha \approx 0.683, \quad B = \frac{22}{15}\alpha \approx 0.999, \tag{4.14}$$

$$C = -\frac{19}{15}\alpha \approx -0.863, \quad D = -\frac{58}{15}\alpha \approx -2.633. \tag{4.15}$$

With the equations in a simpler form, now we address to the analytic solution for the domain-wall problem described in chapter (1). By considering very large planar interfaces, one can assume symmetric solutions with respect to the longitudinal direction, depending only on the coordinate perpendicular to the interface, say x. The first integral to the GL equation can be obtained with the simple integrating factor ψ'

$$\psi - \psi^3 + \psi'' = 0 \Rightarrow \psi\psi' - \psi^3\psi' + \psi'\psi'' = 0 \Rightarrow 2\psi^2 - \psi^4 + 2(\psi')^2 = C_I. \tag{4.16}$$

With the boundary conditions $\psi(\infty) = 1$ and $\psi'(\infty) = 0$, the integration constant becomes determined $C_I = 1$ and the equation can be put in the integral form

$$\int_0^x dx\frac{\psi'}{1-\psi^2} = \int_{\psi(0)}^{\psi(x)} dz\frac{1}{1-z^2} = \tanh^{-1}\left[\psi(x)\right] = x/\sqrt{2} \tag{4.17}$$

and finally it is obtained the solution

$$\psi(x) = \tanh(x/\sqrt{2}). \tag{4.18}$$

In principle, solving Eq. (4.13) may be simpler than the first equation because it is a linear equation on φ and there are standard techniques for solving this type of equations. The only complication is that the left hand side $(1 - 3\psi^2)\varphi + \varphi''$ may not immediately be in the form of a tabled differential equation and, in the case $\psi(x) = \tanh(x/\sqrt{2})$, we found the adequate variable transformation. After we substitute the expression for $\psi(x)$

on Eq. (4.13), we get an inhomogeneous second order differential equation (ANTON; HERR, 1995)

$$\left[1 - 3\tanh^2(x/\sqrt{2})\right]\varphi + \varphi'' = A\tanh(x/\sqrt{2}) + B\tanh^3(x/\sqrt{2}) + C\tanh^5(x/\sqrt{2}) + D\tanh(x)\mathrm{sech}^4(x/\sqrt{2}) \tag{4.19}$$

With the substitution $z(x) = \tanh(x/\sqrt{2})$ one obtains the following equation:

$$\left[6(1-z^2) - 4\right]\varphi - 2z(1-z^2)\frac{d\varphi}{dz} + (1-z^2)^2\frac{d^2\varphi}{dz^2} = 2Az + 2Bz^3 + 2Cz^5 + Dz(1-z^2)^2$$
$$= (2A + 2B + 2C)z + (D - 2B - 2C)z(1-z^2) - (D + 2C)z^3(1-z^2) \tag{4.20}$$

and dividing both sides by $1 - z^2$ it is found that

$$(1-z^2)\frac{d^2\varphi}{dz^2} - 2z\frac{d\varphi}{dz} + \left(6 - \frac{4}{1-z^2}\right)\varphi =$$
$$= (2A + 2B + 2C)\frac{z}{1-z^2} + (D - 2B - 2C)z - (D + 2C)z^3. \tag{4.21}$$

The homogeneous part of Eq. (4.21) is tabled in Ref. (ABRAMOWITZ; STEGUN, 1964) and its solutions are the so-called *Legendre functions* of the first and second kinds (see plots in Fig. 17):

$$P_2^2(z) = 3(1-z^2),$$
$$Q_2^2(z) = \frac{z\left(5 - 3z^2\right)}{1-z^2} + 3\left(1-z^2\right)\tanh^{-1}(z)$$
$$= \frac{2z}{1-z^2} + 3z + 3\left(1-z^2\right)\tanh^{-1}(z), \tag{4.22}$$

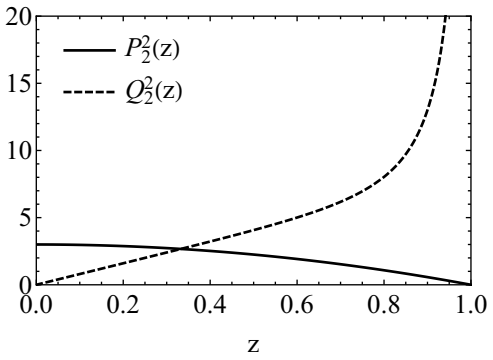

Figure 17 – Plots of the Legendre functions $P_2^2(z)$ (solid line) and $Q_2^2(z)$ (dashed line).

The next step is finding a particular solution, $S_p(z)$, to Eq. (4.21) by looking for the action of the operator

$$\hat{L} \equiv (1-z^2)\frac{d^2}{dz^2} - 2z\frac{d}{dz} + \left(6 - \frac{4}{1-z^2}\right) \tag{4.23}$$

at three particular functions

$$\hat{L}\left(\frac{z}{1-z^2}\right) = 6\frac{z}{1-z^2}, \tag{4.24}$$

$$\hat{L}(z) = -4\frac{z}{1-z^2} + 4z, \tag{4.25}$$

$$\hat{L}\left(z^3\right) = -4\frac{z}{1-z^2} + 10z - 6z^3. \tag{4.26}$$

First, one must notice that $z/(1-z^2)$ is eigenfunction of this operator. Second, the action of $\hat{L}$ in an odd power term results in the term $z/(1-z^2)$ combined with an odd polynomial of the same order. Based on this, consider particular solution of the form of Eq. (4.21)

$$S_p(z) = \alpha_0\frac{z}{1-z^2} + \alpha_1 z + \alpha_3 z^3 \tag{4.27}$$

where one should match up the coeffiecients α_0, α_1 and α_3 with the coefficients of the inhomogeneous term in Eq. (4.21), as shown bellow:

$$\hat{L}\left(S_p\right) = (2A+2B+2C)\frac{z}{1-z^2} + (2D-2B-2C)z - (D+2C)z^3 \tag{4.28}$$

$$= (6\alpha_0 - 4\alpha_1 - 4\alpha_3)\frac{z}{1-z^2} + (4\alpha_1 + 10\alpha_3)z - 6\alpha_3 z^3. \tag{4.29}$$

This system of equations is directly in a triangular form and the solution can be readily obtained:

$$\alpha_0 = \frac{A-C}{3}, \qquad \alpha_1 = -\frac{3B+8C+D}{6}, \qquad \alpha_3 = \frac{2C+D}{6}. \tag{4.30}$$

Now, the last task is to determine the linear combination

$$\varphi(z) = pP_2^2(z) + qQ_2^2(z) + S_p(z) \tag{4.31}$$

of the Legendre functions $P_2^2(z)$ and $Q_2^2(z)$ that obeys the boundary conditions when combined with the particular solution found previously. At $x = 0$, the gap must be null in all orders, therefore

$$0 = \varphi\left[\tanh(0)\right] = pP_2^2(0) + qQ_2^2(0) + S_p(0) = 3p \Rightarrow p = 0. \tag{4.32}$$

The second boundary condition, at $x \to \infty$ ($z = 1$), is a bit more tricky because the general solution has a pole at $z = 1$. To avoid this divergence, we impose the coefficient p to be such that the divergent part of $Q_2^2(z)$ cancels the divergent part of $S_p(z)$, i.e. [1]

$$2q = \alpha_0 \Rightarrow q = -\frac{A-C}{6} \tag{4.33}$$

Then the final solution, plotted in Fig. 18, is

$$\varphi(z) = -\frac{A-C}{6}Q_2^2(z) + S_p(z). \tag{4.34}$$

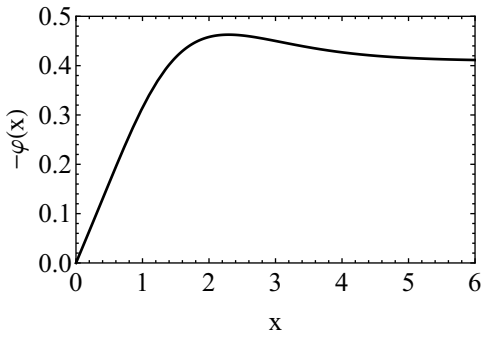

Figure 18 – Plot of the solution of the next-to-leading order contribution of the superconducting gap as function of the distance from the interface.

Note that the maximum absolute value of this function is reached at a distance around $2\xi_{GL}$, differently from the leading order contribution. The complete solution for the superconducting gap, plotted in Fig. 19, is

$$\frac{\Delta(\vec{x},\tau)}{\tau^{1/2}\Psi_\infty} = \tanh(x/\sqrt{2}) - \tau\left[\left(\frac{3}{4} - \frac{47\alpha}{30}\right)\tanh(x/\sqrt{2}) + \left(\frac{3}{4} + \frac{\alpha}{30}\right)(x/\sqrt{2})\mathrm{sech}^2(x/\sqrt{2}) + \frac{16\alpha}{15}\tanh^3(x/\sqrt{2})\right]. \tag{4.35}$$

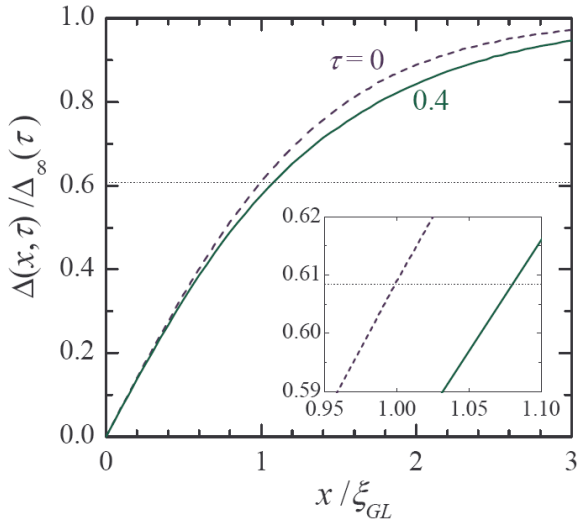

Figure 19 – Plot of the EGL solution for $\Delta(x,\tau)$ given in units of its asymptotic value, the uniform solution $\Delta_\infty(\tau) = \tau^{1/2}\Psi_\infty$, as a function of the relative distance from the interface x/ξ_{GL} for $\tau = 0$ (dashed curve) and $\tau = 0.4$ (solid curve). The dotted horizontal line marks $\delta = \tanh(1/\sqrt{2})$ that determines the condensate healing length according to Eq.

[1] It is easy to prove that non-divergent solutions for φ (that do not involve the term $\frac{z}{1-z^2}$) always reach the uniform solution value at $z = 1$.

From the analytic solution of the EGL equation, it is possible to stablish an equation for determining the healing length of the gap, i.e. the length in which the value of the gap recovers from zero to a certain fraction of the maximum value. We decided to use the cut-off value from the GL solution so that in the limit $\tau \to 0$, the GL value for the healing-length is naturally recovered. Then, the condition for determining the healing-length becomes

$$\frac{\Delta(\xi,\tau)}{\Delta(\infty,\tau)} = \delta = \tanh(1/\sqrt{2}) \approx 0.609 \tag{4.36}$$

and, following the perturbation theory used in the EGL formalism, the healing length will be calculated by considering the leading correction to ξ_{GL}:

$$\xi = \xi_{GL}\left[1 + \epsilon + O\left(\tau^2\right)\right]. \tag{4.37}$$

As expected, $\epsilon \sim \tau$ and then it must be be a small correction in the vicinity of T_c, allowing the Taylor expansion of distances around 1:

$$\frac{\Delta(1+\epsilon,\tau)}{\tau^{1/2}\Psi_\infty} = \psi(1) + \left.\frac{d\psi}{dx}\right|_{x=1}\epsilon + \tau\varphi(1) = \frac{\delta\Delta(\infty,\tau)}{\tau^{1/2}\Psi_\infty} = \delta\left[1 - \left(\frac{3}{2} - \frac{\alpha}{2}\right)\tau\right]. \tag{4.38}$$

which gives

$$\frac{\xi}{\xi_{GL}} = 1 + \left(\frac{3}{4} + \frac{\alpha}{30} - \sqrt{2}\delta\frac{16\alpha}{15}\right)\tau \approx 1 + 0.147\tau. \tag{4.39}$$

The comparison between the numerical solution of ξ found numerically from Eq. (4.36) and the solution from perturbation theory is plotted in Fig. 20. The difference between the numerical and analytical results becomes significant for $\tau > 0.3 - 0.4$, which defines the validity domain of Eq. (4.39) as $\tau \lesssim \tau^* = 0.3 - 0.4$.

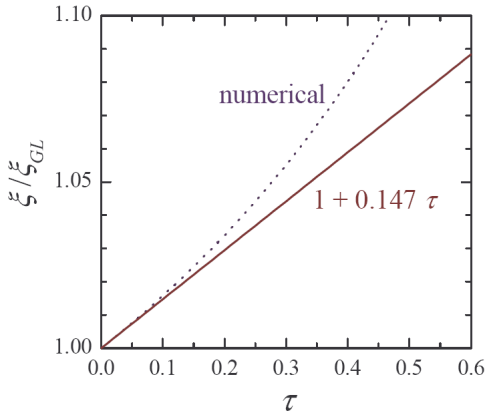

Figure 20 – Condensate healing length versus τ: the analytical result of Eq. (4.39) is given by the dotted line, whereas the full numerical solution of Eq. (4.36) is represented by the solid curve.

4.2 Analytic solution of the EGL equations for two-band superconductors

In this section, the analysis started in chapter 2 is developed in detail, where it was proved that in the case of two-band superconductors both gaps have the same profile in the leading order. For convenience we repeat the set of equations of the EGL formalism

$$\sum_j L_{ij}\Delta_j^{(0)} = 0, \tag{4.40}$$

$$\sum_j L_{ij}\Delta_j^{(1)} = -a_i\Delta_i^{(0)} - b_i|\Delta_i^{(0)}|^2\Delta_i^{(0)} + \mathcal{K}_i\vec{\nabla}^2\Delta_i^{(0)}, \tag{4.41}$$

$$\sum_j L_{ij}\Delta_j^{(2)} = -a_i\Delta_i^{(1)} - b_i\left(2\Delta_i^{(1)}|\Delta_i^{(0)}|^2 + \Delta_i^{*(1)}\Delta_i^{(0)2}\right) + \mathcal{K}_i\vec{\nabla}\Delta_i^{(1)} - F_i\left(\Delta_i^{(0)}\right), \tag{4.42}$$

where

$$\begin{aligned} F_i\left(\Delta_i^{(0)}\right) = &-\frac{a_i}{2}\Delta_i^{(0)} + 2\mathcal{K}_i\vec{\nabla}^2\Delta_i^{(0)} + \mathcal{Q}_i\vec{\nabla}^2(\vec{\nabla}^2\Delta_i^{(0)}) - 2b_i|\Delta_i^{(0)}|^2\Delta_i^{(0)} \\ &- \mathcal{L}_i\left[2\Delta_i^{(0)}|\vec{\nabla}\Delta_i^{(0)}|^2 + 3\Delta_i^{*(0)}(\vec{\nabla}\Delta_i^{(0)})^2 + \Delta_i^{2(0)}\vec{\nabla}^2\Delta_i^{*(0)} + 4|\Delta_i^{(0)}|^2\vec{\nabla}^2\Delta_i^{(0)}\right] \\ &+ c_i|\Delta_i^{(0)}|^4\Delta_i^{(0)} \end{aligned} \tag{4.43}$$

and

$$\mathcal{A} = \ln\left(\frac{2e^{\Gamma}\hbar\omega_c}{\pi T_c}\right), \quad \mathcal{A}_i = N_i(0)\mathcal{A}, \quad a_i = -N_i(0), \quad b_i = N_i(0)\frac{7\zeta(3)}{8\pi^2T_c^2}, \tag{4.44}$$

$$c_i = N_i(0)\frac{93\zeta(5)}{128\pi^4T_c^4}, \quad \mathcal{K}_i = \frac{b_i}{6}\hbar^2v_i^2, \quad \mathcal{Q}_i = \frac{c_i}{30}\hbar^4v_i^4, \quad \mathcal{L}_i = \frac{c_i}{9}\hbar^2v_i^2. \tag{4.45}$$

The matrix

$$L = \begin{pmatrix} \gamma_{11} - N_1(0)\mathcal{A} & \gamma_{12} \\ \gamma_{12} & \gamma_{22} - N_2(0)\mathcal{A} \end{pmatrix} \tag{4.46}$$

plays a central role in this system of equations and studying it can be extremely helpful to solve the EGL equations. As seen in chapter 2, by looking for non-trivial solutions for $\Delta^{(0)}$, one has $\det(L) = 0$, which provides the critical temperature of the system. Instead, let us limit to finding the constant $\mathcal{A}$ (which is directly related to T_c)[2]

$$\mathcal{A} = \frac{1}{GN_1(0)N_2(0)}\left[\frac{g_{11}N_1(0) + g_{22}N_2(0)}{2} + \sqrt{\left[\frac{g_{11}N_1(0) - g_{22}N_2(0)}{2}\right]^2 + g_{12}^2N_1(0)N_2(0)}\right], \tag{4.47}$$

where $G = g_{11}g_{22} - g_{12}^2$. To express the matrix L in a convenient form, let us define the auxiliary parameter S:

$$S = -\frac{\gamma_{11} - N_1(0)\mathcal{A}}{\gamma_{12}} = \frac{g_{22} - N_1(0)G\mathcal{A}}{g_{12}} \tag{4.48}$$

[2] We have chosen the solution with "−" sign once the other one may produce non-physical states.

and then

$$L = -\gamma_{12}\begin{pmatrix} S & -1 \\ -1 & S^{-1} \end{pmatrix}. \tag{4.49}$$

Then, $\lambda_1 = 0$ and $\lambda_2 = -\gamma_{12}(S + S^{-1})$. Also, the eigenvectors of L are

$$\vec{\eta}_1 = \begin{pmatrix} 1 \\ S \end{pmatrix}, \qquad \vec{\eta}_2 = \begin{pmatrix} -S \\ 1 \end{pmatrix} \tag{4.50}$$

Notice that the eigenvectors given by Eq. (4.50) are not normalized. The EGL formalism does not require such a normalization and, in addition, use of the normalized eigenvectors results in more complex expressions. As seen, Eq.(4.40) implies that

$$\vec{\Delta}^{(0)}(\vec{x}) = \Psi(\vec{x})\vec{\eta}_1, \tag{4.51}$$

i.e. the gap profiles are proportional and therefore it is clear that the parameter S is the ratio between the two gaps, which is commonly measured experimentally (IAVARONE et al., 2002; GOLUBOV et al., 2002).

By projecting Eq. (4.41) onto $\vec{\eta}_1$, one finds the equation for the true order parameter of the system, Ψ,

$$a\Psi + b|\Psi|^2\Psi - \mathcal{K}\nabla^2\Psi = 0, \tag{4.52}$$

where we have redefined the parameters

$$a = \sum_i a_i \eta_{+i}^2, \quad b = \sum_i b_i \eta_{+i}^4, \quad \mathcal{K} = \sum_i \mathcal{K}_i \eta_{+i}^2. \tag{4.53}$$

The uniform solution becomes

$$\Psi_\infty = \sqrt{-\frac{a}{b}} = T_c\sqrt{\frac{8\pi^2}{7\zeta(3)}}\sqrt{\frac{1+\chi S^2}{1+\chi S^4}}, \tag{4.54}$$

with the ratio between DOS's $\chi = N_2(0)/N_1(0)$. Also, the healing length of the leading-order solution becomes[3]

$$\xi_{GL} = \sqrt{-\frac{\mathcal{K}}{a}} = \frac{\hbar v_1}{T_c}\sqrt{\frac{7\zeta(3)}{48\pi^2}}\sqrt{\frac{1+\eta\beta^2 S^4}{1+\eta S^2}} \tag{4.55}$$

where [4] $\beta = v_2/v_1$ is the ratio of Fermi velocities and, by expressing Ψ in terms of the uniform solution, $\psi = \Psi/\Psi_\infty$, the equation for the order parameter becomes exactly the GL equation, (4.7). Then leading-order solution for the domain-wall problem becomes

$$\vec{\Delta}^{(0)} = \Psi_\infty \tanh(x/\sqrt{2}\xi_{GL})\vec{\eta}_1 \tag{4.56}$$

[3] This label means that the Ginzburg-Landau contribution corresponds to the leading order term, inasmuch the *EGL* label will correspond to the contribution from the next-to-leading order term, even though both terms were derived in the scope of the EGL foramlism.

[4] In this chapter, β is redefined as the ratio between Fermi velocities between band 1 and 2.

In order to find $\vec{\Delta}^{(1)}$, it is useful to expand it in terms of the eigenvectors of L

$$\vec{\Delta}^{(1)}(\vec{x}) = \Phi_1(\vec{x})\vec{\eta}_1 + \Phi_2(\vec{x})\vec{\eta}_2 \tag{4.57}$$

and then project Eq. (4.42) onto $\vec{\eta}_2$

$$\begin{aligned}\lambda_2|\vec{\eta}_2|^2\Phi_2 &= -\gamma_{12}S^{-1}(1+S^2)^2\varphi_- \\ &= -a'\Psi - b'|\Psi|^2\Psi + \mathcal{K}'\nabla^2\Psi\end{aligned} \tag{4.58}$$

where the new auxiliary parameters were defined

$$a' = \sum_i a_i\eta_{-i}\eta_{+i}, \quad b' = \sum_i b_i\eta_{-i}\eta_{+i}^3, \quad \mathcal{K}' = \sum_i \mathcal{K}_i\eta_{-i}\eta_{+i}. \tag{4.59}$$

This equation can be simplified by using Eq. (4.52) in order to remove the Laplacian term, resulting in

$$\varphi_2(\vec{x}) = \frac{\Phi_2(\vec{x})}{\Psi_0} = \mathcal{G}\left[\left(\frac{\mathcal{K}'}{\mathcal{K}} - \frac{a'}{a}\right)\psi(\vec{x}) - \left(\frac{\mathcal{K}'}{\mathcal{K}} - \frac{b'}{b}\right)\psi^3(\vec{x})\right] \tag{4.60}$$

$$\left.\frac{\varphi_-}{\Psi}\right|_{bulk} = \mathcal{G}\left(\frac{b'}{b} - \frac{a'}{a}\right), \tag{4.61}$$

where in this expression we defined the auxiliary parameter

$$\mathcal{G} = \frac{a}{\lambda_2|\vec{\eta}_2|^2} = \frac{aGS}{g_{12}(1+S^2)^2}. \tag{4.62}$$

This parameter is present only in the multi-band solution of the EGL formalism and then, if this parameter is zero, the system has only one spatial profile for all bands. More specifically if $\mathcal{G} = 0$ then $\varphi_2 = 0$ and then the vector $\Delta^{(1)}$ presents only the contribution from η_1

$$\Delta(\vec{x},\tau) = (\Psi + \tau\varphi_1)\,\vec{\eta}_1. \tag{4.63}$$

Also, from Eq. (4.60), we see that if one has the same density of states at the Fermi level and the same Fermi velocities for each band, the function φ_- is null producing again the case shown in Eq. (4.63). Finally we project Eq (4.42) onto $\vec{\eta}_1$ to obtain the equation for φ_+

$$\begin{aligned}a\Phi_1 + 3b\Psi^2\Phi_2 - \mathcal{K}\nabla^2\Phi_1 &= -a'\Phi_2 - 3b'\Psi^2\Phi_2 + \mathcal{K}'\nabla^2\Phi_2 \\ -\frac{a}{2}\Psi + 2\mathcal{K}\nabla^2\Psi + \mathcal{Q}\nabla^2(\nabla^2\Psi) - 2b\Psi^3 - 5\mathcal{L}&\left[\Psi(\vec{\nabla}\Psi)^2 + \Psi^2\nabla^2\Psi\right] + c|\Psi|^4\Psi\end{aligned} \tag{4.64}$$

where, similarly to the Φ_2 equation, we have redefined the parameters

$$\mathcal{Q} \equiv \sum_i Q_i\eta_{+i}^2, \quad \mathcal{L} \equiv \sum_i \mathcal{L}_i\eta_{+i}^4, \quad c \equiv \sum_i c_i\eta_{+i}^6. \tag{4.65}$$

Expressing Φ_1 in dimensionless units, $\varphi_1(\vec{x}) = \Phi_1(\vec{x})/\Phi_0$, one can use Eq's. (4.52) and (4.60) in order to remove Laplacian terms, and finally the equation for φ_1 becomes identical to that the single-band case

$$(1-3|\psi|^2)\varphi_+ + \nabla^2\varphi_+ = A\Psi + B\Psi^3 + C\Psi^5 + D\Psi(\vec{\nabla}\Psi)^2, \tag{4.66}$$

again, with redefined auxiliary coefficients

$$A = \left(\frac{3}{2} + \frac{a\mathcal{Q}}{\mathcal{K}^2}\right) + \mathcal{G}\left(\frac{\mathcal{K}'}{\mathcal{K}} - \frac{a'}{a}\right)^2, \tag{4.67}$$

$$B = \left(5\frac{a\mathcal{L}}{b\mathcal{K}} - 4\frac{a\mathcal{Q}}{\mathcal{K}^2}\right) - \mathcal{G}\left(4\frac{\mathcal{K}'^2}{\mathcal{K}^2} - 6\frac{b'\mathcal{K}'}{b\mathcal{K}} - 2\frac{a'\mathcal{K}'}{a\mathcal{K}} + 4\frac{a'b'}{ab}\right), \tag{4.68}$$

$$C = \left(\frac{ac}{b^2} + 3\frac{a\mathcal{Q}}{\mathcal{K}^2} - 5\frac{a\mathcal{L}}{b\mathcal{K}}\right) + 3\mathcal{G}\left(\frac{\mathcal{K}'}{\mathcal{K}} - \frac{b'}{b}\right)^2, \tag{4.69}$$

$$D = \left(6\frac{a\mathcal{Q}}{\mathcal{K}^2} - 5\frac{a\mathcal{L}}{b\mathcal{K}}\right) + 6\mathcal{G}\left(\frac{\mathcal{K}'^2}{\mathcal{K}^2} - \frac{b'\mathcal{K}'}{b\mathcal{K}}\right). \tag{4.70}$$

These coefficients are combinations of the auxiliary parameter S, the constant $\alpha\frac{93\zeta(5)}{98\zeta(3)^2}$ and the ratio of microscopic parameters $\chi = \frac{N_2(0)}{N_1(0)}$ and $\beta = \frac{v_2}{v_1}$

$$\frac{ac}{b^2} = -\alpha\frac{(1+\chi S^2)(1+\chi S^6)}{(1+\chi S^4)^2}, \tag{4.71}$$

$$\frac{a\mathcal{Q}}{\mathcal{K}^2} = -\frac{6}{5}\alpha\frac{(1+\chi S^2)(1+\chi\beta^4 S^2)}{(1+\chi\beta^2 S^2)^2}, \tag{4.72}$$

$$\frac{a\mathcal{L}}{b\mathcal{K}} = \frac{2}{3}\alpha\frac{(1+\chi S^2)(1+\chi\beta^2 S^4)}{(1+\chi S^4)(1+\chi\beta^2 S^2)}, \tag{4.73}$$

$$\frac{\mathcal{K}'}{\mathcal{K}} = -S\frac{1-\chi\beta^2}{1+\chi\beta^2 S^2}, \tag{4.74}$$

$$\frac{a'}{a} = -S\frac{1-\chi}{1+\eta S^2}, \tag{4.75}$$

$$\frac{b'}{b} = -S\frac{1-\chi S^2}{1+\chi S^4} \tag{4.76}$$

Thus, we have reduced the problem of finding a solution to that of the single-band case.

$$\begin{aligned}\varphi_+(x) = &-\left(\frac{3A+3B+5C+D}{6}\right)\tanh(x/\sqrt{2}) \\ &+\left(\frac{2C+D}{6}\right)\tanh^3(x/\sqrt{2}) + \left(\frac{C-A}{2}\right)\frac{x}{\sqrt{2}}\mathrm{sech}^2(x/\sqrt{2})\end{aligned} \tag{4.77}$$

and thus we have found the solution for all the components of the gaps

$$\frac{\vec{\Delta}(x,\tau)}{\tau^{1/2}\Psi_\infty} = \psi(x)\vec{\eta}_1 + \tau\left[\varphi_1(x)\vec{\eta}_1 + \varphi_2(x)\vec{\eta}_2\right]. \tag{4.78}$$

Also, once we know a solution, we have developed a method for deriving the leading corrections to the GL coherence length

$$\Delta_i(\xi,\tau) = \delta\Delta_i(\infty,\tau) \tag{4.79}$$

by expanding this length in τ and considering small perturbations from the GL value, i.e. the leading corrections

$$\frac{\xi_i}{\xi_{GL}} = 1 + \left[\left(\frac{C-A}{2}\right) + \delta\sqrt{2}\left(\frac{2C+D}{6}\right) - \delta\sqrt{2}\mathcal{G}\left(\frac{\mathcal{K}'}{\mathcal{K}} - \frac{b'}{b}\right)\varepsilon_i\right]\tau \tag{4.80}$$

where ξ_i means the EGL result for the healing length in band $i = \{1,2\}$, also ε_i is the ratio between the components of the eigenvectors $\vec{\eta}_2$ and $\vec{\eta}_1$, i.e. $\varepsilon_1 = -S$ and $\varepsilon_2 = 1/S$.

4.2.1 Deviation between healing lengths

Let us introduce the deviation rate of healing lengths

$$\frac{1}{\xi_{GL}}\frac{d(\xi_1-\xi_2)}{d\tau} = \left(\frac{C-A}{2}\right) + \delta\sqrt{2}\left(\frac{2C+D}{6}\right) - \delta\sqrt{2}\mathcal{G}\left(\frac{\mathcal{K}'}{\mathcal{K}} - \frac{b'}{b}\right)\varepsilon_i \tag{4.81}$$

This quantity can serve as the measure for the length scale disparity because the difference between the band healing lengths is usually most pronounced at low temperatures $T \ll T_c$. When analysing this expression, it is found that the ratio of Fermi velocities plays an important role, as expected, to the deviation between gap healing lengths. Notwithstanding, in Ref. (ICHIOKA; KOGAN; SCHMALIAN, 2017), Ichioka et al. it is discussed some different physical picture. In order to stablish that the deviation between healing lengths is a negligible feature in multi-band superconductors, which they called named "locking" of length scales, the authors performed numerical simulations of the microscopic theory of superconductivity in many situations with respect to the density of states and couplings, but they only used one single value, $\beta = 3$, for the ratio of Fermi velocities. The authors intended to have different coherence lengths in the limit of fully decoupled bands but it is not clear to us why they only used this value for β knowing that the Fermi velocities play such an important role on the characteristic lengths. In fact, this rate of deviation found to have strong dependence on β, as seen in Fig. 21(a). The 3D plot of the deviation rate versus $\lambda_{12}/\lambda_{11}$ and β is presented in Fig. 21(a). Details of the dependence on β can be found in Fig. 21(b). The data are shown for $\lambda_{12}/\lambda_{11} > 0.1$ in order to check the expectation (ICHIOKA; KOGAN; SCHMALIAN, 2017) that the difference between the band healing lengths is negligible for such values. For the sake of illustration we choose $\lambda_{11} = 0.6$, $\lambda_{22} = 0.4$, and $\chi = 1$. Notice that this choice of the couplings and the band DOS's ratio is not crucial: similar results are obtained for other sets of microscopic parameters. From Fig. 21, it is seen that $d(\xi_2 - \xi_1)/d\tau$ is monotonically increasing with respect to β while monotonically decreasing with respect to λ_{12}. Basically, there are two

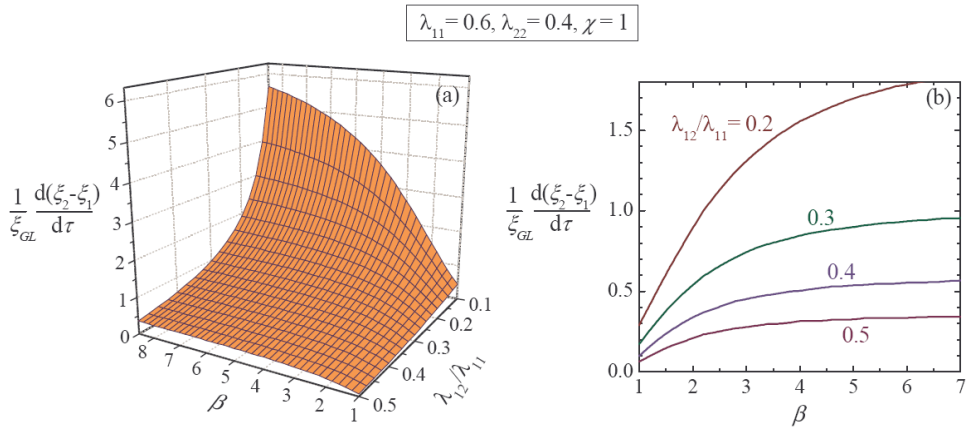

Figure 21 – Deviation rate as function of the ratio of Fermi velocities and the normalized interband coupling.

contributions to the final values of the healing lengths competing: the intra-band and the inter-band interaction. As each band has a proper value for the Fermi velocity, they should have different healing lengths but (remember that, in the regime of decoupled bands, $\xi_i \propto v_i$), once they overlap each other in the same sample, the inter-band coupling tend to smooth these discrepancies. Furthermore, it is important to note that the terms in Eq's. (4.74), (4.75) and (4.76) are bounded with respect to χ, β and S, i.e. the exponents in the numerators and denominators are equal. Even though, before these terms saturate with respect to β one can have significant discrepancies between healing lengths. In quantitative terms, at $T = 0.9T_c$, one has a deviation from 5% to 55% ξ_{GL}, which indicates to be even larger for lower temperatures. Such deviations can produce extremely unusual behaviour to the vortex lattice, such as fractional vortices (BABAEV, 2002; NA; SILVA; MILOSEVIC, 2012; LIN; BULAEVSKII, 2013a; LIN; BULAEVSKII, 2013b; SILVA et al., 2014), enhancement of intertype superconductivity (VAGOV et al., 2016), broken-symmetry vortex patterns (CURRAN et al., 2015), etc.

Let us analyse in detail the limit of nearly decoupled bands. First, by Eq's. (4.47) and (4.48), one can obtain the limit of nearly decoupled regime approximation $g_{12} \to 0$ for the parameter

$$S \to \frac{g_{12}}{g_{11} - g_{22}\chi}. \tag{4.82}$$

Also, one finds that by examining the dependence of the deviation rate with respect to β one finds that

As an application to real materials we considered the microscopic parameters of MgB_2. This case illustrates how the ratio of Fermi velocities has great importance when considering multi-band superconductors. As it is widely known, this material presented in many experiments two clearly distinct superconducting gaps, being actually a pair of very close Fermi sheets each one of them. The σ band is stronger (1) while the π band

is the weaker (2). Single-crystals of this material is formed by graphite-type B layers separated by hexagonal close-packed layers of Mg and it presents anisotropy in the Fermi velocities. The averaged band Fermi velocities in the $a-b$ plane can be estimated as $v_1^{(a-b)} = 4.4\times10^5 m/s$ and $v_2^{(a-b)} = 5.35\times10^5 m/s$. However, the motion of charge carriers in the c direction changes dramatically due to the quasi-2D character of the σ band. In particular, one obtains $v_1^{(c)} = 7\times10^4 m/s$, almost an order of magnitude smaller than $v_1^{(a-b)}$, while for the 3D π band the Fermi velocity in the c direction $v_2^{(c)} = 6\times10^5 m/s$ remains close to $v_2^{(a-b)}$. The ratios between Fermi velocities vary almost one order of magnitude, i.e. $\beta^{(a-b)} = 1.2$ and $\beta^{(c)} = 8.7$, and therefore, as seen before, it is expected that this disparity will produce two kinds of situations when comparing the band healing lengths. As can be seen in Fig. 22(a) and (b), the gap profiles at $\tau = 0.07$ present almost identical profile for $\beta = \beta^{(a-b)}$ while they differ significantly for $\beta^{(c)}$, which agrees with the previous discussion. Note that we are not dealing with the anisotropic version of the EGL equations in this chapter, instead we are considering long samples of single-crystals and measurements of the symmetric cases, where the material is effectively 1D. Here we utilize the dimensionless coupling constants and DOS's ratio reported for MgB_2 in Ref. (): $\lambda_{11} = 2.41$, $\lambda_{22} = 0.78$, $\lambda_{12} = 0.37 \approx 0.15\lambda_{11}$, and $\chi = 1.37$. Using the dotted horizontal line in both panels, one can estimate that the deviation between the band healing lengths is close to 0.07 ξ_{GL} in panel (a) while increasing up to 0.3 ξ_{GL} in panel (b).

An important feature appeared in Fig. 22(b): the solution for gap 1 is not a monotonic function of the distance. This is due to the growth of the coefficient of the leading correction because, as seen in Fig. 18, this is a characteristic of this term only. We believe that this is an undesired result of the perturbation theory and that it should not be present if higher order corrections could be calculated. However, the gap profiles are clearly unequal, once the weaker band has essentially one strong change of inclination around $1\xi_{GL}$ and the stronger band rises quickly and present this strange shape. Thus we find that the band condensates have different healing lengths and, in addition, their spatial profiles are not similar. Based on this observation, one can expect that reducing the deviation between the band healing lengths does not necessarily mean that the system approaches an effectively single-component regime. A mismatch between the band-condensate spatial profiles can still remain, reflecting an essential role of the multiple-condensate structure even for a negligible difference between the band healing lengths.

Finally, we plot in Fig's.22(c) and (d) the healing lengths for both bands as a function of τ from the numerical solution of Eq. (4.79) and from the analytic expression (4.80). It is important to note that these figures give an idea of the deviation between each band healing length and the GL coherence length. This quantity is also strongly dependent of the ratio of Fermi velocities. In plot (c), for the case $\beta^{(a-b)}$, one can see that

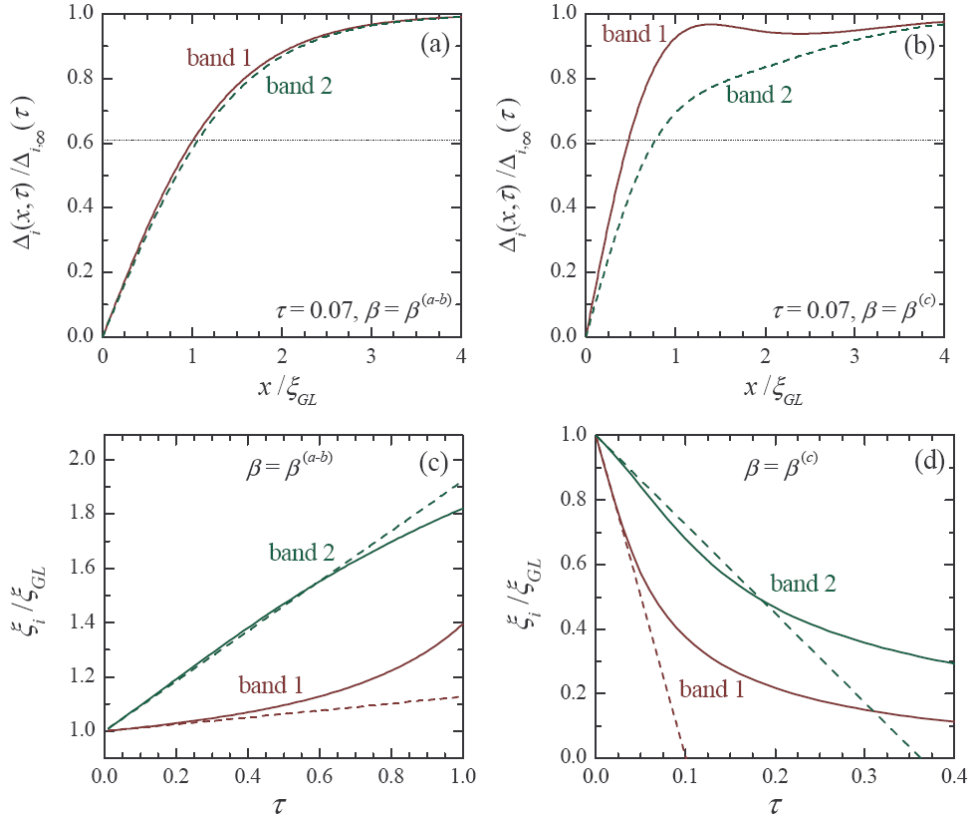

Figure 22 – (a) EGL solution for the band gap $\Delta_i(x,\tau)$ [in units of its asymptotic value $\Delta_{i,\infty}(\tau)$] as a function of the distance from the interface (in units of ξ_{GL}) calculated at $\tau = 0.07$ and $\beta = \beta^{(a-b)}$; the solid and dashed curves represent bands 1 and 2, respectively. (b) The same as in panel (a) but for $\beta = \beta^{(c)}$. (c) The relative band healing length ξ_i/ξ_{GL} versus τ at $\beta = \beta^{(a-b)}$: the analytical result of Eq. (4.80) is given by the (c) dashed line, while the full numerical solution of Eq.(4.79) is represented by the solid curve. (d) The same as in (c) but now for $\beta = \beta^{(c)}$. The dotted lines in panels (a) and (b) mark $\delta = \tanh(1/\sqrt{2})$ that determines the band healing length according to Eq. (4.80). The validity domain of the τ expansion can be estimated as $\tau \lesssim \tau^* = 0.4 - 0.5$ for $\beta = \beta^{(a-b)}$ and $\tau \lesssim \tau^* = 0.05 - 0.07$ for $\beta = \beta^{(c)}$.

both healing lengths increase with temperature, i.e. the leading correction is positive for this set of microscopic parameter. In plot (c), for the case $\beta^{(c)}$, the contrary happens. It is interesting to note that in the single band case, the expression was universal and the deviation was very small. Now in the multi-band case we see a completely different scenario, which reinforces the idea that multi-band systems have the possibility of completely new phenomena. One can also learn from Figs.22(c) and (d) that the validity domain of the two-band EGL formalism is strongly dependent on the ratio of the band Fermi velocities. In particular, for $\beta = \beta^{(a-b)}$ the analytical results for the band healing lengths are close to the numerical solutions of Eq. (4.79) up to $\tau = 0.4 - 0.5$ so that the upper boundary of the validity domain is estimated as $\tau^* = 0.4 - 0.5$. From Fig.22(d) we find the considerably smaller value $\tau^* = 0.05 - 0.07$. This shrinking of the validity

domain at $\beta = \beta^{(c)}$ is a manifestation of the fact that, for great disparity between the band Fermi velocities, the deviations of the band healing lengths from the GL coherence length (and also from each other) so rapidly increase with τ that higher orders in τ should be incorporated already for $\tau \gtrsim 0.1$.

5 CONCLUSIONS

"Quo usque tandem abutere,
Catilina, patientia nostra?"

"How long, Catiline, will you go
on abusing our patience?"

Cicero

The thesis is focused on superconducting phenomena that can not be captured by the standard Ginzburg-Landau (GL) theory. Furthermore, the phenomena of interest can hardly be investigated in necessary detail by means of the full microscopic formalism, due to abnormal technical difficulties. This is why the present study is based on the extended GL (EGL) formalism (SHANENKO et al., 2011) that goes to one order beyond the standard GL theory in the perturbation expansion of the microscopic equations over the small proximity to the critical temperature $\tau = 1 - T/T_c$.

The first problem investigated in the present thesis concerns the intertype (IT) superconductivity regime (i.e., neither type I nor type II) in anisotropic superconductors. We have developed a scaling approach for anisotropic superconductors, to effectively isotropize the system, and so constructed a way of extracting anisotropic results from an auxiliary isotropic model. In particular, we have demonstrated that the self-consistency equation for the order parameter can be reduced to its auxiliary isotropic variant in any order of the perturbation theory in the small deviation from the critical temperature $\tau = 1-T/T_c$. This means that previous results of the isotropic GL and EGL theories can be used to get the corresponding anisotropic results by simply applying the inverse scaling. We have found that the self-dual Bogomolnyi regime, where the superconducting state is specified by the duality between the condensate and magnetic flux, sustains in the anisotropic case, still separating the standard superconductivity types I and II. We have calculated the intertype (IT) domain boundaries for anisotropic superconductors, based on the results for the IT regime obtained previously within the isotropic EGL theory. While in the isotropic case the superconductivity type of the system is controlled by the phase diagram in the (κ, T) plane (with κ the GL parameter), one should keep in mind that for the anisotropic system, the magnetic and coherence lengths are direction dependent. The GL parameter κ depends on the direction as well, i.e., κ_x, κ_y, and κ_z are different for the principle axis x, y, and z. Then, for the magnetic field along, say, the z direction we have obtained that the superconductivity-type phase diagram is controlled by the three parameters κ_x, κ_y, and T. Then, at $T = T_c$ the Bogomolnyi regime is given

by the curve $\sqrt{\kappa_x \kappa_y} = 1/\sqrt{2}$ in the (κ_x, κ_y) plane, i.e., type II is above this curve and type I is below. Below T_c this curve unfolds in a finite IT domain in the (κ_x, κ_y) plane. The relevant expressions for the other principle directions can be obtained by the circular permutation of x, y, and z. Our results demonstrate that there can be a situation when the superconductivity type of the system of interest depends on the direction of the applied magnetic field. It is of importance that this conclusion is in agreement with the experimental results for TaN.

The second problem considered in this thesis deals with the difference between the spatial profiles of the band condensates in multi-band superconductors. The aim of the present study is to demonstrate that a notable difference between the band length scales in multi-band superconductors can appear far beyond the regime of nearly decoupled bands, contrary to the common expectation. We have analytically calculated the band-dependent corrections to the GL coherence length for the two-band case. Our study has demonstrated that a deviation between the resulting band healing lengths is a product of complex interplay between different tendencies mainly governed by the interband interactions and band Fermi velocities. The interband coupling tends to wash out the difference between the band spatial scales while different band velocities help it to sustain. As a result, the band healing lengths can significantly deviate from each other far beyond the regime of nearly decoupled bands. Our results allow for a deeper insight on how the band lengthscales depend on microscopic parameters and will certainly be appealing to experimentalists, as our conclusions are relevant for the spatial distribution of the superconducting condensate in the vortex core of multi-band materials.

BIBLIOGRAPHY

ABRAMOWITZ, M.; STEGUN, I. A. *Handbook of mathematical functions with formulas, graphs, and mathematical tables*. [S.l.: s.n.], 1964. v. 55. Cited at page 60.

ABRIKOSOV, A. The magnetic properties of superconducting alloys. *Journal of Physics and Chemistry of Solids*, v. 2, n. 3, p. 199 – 208, 1957. ISSN 0022-3697. Disponível em: <http://www.sciencedirect.com/science/article/pii/0022369757900835>. Cited at page 23.

ABRIKOSOV, A. A. On the magnetic properties of superconductors of the second group. *J. Exptl. Theoret. Phys.*, URSS, v. 32, p. 1174–1182, 1957. Cited at page 23.

ABRIKOSOV, A. A.; DZYALOSHINSKI, I. E.; GOR'KOV, L. P. *Quantum Field Theoretical Methods in Statistical Physics*. [S.l.]: Pergamon, 1965. Cited at page 29.

ANTON, H.; HERR, A. *Calculus with analytic geometry*. Wiley, 1995. ISBN 9780471594956. Disponível em: <https://books.google.com.br/books?id=y6PgAAAAMAAJ>. Cited at page 60.

ASKERZADE, I. N.; GENCER, A.; GüçLü, N. On the Ginzburg-Landau analysis of the upper critical field h_c2 in mgb_2. *Superconductor Science and Technology*, v. 15, n. 2, p. L13, 2002. Disponível em: <http://stacks.iop.org/0953-2048/15/i=2/a=102>. Cited at page 41.

AUER, J.; ULLMAIER, H. Magnetic behavior of type-II superconductors with small Ginzburg-Landau parameters. *Phys. Rev. B*, v. 7, n. 136, 1973. Cited 2 times at page 8 and 9.

BABAEV, E. Vortices with fractional flux in two-gap superconductors and in extended faddeev model. *Phys. Rev. Lett.*, American Physical Society, v. 89, p. 067001, Jul 2002. Disponível em: <https://link.aps.org/doi/10.1103/PhysRevLett.89.067001>. Cited at page 69.

BABAEV, E.; SPEIGHT, M. Semi-meissner state and neither type-I nor type-II superconductivity in multicomponent superconductors. *Phys. Rev. B*, American Physical Society, v. 72, p. 180502, Nov 2005. Disponível em: <http://link.aps.org/doi/10.1103/PhysRevB.72.180502>. Cited at page 41.

BARDEEN, J.; COOPER, L. N.; SCHRIEFFER, J. R. Microscopic theory of superconductivity. *Phys. Rev.*, American Physical Society, v. 106, p. 162–164, Apr 1957. Disponível em: <https://link.aps.org/doi/10.1103/PhysRev.106.162>. Cited at page 27.

BARDEEN, J.; PINES, D. Electron-phonon interaction in metals. *Phys. Rev.*, American Physical Society, v. 99, p. 1140–1150, Aug 1955. Disponível em: <https://link.aps.org/doi/10.1103/PhysRev.99.1140>. Cited at page 26.

BOORSE, H. A. Superconducting electronic specific heats, the "exponential law," and the Bardeen, Cooper, Schrieffer theory. *Phys. Rev. Lett.*, American Physical Society, v. 2, p. 391–393, May 1959. Disponível em: <https://link.aps.org/doi/10.1103/PhysRevLett.2.391>. Cited at page 39.

BOUQUET, F. et al. Specific heat of $Mg^{11}B_2$: Evidence for a second energy gap. *Phys. Rev. Lett.*, American Physical Society, v. 87, p. 047001, Jul 2001. Disponível em: <https://link.aps.org/doi/10.1103/PhysRevLett.87.047001>. Cited at page 41.

BOUQUET, F. et al. Phenomenological two-gap model for the specific heat of mgb_2. *Europhys. Lett.*, v. 56, n. 6, p. 856–862, 2001. Disponível em: <https://doi.org/10.1209/epl/i2001-00598-7>. Cited at page 41.

BRANDT, E. H.; DAS, M. P. Attractive vortex interaction and the intermediate-mixed state of superconductors. *J. Supercond. Nov. Magn.*, v. 24, n. 57, 2011. Cited 2 times at page 8 and 9.

Bruce Lee. *The Pierre Berton Show*. 1971. Disponível em: <https://www.youtube.com/watch?v=uk1lzkH-e4U>. Cited at page 7.

BUD'KO, S. L. et al. Boron isotope effect in superconducting mgb_2. *Phys. Rev. Lett.*, American Physical Society, v. 86, p. 1877–1880, Feb 2001. Disponível em: <https://link.aps.org/doi/10.1103/PhysRevLett.86.1877>. Cited at page 41.

BUZEA, C.; YAMASHITA, T. Review of the superconducting properties of mgb_2. *Superconductor Science and Technology*, v. 14, n. 11, p. R115, 2001. Disponível em: <http://stacks.iop.org/0953-2048/14/i=11/a=201>. Cited at page 41.

COOPER, L. N. Bound electron pairs in a degenerate Fermi gas. *Phys. Rev.*, American Physical Society, v. 104, p. 1189–1190, Nov 1956. Disponível em: <https://link.aps.org/doi/10.1103/PhysRev.104.1189>. Cited at page 26.

CURRAN, P. J. et al. Spontaneous symmetry breaking in vortex systems with two repulsive lengthscales. *Scientific Reports*, v. 5, 2015. Cited at page 69.

ESSMANN, U. Observation of the mixed state. *Physica*, v. 55, p. 83 – 93, 1971. ISSN 0031-8914. Disponível em: <http://www.sciencedirect.com/science/article/pii/0031891471902448>. Cited at page 46.

FETTER, A.; WALECKA, J. *Quantum Theory of Many-particle Systems*. [S.l.]: Dover Publications, 2003. (Dover Books on Physics). Cited at page 38.

FEYNMAN, R.; LEIGHTON, R.; SANDS, M. *The Feynman Lectures on Physics, Vol. III: The New Millennium Edition: Quantum Mechanics*. Basic Books, 2011. (The Feynman Lectures on Physics). ISBN 9780465025015. Disponível em: <https://books.google.com.br/books?id=KsnbNL_rh04C>. Cited at page 16.

FRÖHLICH, H. Theory of the superconducting state. I. the ground state at the absolute zero of temperature. *Phys. Rev.*, American Physical Society, v. 79, p. 845–856, Sep 1950. Disponível em: <https://link.aps.org/doi/10.1103/PhysRev.79.845>. Cited at page 26.

GENNES, P. D. *Superconductivity Of Metals And Alloys*. Westview Press, 1999. (Advanced Books Classics Series). ISBN 9780813345840. Disponível em: <https://books.google.com.br/books?id=ZMf_ticFcWYC>. Cited at page 26.

GINSBERG, D. M.; RICHARDS, P. L.; TINKHAM, M. Apparent structure on the far infrared energy gap in superconducting lead and mercury. *Phys. Rev. Lett.*, American Physical Society, v. 3, p. 337–338, Oct 1959. Disponível em: <https://link.aps.org/doi/10.1103/PhysRevLett.3.337>. Cited at page 40.

GIUBILEO, F. et al. Two-gap state density in mgb_2: A true bulk property or a proximity effect? *Phys. Rev. Lett.*, American Physical Society, v. 87, p. 177008, Oct 2001. Disponível em: <https://link.aps.org/doi/10.1103/PhysRevLett.87.177008>. Cited at page 41.

GOLUBOV, A. A. et al. Specific heat of mgb_2 in a one- and a two-band model from first-principles calculations. *Journal of Physics: Condensed Matter*, v. 14, n. 6, p. 1353, 2002. Disponível em: <http://stacks.iop.org/0953-8984/14/i=6/a=320>. Cited 2 times at page 41 and 65.

GOR'KOV, L. P. On the energy spectrum of superconductors. *J. Exptl. Theoret. Phys.*, U.S.S.R., v. 34(7), 1958. Cited at page 29.

GOR'KOV, L. P. Microscopic derivation of the Ginzburg-Landau equations in the theory of superconductivity. *J. Explt. Theoret. Phys.*, U.S.S.R., v. 36(9), 1959. Cited 2 times at page 29 and 38.

GOR'KOV, L. P.; MELIK-BARKHUDAROV, T. K. Microscopic derivation of the Ginzburg-Landau equations for an anisotropic superconductor. *J. Explt. Theoret. Phys*, v. 18, 1964. Cited 2 times at page 40 and 52.

HESS, H. F. et al. Scanning-tunneling-microscope observation of the Abrikosov flux lattice and the density of states near and inside a fluxoid. *Phys. Rev. Lett.*, American Physical Society, v. 62, p. 214–216, Jan 1989. Disponível em: <https://link.aps.org/doi/10.1103/PhysRevLett.62.214>. Cited at page 25.

HIRSCH, J. E. Electrodynamics of superconductors. *Phys. Rev. B*, American Physical Society, v. 69, p. 214515, Jun 2004. Cited at page 17.

HOHENBERG, P. C.; WERTHAMER, N. R. Anisotropy and temperature dependence of the upper critical field of type-II superconductors. *Phys. Rev.*, American Physical Society, v. 153, p. 493–497, Jan 1967. Disponível em: <https://link.aps.org/doi/10.1103/PhysRev.153.493>. Cited at page 40.

HOWARD, I. K. H is for enthalpy, thanks to Heike Kamerlingh Onnes and Alfred W. Porter. *Journal of Chemical Education*, v. 79, n. 6, p. 697, 2002. Cited at page 15.

IAVARONE, M. et al. Two-band superconductivity in mgb_2. *Phys. Rev. Lett.*, American Physical Society, v. 89, p. 187002, Oct 2002. Disponível em: <https://link.aps.org/doi/10.1103/PhysRevLett.89.187002>. Cited 2 times at page 41 and 65.

ICHIOKA, M.; KOGAN, V. G.; SCHMALIAN, J. Locking of length scales in two-band superconductors. *Phys. Rev. B*, American Physical Society, v. 95, p. 064512, Feb 2017. Disponível em: <https://link.aps.org/doi/10.1103/PhysRevB.95.064512>. Cited at page 68.

KARAPETROV, G. et al. Scanning tunneling spectroscopy in mgb_2. *Phys. Rev. Lett.*, American Physical Society, v. 86, p. 4374–4377, May 2001. Disponível em: <https://link.aps.org/doi/10.1103/PhysRevLett.86.4374>. Cited at page 41.

KLEINER, W. H.; ROTH, L. M.; AUTLER, S. H. Bulk solution of Ginzburg-Landau equations for type II superconductors: Upper critical field region. *Phys. Rev.*, American Physical Society, v. 133, p. A1226–A1227, Mar 1964. Disponível em: <https://link.aps.org/doi/10.1103/PhysRev.133.A1226>. Cited 2 times at page 24 and 25.

KLEMM, R. A.; CLEM, J. R. Lower critical field of an anisotropic type-II superconductor. *Phys. Rev. B*, American Physical Society, v. 21, p. 1868–1875, Mar 1980. Disponível em: <https://link.aps.org/doi/10.1103/PhysRevB.21.1868>. Cited at page 53.

KOGAN, V. G.; SCHMALIAN, J. Ginzburg-Landau theory of two-band superconductors: Absence of type-1.5 superconductivity. *Phys. Rev. B*, American Physical Society, v. 83, p. 054515, Feb 2011. Disponível em: <http://link.aps.org/doi/10.1103/PhysRevB.83.054515>. Cited 2 times at page 41 and 46.

KONSIN, P.; SORKIN, B. A generalized two-band model for the superconductivity in mgb_2. *Superconductor Science and Technology*, v. 17, n. 12, p. 1472, 2004. Disponível em: <http://stacks.iop.org/0953-2048/17/i=12/a=019>. Cited at page 41.

KRÄGELOH, U. Der zwischenzustand bei supraleitern zweiter art. *physica status solidi (b)*, v. 42, n. 2, p. 559–576. Disponível em: <https://onlinelibrary.wiley.com/doi/abs/10.1002/pssb.19700420210>. Cited at page 46.

KRÄGELOH, U. Flux line lattices in the intermediate state of superconductors with ginzburg landau parameters near 12. *Physics Letters A*, v. 28, n. 9, p. 657 – 658, 1969. ISSN 0375-9601. Disponível em: <http://www.sciencedirect.com/science/article/pii/0375960169904939>. Cited at page 46.

KUMPF, U. Magnetisierungskurven von supraleitern zweiter art mit kleinen ginzburg-landau-parametern. *physica status solidi (b)*, v. 44, n. 2, p. 829–843, 1971. Disponível em: <https://onlinelibrary.wiley.com/doi/abs/10.1002/pssb.2220440243>. Cited at page 46.

LANDAU, L. On the theory of phase transitions. *Zh. Eksp. Teor. Fiz.*, v. 7, p. 19–32, 1937. Cited at page 19.

LAWRENCE, W. E.; DONIACH, S. *Proc. 12th Int. Conf. Low Temp. Phys.* [S.l.: s.n.]. Cited at page 52.

LIN, S.-Z.; BULAEVSKII, L. N. Dissociation transition of a composite lattice of magnetic vortices in the flux-flow regime of two-band superconductors. *Phys. Rev. Lett.*, American Physical Society, v. 110, p. 087003, Feb 2013. Disponível em: <https://link.aps.org/doi/10.1103/PhysRevLett.110.087003>. Cited at page 69.

LIN, S.-Z.; BULAEVSKII, L. N. Dissociation transition of a composite lattice of magnetic vortices in the flux-flow regime of two-band superconductors. *Phys. Rev. Lett.*, American Physical Society, v. 110, p. 087003, Feb 2013. Disponível em: <https://link.aps.org/doi/10.1103/PhysRevLett.110.087003>. Cited at page 69.

LIU, A. Y.; MAZIN, I. I.; KORTUS, J. Beyond Eliashberg superconductivity in MgB_2: Anharmonicity, two-phonon scattering, and multiple gaps. *Phys. Rev. Lett.*, American Physical Society, v. 87, p. 087005, Aug 2001. Disponível em: <https://link.aps.org/doi/10.1103/PhysRevLett.87.087005>. Cited at page 41.

LONDON, F. *Superfluids*. [S.l.]: Wiley, 1950. (Structure of matter series, v. 1). Cited at page 17.

MAXWELL, E. Isotope effect in the superconductivity of mercury. *Phys. Rev.*, American Physical Society, v. 78, p. 477–477, May 1950. Disponível em: <https://link.aps.org/doi/10.1103/PhysRev.78.477>. Cited at page 26.

MAZIN, I.; ANTROPOV, V. Electronic structure, electron–phonon coupling, and multiband effects in mgb_2. *Physica C: Superconductivity*, v. 385, n. 1, p. 49 – 65, 2003. ISSN 0921-4534. Disponível em: <http://www.sciencedirect.com/science/article/pii/S0921453402022992>. Cited at page 41.

MORSE, R. W.; OLSEN, T.; GAVENDA, J. D. Evidence for anisotropy of the superconducting energy gap from ultrasonic attenuation. *Phys. Rev. Lett.*, American Physical Society, v. 3, p. 15–16, Jul 1959. Disponível em: <https://link.aps.org/doi/10.1103/PhysRevLett.3.15>. Cited at page 39.

MOSER, E.; SEIDL, E.; WEBER, H. W. Superconductive properties of vanadium and their impurity dependence. *Journal of Low Temperature Physics*, v. 49, n. 5, p. 585–607, Dec 1982. ISSN 1573-7357. Disponível em: <https://doi.org/10.1007/BF00681903>. Cited at page 55.

MOSHCHALKOV, V. et al. Type-1.5 superconductivity. *Phys. Rev. Lett.*, American Physical Society, v. 102, p. 117001, Mar 2009. Disponível em: <http://link.aps.org/doi/10.1103/PhysRevLett.102.117001>. Cited at page 41.

NA, J. C. P.; SILVA, C. C. de S.; MILOSEVIC, M. V. Stability of fractional vortex states in a two-band mesoscopic superconductor. *Phys. Rev. B*, American Physical Society, v. 86, p. 024512, Jul 2012. Disponível em: <https://link.aps.org/doi/10.1103/PhysRevB.86.024512>. Cited at page 69.

NAGAMATSU, J. et al. Superconductivity at 39k in magnesium diboride. *Nature*, Macmillian Magazines Ltd., v. 410, 2001. Cited at page 41.

OGG, R. A. Bose-Einstein condensation of trapped electron pairs. phase separation and superconductivity of metal-ammonia solutions. *Phys. Rev.*, American Physical Society, v. 69, p. 243–244, Mar 1946. Disponível em: <https://link.aps.org/doi/10.1103/PhysRev.69.243>. Cited at page 25.

OUBOTER, R. de B. Superconductivity: Discoveries during the early years of low temperature research at Leiden 1908-1914. *IEEE Transactions on Magnetics*, v. 23, n. 2, p. 355–370, 1987. Cited at page 14.

PECHENIK, E. et al. Unconventional vortices in multicomponent Ginzburg-Landau theory. *Phys. Rev. B*, American Physical Society, v. 65, p. 214532, Jun 2002. Disponível em: <https://link.aps.org/doi/10.1103/PhysRevB.65.214532>. Cited at page 41.

PINES, D. Superconductivity in the periodic system. *Phys. Rev.*, American Physical Society, v. 109, p. 280–287, Jan 1958. Disponível em: <https://link.aps.org/doi/10.1103/PhysRev.109.280>. Cited at page 26.

PIPPARD, A. B. An experimental and theoretical study of the relation between magnetic field and current in a superconductor. *Proceedings of the Royal Society of London A: Mathematical, Physical and Engineering Sciences*, The Royal Society, v. 216, n. 1127, p. 547–568, 1953. ISSN 0080-4630. Disponível em: <http://rspa.royalsocietypublishing.org/content/216/1127/547>. Cited at page 18.

POPOV, V. N. *Functional Integrals and Collective Excitations*. [S.l.]: Cambrige University Press, 1987. Cited at page 47.

PROZOROV, R. Equilibrium topology of the intermediate state in type-I superconductors of different shapes. *Phys. Rev. Lett.*, American Physical Society, v. 98, p. 257001, Jun 2007. Disponível em: <https://link.aps.org/doi/10.1103/PhysRevLett.98.257001>. Cited at page 46.

REYNOLDS, C. A. et al. Superconductivity of isotopes of mercury. *Phys. Rev.*, American Physical Society, v. 78, p. 487–487, May 1950. Disponível em: <https://link.aps.org/doi/10.1103/PhysRev.78.487>. Cited at page 26.

RICHARDS, P. L.; TINKHAM, M. Far-infrared energy gap measurements in bulk superconducting In, Sn, Hg, Ta, V, Pb, and Nb. *Phys. Rev.*, American Physical Society, v. 119, p. 575–590, Jul 1960. Disponível em: <https://link.aps.org/doi/10.1103/PhysRev.119.575>. Cited at page 40.

SARAIVA, T. T. et al. Multiband superconductors: Disparity between band length scales. *Phys. Rev. B*, American Physical Society, v. 96, p. 134521, Oct 2017. Disponível em: <https://link.aps.org/doi/10.1103/PhysRevB.96.134521>. Cited 2 times at page 8 and 9.

SAUERZOPF, F. M. et al. Anisotropy effects in tantalum, niobium, and vanadium down to the millikelvin temperature range. *Journal of Low Temperature Physics*, v. 66, n. 3, p. 191–208, Feb 1987. ISSN 1573-7357. Disponível em: <https://doi.org/10.1007/BF00681821>. Cited at page 55.

SCHAFROTH, M. R. Superconductivity of a charged ideal bose gas. *Phys. Rev.*, American Physical Society, v. 100, p. 463–475, Oct 1955. Disponível em: <https://link.aps.org/doi/10.1103/PhysRev.100.463>. Cited at page 26.

SHANENKO, A. A. et al. Extended Ginzburg-Landau formalism for two-band superconductors. *Phys. Rev. Lett.*, American Physical Society, v. 106, p. 047005, Jan 2011. Disponível em: <http://link.aps.org/doi/10.1103/PhysRevLett.106.047005>. Cited 5 times at page 8, 9, 41, 46, and 73.

SILVA, R. M. da et al. Distinct magnetic signatures of fractional vortex configurations in multiband superconductors. *Applied Physics Letters*, v. 105, n. 23, p. 232601, 2014. Cited at page 69.

SUHL, H.; MATTHIAS, B. T.; WALKER, L. R. Bardeen-Cooper-Schrieffer theory of superconductivity in the case of overlapping bands. *Phys. Rev. Lett.*, American Physical Society, v. 3, p. 552–554, Dec 1959. Disponível em: <http://link.aps.org/doi/10.1103/PhysRevLett.3.552>. Cited 3 times at page 40, 41, and 45.

TILLEY, D.; GURP, G. V.; BERGHOUT, C. Anisotropy of the critical nucleation fields in superconductors. *Physics Letters*, v. 12, n. 4, p. 305 – 306, 1964. ISSN 0031-9163. Disponível em: <http://www.sciencedirect.com/science/article/pii/0031916364909679>. Cited at page 40.

TINKHAM, M. *Introduction to Superconductivity*. Second. [S.l.]: McGraw-Hill, 1996. Cited 4 times at page 18, 23, 25, and 27.

TRÄUBLE, H.; ESSMANN, U. Flux-line arrangement in superconductors as revealed by direct observation. *Journal of Applied Physics*, v. 39, n. 9, p. 4052–4059, 1968. Disponível em: <https://doi.org/10.1063/1.1656923>. Cited at page 24.

VAGOV, A. et al. Superconductivity between standard types: Multiband versus single-band materials. *Phys. Rev. B*, American Physical Society, v. 93, p. 174503, May 2016. Disponível em: <https://link.aps.org/doi/10.1103/PhysRevB.93.174503>. Cited 9 times at page 8, 9, 46, 47, 49, 50, 51, 56, and 69.

VAGOV, A. V. et al. Extended Ginzburg-Landau formalism: Systematic expansion in small deviation from the critical temperature. *Phys. Rev. B*, American Physical Society, v. 85, p. 014502, Jan 2012. Disponível em: <http://link.aps.org/doi/10.1103/PhysRevB.85.014502>. Cited 4 times at page 8, 9, 37, and 41.

WEBER, H. W.; SPORNA, J. F.; SEIDL, E. Transition from type-II to type-I superconductivity with magnetic field direction. *Phys. Rev. Lett.*, American Physical Society, v. 41, p. 1502–1506, Nov 1978. Disponível em: <https://link.aps.org/doi/10.1103/PhysRevLett.41.1502>. Cited 2 times at page 55 and 56.

APPENDIX A – ANALYTIC DETAILS OF THE EGL FORMALISM

This appendix contains the thorough derivation of the equations of motion of the thermal Green's functions. The generalization to an arbitrary number of bands is quite straightforward.

A.1 Equations of motion for the thermal Green functions

In order to derive the equations of motion of the field-operators one must calculate their commutators with the Hamiltonian operator, $\mathcal{H}_{BCS}$. For instance, one must combine the expression for the field-operators in the Heisenberg's picture:

$$\psi_\sigma(\vec{x},\mathrm{t}) = \exp(\mathcal{H}_{BCS}\mathrm{t}/\hbar)\ \psi_\sigma(\vec{x})\ \exp(-\mathcal{H}_{BCS}\mathrm{t}/\hbar), \tag{A.1}$$

$$\overline{\psi}_\sigma(\vec{x},\mathrm{t}) = \exp(\mathcal{H}_{BCS}\mathrm{t}/\hbar)\ \psi^\dagger_\sigma(\vec{x})\ \exp(-\mathcal{H}_{BCS}\mathrm{t}/\hbar) \tag{A.2}$$

and calculate their the commutator of these operators with $\mathcal{H}_{BCS}$. Also one must define the nature of the particles in question. In this case, it is defined to be the fermionic kind:

$$\left\{\psi_\sigma(\vec{x}), \psi^\dagger_{\sigma'}(\vec{x}')\right\} = \delta_{\sigma,\sigma'}\delta(\vec{x}-\vec{x}'), \tag{A.3}$$

$$\{\psi_\sigma(\vec{x}), \psi_{\sigma'}(\vec{x}')\} = 0. \tag{A.4}$$

The equation of motion for the destruction field-operator is

$$\begin{aligned}
-\hbar\partial_\mathrm{t}\psi_\uparrow(\vec{x},\mathrm{t}) &= [\psi_\uparrow(\vec{x},\mathrm{t}), \mathcal{H}_{BCS}] \\
&= \exp(\mathcal{H}_{BCS}\mathrm{t}/\hbar)\ [\psi_\uparrow(\vec{x}), \mathcal{H}_{BCS}]\ \exp(-\mathcal{H}_{BCS}\mathrm{t}/\hbar) \\
&= \exp(\mathcal{H}_{BCS}\mathrm{t}/\hbar)\left(\left[\psi_\uparrow(\vec{x}), \sum_\sigma \int d^D y\ \psi^\dagger_\sigma(\vec{y})\mathcal{T}_y\psi_\sigma(\vec{y})\right] + \right. \\
&\quad \left. + \left[\psi_\uparrow(\vec{x}), \int d^D y\ \psi^\dagger_\uparrow(\vec{y})\psi^\dagger_\downarrow(\vec{y})\Delta(\vec{y}) + \Delta^*(\vec{y})\psi_\downarrow(\vec{y})\psi_\uparrow(\vec{y})\right]\right)\exp(-\mathcal{H}_{BCS}\mathrm{t}/\hbar)
\end{aligned} \tag{A.5}$$

where it was used the fact that the comutator of an operator and its exponential operator is null.

The first equation of motion is calculated as the following[1]:

$$\begin{aligned}
\left[\psi_\uparrow(\vec{x}), \sum_\sigma \int d^D y\ \psi^\dagger_\sigma(\vec{y})\mathcal{T}_y\psi_\sigma(\vec{y})\right] &= \sum_\sigma \int d^D y \left[\psi_\uparrow(\vec{x}), \psi^\dagger_\sigma(\vec{y})\mathcal{T}_y\psi_\sigma(\vec{y})\right] \\
&= \sum_\sigma \int d^D y \left(\underbrace{\psi_\uparrow(\vec{x})\psi^\dagger_\sigma(\vec{y})}\mathcal{T}_y\psi_\sigma(\vec{y}) - \psi^\dagger_\sigma(\vec{y})\mathcal{T}_y\underbrace{\psi_\sigma(\vec{y})\psi_\uparrow(\vec{x})}\right) \\
&= \sum_\sigma \int d^D y \left(\left(\delta_{\uparrow,\sigma}\delta(\vec{x}-\vec{y}) - \psi^\dagger_\sigma(\vec{y})\psi_\uparrow(\vec{x})\right)\mathcal{T}_y\psi_\sigma(\vec{y}) - \psi^\dagger_\sigma(\vec{y})\mathcal{T}_y\psi_\sigma(\vec{y})\psi_\uparrow(\vec{x})\right) \\
&= \sum_\sigma \int d^D y \left(\delta_{\uparrow,\sigma}\delta(\vec{x}-\vec{y})\mathcal{T}_y\psi_\sigma(\vec{y}) + \psi^\dagger_\sigma(\vec{y})\mathcal{T}_y\psi_\sigma(\vec{y})\psi_\uparrow(\vec{x}) - \psi^\dagger_\sigma(\vec{y})\mathcal{T}_y\psi_\sigma(\vec{y})\psi_\uparrow(\vec{x})\right) \\
&= \mathcal{T}_x\psi_\uparrow(\vec{x}) \qquad \text{(A.6)}
\end{aligned}$$

and the second term as the following

$$\begin{aligned}
&\left[\psi_\uparrow(\vec{x}), \int d^D y \left(\psi^\dagger_\uparrow(\vec{y})\psi^\dagger_\downarrow(\vec{y})\Delta(\vec{y}) + \Delta^*(\vec{y})\psi_\downarrow(\vec{y})\psi_\uparrow(\vec{y})\right)\right] = \\
&= \int d^D y \left[\psi_\uparrow(\vec{x}), \psi^\dagger_\uparrow(\vec{y})\psi^\dagger_\downarrow(\vec{y})\Delta(\vec{y}) + \Delta^*(\vec{y})\psi_\downarrow(\vec{y})\psi_\uparrow(\vec{y})\right] \\
&= \int d^D y \left(\underbrace{\psi_\uparrow(\vec{x})\psi^\dagger_\uparrow(\vec{y})}\psi^\dagger_\downarrow(\vec{y})\Delta(\vec{y}) - \psi^\dagger_\uparrow(\vec{y})\underbrace{\psi^\dagger_\downarrow(\vec{y})\psi_\uparrow(\vec{x})}\Delta(\vec{y}) + \right. \\
&\quad \left. + \Delta^*(\vec{y})\underbrace{\psi_\uparrow(\vec{x})\psi_\downarrow(\vec{y})}\psi_\uparrow(\vec{y}) - \Delta^*(\vec{y})\psi_\downarrow(\vec{y})\underbrace{\psi_\uparrow(\vec{y})\psi_\uparrow(\vec{x})}\right) \\
&= \int d^D y \left(\left(\delta(\vec{x}-\vec{y}) - \psi^\dagger_\uparrow(\vec{y})\psi_\uparrow(\vec{x})\right)\psi^\dagger_\downarrow(\vec{y})\Delta(\vec{y}) + \psi^\dagger_\uparrow(\vec{y})\psi_\uparrow(\vec{x})\psi^\dagger_\downarrow(\vec{y})\Delta(\vec{y})\right. \\
&\quad \left. -\Delta^*(\vec{y})\psi_\downarrow(\vec{y})\psi_\uparrow(\vec{x})\psi_\uparrow(\vec{y}) + \Delta^*(\vec{y})\psi_\downarrow(\vec{y})\psi_\uparrow(\vec{x})\psi_\uparrow(\vec{y})\right) \\
&= \psi^\dagger_\downarrow(\vec{x})\Delta(\vec{x}) \qquad \text{(A.7)}
\end{aligned}$$

And finaly the equation of motion for the destruction field operator in the Heisenberg's picture is

$$\begin{aligned}
-\hbar\partial_t\psi_\uparrow(\vec{x},t) &= \exp(\mathcal{H}_{BCS}t/\hbar)\left[\mathcal{T}_x\psi_\uparrow(\vec{x}) + \psi^\dagger_\downarrow(\vec{x})\Delta(\vec{x})\right]\exp(-\mathcal{H}_{BCS}t/\hbar) \\
&= \mathcal{T}_x\psi_\uparrow(\vec{x},t) + \Delta(\vec{x})\overline{\psi}_\downarrow(\vec{x},t) \qquad \text{(A.8)}
\end{aligned}$$

In a similar way we can find the equation of motion for the creation operator in the Heisenberg's picture:

$$\begin{aligned}
&-\hbar\partial_t\overline{\psi}_\downarrow(\vec{x},t) = \left[\overline{\psi}_\downarrow(\vec{x},t), \mathcal{H}_{BCS}\right] \\
&= \exp(\mathcal{H}_{BCS}t/\hbar)\left[\psi^\dagger_\downarrow(\vec{x}), \mathcal{H}_{BCS}\right]\exp(-\mathcal{H}_{BCS}t/\hbar) \\
&= \exp(\mathcal{H}_{BCS}t/\hbar)\left(\left[\psi^\dagger_\downarrow(\vec{x}), \sum_\sigma \int d^D y\ \psi^\dagger_\sigma(\vec{y})\mathcal{T}_y\psi_\sigma(\vec{y})\right] + \right. \\
&\left. + \left[\psi^\dagger_\downarrow(\vec{x}), \int d^D y\ \psi^\dagger_\uparrow(\vec{y})\psi^\dagger_\downarrow(\vec{y})\Delta(\vec{y}) + \Delta^*(\vec{y})\psi_\downarrow(\vec{y})\psi_\uparrow(\vec{y})\right]\right)\exp(-\mathcal{H}_{BCS}t/\hbar) \qquad \text{(A.9)}
\end{aligned}$$

[1] The underbraces in the equation below indicate the terms where commutators are applied.

again, it was used the fact that the comutator of an operator and its exponential operator is null. The first commutator is calculated as

$$\begin{aligned}
\left[\psi_\downarrow^\dagger(\vec{x}), \sum_\sigma \int d^D y\ \psi_\sigma^\dagger(\vec{y})\mathcal{T}_y\psi_\sigma(\vec{y})\right] &= \sum_\sigma \int d^D y \left[\psi_\downarrow^\dagger(\vec{x}), \psi_\sigma^\dagger(\vec{y})\mathcal{T}_y\psi_\sigma(\vec{y})\right] \\
&= \sum_\sigma \int d^D y \left(\underbrace{\psi_\downarrow^\dagger(\vec{x})\psi_\sigma^\dagger(\vec{y})}\mathcal{T}_y\psi_\sigma(\vec{y}) - \psi_\sigma^\dagger(\vec{y})\mathcal{T}_y\underbrace{\psi_\sigma(\vec{y})\psi_\downarrow^\dagger(\vec{x})}\right) \\
&= \sum_\sigma \int d^D y \left(-\psi_\sigma^\dagger(\vec{y})\psi_\downarrow^\dagger(\vec{x})\mathcal{T}_y\psi_\sigma(\vec{y}) - \psi_\sigma^\dagger(\vec{y})\mathcal{T}_y\left(\delta_{\sigma,\downarrow}\delta(\vec{x}-\vec{y}) - \psi_\downarrow^\dagger(\vec{x})\psi_\sigma(\vec{y})\right)\right) \\
&= \sum_\sigma \int d^D y \left(-\psi_\sigma^\dagger(\vec{y})\psi_\downarrow^\dagger(\vec{x})\mathcal{T}_y\psi_\sigma(\vec{y}) + \psi_\sigma^\dagger(\vec{y})\psi_\downarrow^\dagger(\vec{x})\mathcal{T}_y\psi_\sigma(\vec{y}) - \psi_\sigma^\dagger(\vec{y})\delta_{\sigma,\downarrow}\mathcal{T}_y\delta(\vec{y}-\vec{x})\right) \\
&= -\mathcal{T}_x^*\psi_\downarrow^\dagger(\vec{x}),
\end{aligned} \tag{A.10}$$

where in the last step it was used that the only term changing sign is the one which involves the first derivative

$$\int d^D y \psi_\sigma^\dagger(\vec{y})\vec{A}(\vec{y})\cdot\vec{\nabla}\delta(\vec{y}-\vec{x}) = -\int d^D y \delta(\vec{y}-\vec{x})\vec{A}(\vec{y})\cdot\vec{\nabla}\psi_\sigma^\dagger(\vec{y}) = -\vec{A}\cdot\vec{\nabla}\psi_\sigma^\dagger(\vec{x}) \tag{A.11}$$

and thus the complex conjugate $\mathcal{T}_y^*$ appears in the final expression of Eq. A.10. The second term as the following

$$\begin{aligned}
&\left[\psi_\downarrow^\dagger(\vec{x}), \int d^D y \left(\psi_\uparrow^\dagger(\vec{y})\psi_\downarrow^\dagger(\vec{y})\Delta(\vec{y}) + \Delta^*(\vec{y})\psi_\downarrow(\vec{y})\psi_\uparrow(\vec{y})\right)\right] = \\
&= \int d^D y \left[\psi_\downarrow^\dagger(\vec{x}), \psi_\uparrow^\dagger(\vec{y})\psi_\downarrow^\dagger(\vec{y})\Delta(\vec{y}) + \Delta^*(\vec{y})\psi_\downarrow(\vec{y})\psi_\uparrow(\vec{y})\right] \\
&= \int d^D y \left(\underbrace{\psi_\downarrow^\dagger(\vec{x})\psi_\uparrow^\dagger(\vec{y})}\psi_\downarrow^\dagger(\vec{y})\Delta(\vec{y}) - \psi_\uparrow^\dagger(\vec{y})\underbrace{\psi_\downarrow^\dagger(\vec{y})\psi_\downarrow^\dagger(\vec{x})}\Delta(\vec{y}) + \right. \\
&\quad \left. + \Delta^*(\vec{y})\underbrace{\psi_\downarrow^\dagger(\vec{x})\psi_\downarrow(\vec{y})}\psi_\uparrow(\vec{y}) - \Delta^*(\vec{y})\psi_\downarrow(\vec{y})\underbrace{\psi_\uparrow(\vec{y})\psi_\downarrow^\dagger(\vec{x})}\right) \\
&= \int d^D y \left(-\psi_\uparrow^\dagger(\vec{y})\psi_\downarrow^\dagger(\vec{x})\psi_\downarrow^\dagger(\vec{y})\Delta(\vec{y}) + \psi_\uparrow^\dagger(\vec{y})\psi_\downarrow^\dagger(\vec{x})\psi_\downarrow^\dagger(\vec{y})\Delta(\vec{y}) + \right. \\
&\quad \left. + \Delta^*(\vec{y})\delta(\vec{x}-\vec{y})\psi_\uparrow(\vec{y}) - \Delta^*(\vec{y})\psi_\downarrow(\vec{y})\psi_\downarrow^\dagger(\vec{x})\psi_\uparrow(\vec{y}) + \Delta^*(\vec{y})\psi_\downarrow(\vec{y})\psi_\downarrow^\dagger(\vec{x})\psi_\uparrow(\vec{y})\right) \\
&= \Delta^*(\vec{x})\psi_\uparrow(\vec{x})
\end{aligned} \tag{A.12}$$

and finally the equation of motion for the creation field-operator in the Heisenberg's picture is:

$$-\hbar\partial_t\overline{\psi}_\downarrow(\vec{x},t) = -\mathcal{T}_x^*\overline{\psi}_\downarrow(\vec{x},t) + \Delta^*(\vec{x})\psi_\uparrow(\vec{x},t) \tag{A.13}$$

The set of equations of motion of the field operators can be written in matrix form as

$$-\hbar\partial_t\begin{pmatrix}\psi_\uparrow(\vec{x},t)\\ \overline{\psi}_\downarrow(\vec{x},t)\end{pmatrix} = \begin{pmatrix}\mathcal{T}_x & \Delta(\vec{x})\\ \Delta^*(\vec{x}) & -\mathcal{T}_x^*\end{pmatrix}\begin{pmatrix}\psi_\uparrow(\vec{x},t)\\ \overline{\psi}_\downarrow(\vec{x},t)\end{pmatrix} \tag{A.14}$$

One can obtain the equations of motion of the Green's functions from Eq. (2.10)

$$
\begin{aligned}
-\hbar\partial_\tau \mathcal{G}(\vec{x},\tau;\vec{x}',\tau') &= \partial_\tau \left\langle T_\tau \psi_\uparrow(\vec{x},\tau)\overline{\psi}_\uparrow(\vec{x}',\tau')\right\rangle = \\
&= \partial_\tau \left\langle \theta(\tau-\tau')\psi_\uparrow(\vec{x},\tau)\overline{\psi}_\uparrow(\vec{x}',\tau') - \theta(\tau'-\tau)\overline{\psi}_\uparrow(\vec{x}',\tau')\psi_\uparrow(\vec{x},\tau)\right\rangle = \\
&= \left\langle \left[\delta(\tau-\tau')\psi_\uparrow(\vec{x},\tau) + \theta(\tau-\tau')\partial_\tau\psi_\uparrow(\vec{x},\tau)\right]\overline{\psi}_\uparrow(\vec{x}',\tau') + \right. \\
&\quad \left. +\delta(\tau'-\tau)\overline{\psi}_\uparrow(\vec{x}',\tau')\psi_\uparrow(\vec{x},\tau) - \theta(\tau'-\tau)\overline{\psi}_\uparrow(\vec{x}',\tau')\partial_\tau\psi_\uparrow(\vec{x},\tau)\right\rangle = \\
&= \left\langle \delta(\tau-\tau')\left\{\psi_\uparrow(\vec{x},\tau),\overline{\psi}_\uparrow(\vec{x}',\tau')\right\} - \frac{1}{\hbar}\theta(\tau-\tau')\left[\mathcal{T}_x\psi_\uparrow(\vec{x},\tau) + \Delta(\vec{x})\overline{\psi}_\downarrow(\vec{x},\tau)\right]\times\right. \\
&\quad \left.\times\overline{\psi}_\uparrow(\vec{x}',\tau') + \frac{1}{\hbar}\theta(\tau'-\tau)\overline{\psi}_\uparrow(\vec{x}',\tau')\left[\mathcal{T}_x\psi_\uparrow(\vec{x},\tau) + \Delta(\vec{x})\overline{\psi}_\downarrow(\vec{x},\tau)\right]\right\rangle
\end{aligned}
\tag{A.15}
$$

where θ is the Heaviside's step function and we used the equation of motion for the destruction operator.

$$
\begin{aligned}
&-\hbar\partial_\tau \mathcal{G}(\vec{x},\tau;\vec{x}',\tau') = \\
&\quad = \delta(\tau-\tau')\delta(\vec{x}-\vec{x}') + \\
&\quad +\mathcal{T}_x\left(-\frac{1}{\hbar}\left\langle\theta(\tau-\tau')\psi_\uparrow(\vec{x},\tau)\overline{\psi}_\uparrow(\vec{x}',\tau') - \theta(\tau'-\tau)\overline{\psi}_\uparrow(\vec{x}',\tau')\psi_\uparrow(\vec{x},\tau)\right\rangle\right) \\
&\quad +\Delta(\vec{x})\left(-\frac{1}{\hbar}\left\langle\theta(\tau-\tau')\overline{\psi}_\downarrow(\vec{x},\tau)\overline{\psi}_\uparrow(\vec{x}',\tau') - \theta(\tau'-\tau)\overline{\psi}_\uparrow(\vec{x}',\tau')\overline{\psi}_\downarrow(\vec{x},\tau)\right\rangle\right) \\
&\quad = \delta(\tau-\tau')\delta(\vec{x}-\vec{x}') + \mathcal{T}_x\mathcal{G}(\vec{x},\tau;\vec{x}',\tau') + \Delta(\vec{x})\overline{\mathcal{F}}(\vec{x},\tau;\vec{x}',\tau')
\end{aligned}
\tag{A.16}
$$

We obtained a differential equation for the Green's Function $\mathcal{G}(\vec{x},\tau;\vec{x}',\tau')$. Note that, in this process, another Green's function $\overline{\mathcal{F}}(\vec{x},\tau;\vec{x}',\tau')$ emerged.

Let us obtain the equation of motion for this other Green's function

$$
\begin{aligned}
-\hbar\partial_\tau\overline{\mathcal{F}}(\vec{x},\tau;\vec{x}',\tau') &= \partial_\tau\left\langle T_\tau\overline{\psi}_\downarrow(\vec{x},\tau)\overline{\psi}_\uparrow(\vec{x}',\tau')\right\rangle = \\
&= \left\langle\delta(\tau-\tau')\overline{\psi}_\downarrow(\vec{x},\tau)\overline{\psi}_\uparrow(\vec{x}',\tau') + \theta(\tau-\tau')\partial_\tau\overline{\psi}_\downarrow(\vec{x},\tau)\overline{\psi}_\uparrow(\vec{x}',\tau') + \right. \\
&\quad \left. + \delta(\tau-\tau')\overline{\psi}_\downarrow(\vec{x},\tau)\overline{\psi}_\uparrow(\vec{x}',\tau') - \theta(\tau'-\tau)\overline{\psi}_\uparrow(\vec{x}',\tau')\partial_\tau\overline{\psi}_\downarrow(\vec{x},\tau)\right\rangle = \\
&= -\frac{1}{\hbar}\left\langle\theta(\tau-\tau')\left[-\mathcal{T}_x^*\overline{\psi}_\downarrow(\vec{x},\tau) + \Delta^*(\vec{x})\psi_\uparrow(\vec{x},\tau)\right]\overline{\psi}_\uparrow(\vec{x}',\tau') - \right. \\
&\quad \left. - \theta(\tau'-\tau)\overline{\psi}_\uparrow(\vec{x}',\tau')\left[-\mathcal{T}_x^*\overline{\psi}_\downarrow(\vec{x},\tau) + \Delta^*(\vec{x})\psi_\uparrow(\vec{x},\tau)\right]\right\rangle \Rightarrow
\end{aligned}
$$

$$
-\hbar\partial_\tau\overline{\mathcal{F}}(\vec{x},\tau;\vec{x}',\tau') = \Delta^*(\vec{x})\mathcal{G}(\vec{x},\tau;\vec{x}',\tau') - \mathcal{T}_x^*\overline{\mathcal{F}}(\vec{x},\tau;\vec{x}',\tau') \tag{A.17}
$$

For this Green's function we do not have δ function in the equation of motion, which is the reason why its is called "anomalous".

We can use matrix notation to condense these equations

$$-\hbar\partial_\tau \begin{pmatrix} \mathcal{G}(\vec{x},\tau;\vec{x}',\tau') \\ \overline{\mathcal{F}}(\vec{x},\tau;\vec{x}',\tau') \end{pmatrix} = \delta(\tau-\tau')\delta(\vec{x}-\vec{x}') \begin{pmatrix} 1 \\ 0 \end{pmatrix} + \underbrace{\begin{pmatrix} \mathcal{T}_x & \Delta(\vec{x}) \\ \Delta^*(\vec{x}) & -\mathcal{T}_x^* \end{pmatrix}}_{\mathcal{H}_{BdG}} \begin{pmatrix} \mathcal{G}(\vec{x},\tau;\vec{x}',\tau') \\ \overline{\mathcal{F}}(\vec{x},\tau;\vec{x}',\tau') \end{pmatrix} \tag{A.18}$$

In a similar way, we can calculate the system of equations for the other pair of Green's functions

$$-\hbar\partial_\tau \begin{pmatrix} \mathcal{F}(\vec{x},\tau;\vec{x}',\tau') \\ \overline{\mathcal{G}}(\vec{x},\tau;\vec{x}',\tau') \end{pmatrix} = \delta(\tau-\tau')\delta(\vec{x}-\vec{x}') \begin{pmatrix} 0 \\ 1 \end{pmatrix} + \begin{pmatrix} \mathcal{T}_x & \Delta(\vec{x}) \\ \Delta^*(\vec{x}) & -\mathcal{T}_x^* \end{pmatrix} \begin{pmatrix} \mathcal{F}(\vec{x},\tau;\vec{x}',\tau') \\ \overline{\mathcal{G}}(\vec{x},\tau;\vec{x}',\tau') \end{pmatrix} \tag{A.19}$$

And we can define a more general matrix which involves all Green's functions

$$G(\vec{x},\tau;\vec{x}',\tau') \equiv \begin{pmatrix} \mathcal{G}(\vec{x},\tau;\vec{x}',\tau') & \mathcal{F}(\vec{x},\tau;\vec{x}',\tau') \\ \overline{\mathcal{F}}(\vec{x},\tau;\vec{x}',\tau') & \overline{\mathcal{G}}(\vec{x},\tau;\vec{x}',\tau') \end{pmatrix}, \quad \check{1} \equiv \begin{pmatrix} 1 & 0 \\ 0 & 1 \end{pmatrix} \tag{A.20}$$

$$-\hbar\partial_\tau G(\vec{x},\tau;\vec{x}',\tau') = \delta(\tau-\tau')\delta(\vec{x}-\vec{x}')\check{1} + \mathcal{H}_{BdG}G(\vec{x},\tau;\vec{x}',\tau') \tag{A.21}$$

A.2 Main integrals of the EGL formalism

In this section the integrals appearing in the EGL formalism are derived in full detail. As described in chapter 2, the τ expansion of the relevant quantities is the best way of separating terms into the correct equation. Therefore, the all the integrals here are presented already within the expanded form.

A.2.1 Terms involving K_a

In the $\tau^{1/2}$ component of the gap expansion given by Eq. (2.47), appears the following integral[2]:

$$\begin{aligned} I_{a1} &= \int \mathrm{d}^3z K_a(\vec{z}) = -gT \lim_{\eta\to 0^+} \sum_\omega \int \mathrm{d}^3z \, \exp(-i\omega\eta)\mathcal{G}_\omega^{(0)}(\vec{z})\overline{\mathcal{G}}_\omega^{(0)}(-\vec{z}) = \\ &= -gT \lim_{\eta\to 0^+} \sum_\omega \int \mathrm{d}^3z \int \frac{\mathrm{d}^3k}{(2\pi)^3}\frac{\mathrm{d}^3k'}{(2\pi)^3} \exp(-i\omega\eta)\frac{\exp(i\vec{k}\cdot\vec{z})}{i\hbar\omega_n-\xi_k}\frac{\exp(-i\vec{k}'\cdot\vec{z})}{i\hbar\omega_n+\xi_{k'}} = \\ &= -gT \lim_{\eta\to 0^+} \sum_\omega \int \frac{\mathrm{d}^3k\mathrm{d}^3k'}{(2\pi)^3}\frac{\exp(-i\omega\eta)}{i\hbar\omega_n-\xi_k}\frac{\exp[-i\vec{x}\cdot(\vec{k}'-\vec{k})]}{i\hbar\omega_n+\xi_{k'}} \underbrace{\frac{1}{(2\pi)^3}\int \mathrm{d}^3y \, \exp[i\vec{y}\cdot(\vec{k}'-\vec{k})]}_{\delta(\vec{k}'-\vec{k})} \\ &= -gT \lim_{\eta\to 0^+} \sum_\omega \int \frac{\mathrm{d}^3k}{(2\pi)^3}\frac{\exp(-i\omega\eta)}{2\xi_k}\left(\frac{1}{i\hbar\omega_n-\xi_{k'}}-\frac{1}{i\hbar\omega_n+\xi_{k'}}\right) \end{aligned} \tag{A.22}$$

[2] This is the only term in which it is necessary to keep the limit of $\eta \to 0$. In all other terms the limit and the integrals are interchangeable.

As this integral cannot be directly solved, one must invert the summation over Matsubara frequencies and the integral over $\vec{k}$. The problem now is to calculate

$$\lim_{\eta\to 0^+}\sum_{\omega}\exp(-i\omega\eta)\frac{1}{i\hbar\omega\pm\xi_k}. \tag{A.23}$$

This can be done by the Matsubara's weighing function

$$f(z)=\frac{\mp\beta}{\exp(\pm\beta z)+1}\frac{\exp(-z\eta/\hbar)}{z\mp\xi_k} \tag{A.24}$$

Such that the contour integral along the paths described in Fig's. () produces the summation of Eq. (A.23)

$$\frac{1}{2\pi i}\lim_{\eta\to 0^+}\oint_C\frac{\mp\beta}{\exp(\pm\beta z)+1}\frac{\exp(-z\eta/\hbar)}{z\mp\xi_k}=\lim_{\eta\to 0^+}\sum_{\omega}\frac{\exp(-i\omega_n\eta)}{i\hbar\omega_n\mp\xi_k}+\frac{\beta}{\exp(\mp\beta\xi_k)+1}=0 \tag{A.25}$$

Therefore, the problem reduces to

$$\begin{aligned} I_{a1} &= -gT\int\frac{\mathrm{d}^3k}{(2\pi)^3}\left(-\frac{\beta}{\exp(-\beta\xi_k)+1}+\frac{\beta}{\exp(\beta\xi_k)+1}\right)\\ &= -g\int\frac{\mathrm{d}^3k}{(2\pi)^3}\frac{1}{2\xi_k}\frac{1-\exp(\beta\xi_k)}{\exp(\beta\xi_k)+1}=g\int\frac{\mathrm{d}^3k}{(2\pi)^3}\frac{1}{2\xi_k}\tanh(\beta\xi_k/2)\\ &= g\int_0^{\hbar\omega_D}\mathrm{d}\xi N(\xi)\frac{\tanh(\beta\xi/2)}{\xi}\approx gN(0)\int_0^{\hbar\beta\omega_D/2}\mathrm{d}x\frac{\tanh(x)}{x}. \end{aligned} \tag{A.26}$$

In general, the last integral cannot be solved in terms of known functions. As the physical limit of this formalism is restricted to the case when $\hbar\omega_D\gg T$, it can be approximated to

$$\begin{aligned} \int_0^{\hbar\beta\omega_D/2}\mathrm{d}x\frac{\tanh(x)}{x} &= \int_0^{\hbar\beta\omega_D/2}\mathrm{d}x\left[\frac{\mathrm{d}\ln(x)}{\mathrm{d}x}\right]\tanh(x)\approx\ln\left(\frac{\hbar\beta\omega_D}{2}\right)-\int_0^{\infty}\mathrm{d}x\ \ln(x)\sec^2(x)\\ &= \ln\left(\frac{\hbar\beta\omega_D}{2}\right)+\Gamma-\ln(\pi/4)=\ln\left(\frac{2e^{\gamma}\hbar\omega_D}{\pi T}\right). \end{aligned} \tag{A.27}$$

And finally,

$$I_{a1}=gN(0)\ln\left(\frac{2e^{\gamma}\hbar\omega_D}{\pi T}\right). \tag{A.28}$$

where $\gamma\approx 0.577$ is the Euler-Mascheroni constant.

The next integral related to K_a appears in the $\tau^{3/2}$ contribution

$$I_{a2}^{i,j}=\frac{1}{2!}\int\mathrm{d}^3z\ K_a(\vec{z})z_iz_j=-\frac{1}{2}gT\sum_{\omega}\int\mathrm{d}^3z\ \mathcal{G}_{\omega}^{(0)}(\vec{z})\overline{\mathcal{G}}_{\omega}^{(0)}(-\vec{z})z_iz_j. \tag{A.29}$$

By using a property of Fourier's transforms, the components of the vector $\vec{z}$ in the integrals can be expressed as derivatives in the Fourier space

$$\int \mathrm{d}^3z\ \exp(-i\vec{k}\cdot\vec{z})\mathcal{G}^{(0)}_\omega(\vec{z})z_j = \int \mathrm{d}\vec{z}\ (i\partial_{k_j})\exp(-i\vec{k}\cdot\vec{z})\mathcal{G}^{(0)}_\omega(\vec{z}) = i\partial_{k_j}\tilde{\mathcal{G}}^{(0)}_\omega(\vec{k}) \quad \text{(A.30)}$$

$$\int \mathrm{d}^3z\ \exp(-i\vec{k}\cdot\vec{z})\overline{\mathcal{G}}^{(0)}_\omega(-\vec{z})z_j = \int \mathrm{d}\vec{z}(i\partial_{k_j})\exp(-i\vec{k}\cdot\vec{z})\overline{\mathcal{G}}^{(0)}_\omega(-\vec{z}) = i\partial_{k_j}\overline{\mathcal{G}}^{(0)}_\omega(\vec{k}) \quad \text{(A.31)}$$

where $\mathcal{G}^{(0)}_\omega(\vec{k})$ and $\overline{\mathcal{G}}^{(0)}_\omega(\vec{k})$ are the Fourier's transform of the unperturbed Green's functions. Moreover, by the convolution theorem, the integral above can be rewritten in terms of the Fourier's transform of the unperturbed Green's functions[3], which gives

$$\begin{aligned} I^{i,j}_{a2} &= \frac{1}{2}gT\sum_\omega\int\frac{d^3k}{(2\pi)^3}\left(\partial_{k_i}\frac{1}{i\hbar\omega-\xi_k}\right)\left(\partial_{k_j}\frac{1}{i\hbar\omega+\xi_k}\right) \\ &= \frac{1}{2}gT\sum_\omega\int\frac{d^3k}{(2\pi)^3}\frac{-\frac{\hbar^2}{m}k_i}{(i\hbar\omega-\xi_k)^2}\frac{\frac{\hbar^2}{m}k_j}{(i\hbar\omega+\xi_k)^2} \end{aligned} \quad \text{(A.32)}$$

In the case of spherical Fermi surfaces the integrals are non-zero, clearly, only when $i = j$ and also k_i^2 can be substituted by $k^2/3$, then

$$\begin{aligned} I^{i,j}_{a2} &= \frac{\delta_{ij}}{3}gT\left(\frac{\hbar^2}{m}\right)\sum_\omega\int\frac{d^3k}{(2\pi)^3}\frac{\xi_k+\mu}{(\hbar^2\omega^2+\xi_k^2)^2} \\ &\approx \frac{\delta_{ij}}{3}gT\left(\frac{\hbar^2}{m}\right)N(0)\sum_\omega\int_{-\hbar\omega_D}^{\hbar\omega_D}d\xi\frac{\xi+\mu}{(\hbar^2\omega^2+\xi^2)^2}. \end{aligned} \quad \text{(A.33)}$$

By parity, one can easily reduce the expression above to[4]

$$\begin{aligned} I^{i,j}_{a2} &\approx \frac{\delta_{ij}}{3}gT\left(\frac{\hbar^2}{m}\right)\frac{mv_F^2}{2}N(0)\sum_\omega\frac{1}{|\hbar\omega|^3}\underbrace{\int_{-\infty}^{\infty}\frac{1}{(1+x^2)^2}}_{\pi/2} \\ &= \frac{\delta_{ij}}{3}gT\frac{\hbar^2v_F^2}{2}N(0)\frac{\pi}{2}\frac{2}{(2\pi T)^3}\underbrace{\sum_{n=1}^{\infty}\frac{1}{(n+1/2)^3}}_{7\zeta(3)} \\ &= \frac{\delta_{ij}}{6}\frac{7\zeta(3)}{8\pi^2T^2}\hbar^2v_F^2 = \delta_{ij}\mathcal{K}[1+2\tau+O(\tau^2)] \end{aligned} \quad \text{(A.34)–(A.35)}$$

In case of anisotropic Fermi surfaces, the terms with mixed components of the vector $\vec{z}$ can contribute to the final expression. This is not a critical issue in the elliptic

[3] In these derivations it is applied a generalization of the convolution theorem to more dimensions and products of more functions: given the convolution of two functions f and g with their respective Fourier transforms $\tilde{f}$ and $\tilde{g}$, $(f\otimes g)(z) = \int dx f(x)g(z-x)$, then $f\otimes g = \int dk\tilde{f}(z)\tilde{g}(k)\exp(-ikx)$.

[4] In the summation over the Matsubara's frequencies, one should rememner that $\sum_{n=1}^{\infty}\frac{1}{(n+1/2)^l} = (2^l-1)\zeta(l)$

case because one can find a new set of coordinates through a linear transformation in which these mixed terms are zero again. In this case, the dispersion relation becomes

$$\xi_k = \sum_j \frac{\hbar^2 k_j^2}{2m_j} - \mu \tag{A.36}$$

and, taking over from Eq. (A.32),

$$\begin{aligned} I_{a2}^{i,j} &= \frac{1}{2} gT \sum_\omega \int \frac{d^3k}{(2\pi)^3} \left(\partial_{k_i} \frac{1}{i\hbar\omega - \xi_k}\right)\left(\partial_{k_j} \frac{1}{i\hbar\omega + \xi_k}\right) \\ &= \frac{1}{2} gT \sum_\omega \int \frac{d^3k}{(2\pi)^3} \frac{-\frac{\hbar^2}{m_i} k_i}{(i\hbar\omega - \xi_k)^2} \frac{\frac{\hbar^2}{m_j} k_j}{(i\hbar\omega + \xi_k)^2} \end{aligned} \tag{A.37}$$

Now rescaling $\vec{k}$ in terms of the principal axis, it is obtained a spherical domain of integration

$$\tilde{k}_i = \sqrt{m_i} k_i \tag{A.38}$$

and thus the single electron energy becomes

$$\xi_{\tilde{k}} = \sum_q \frac{\hbar^2 k_q^2}{2m_q} = \left(\frac{\hbar^2 \tilde{k}^2}{2\tilde{m}}\right) \tag{A.39}$$

The symmetry of the integrand makes only diagonal terms ($i = j$) non-zero again and after making the change of variable $\frac{d^3\tilde{k}}{(2\pi)^3} \to N(\xi)d\xi$ (integrated up to the cut-off energy $\hbar\omega_c$), one can follow the same steps as in the isotropic case to arrive at

$$I_{a2}^{i,j} = \frac{1}{6} N(0) \frac{7\zeta(3)}{8\pi^2 T^2} \hbar^2 v_i^2 \delta_{i,j} = \mathcal{K}_i [1 + 2\tau + O(\tau^2)]. \tag{A.40}$$

A similar integral appears in the current equation but instead of having a second derivative of the gaps, one has first derivative of the gap and first derivative of the unperturbed Green functions.

The next term we analyse is

$$\int \mathrm{d}\vec{z} K_a(\vec{z}) \frac{\left(\vec{z} \cdot \vec{\nabla}\right)^4}{4!} \Delta(\vec{x}) = \int \mathrm{d}\vec{z} K_a(\vec{z}) \left[\frac{1}{4!} \sum_n z_n^4 \partial_n^4 + \frac{1}{8} \sum_{n \neq m} z_m z_n \partial_m \partial_n\right] \Delta(\vec{x}) \tag{A.41}$$

So we have to calculate two kinds of integrals

$$\int \mathrm{d}\vec{z} K_a(\vec{z}) z_n^4 \tag{A.42}$$

$$\int \mathrm{d}\vec{z} K_a(\vec{z}) z_n^2 z_m^2, \text{ where (m}\neq \text{n)}. \tag{A.43}$$

The first can be solved as

$$\int \mathrm{d}\vec{z} K_a(\vec{z}) z_n^4 \to \int \mathrm{d}\vec{z} K_a(\vec{z}) z_1^4 =$$
$$= \; gT\left[\frac{\pi N(0)}{k_F}\right]^2 \underbrace{\int_0^\infty \mathrm{d}z \frac{z^4}{\sinh(z/\xi_T)}}_{\xi_T^5 2(1-2^{-5})\Gamma(5)\zeta(5)} \underbrace{\int_{-1}^{1} \mathrm{d}(\cos\theta)\sin^4\theta}_{16/15} \underbrace{\int_0^{2\pi} \mathrm{d}\phi \cos^4\phi}_{3\pi/4} = \frac{4}{5} c\hbar^4 v_F^4 \quad \text{(A.44)}$$

and the second

$$\int \mathrm{d}\vec{z} K_a(\vec{z}) z_m^2 z_n^2 \to \int \mathrm{d}\vec{z} K_a(\vec{z}) z_1^2 z_2^2 =$$
$$= gT\left[\frac{\pi N(0)}{k_F}\right]^2 \underbrace{\int_0^\infty \mathrm{d}z \frac{z^4}{\sinh(z/\xi_T)}}_{\xi_T^5 2(1-2^{-5})\Gamma(5)\zeta(5)} \underbrace{\int_{-1}^{1} \mathrm{d}(\cos\theta)\sin^4\theta}_{16/15} \underbrace{\int_0^{2\pi} \mathrm{d}\phi \sin^2\phi\cos^2\phi}_{\pi/4} = \frac{4}{15} c\hbar^4 v_F^4. \quad \text{(A.45)}$$

The final expression becomes

$$\int \mathrm{d}\vec{z} K_a(\vec{z}) \frac{\left(\vec{z}\cdot\vec{\nabla}\right)^4}{4!} \Delta(\vec{x}) = \frac{c}{30}\hbar^4 v_F^4 \left[\sum_n \partial_n^2 + \sum_{n\neq m} \partial_m^2 \partial_n^2\right] \overline{\Delta}(\vec{x}) = Q\nabla^2(\nabla^2\Delta). \quad \text{(A.46)}$$

A.2.2 Terms involving K_b

The first integral related to the kernel K_b appears in the gap expansion, Eq. (2.47), in the form

$$b_1 = \int \mathrm{d}^3 y_1 \mathrm{d}^3 y_2 \mathrm{d}^3 y_3 K_b(\vec{x}, \vec{y}_1, \vec{y}_2, \vec{y}_3) \quad \text{(A.47)}$$
$$= -gT \sum_\omega \int \mathrm{d}^3 y_1 \mathrm{d}^3 y_2 \mathrm{d}^3 y_3 \mathcal{G}_\omega^{(0)}(\vec{x}, \vec{y}_1) \overline{\mathcal{G}}_\omega^{(0)}(\vec{y}_1, \vec{y}_2) \mathcal{G}_\omega^{(0)}(\vec{y}_2, \vec{y}_3) \overline{\mathcal{G}}_\omega^{(0)}(\vec{z}_3, \vec{x}) \quad \text{(A.48)}$$

and the convolution theorem can be applied in order to express this expression in terms of the Fourier transforms of the unperturbed Green's functions

$$b_1 = -gT \sum_\omega \int \frac{\mathrm{d}^3 k}{(2\pi)^3} \frac{1}{(i\hbar\omega_n - \xi_k)^2} \frac{1}{(i\hbar\omega_n + \xi_k)^2}$$
$$\approx -gT \sum_\omega N(0) \int_{-\hbar\omega_D}^{\hbar\omega_D} d\xi \frac{1}{(\hbar^2\omega_n^2 + \xi^2)^2} \approx -gT \sum_\omega \frac{1}{|\hbar\omega|^3} 2 \underbrace{\int_0^\infty \frac{1}{(1+x^2)^2}}_{\pi/4}$$
$$= -gN(0)T \frac{\pi}{2\hbar^3\pi^3} 2 \sum_{n=0}^{\infty} \frac{\beta^3\hbar^3}{(2n+1)^3} = -gN(0)\frac{7\zeta(3)}{8\pi^2 T^2} \quad \text{(A.49)}$$

The next term involving involving K_b is of order $\tau^{5/2}$ and then one must consider that three Δ's appear in this kernel,which gives already a $\tau^{3/2}$ exponent remaining two gradient operators (coming from the Taylor expansions) which might appear in the forms

$$\left(\vec{z}\cdot\vec{\nabla}\right)\Delta(\vec{x}) = \sum_n z_n \partial_n \Delta(\vec{x}) \tag{A.50}$$

or

$$\left(\vec{z}\cdot\vec{\nabla}\right)^2\Delta(\vec{x}) = \sum_{mn} z_m z_n \partial_m \partial_n \Delta(\vec{x}). \tag{A.51}$$

The symmetry of the kernel allows us to solve integrals for a given pair of components z_m, z_n and extend the result to other direction. Essentially, different terms appear from the gap expansion, which produce some kinds of integrals, in summary they are

$$\int \prod_{j=1}^{3} \mathrm{d}\vec{z}_j K_b\left(\{\vec{z}\}_3\right)\left[\left(\vec{z}_1\cdot\vec{\nabla}\right)\Delta(\vec{x})\right]\Delta^*(\vec{x})\left[\left(\vec{z}_3\cdot\vec{\nabla}\right)\Delta(\vec{x})\right] \Rightarrow \int \prod_{j=1}^{3} \mathrm{d}\vec{z}_j K_b\left(\{\vec{z}\}_3\right) z_{1m} z_{3n} \tag{A.52}$$

$$\int \prod_{j=1}^{3} \mathrm{d}\vec{z}_j K_b\left(\{\vec{z}\}_3\right)\left[\left(\vec{z}_1\cdot\vec{\nabla}\right)\Delta(\vec{x})\right]\left[\left(\vec{z}_2\cdot\vec{\nabla}\right)\Delta^*(\vec{x})\right]\Delta(\vec{x}) \Rightarrow \int \prod_{j=1}^{3} \mathrm{d}\vec{z}_j K_b\left(\{\vec{z}\}_3\right) z_{1m} z_{2n} \tag{A.53}$$

$$\int \prod_{j=1}^{3} \mathrm{d}\vec{z}_j K_b\left(\{\vec{z}\}_3\right)|\Delta(\vec{x})|^2 \frac{\left(\vec{z}_1\cdot\vec{\nabla}\right)^2}{2!}\Delta(\vec{x}) \Rightarrow \int \prod_{j=1}^{3} \mathrm{d}\vec{z}_j K_b\left(\{\vec{z}\}_3\right) z_{1m} z_{1n} \tag{A.54}$$

$$\int \prod_{j=1}^{3} \mathrm{d}\vec{z}_j K_b\left(\{\vec{z}\}_3\right)\Delta^2(\vec{x}) \frac{\left(\vec{z}_2\cdot\vec{\nabla}\right)^2}{2!}\Delta^*(\vec{x}) \Rightarrow \int \prod_{j=1}^{3} \mathrm{d}\vec{z}_j K_b\left(\{\vec{z}\}_3\right) z_{2m} z_{2n} \tag{A.55}$$

Because of the symmetry of K_b and the relation

$$\overline{\mathcal{G}}^{(0)}_{\omega}(\vec{z}) = -\mathcal{G}^{(0)}_{-\omega}(-\vec{z}), \tag{A.56}$$

we can permute $\vec{z}_1$ and $\vec{z}_3$ as

$$\begin{aligned} K_b\left(\vec{z}_1,\vec{z}_2,\vec{z}_3\right) &= -gT\sum_{\omega}\mathcal{G}^{(0)}_{\omega}(-\vec{z}_1)\overline{\mathcal{G}}^{(0)}_{\omega}(\vec{z}_1-\vec{z}_2)\mathcal{G}^{(0)}_{\omega}(\vec{z}_2-\vec{z}_3)\overline{\mathcal{G}}^{(0)}_{-\omega}(\vec{z}_3) \\ &= -gT\sum_{\omega}\overline{\mathcal{G}}^{(0)}_{-\omega}(\vec{z}_1)\mathcal{G}^{(0)}_{-\omega}(\vec{z}_2-\vec{z}_1)\overline{\mathcal{G}}^{(0)}_{-\omega}(\vec{z}_3-\vec{z}_2)\mathcal{G}^{(0)}_{-\omega}(-\vec{z}_3) = \\ &= -gT\sum_{\omega}\mathcal{G}^{(0)}_{-\omega}(-\vec{z}_3)\overline{\mathcal{G}}^{(0)}_{-\omega}(\vec{z}_3-\vec{z}_2)\mathcal{G}^{(0)}_{-\omega}(\vec{z}_2-\vec{z}_1)\overline{\mathcal{G}}^{(0)}_{-\omega}(\vec{z}_1) = \\ &= K_b\left(\vec{z}_3,\vec{z}_2,\vec{z}_1\right) \end{aligned} \tag{A.57}$$

Each of these terms can be cast in terms of the Fourier transforms of the unperturbed Greens functions[5]

$$\begin{aligned}
\int \prod_{j=1}^{3} \mathrm{d}\vec{z}_j K_b\left(\{\vec{z}\}_3\right) z_{1m} z_{3n} &= gT \sum_{\omega} \int \prod_{j=1}^{3} \mathrm{d}\vec{z}_j (-z_{1m}) \mathcal{G}_{\omega}^{(0)}(-\vec{z}_1) \overline{\mathcal{G}}_{\omega}^{(0)}(\vec{z}_1 - \vec{z}_2) \times \\
&\quad \times \mathcal{G}_{\omega}^{(0)}(\vec{z}_2 - \vec{z}_3) z_{3n} \overline{\mathcal{G}}_{\omega}^{(0)}(\vec{z}_3) \\
&= gT \sum_{\omega} \int \frac{\mathrm{d}^3 k}{(2\pi)^3} \left[(i\partial_{k_m}) \frac{1}{i\hbar\omega - \xi_k} \right] \frac{1}{i\hbar\omega + \xi_k} \frac{1}{i\hbar\omega - \xi_k} \left[(-i\partial_{k_n}) \frac{1}{i\hbar\omega + \xi_k} \right] \\
&= gT \sum_{\omega} \int \frac{\mathrm{d}^3 k}{(2\pi)^3} \frac{-\frac{\hbar^2}{m} k_m}{(i\hbar\omega - \xi_k)^2} \frac{1}{i\hbar\omega + \xi_k} \frac{1}{i\hbar\omega - \xi_k} \left[-\frac{-\frac{\hbar^2}{m} k_n}{(i\hbar\omega + \xi_k)^2} \right] \\
&= gT \frac{\hbar^2}{m} \frac{2}{3} N(0) \delta_{mn} \sum_{\omega} \int_{-\infty}^{\infty} \mathrm{d}\xi \frac{2(\xi + \mu)}{(-\hbar^2\omega^2 - \xi^2)^3} \\
&= -gT \frac{\hbar^4 k_F^2}{m^2} \frac{2}{3} N(0) \delta_{mn} \sum_{\omega} \int_{-\infty}^{\infty} \mathrm{d}\xi \frac{1}{(\hbar^2\omega^2 + \xi^2)^3},
\end{aligned} \tag{A.58}$$

and

$$\begin{aligned}
\int \prod_{j=1}^{3} \mathrm{d}\vec{z}_j K_b\left(\{\vec{z}\}_3\right) z_{1m} z_{3n} &= -gT \frac{2}{3} N(0) \hbar^2 v_F^2 \delta_{mn} \underbrace{\sum_{\omega} \frac{1}{|\hbar\omega|^5}}_{31\zeta(5)/(2\pi T)^5} \underbrace{\int_{-\infty}^{\infty} \mathrm{d}\alpha \frac{1}{(1+\alpha^2)^3}}_{3\pi/8} \\
&= -\underbrace{\frac{gN(0)}{128\pi^4 T^4} 31\zeta(5)}_{c/3} \hbar^2 v_F^2 \delta_{mn}.
\end{aligned} \tag{A.59}$$

So we have

$$\begin{aligned}
&\int \prod_{j=1}^{3} \mathrm{d}\vec{z}_j K_b\left(\{\vec{z}\}_3\right) \left[\left(\vec{z}_1 \cdot \overline{\nabla}\right) \overline{\Delta}(\vec{x}) \right] \overline{\Delta}^*(\vec{x}) \left[\left(\vec{z}_3 \cdot \overline{\nabla}\right) \overline{\Delta}(\vec{x}) \right] \\
&\quad = -\frac{c}{3} \hbar^2 v_F^2 [1 + O(\tau)] \sum_{mn} \overline{\Delta}^*(\vec{x}) \delta_{mn} \partial_m \overline{\Delta}(\vec{x}) \partial_n \overline{\Delta}(\vec{x}) = -\frac{c}{3} \hbar^2 v_F^2 [1 + O(\tau)] \overline{\Delta}^*(\vec{x}) \left[\overline{\nabla} \overline{\Delta}(\vec{x}) \right]^2
\end{aligned} \tag{A.60}$$

For terms involving $\vec{z}_2$, we rewrite them as

$$z_{2n} z_{1m} = (z_{1n} - z_{1n} + z_{2n}) z_{1m} = (-z_{1n})(-z_{1m}) + (z_{1n} - z_{2n})(-z_{1m}) \tag{A.61}$$

$$\begin{aligned}
z_{2n} z_{2m} &= (-z_{2n})(-z_{2m}) = (z_{1n} - z_{1n} - z_{2n})(z_{1m} - z_{1m} - z_{2m}) \\
&= (z_{1n} - z_{2n})(z_{1m} - z_{2m}) + (z_{1n} - z_{2n})(-z_{1m}) + (z_{1m} - z_{2m})(-z_{1n}) + (-z_{1m})(-z_{1n})
\end{aligned} \tag{A.62}$$

[5] We used the useful property of Fourier transforms: $\int \mathrm{d}^3 z f(\vec{z}) z_m^l \mathrm{e}^{-i\vec{k}\cdot\vec{z}} = \int \mathrm{d}^3 z f(\vec{z}) (i\partial_{k_m})^l \mathrm{e}^{-i\vec{k}\cdot\vec{z}} = (i\partial_{k_m})^l \int \mathrm{d}^3 z f(\vec{z}) \mathrm{e}^{-i\vec{k}\cdot\vec{z}} = (i\partial_{k_m})^l F(\vec{k})$.

thus

$$
\begin{aligned}
&= -gT\sum_{\omega}\int\frac{\mathrm{d}^3k}{(2\pi)^3}\frac{1}{i\hbar\omega-\xi_k}\left[(i\partial_{k_m})(i\partial_{k_n})\frac{1}{i\hbar\omega+\xi_k}\right]\frac{1}{i\hbar\omega-\xi_k}\frac{1}{i\hbar\omega+\xi_k}\\
&\quad - gT\sum_{\omega}\int\frac{\mathrm{d}^3k}{(2\pi)^3}\left[(-i\partial_{k_m})\frac{1}{i\hbar\omega-\xi_k}\right]\left[(i\partial_{k_n})\frac{1}{i\hbar\omega+\xi_k}\right]\frac{1}{i\hbar\omega-\xi_k}\frac{1}{i\hbar\omega+\xi_k}\\
&\quad - gT\sum_{\omega}\int\frac{\mathrm{d}^3k}{(2\pi)^3}\left[(-i\partial_{k_n})\frac{1}{i\hbar\omega-\xi_k}\right]\left[(i\partial_{k_m})\frac{1}{i\hbar\omega+\xi_k}\right]\frac{1}{i\hbar\omega-\xi_k}\frac{1}{i\hbar\omega+\xi_k}\\
&\quad - gT\sum_{\omega}\int\frac{\mathrm{d}^3k}{(2\pi)^3}\left[(-i\partial_{k_m})(-i\partial_{k_n})\frac{1}{i\hbar\omega-\xi_k}\right]\frac{1}{i\hbar\omega+\xi_k}\frac{1}{i\hbar\omega-\xi_k}\frac{1}{i\hbar\omega+\xi_k} \qquad \text{(A.63)}\\
&= gT\sum_{\omega}\int\frac{\mathrm{d}^3k}{(2\pi)^3}\frac{1}{i\hbar\omega-\xi_k}\left[2\frac{\left(-\frac{\hbar^2}{m}\right)^2k_mk_n}{(i\hbar\omega+\xi_k)^3}-\frac{-\frac{\hbar^2}{m}\delta_{mn}}{(i\hbar\omega+\xi_k)^2}\right]\frac{1}{i\hbar\omega-\xi_k}\frac{1}{i\hbar\omega+\xi_k}-\\
&\quad - gT\sum_{\omega}\int\frac{\mathrm{d}^3k}{(2\pi)^3}\frac{-\frac{\hbar^2}{m}k_m}{(i\hbar\omega-\xi_k)^2}\left[-\frac{-\frac{\hbar^2}{m}k_n}{(i\hbar\omega+\xi_k)^2}\right]\frac{1}{i\hbar\omega-\xi_k}\frac{1}{i\hbar\omega+\xi_k}-\\
&\quad - gT\sum_{\omega}\int\frac{\mathrm{d}^3k}{(2\pi)^3}\frac{-\frac{\hbar^2}{m}k_n}{(i\hbar\omega-\xi_k)^2}\left[-\frac{-\frac{\hbar^2}{m}k_m}{(i\hbar\omega+\xi_k)^2}\right]\frac{1}{i\hbar\omega-\xi_k}\frac{1}{i\hbar\omega+\xi_k}+\\
&\quad + gT\sum_{\omega}\int\frac{\mathrm{d}^3k}{(2\pi)^3}\left[2\frac{\left(-\frac{\hbar^2}{m}\right)^2k_mk_n}{(i\hbar\omega-\xi_k)^3}-\frac{-\frac{\hbar^2}{m}\delta_{mn}}{(i\hbar\omega-\xi_k)^2}\right]\frac{1}{i\hbar\omega+\xi_k}\frac{1}{i\hbar\omega-\xi_k}\frac{1}{i\hbar\omega+\xi_k}
\end{aligned}
$$

(A.64)

And finally

$$\int \prod_{j=1}^{3} \mathrm{d}\vec{z}_j K_b\left(\{\vec{z}\}_3\right) z_{2m} z_{2n} =$$

$$= gN(0)T \sum_{\omega} \int_{-\infty}^{\infty} \mathrm{d}\xi \left[2\frac{\left(-\frac{\hbar^2}{m}\right)^2 \frac{k^2}{3}\delta_{mn}}{(\hbar^2\omega^2+\xi^2)^4}(i\hbar\omega-\xi)^2 - \frac{-\frac{\hbar^2}{m}\delta_{mn}}{(-\hbar^2\omega^2-\xi^2)^3}(i\hbar\omega-\xi) \right]$$

$$+ 2gN(0)T \sum_{\omega} \int_{-\infty}^{\infty} \mathrm{d}\xi \frac{\left(-\frac{\hbar^2}{m}\right)^2 \frac{k^2}{3}\delta_{mn}}{(\hbar^2\omega^2+\xi^2)^4}(\hbar^2\omega^2+\xi^2)+$$

$$+ gN(0)T \sum_{\omega} \int_{-\infty}^{\infty} \mathrm{d}\xi \left[2\frac{\left(-\frac{\hbar^2}{m}\right)^2 \frac{k^2}{3}\delta_{mn}}{(\hbar^2\omega^2+\xi^2)^4}(i\hbar\omega+\xi)^2 - \frac{-\frac{\hbar^2}{m}\delta_{mn}}{(-\hbar^2\omega^2-\xi^2)^3}(i\hbar\omega+\xi) \right] \tag{A.65}$$

$$= gN(0)T\frac{2}{3}\left(-\frac{\hbar^2}{m}\right) \sum_{\omega} \int_{-\infty}^{\infty} \mathrm{d}\xi \frac{2(\xi+\mu)(-\hbar^2\omega^2+3\xi^2)\delta_{mn}}{(\hbar^2\omega^2+\xi^2)^4} =$$

$$= -gN(0)T\frac{2}{3}\frac{\hbar^2}{m}\frac{\hbar^2 k_F^2}{m} \sum_{\omega} \int_{-\infty}^{\infty} \mathrm{d}\xi \frac{(-\hbar^2\omega^2+3\xi^2)\delta_{mn}}{(\hbar^2\omega^2+\xi^2)^4} =$$

$$= -gN(0)T\frac{2}{3}\hbar^2 v_F^2 \delta_{mn} \underbrace{\sum_{\omega} \frac{1}{|\hbar\omega|^5}}_{31\zeta(5)/(2\pi T)^5} \underbrace{\int_{-\infty}^{\infty} \mathrm{d}\alpha \frac{(3\alpha^2-1)}{(1+\alpha^2)^4}}_{-\pi/8} = gN(0)\frac{31\zeta(5)}{3\times 128\pi^4 T^4}\hbar^2 v_F^2 \delta_{mn}$$

$$= \frac{c\hbar^2 v_F^2}{9}[1+O(\tau)]\delta_{mn} = \mathcal{L}[1+O(\tau)]\delta_{mn} \tag{A.66}$$

which produces the coefficient $\mathcal{L}$ of the EGL formalism

$$\int \prod_{j=1}^{3} \mathrm{d}\vec{z}_j K_b\left(\{\vec{z}\}_3\right) \Delta^2(\vec{x}) \frac{\left(\vec{z}_2\cdot\vec{\nabla}\right)^2}{2!}\Delta^*(\vec{x})$$

$$= -\mathcal{L}\sum_{mn} \delta_{mn}\Delta^2(\vec{x})\partial_m\partial_n\Delta^*(\vec{x}) = -\mathcal{L}\Delta^2(\vec{x})\vec{\nabla}^2\Delta^*(\vec{x}) \tag{A.67}$$

and can be similarly calculated for the other terms involving second derivatives and

three gaps.

A.2.3 Terms involving K_c

This last term involves only one term of the order $\tau^{5/2}$:

$$
\begin{aligned}
c_1 &= \int \prod_{j=1}^{5} \mathrm{d}\vec{z}_j K_c\left(\{\vec{z}\}_5\right) = \\
&= -gT \int \prod_{j=1}^{5} \mathrm{d}\vec{z}_j \sum_{\omega} \exp(-i\omega\eta)\mathcal{G}_{\omega}^{(0)}(-\vec{z}_1)\overline{\mathcal{G}}_{\omega}^{(0)}(\vec{z}_1,\vec{z}_2)\times \\
&\qquad \times = \mathcal{G}_{\omega}^{(0)}(\vec{z}_2,\vec{z}_3)\overline{\mathcal{G}}_{\omega}^{(0)}(\vec{z}_3,\vec{z}_4)\mathcal{G}_{\omega}^{(0)}(\vec{z}_4,\vec{z}_5)\overline{\mathcal{G}}_{\omega}^{(0)}(\vec{z}_5) = \\
&= -gT \sum_{\omega} \int \frac{\mathrm{d}^D k}{(2\pi)^D} \left[\frac{1}{(i\hbar\omega - \xi_k)(i\hbar\omega + \xi_k)}\right]^3 = gT \sum_{\omega} \int \frac{\mathrm{d}^D k}{(2\pi)^D} \frac{1}{(\hbar^2\omega^2 + \xi_k^2)^3} = \\
&= 2gN(0)T \underbrace{\sum_{n=0}^{\infty} \frac{1}{|\pi T(2n+1)|^5}}_{31\zeta(5)/(2\pi T)^5} \underbrace{\int_{-\infty}^{\infty} \mathrm{d}x \frac{1}{(1+x^2)^3}}_{3\pi/8} = N(0)\frac{93\zeta(5)}{128\pi^4 T^4} \\
&= \underbrace{\frac{93\zeta(5)N(0)}{128\pi^4 T_c^4}}_{\equiv c}[1 + O(\tau)]
\end{aligned}
\tag{A.68}
$$

APPENDIX B – SCIENTIFIC PUBLICATIONS PRODUCED DURING THE DOCTORAL COURSE

B.1 Publications related to the Thesis

PHYSICAL REVIEW B **96**, 134521 (2017)

Multiband superconductors: Disparity between band length scales

Tiago T. Saraiva, C. C. de Souza Silva, J. Albino Aguiar, and A. A. Shanenko
Departamento de Física, Universidade Federal de Pernambuco, Av. Jorn. Aníbal Fernandes, s/n, Cidade Universitária 50740-560, Recife, PE, Brazil
(Received 30 January 2017; published 27 October 2017)

Multiple condensates in a superconducting material can interfere constructively or destructively and this leads to unconventional effects not inherent in single-band superconductors. Such effects can be pronounced when the spatial scales (healing lengths) of different band condensates deviate from each other. Here we show that, contrary to usual expectations, this deviation can be considerable even far beyond the regime of nearly decoupled bands, being affected by difference between the band Fermi velocities. Our study is performed within the extended Ginzburg-Landau (GL) formalism that goes to one order beyond the GL theory in the perturbation expansion of the microscopic equations over the proximity to T_c. The formalism makes it possible to obtain closed analytical results for the profiles of the band condensates and for their healing lengths and, at the same time, captures the difference between the healing lengths which does not appear in the standard GL domain.

DOI: 10.1103/PhysRevB.96.134521

I. INTRODUCTION

Interest in spatial scales of the contributing band condensates in multiband superconductors arises in the context of a search for unusual physics not inherent in single-band materials. When coexisting in one system, multiple condensates can interfere (interact) constructively or destructively and this may lead to unusual coherent phenomena [1] such as, e.g., fractional vortices [2–7], chiral solitons [8,9], a hidden criticality [10], an enhancement of the intertype superconductivity [11], a giant paramagnetic Meissner effect [12], broken-symmetry vortex patterns [13], etc. Such phenomena are sensitive to the difference between the coherence length scales of available bands and one can expect that the most promising regime for observing exotic superconducting phenomena is when the spatial profiles of different band condensates mismatch. For example, one can imagine two coexisting superconducting condensates with so different healing lengths that these condensates, when taken separately, belong to superconductivity types I and II. Then, the question arises about the superconductivity type of the aggregate condensate that incorporates so different coherent entries. This question has lead to the assumption about a special multiband superconductivity type [14] and stimulated intense debates in the literature (see Refs. [15–17] and references therein). The consequent microscopic calculations proved that the classification of the superconductivity types does not change in multiband superconductors [11]. However, the intertype domain, located in the phase diagram between types I and II and negligible in single-band superconductors, tends to expand significantly in the presence of multiple bands with competing spatial scales [11]. The intertype superconductivity is governed by the Bogomolnyi self-duality [18,19] resulting in exotic flux configurations such as lattices of superconducting islands, labyrinths of vortices, and mixtures of vortex clusters and giant vortices [20]. Thus the appearance of the competing band length scales can dramatically change the superconductor magnetic properties as compared to those in single-band materials.

It has been known [21] since the 1960s but also confirmed recently [16,17] that the spatial profiles of different band condensates in multiband superconductors are the same in the Ginzburg-Landau (GL) domain, i.e., when only contributions to the band superconducting gaps of order $\tau^{1/2}$ are included (with $\tau = 1 - T/T_c$ the proximity to the critical temperature). However, a general analysis of the τ expansion of the two-band BCS equations [17,22] has revealed that the spatially dependent band gaps are not any longer proportional to one another when contributions of order $\tau^{3/2}$ and higher are incorporated. In other words, the healing lengths of band condensates are generally different in multiband superconductors and this difference disappears only in the limit $T \to T_c$. This result has been confirmed [23] by numerical investigations of the two-band extended GL (EGL) formalism [17,22] that goes to one order beyond the GL theory in the τ expansion of the microscopic equations. It is also in agreement with the analysis of the long-range asymptotes of superconducting gaps in the single-vortex solution of two-gap systems [24].

Recently the band healing lengths have been extracted from experimental data for several two-band superconducting compounds. By fitting the results for the spatial distribution of the zero-bias DOS (density of states) in $NbSe_2$, $NbSe_{1.8}S_{0.2}$, and $CaKFe_4As_4$ [25,26], it has been found that the two-band healing lengths are close to one another in these materials even down to low temperatures $T \ll T_c$. Based on numerical investigations of the two-band Eilenberger equations and keeping in mind those experimental findings, the authors of Ref. [27] have suggested that the band healing lengths remain close to each other below T_c in general and this "locking of the length scales" is released only for nearly decoupled bands. According to Ref. [27], such a regime is approached when the interband coupling is by an order of magnitude smaller than the intraband couplings.

In the present work we demonstrate that in fact the band healing lengths can significantly deviate from each other far beyond the regime of nearly decoupled bands. This deviation is governed by disparity between the band Fermi velocities. Notice that the dependence of the healing lengths on the characteristic velocities has not been studied in much detail, especially in the case of significant interaction between band condensates. The investigation of Ref. [27] was focused on effects of the interband coupling only. From the asymptotic results of Ref. [24] one can see that the spatial profiles of the

band condensates are sensitive to the band Fermi velocities but the related calculations have been done for extremely small interband couplings; see Fig. 3 in Ref. [24].

Our calculations are performed for a clean two-band system with the s-wave pairing and spherical Fermi surfaces in both bands. The present study does not focus on a particular superconducting material but considers general trends of the band-dependent corrections to the GL coherence length as functions of the band Fermi velocities and interband coupling. Our investigation is done within the EGL formalism [17,22,28], where the lowest contribution of order $\tau^{1/2}$ and the leading correction of order $\tau^{3/2}$ are included in superconducting band-dependent gaps. The main ideas of this approach are similar to those realized in the 1970s for single-band superconductors by Jacobs [29–32], who introduced the τ expansion to correct the so-called Neumann-Tewordt functional [33,34]. (An interested reader can find relevant details in Ref. [11].) Including the perturbative corrections to the GL equations does not simply improve the accuracy of quantitative results but allows for capturing effects that are not accessible in the standard GL approach. As already mentioned above, the difference between the band healing lengths in multiband superconductors is one of such fundamental effects. We employ the perturbation expansion in τ rather than the full microscopic equations because the deviation between the band length scales beyond the regime of nearly decoupled bands is clearly seen already when including corrections of order $\tau^{3/2}$ in superconducting gaps. Furthermore, the perturbative approach yields closed analytical expressions for the spatial profiles of the band condensates and their healing lengths. This allows for a deeper insight on how the band length scales depend on microscopic parameters and will certainly be appealing to experimentalists, as our conclusions are relevant for the spatial distribution of the superconducting condensate in the vortex core of multiband materials.

Our paper is organized as follows. In Sec. II we introduce an analytical solution to the EGL formalism which makes it possible to explicitly find the leading correction in τ to the GL coherence length. To simplify our presentation, we first discuss the single-band case where calculations and resulting expressions are relatively simpler. In Sec. III we generalize the solution to the case of two contributing bands. Based on this generalization, we again calculate the leading correction to the GL coherence length but now this correction becomes band dependent. Then we investigate the band healing lengths as functions of the relevant microscopic parameters. Our conclusions are given in Sec. IV.

II. ANALYTICAL SOLUTION AND HEALING LENGTH IN SINGLE-BAND SUPERCONDUCTOR

In order to calculate the band-dependent corrections to the GL coherence length, we employ the EGL formalism and consider a spatially nonuniform configuration where the superconducting condensate (including all its band components) is severely suppressed at some point(s). In this case each band component recovers its bulk value in a distance that can be called the band healing length. When $T \to T_c$, the latter approaches the GL coherence length that is unique for all contributing bands [16,17,21]. There are two similar possibilities to arrange such a configuration, viz. by considering a vortex solution in the presence of a magnetic field or by invoking appropriate boundary conditions. Both of these possibilities result in similar band-dependent corrections to the GL coherence length and, as we are interested in the regime with significantly different band length scales, the particular choice of one of these options is not important. Technically it is easier to work with zero magnetic field, and so we follow the way employed in Ref. [23] and consider the widely used spatial configuration [35], where the superconducting condensate occupies a half space $x > 0$ and is completely suppressed for $x \leqslant 0$; see Fig. 1. By construction, spatial variations of the condensate over any length scale smaller than (or of the order of) the Cooper-pair radius are beyond the EGL formalism. This is why our choice of the boundary conditions cannot produce any Friedel-like oscillations (typical of the superconductor-insulator interface; see, e.g., Ref. [36]) but yields a spatial profile of the condensate similar to that in the vortex core. (By the same reason any features of the Kramer-Pesch collapse in the vortex core are also beyond our consideration [37,38].)

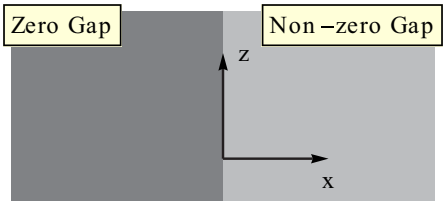

FIG. 1. Sketch of our calculational setup: the plane $x = 0$ separates domains with zero ($x < 0$) and nonzero ($x > 0$) gaps so we have the Dirichlet boundary condition for the superconducting gap(s) at the interface $x = 0$. The system remains symmetric under translations in y and z directions.

The main difficulty in finding the condensate spatial distribution within the EGL formalism concerns solving the gap equation in the lowest order in $\tau = 1 - T/T_c$, i.e., the nonlinear GL equation. The corrections to the GL result are governed by a linear equation [17,22,28] that can be solved analytically in many important cases. An advantage of the chosen spatial configuration given by Fig. 1 is that the solution to the GL equation can be written in this case in a closed analytical form [35,39]. Below we show that the leading corrections in τ to this solution can also be found analytically and therefore one can calculate the corresponding band-dependent correction to the GL coherence length in an explicit form.

The simplest way to introduce the analytical procedure of interest is to first consider the single-band case. Such an auxiliary study is presented in this section.

As already mentioned in the Introduction, within the EGL formalism the superconducting gap incorporates two terms [17,22,28], i.e., the GL contribution of order $\tau^{1/2}$ and its leading correction of order $\tau^{3/2}$. In particular, for the single-band case one obtains [28]

$$\Delta(\mathbf{r},\tau) = \tau^{1/2}[\Delta^{(0)}(\mathbf{r}) + \tau\Delta^{(1)}(\mathbf{r}) + O(\tau^2)], \qquad (1)$$

where the spatial distribution of the superconducting gap in the lowest order $\Delta^{(0)}(\mathbf{r})$ obeys the GL equation

$$a\Delta^{(0)} + b|\Delta^{(0)}|^2\Delta^{(0)} - \mathcal{K}\nabla^2\Delta^{(0)} = 0, \qquad (2)$$

TABLE I. Dimensionless coefficients for the single-band and two-band systems, $\alpha = 93\zeta(5)/[98\zeta^2(3)] \approx 0.68$. For the two-band case we have $\lambda_{ij} = g_{ij}N(0)$, with g_{ij} the interaction coupling constant and $N(0) = N_1(0) + N_2(0)$ the total DOS, $\chi = N_2(0)/N_1(0)$, and $\beta = v_{F2}/v_{F1}$, where v_{Fi} is the band Fermi velocity.

Auxiliary coefficient	Single-band expression	Two-band expression
$\frac{ac}{b^2}$	$-\alpha$	$-\alpha\frac{(1+\chi S^2)(1+\chi S^6)}{(1+\chi S^4)^2}$
$\frac{a\mathcal{Q}}{\mathcal{K}^2}$	$-\frac{6}{5}\alpha$	$-\frac{6}{5}\alpha\frac{(1+\chi S^2)(1+\chi\beta^4 S^2)}{(1+\chi\beta^2 S^2)^2}$
$\frac{a\mathcal{L}}{b\mathcal{K}}$	$-\frac{2}{3}\alpha$	$-\frac{2}{3}\alpha\frac{(1+\chi S^2)(1+\chi\beta^2 S^4)}{(1+\chi S^4)(1+\chi\beta^2 S^2)}$
$\frac{a'}{a}$		$-S\frac{1-\chi}{1+\chi S^2}$
$\frac{b'}{b}$		$-S\frac{1-\chi S^2}{1+\chi S^4}$
$\frac{\mathcal{K}'}{\mathcal{K}}$		$-S\frac{1-\chi\beta^2}{1+\chi\beta^2 S^2}$
A	$\left(\frac{3}{2}+\frac{a\mathcal{Q}}{\mathcal{K}^2}\right) = \frac{3}{2}-\frac{6}{5}\alpha$	$\left(\frac{3}{2}+\frac{a\mathcal{Q}}{\mathcal{K}^2}\right)+\mathcal{G}\left(\frac{\mathcal{K}'}{\mathcal{K}}-\frac{a'}{a}\right)^2$
B	$\left(5\frac{a\mathcal{L}}{b\mathcal{K}}-4\frac{a\mathcal{Q}}{\mathcal{K}^2}\right) = \frac{22}{15}\alpha$	$\left(5\frac{a\mathcal{L}}{b\mathcal{K}}-4\frac{a\mathcal{Q}}{\mathcal{K}^2}\right)-\mathcal{G}\left(4\frac{\mathcal{K}'^2}{\mathcal{K}^2}-6\frac{b'\mathcal{K}'}{b\mathcal{K}}-2\frac{a'\mathcal{K}'}{a\mathcal{K}}+4\frac{a'b'}{ab}\right)$
C	$\left(\frac{ac}{b^2}+3\frac{a\mathcal{Q}}{\mathcal{K}^2}-5\frac{a\mathcal{L}}{b\mathcal{K}}\right) = -\frac{19}{15}\alpha$	$\left(\frac{ac}{b^2}+3\frac{a\mathcal{Q}}{\mathcal{K}^2}-5\frac{a\mathcal{L}}{b\mathcal{K}}\right)+3\mathcal{G}\left(\frac{\mathcal{K}'}{\mathcal{K}}-\frac{b'}{b}\right)^2$
D	$\left(6\frac{a\mathcal{Q}}{\mathcal{K}^2}-5\frac{a\mathcal{L}}{b\mathcal{K}}\right) = -\frac{58}{15}\alpha$	$\left(6\frac{a\mathcal{Q}}{\mathcal{K}^2}-5\frac{a\mathcal{L}}{b\mathcal{K}}\right)+6\mathcal{G}\left(\frac{\mathcal{K}'^2}{\mathcal{K}^2}-\frac{b'\mathcal{K}'}{b\mathcal{K}}\right)$
S		$\frac{1}{2\lambda_{12}}\left(\lambda_{22}-\frac{\lambda_{11}}{\chi}+\sqrt{\left(\lambda_{22}-\frac{\lambda_{11}}{\chi}\right)^2+4\frac{\lambda_{12}^2}{\chi}}\right)$
$\mathcal{G}$		$-\frac{\lambda_{11}\lambda_{22}-\lambda_{12}^2}{\lambda_{12}}\frac{S(1+\chi S^2)}{(1+\chi)(1+S^2)^2}$

and the leading correction in τ is controlled by the linear equation

$$(a + 2b|\Delta^{(0)}|^2 + \Delta^{(0)2})\Delta^{(1)} - \mathcal{K}\nabla^2\Delta^{(1)} = F[\Delta^{(0)}], \quad (3)$$

with the right-hand side $F = F[\Delta^{(0)}]$ given by

$$\begin{aligned} F = &-\frac{a}{2}\Delta^{(0)} + 2\mathcal{K}\nabla^2\Delta^{(0)} + \mathcal{Q}\nabla^2(\nabla^2\Delta^{(0)}) - 2b|\Delta^{(0)}|^2\Delta^{(0)} \\ &- \mathcal{L}[2\Delta^{(0)}|\nabla\Delta^{(0)}|^2 + 3\Delta^{(0)*}(\nabla\Delta^{(0)})^2 + \Delta^{(0)2}\nabla^2\Delta^{(0)*} \\ &+ 4|\Delta^{(0)}|^2\nabla^2\Delta^{(0)}] + c|\Delta^{(0)}|^4\Delta^{(0)}. \end{aligned} \quad (4)$$

The material coefficients a, b, $\mathcal{K}$, c, $\mathcal{Q}$, and $\mathcal{L}$ in Eqs. (2), (3), and (4) are calculated with a specific model of the charge-carrier states. For the illustration we choose a single-band system in the clean limit and with a 3D Fermi surface. Then the material coefficients are obtained as [28]

$$\begin{aligned} &a = -N(0), \quad b = N(0)\frac{7\zeta(3)}{8\pi^2 T_c^2}, \quad \mathcal{K} = \frac{b}{6}\hbar^2 v_F^2, \\ &c = N(0)\frac{93\zeta(5)}{128\pi^4 T_c^4}, \quad \mathcal{Q} = \frac{c}{30}\hbar^4 v_F^4, \quad \mathcal{L} = \frac{c}{9}\hbar^2 v_F^2, \end{aligned} \quad (5)$$

where $N(0)$ is the DOS, v_F denotes the Fermi velocity, and $\zeta(\ldots)$ is the Riemann zeta function. The critical temperature is given by the ordinary weak-coupling expression $T_c = (2e^{\Gamma}/\pi)\hbar\omega_c \exp[-1/gN(0)]$, with g the Gor'kov coupling constant, ω_c the energy cutoff, and $\Gamma \approx 0.58$ the Euler constant. Notice that matching the proper orders in the perturbation expansion in τ requires one to explicitly display the temperature dependence of both contributions to $\Delta(\mathbf{r},\tau)$. This is why the material coefficient a appearing in the GL equation does not include τ. In addition, the spatial coordinates (and all characteristic lengths) are scaled as $\tau^{1/2}\mathbf{r}$, which introduces the corresponding scaling in the spatial gradients $\nabla \propto \tau^{1/2}$; see Ref. [28].

In the problem of interest the gap function $\Delta(\mathbf{r},\tau)$ can be chosen real and, due to the symmetry of the system, we have $\Delta(\mathbf{r},\tau) = \Delta(x,\tau)$. In this case, the relevant equations can be considerably simplified by introducing the dimensionless variables

$$\bar{x} = x/\xi_{\mathrm{GL}}, \quad \psi = \Delta^{(0)}/\Psi_0, \quad \varphi = \Delta^{(1)}/\Psi_0, \quad (6)$$

where $\xi_{\mathrm{GL}} = \sqrt{-\mathcal{K}/a}$ is the GL coherence length (multiplied by $\tau^{1/2}$ due to the scaling) and $\Psi_0 = \sqrt{-a/b}$ is the bulk solution of the GL equation (2). Below the bar over x is suppressed (this does cause any confusion). Then, the basic equations acquire the form

$$\psi - \psi^3 + \psi'' = 0, \quad (7)$$

$$(1 - 3\psi^2)\varphi + \varphi'' = f[\psi], \quad (8)$$

where $f = F/(a\Psi_0)$, after exclusion of higher gradients with the help of the GL equation, reads

$$f = A\psi + B\psi^3 + C\psi^5 + D\psi\psi'^2. \quad (9)$$

The dimensionless coefficients A, B, C, and D are given in Table I. Since they are written in terms of the number $\alpha = 93\zeta(5)/[98\zeta^2(3)] \approx 0.68$, the solution of Eq. (8) is material independent. So, the order parameter $\Delta(x,\tau)$ obtained within the single-band EGL formalism depends on microscopic characteristics only through Ψ_0 and ξ_{GL}, similar to the solution of the GL equation. However, as will be seen in Sec. III, the two-band case exhibits a more complex scenario. The relevant boundary conditions for Eqs. (7) and (8) are given by

$$\psi(0) = \psi'(\infty) = 0, \quad \varphi(0) = \varphi'(\infty) = 0, \quad (10)$$

i.e., $\Delta(x,\tau)$ vanishes at the interface $x = 0$ and rises to its asymptotic (bulk) value when $x \to \infty$.

As is well known [39], the solution for the 1D nonlinear Schrödinger equation (7) with the boundary conditions (10) is

given by ($x > 0$)

$$\psi(x) = \tanh(x/\sqrt{2}). \tag{11}$$

The key point in solving Eq. (8) is switching to the new variable ψ defined by Eq. (11). Written in terms of ψ, Eq. (8) reads

$$D_L\varphi = 2f/(1-\psi^2), \tag{12}$$

where D_L is the operator of the associated Legendre differential equation for the azimuthal quantum number 2 and magnetic quantum number 2, i.e.,

$$D_L = (1-\psi^2)\frac{d^2}{d\psi^2} - 2\psi\frac{d}{d\psi} + \left(6 - \frac{4}{1-\psi^2}\right). \tag{13}$$

The homogeneous equation $D_L\varphi = 0$ is well known [40] and its general solution is given by a linear combination of the first- and second-kind associated Legendre functions which, in the case of interest, write

$$\begin{aligned} P_2^2(\psi) &= 3(1-\psi^2), \\ Q_2^2(\psi) &= \frac{2\psi}{1-\psi^2} + 3\psi + 3(1-\psi^2)\tanh^{-1}(\psi). \end{aligned} \tag{14}$$

As Eq. (12) is inhomogeneous, its general solution is given by the sum of its particular solution $S_p(\psi)$ and a general solution of the corresponding homogeneous equation. To specify $S_p(\psi)$, one first notes that

$$\begin{aligned} D_L\left(\frac{\psi}{1-\psi^2}\right) &= \frac{6\psi}{1-\psi^2}, \quad D_L\psi = -\frac{4\psi}{1-\psi^2} + 4\psi, \\ D_L\psi^3 &= -\frac{4\psi}{1-\psi^2} + 10\psi - 6\psi^3. \end{aligned} \tag{15}$$

Then, it remains to mention that the right-hand side of Eq. (12) can be rearranged as

$$\begin{aligned} \frac{2f}{1-\psi^2} =& (2A+2B+2C)\frac{\psi}{1-\psi^2} - (2B+2C-D)\psi \\ &- (2C+D)\psi^3. \end{aligned} \tag{16}$$

Now, based on Eqs. (15) and (16), it is fairly easy to see that $S_p(\psi)$ can be written as

$$S_p = \alpha_0\frac{\psi}{1-\psi^2} + \alpha_1\,\psi + \alpha_3\,\psi^3, \tag{17}$$

where the coefficients α_0, α_1, and α_3 are obtained when plugging Eq. (17) into Eq. (12) and using the rearrangement given by Eq. (16). The resulting system of equations for the coefficients α_0, α_1, and α_3 is of the triangular form, and so one easily obtains

$$\begin{aligned} &\alpha_0 = (A-C)/3, \quad \alpha_1 = -(3B+8C+D)/6, \\ &\alpha_3 = (2C+D)/6. \end{aligned} \tag{18}$$

Now we have everything at our disposal to find the solution of Eq. (12). The first-kind Legendre function cannot contribute as we have $P_2^2(0) = 3$, $Q_2^2(0) = 0$, and $S_p(0) = 0$; see the boundary conditions in Eq. (10). Moreover, since the solution in question should be uniform for $x \to \infty$ ($\psi \to 1$), the divergent term $\frac{\psi}{1-\psi^2}$ that appears in $S_p(\psi)$ and $Q_2^2(\psi)$ must be eliminated by an appropriate choice of the coefficient for $Q_2^2(\psi)$. As a result, we get

$$\varphi = -\frac{A-C}{6}\,Q_2^2(\psi) + S_p(\psi), \tag{19}$$

where the boundary conditions (10) are certainly satisfied.

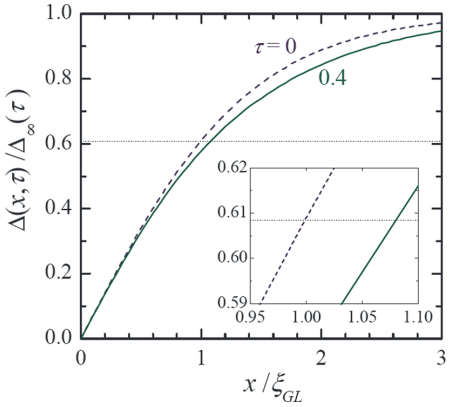

FIG. 2. EGL solution for $\Delta(x,\tau)$ given in units of its asymptotic value $\Delta_\infty(\tau)$ as a function of the relative distance from the interface x/ξ_{GL} for $\tau = 0$ (dashed curve) and $\tau = 0.4$ (solid curve). The dotted horizontal line marks $\delta = \tanh(1/\sqrt{2})$ that determines the condensate healing length according to Eq. (21).

After combining Eqs. (1), (11), and (19), the superconducting gap calculated up to order $\tau^{3/2}$ is given by

$$\begin{aligned} \frac{\Delta(x,\tau)}{\tau^{1/2}\Psi_0} =& \tanh(x/\sqrt{2}) - \tau\Bigg[\tanh(x/\sqrt{2})\left(\frac{3}{4} - \frac{47\alpha}{30}\right) \\ &+ (x/\sqrt{2})\,\mathrm{sech}^2(x/\sqrt{2})\left(\frac{3}{4} + \frac{\alpha}{30}\right) \\ &+ \tanh^3(x/\sqrt{2})\,\frac{16\alpha}{15}\Bigg], \end{aligned} \tag{20}$$

where α is the material-independent number, as already mentioned previously; see Table I. The spatial profile of the order parameter is shown in Fig. 2 for $\tau = 0$ and $\tau = 0.4$. At $\tau = 0$ the EGL solution coincides with the GL result while below T_c it deviates from the GL order parameter, recovering the asymptotic value slower than this occurs in the GL scenario. To quantify this deviation, we define the healing length ξ as the distance at which the gap taken in units of $\Delta_\infty(\tau) = \lim_{x\to\infty}\Delta(x,\tau)$ reaches the characteristic value $\delta = \tanh(1/\sqrt{2}) \approx 0.61$, i.e.,

$$\Delta(\xi,\tau)/\Delta_\infty(\tau) = \delta. \tag{21}$$

This definition is chosen so that the GL coherence length is recovered in the limit $\tau \to 0$. Based on Eqs. (20) and (21), one is able to get the τ expansion for ξ. Indeed, by expanding $\Delta(\xi,\tau)$ in Eq. (21) over a small deviation of ξ from the GL coherence length [the latter is 1 in the dimensionless units of Eq. (6)], we obtain

$$\frac{\Delta(\xi,\tau)}{\tau^{1/2}\Psi_0} \approx \psi(1) + \left.\frac{d\psi}{d\xi}\right|_{\xi=1}\delta\xi + \tau\varphi(1), \tag{22}$$

where only the terms up to order τ are included and it is taken into consideration that $\delta\xi = \xi - 1 \propto \tau$. Then, plugging

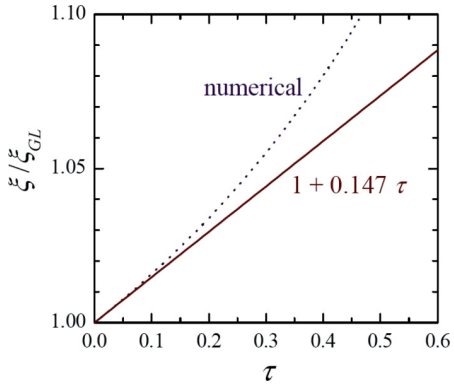

FIG. 3. Condensate healing length versus τ: the analytical result of Eq. (23) is given by the dotted line, whereas the full numerical solution of Eq. (21) is represented by the solid curve. The difference between the numerical and analytical results becomes significant for $\tau > 0.3-0.4$, which defines the validity domain of Eq. (23) as $\tau \lesssim \tau^* = 0.3-0.4$; see the related discussion in the main text.

Eq. (22) into the definition of the healing length (21), we get the ratio $\xi/\xi_{\rm GL}$ in the lowest and next-to-lowest orders in τ as

$$\xi/\xi_{\rm GL} = 1 + \tau\left(\frac{3}{4} + \frac{\alpha}{30} - \sqrt{2}\delta\frac{16\alpha}{15}\right) \approx 1 + 0.147\tau. \quad (23)$$

The result given by Eq. (23) is material independent, in agreement with Eq. (20). The difference between the EGL healing length and $\xi_{\rm GL}$ is not pronounced, e.g., even at $\tau = 0.4$ it is about 5%. However, a similar analytical treatment will be invoked in Sec. III for a system with two contributing bands where the situation changes crucially.

In Fig. 3 the analytical result (23) obtained by expanding Eq. (21) is compared with a numerical solution of Eq. (21) for ξ. Notice that the left-hand side of Eq. (21) is not a linear function of τ and so the solution for ξ is given by an infinite series in powers of τ. However, only the contribution of order τ is relevant here because the higher orders are incomplete. As is seen from Fig. 3, the difference between the numerical and analytical results becomes significant for $\tau > 0.3-0.4$, where higher orders in τ make considerable contributions to ξ. This gives the material-independent validity domain for our results as $\tau \lesssim \tau^* = 0.3-0.4$. For $\tau > \tau^*$ one expects that higher orders in τ can play a role in $\Delta(x,\tau)$. A similar estimate is obtained under the criterion that ξ should be larger than the characteristic length of the integral kernels involved in the expansion of the gap equation over the powers of the order parameter [23,39], i.e., $\xi > \hbar v_F/(2\pi T)$. We recall that the assumption of small Δ results in a nonlinear integral gap equation. To get a simpler differential-equation structure, one needs to invoke a gradient expansion, and its validity is controlled by the above inequality. When utilizing Eq. (23) for the healing length, this inequality is reduced to $\tau < 0.35$. It is worth noting here that in many cases the qualitative predictions of the EGL theory (and sometimes even quantitative results) still hold down to low temperatures $T \ll T_c$; see discussions and examples in Refs. [11,22,28].

The analytical solution constructed in this section for single-band systems can be generalized to the case of multi-band superconductors. Thus we proceed further and consider a more complicated variant with two available bands.

III. LENGTH SCALES IN TWO-BAND SUPERCONDUCTOR

A. Analytical solution for band gaps

In the present section we again employ the spatial configuration of Fig. 1 but the right half-space is now occupied by a two-band superconductor so that both superconducting gaps vanish at the interface $x = 0$. Our starting point is the self-consistency BCS equation which is written for the two-band case as (see, e.g., Ref. [22])

$$\vec{\Delta}(\mathbf{r},\tau) = \check{g}\,\vec{R}[\vec{\Delta}(\mathbf{r},\tau)], \quad (24)$$

where $\check{g}$ is the 2×2 matrix of the coupling constants g_{ij}, $\vec{\Delta}(\mathbf{r},\tau)$ is the column of the band gaps $\Delta_i(\mathbf{r},\tau)$ $(i = 1,2)$, and the elements of $\vec{R}$ are the band-dependent anomalous Green functions $R_i = \langle\hat{\psi}_{i\uparrow}(\mathbf{r})\hat{\psi}_{i\downarrow}(\mathbf{r})\rangle$ [22]. It is convenient to rearrange R_i in order to separate its lowest-order contribution, i.e.,

$$R_i = N_i(0)\mathcal{A}\Delta_i + \Omega_i, \quad (25)$$

where $N_i(0)$ is the band DOS and $\mathcal{A} = \ln[2e^{\Gamma}\hbar\omega_c/(\pi\, T_c)]$, with Γ and ω_c already introduced earlier in Sec. II. Then, the self-consistency equation (24) reads

$$\check{L}\vec{\Delta}(\mathbf{r},\tau) = \vec{\Omega}[\vec{\Delta}(\mathbf{r},\tau)], \quad (26)$$

where $\check{L}$ is the matrix with the entries $L_{ij} = \gamma_{ij} - \delta_{ij}N_i(0)\mathcal{A}$, δ_{ij} is the Kronecker symbol, and γ_{ij} is the element of the inverted interaction matrix $\check{\gamma} = \check{g}^{-1}$. Following Ref. [22], we expand $\vec{\Delta}$ in τ as

$$\vec{\Delta} = \tau^{1/2}[\vec{\Delta}^{(0)} + \tau\vec{\Delta}^{(1)} + \tau^2\vec{\Delta}^{(2)} + O(\tau^3)]. \quad (27)$$

The corresponding expansion for $\vec{\Omega}$ is of the form [22]

$$\vec{\Omega} = \tau^{1/2}[\tau\vec{\Omega}^{(1)} + \tau^2\vec{\Omega}^{(2)} + O(\tau^3)], \quad (28)$$

with

$$\Omega_i^{(1)} = -a_i\Delta_i^{(0)} - b_i\left|\Delta_i^{(0)}\right|^2\Delta_i^{(0)} + \mathcal{K}_i\nabla^2\Delta_i^{(0)} \quad (29)$$

and

$$\Omega_i^{(2)} = -a_i\Delta_i^{(1)} - b_i\left(2\left|\Delta_i^{(0)}\right|^2\Delta_i^{(1)} + \Delta_i^{(0)2}\Delta_i^{(1)*}\right) + \mathcal{K}_i\nabla^2\Delta_i^{(1)} + F_i\left[\Delta_i^{(0)}\right]. \quad (30)$$

Here a_i, b_i, and $\mathcal{K}_i$ depend on a chosen model of the charge-carrier band states and $F_i[\Delta_i^{(0)}]$ is given by Eq. (4) where $\Delta^{(0)}$ is replaced by $\Delta_i^{(0)}$ and the coefficients a, b, c, $\mathcal{K}$, $\mathcal{Q}$, and $\mathcal{L}$ acquire the band index i. To demonstrate disparity between the band length scales beyond the regime of nearly decoupled bands, it is not necessary to consider unconventional pairing symmetries or anisotropic systems. We choose a simple variant of two bands with 3D Fermi surfaces in the clean limit. So the relevant microscopic parameters are the couplings $g_{ij} = g_{ji}$, the band Fermi velocities v_{Fi}, and the band DOSs $N_i(0)$ $(i,j = 1,2)$. Then the band material coefficients a_i, b_i, c_i, $\mathcal{K}_i$, $\mathcal{Q}_i$, and $\mathcal{L}_i$ are given by Eq. (5) but with $N(0)$ and v_F replaced by $N_i(0)$ and v_{Fi}. Similar to the single-band case, the spatial coordinates (and the healing lengths) are scaled as $\tau^{1/2}\mathbf{r}$

so that $\nabla \propto \tau^{1/2}$; see Refs. [22,28]. Notice that due to the rearrangement (25), the lowest nonzero order in the τ expansion of $\vec{\Omega}$ is $\tau^{3/2}$, i.e., $\vec{\Omega}^{(0)} = 0$. We also remark that, to find the multiband self-consistency equation in a given order in τ, one needs to expand the band gaps up to the same order. This is a distinctive feature of the multiband formalism that does not appear in the single-band equations. As the equation for the leading correction to the GL contribution in band gaps results from the self-consistency equation taken in order $\tau^{5/2}$ [see Eq. (46) below], one needs to explicitly display the contribution of order $\tau^{5/2}$ in Eq. (27) and introduce $\vec{\Delta}^{(2)}$.

Taken in order $\tau^{1/2}$, the self-consistency equation (26) yields

$$\check{L}\vec{\Delta}^{(0)} = 0. \tag{31}$$

For obtaining a nontrivial solution for $\Delta_i^{(0)}$ it must be true that

$$\det \check{L} = [\gamma_{11} - N_1(0)\mathcal{A}][\gamma_{22} - N_2(0)\mathcal{A}] - \gamma_{12}^2 = 0, \tag{32}$$

and T_c is the largest root of Eq. (32). In addition, Eq. (31) dictates that the gap vector $\vec{\Delta}^{(0)}$ is proportional to the eigenvector of the matrix $\check{L}$ with the zero eigenvalue, i.e.,

$$\vec{\Delta}^{(0)}(\mathbf{r}) = \Psi(\mathbf{r})\vec{\eta}_1. \tag{33}$$

Therefore, in order $\tau^{1/2}$, the band gaps are proportional to one another [17,22] and $\Psi(\mathbf{r})$ (which controls the spatial profile of both band condensates) is the Landau order parameter of the two-band system. To express $\vec{\eta}_1$ in a convenient form, we introduce the auxiliary quantity

$$S = -\frac{\gamma_{11} - N_1(0)\mathcal{A}}{\gamma_{12}} = \frac{g_{22} - N_1(0)G\mathcal{A}}{g_{12}}, \tag{34}$$

where $G = g_{11}g_{22} - g_{12}^2$ is the determinant of $\check{g}$. Based on this definition, we can choose two eigenvectors of $\check{L}$ as

$$\vec{\eta}_1 = \begin{pmatrix} 1 \\ S \end{pmatrix}, \quad \vec{\eta}_2 = \begin{pmatrix} -S \\ 1 \end{pmatrix}, \tag{35}$$

with the eigenvalues

$$w_1 = 0, \quad w_2 = -\gamma_{12}(S + S^{-1}). \tag{36}$$

Notice that the eigenvectors given by Eq. (35) are not normalized. The EGL formalism does not require such a normalization and, in addition, use of the normalized eigenvectors results in more complex expressions.

Taken in order $\tau^{3/2}$, the self-consistency equation (26) is reduced to

$$\check{L}\vec{\Delta}^{(1)} = \vec{\Omega}^{(1)}. \tag{37}$$

The two projections of Eq. (37) onto $\vec{\eta}_1$ and $\vec{\eta}_2$ should be examined. The projection onto $\vec{\eta}_1$ yields the two-band GL equation

$$a\Psi + b|\Psi|^2\Psi - \mathcal{K}\nabla^2\Psi = 0, \tag{38}$$

where the coefficients a, b, and $\mathcal{K}$ [redefined as compared to Eq. (2)] are averages over the contributing bands

$$a = \sum_i a_i\eta_{1i}^2, \quad b = \sum_i b_i\eta_{1i}^4, \quad \mathcal{K} = \sum_i \mathcal{K}_i\eta_{1i}^2, \tag{39}$$

with η_{1i} the component of $\vec{\eta}_1$. The uniform solution of Eq. (38) is given by

$$\Psi_0 = \sqrt{-\frac{a}{b}} = \sqrt{\frac{8\pi^2T_c^2}{7\zeta(3)}\,\frac{1+\chi S^2}{1+\chi S^4}}, \tag{40}$$

with $\chi = N_2(0)/N_1(0)$. The GL coherence length writes

$$\xi_{\mathrm{GL}} = \sqrt{-\frac{\mathcal{K}}{a}} = \sqrt{\hbar^2 v_{F1}^2\,\frac{7\zeta(3)}{48\pi^2T_c^2}\,\frac{1+\chi\beta^2S^2}{1+\chi S^2}}, \tag{41}$$

with $\beta = v_{F2}/v_{F1}$. As seen, due to the two-band modification of the coefficients a, b, and $\mathcal{K}$, Ψ_0 and ξ_{GL} depend on the material parameters not only through T_c but also incorporate S, χ, and β. Keeping in mind that the band-gap functions do not depend on the spatial coordinates y and z and introducing dimensionless units similar to that of the single-band case (6), we obtain that $\psi(x) = \Psi/\Psi_0$ obeys Eq. (7) (the band gaps are chosen real). As the boundary conditions for ψ in the two-band case are also given by Eq. (10), the solution remains $\psi = \tanh(x/\sqrt{2})$.

The next step is investigating the projection of Eq. (37) onto $\vec{\eta}_2$. We first define the expansion

$$\vec{\Delta}^{(1)}(\mathbf{r}) = \sum_\alpha \Phi_\alpha(\mathbf{r})\vec{\eta}_\alpha, \tag{42}$$

where the index α enumerates the eigenvectors of $\check{L}$ and should not be confounded with the band index i. Now, by projecting Eq. (37) onto $\vec{\eta}_2$, we obtain

$$w_2\,\vec{\eta}_2^{\dagger}\vec{\eta}_2\,\Phi_2 = -a'\Psi - b'|\Psi|^2\Psi + \mathcal{K}'\nabla^2\Psi, \tag{43}$$

where $\vec{\eta}_2^{\dagger} = (\eta_{21}, \eta_{22})$ and

$$a' = \sum_i a_i\eta_{1i}\eta_{2i}, \quad b' = \sum_i b_i\eta_{1i}^3\eta_{2i}, \quad \mathcal{K}' = \sum_i \mathcal{K}_i\eta_{1i}\eta_{2i}. \tag{44}$$

Employing Eq. (38) and introducing the dimensionless functions $\varphi_\alpha = \Phi_\alpha/\Psi_0$, one rewrites Eq. (43) as

$$\varphi_2 = \mathcal{G}\left[\left(\frac{\mathcal{K}'}{\mathcal{K}} - \frac{a'}{a}\right)\psi - \left(\frac{\mathcal{K}'}{\mathcal{K}} - \frac{b'}{b}\right)\psi^3\right], \tag{45}$$

with $\mathcal{G} = a/(w_2\vec{\eta}_2^{\dagger}\vec{\eta}_2)$.

When considered in order $\tau^{5/2}$, the self-consistency equation (26) is of the form

$$\check{L}\vec{\Delta}^{(2)} = \vec{\Omega}^{(2)}. \tag{46}$$

Projecting this equation onto $\vec{\eta}_1$, one finds

$$a\Phi_1 + b(2|\Psi|^2\Phi_1 + \Psi^2\Phi_1^*) - \mathcal{K}\nabla^2\Phi_1 = \mathcal{F}[\Phi_2, \Psi], \tag{47}$$

with

$$\mathcal{F}[\Phi_2, \Psi] = -a'\Phi_2 - b'(2|\Psi|^2\Phi_2 + \Psi^2\Phi_2^*) + \mathcal{K}'\nabla^2\Phi_2 + F[\Psi]. \tag{48}$$

Here $F[\Psi]$ is given by Eq. (4) but with $\Delta^{(0)}$ replaced by Ψ and the coefficients a, b, $\mathcal{K}$, $\mathcal{Q}$, $\mathcal{L}$, and c redefined according to Eq. (39) and

$$\mathcal{Q} = \sum_i \mathcal{Q}_i\eta_{1i}^2, \quad \mathcal{L} = \sum_i \mathcal{L}_i\eta_{1i}^4, \quad c = \sum_i c_i\eta_{1i}^6. \tag{49}$$

As Φ_2 obeys Eq. (43), the right-hand side of Eq. (47) can be expressed only in terms of Ψ. Then, using the dimensionless functions $\varphi_1(x)$ and $\psi(x)$ and switching to the variable $\psi = \tanh(x/\sqrt{2})$, we obtain for φ_1 an equation that is formally the same as Eq. (12). However, now the coefficients A, B, C, and D appearing in $f[\psi]$ are given by new expressions; see Table I. The boundary conditions for φ_1 are also the same as those for φ in the single-band case; see Eq. (10). Thus the whole solution procedure for φ_1 can be performed through the same steps.

Finally, the complete expression for $\vec{\Delta}(x,\tau)$ up to order $\tau^{3/2}$ can be assembled as

$$\frac{\vec{\Delta}(x,\tau)}{\tau^{1/2}\Psi_0} = \psi(x)\vec{\eta}_1 + \tau[\varphi_1(x)\vec{\eta}_1 + \varphi_2(x)\vec{\eta}_2], \tag{50}$$

where ψ obeys Eq. (11), φ_1 is given by the right-hand side of Eq. (19) with the coefficients A, B, C, and D modified for the two-band case (see Table I), and φ_2 satisfies Eq. (45). As seen, the difference between the spatial profiles of the band gaps appears in the leading correction to the GL result due to the presence of the term $\varphi_2(x)\vec{\eta}_2$, as has been already mentioned in previous works [17,22]. However, one should take into consideration that φ_2 can be equal to zero for some specific combinations of the microscopic parameters. For example, it happens when $G = 0$, resulting in $\mathcal{G} = 0$. As $w_2 \to \infty$ for $G \to 0$, the spatial profiles of the band condensates remain the same for $G = 0$ in any order of the perturbation expansion in τ. One can get a feeling about this case by examining the projection of Eq. (46) onto $\vec{\eta}_2$: it is obviously equal to zero as being inversely proportional to w_2.

B. Deviation between band healing lengths

The band healing lengths ξ_i are calculated by applying the criterion of Eq. (21) to the band gaps Δ_i given by Eq. (50) so that we have

$$\Delta_i(\xi_i,\tau)/\Delta_{i,\infty}(\tau) = \delta, \tag{51}$$

where $\Delta_{i,\infty}(\tau) = \lim_{x\to\infty}\Delta_i(x,\tau)$. The solution of Eq. (51), up to the leading correction to the GL coherence length, is of the form

$$\xi_i/\xi_{\rm GL} = 1 + \tau\left\{\frac{A-C}{2} + \sqrt{2}\delta\left[\frac{2C+D}{6} + \mathcal{G}\left(\frac{b'}{b} - \frac{\mathcal{K}'}{\mathcal{K}}\right)\varepsilon_i\right]\right\}, \tag{52}$$

with $\varepsilon_1 = -S$, $\varepsilon_2 = 1/S$, and $\delta = \tanh(1/\sqrt{2})$. In agreement with the above discussion about the spatial profiles of the band condensates, see Eq. (50), we find that the healing lengths become generally different in the leading correction to the GL coherence length. (One should keep in mind, of course, exceptions when $\varphi_2 = 0$, e.g., for $G = 0$.) We introduce the deviation rate of the band healing lengths $d(\xi_2 - \xi_1)/d\tau$ given by

$$\frac{1}{\xi_{\rm GL}}\frac{d(\xi_2-\xi_1)}{d\tau} = \mathcal{G}\delta\sqrt{2}(S + S^{-1})\left(\frac{b'}{b} - \frac{\mathcal{K}'}{\mathcal{K}}\right). \tag{53}$$

This quantity can serve as the measure for the length scale disparity because the difference between the band healing lengths is usually most pronounced at low temperatures $T \ll T_c$. (It is important to note that the effect in question can be further enhanced in the presence of a hidden criticality [10] but the latter is not captured in the leading correction to the GL theory.) Notice that all dimensionless quantities that appear in Eq. (53), and also in Eqs. (50) and (52), depend on the material parameters through the dimensionless couplings $\lambda_{ij} = g_{ij}N(0)$ $[N(0) = N_1(0) + N_2(0)]$, the band DOS's ratio χ, and the ratio of the band Fermi velocities β. The corresponding expressions are displayed in Table I.

By examining Eq. (53) one finds that the deviation rate is strongly dependent on the relative interband coupling $\lambda_{12}/\lambda_{11}$, in agreement with the results of Ref. [27]. However, our study demonstrates that the difference between the healing lengths is also very sensitive to the ratio of the band Fermi velocities $\beta = v_{F2}/v_{F1}$. The 3D plot of the deviation rate versus $\lambda_{12}/\lambda_{11}$ and β is presented in Fig. 4(a). Details of the dependence on β can be found in Fig. 4(b). The data are shown for $\lambda_{12}/\lambda_{11} > 0.1$ in order to check the expectation [27] that the difference between the band healing lengths is negligible for such values

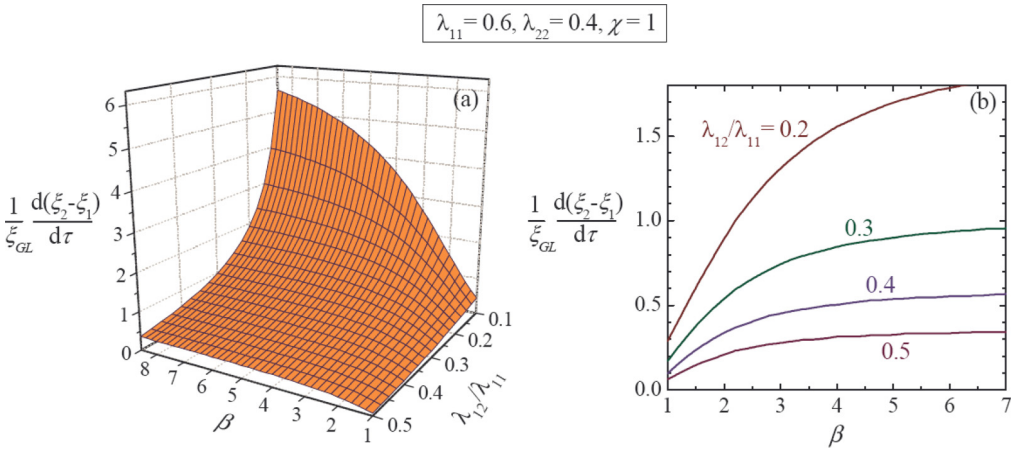

FIG. 4. (a) Deviation rate of the band healing lengths in units of the GL coherence length [see Eq. (53)] versus the ratio of the band Fermi velocities β and the relative interband coupling $\lambda_{12}/\lambda_{11}$ as calculated at $\chi = N_2(0)/N_1(0) = 1$. (b) The same quantity as in panel (a) but now given as a function of β for the relative interband couplings 0.2, 0.3, 0.4, and 0.5.

of the relative interband coupling. For the sake of illustration we choose $\lambda_{11} = 0.6$, $\lambda_{22} = 0.4$, and $\chi = 1$. Notice that this choice of the intraband couplings and the band DOS's ratio is not crucial: similar results are obtained for other sets of λ_{11}, λ_{22}, and χ. In our consideration band 1 is a stronger band. It means that $\lambda_{11} - \chi\lambda_{22} > 0$, i.e., the critical temperature of band 1 considered as an independent superconductor (i.e., at $\lambda_{12} = 0$) is higher than the superconducting temperature of the decoupled band 2.

From Fig. 4(a) it is seen that $d(\xi_2 - \xi_1)/d\tau$ is most pronounced when $\beta > 2{-}3$ and $\lambda_{12}/\lambda_{11} < 0.3$. In particular, for these parameters we find that $\xi_2 - \xi_1$ taken at $\tau = 0.1$ varies from $0.1\xi_{\rm GL}$ up to almost $0.6\xi_{\rm GL}$. We emphasize that such significant deviation between the band length scales develops almost near T_c. As already mentioned above, the difference of the band healing lengths is further increased when lowering the temperature. Another important feature of the plot in Fig. 4(a) is an increase of the deviation rate with rising β. Though this increase is more profound at $\lambda_{12}/\lambda_{11} = 0.1{-}0.2$, its effect is clearly seen also for larger interband couplings. For example, at $\lambda_{12}/\lambda_{11} = 0.3$ we find that $d(\xi_2 - \xi_1)/d\tau \approx \xi_{\rm GL}$ for $\beta > 5$ while being about $0.2\xi_{\rm GL}$ at $\beta = 1$; see Fig. 4(b). Even at $\lambda_{12}/\lambda_{11} = 0.5$ the deviation rate increases from $0.1\xi_{\rm GL}$ at $\beta = 1$ up to almost $0.4\xi_{\rm GL}$ at $\beta = 3$. The region of the fast growth of the deviation rate as a function of β shrinks when the interband coupling rises. In particular, at $\lambda_{12}/\lambda_{11} = 0.5$ a saturation is almost reached at $\beta \approx 4$, while at $\lambda_{12}/\lambda_{11} = 0.2$ the increase is still pronounced for $\beta = 6$. As seen, the effect of β on the deviation between the band healing lengths is rather important. When $\beta > 5$, the deviation rate is not negligible even for interband couplings $\lambda_{12}/\lambda_{11} = 0.4{-}0.5$, i.e., far beyond the regime of nearly decoupled bands.

The underlying physics for the dependence of the deviation rate on $\lambda_{12}/\lambda_{11}$ is that the interband interactions tend to wash out any difference between the contributing band condensates. To clarify the reason behind the impact of the ratio of the band Fermi velocities, one can recall that for the decoupled bands in the clean limit $\xi_i \propto v_{Fi}$ and so $\xi_2 - \xi_1 \propto v_{F2} - v_{F1}$. Hence the larger the difference of the band Fermi velocities, the more pronounced the deviation between the band length scales of two decoupled condensates and, physically, this trend should sustain for small interband couplings. One can note, however, that the relation $\xi_i \propto v_{Fi}$ is oversimplified because it is not applicable at all temperatures below T_c. In particular, it is not correct in the so-called passive regime of band 2 which is realized at temperatures above T_{c2}, i.e., the superconducting temperature of band 2 taken as a separate superconductor ($T_{c2} < T_c$). For more detail, it is instructive to examine the right-hand side of Eq. (53) in the limit $\lambda_{12} \to 0$. Using the explicit form of S given in Table I and taking into account that $\lambda_{11} - \chi\lambda_{22} > 0$ (band 1 is a stronger band), we derive for $\lambda_{12} \to 0$

$$S \to \lambda_{12}/(\lambda_{11} - \chi\lambda_{22}). \tag{54}$$

As seen, S goes to zero for zero interband coupling and so does φ_2 ($\mathcal{G} \to 0$); see Eq. (45) and Table I. Then Eq. (50) dictates that the occupation of band 2 becomes zero. It is clear that one can hardly use the standard relation $\xi_2 \propto v_{F2}$ in the absence of the condensed state. However, the zero-interband-coupling limit for ξ_2 and so for the deviation rate still exist. In particular, we obtain in the limit $\lambda_{12} \to 0$

$$\frac{1}{\xi_{\rm GL}}\frac{d(\xi_2 - \xi_1)}{d\tau} \propto \beta^2. \tag{55}$$

Based on Eq. (55), one concludes that the deviation rate is very sensitive to the ratio of the band Fermi velocities and enhanced when the Fermi velocity of the weaker band is larger than that of the stronger band, in a qualitative agreement with our results in Fig. 4. We remark that at $\chi = 1$ Eq. (55) is quantitatively correct only for $\lambda_{12}/\lambda_{11} \lesssim 0.01$. Indeed, our results given in Fig. 4 exhibit a saturation for large β which is clearly an effect of interband interactions.

Above we have considered how the rate of the deviation between the healing lengths is sensitive to the relative interband coupling and the ratio of the band Fermi velocities. It has been mentioned that the qualitative picture of our results is not sensitive to particular values of the intraband couplings and the band DOS's ratio. However, quantitative changes due to variations in λ_{11}, λ_{22}, and χ can be considerable. This is illustrated in Fig. 5, where $d(\xi_2 - \xi_1)/d\tau$ is shown versus $\lambda_{12}/\lambda_{22}$ and β for the same intraband couplings as in Fig. 4 but for the DOS's ratio $\chi = 0.2$. What is seen immediately in

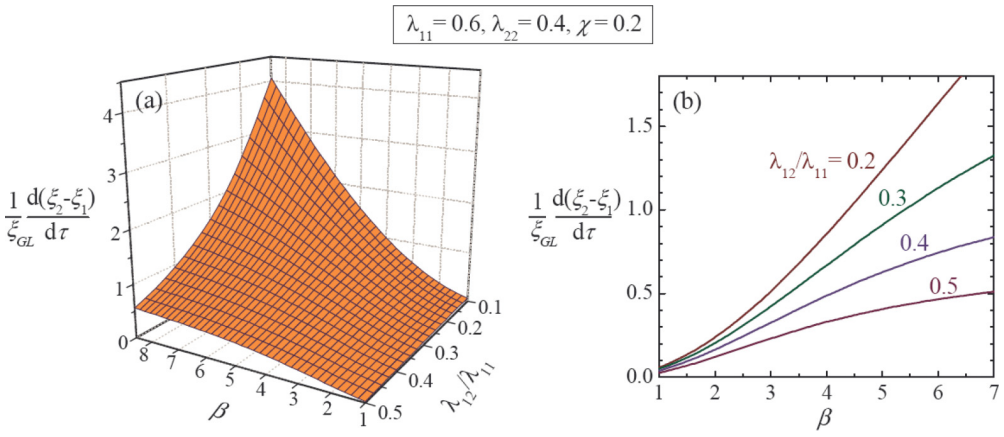

FIG. 5. (a) Deviation rate (53) versus $\beta = v_{F2}/v_{F1}$ and $\lambda_{12}/\lambda_{11}$ for the same intraband couplings as in Fig. 4 but the band DOS's ratio is now changed to $\chi = 0.2$. (b) The deviation rate as a function of β for $\lambda_{12}/\lambda_{11} = 0.2$, 0.3, 0.4, and 0.5; the other microscopic parameters are the same as in panel (a).

Fig. 5(a) is that the maximum at large β and small λ_{12} is less pronounced, being smaller by a factor of about 1.4 as compared to the case of $\chi = 1$. It might seem that the deviation between the band length scales is generally reduced here. However, this is not correct. In particular, one can see in Fig. 5(b) that for large interband couplings and large ratios of the band Fermi velocities, the deviation rate is in fact enhanced as compared to its values for the same parameters in the previous case with $\chi = 1$. For example, at $\lambda_{12}/\lambda_{22} = 0.4$ and 0.5 such an enhancement is about 50%. In addition, the growth of the deviation rate with β is generally more pronounced for $\chi = 0.2$. For instance, at $\lambda_{12}/\lambda_{11} = 0.4$ it increases from $0.05\xi_{\rm GL}$ at $\beta = 1$ up to $0.85\xi_{\rm GL}$ at $\beta = 7$, see Fig. 5(b), while in Fig. 4(b) the deviation rate calculated for the same interband coupling is $0.1\xi_{\rm GL}$ at $\beta = 1$ and $0.6\xi_{\rm GL}$ at $\beta = 7$.

Thus the interband interactions tend to weaken the deviation between the band length scales while disparity between the band Fermi velocities tend to strengthen it. Changes in other microscopic parameters, like χ, add nuances highlighting complexity of this confrontation. A balance between these two confronting tendencies results in the disparity between the band length scales far beyond the regime of nearly decoupled band condensates.

C. Discussion

To have an idea about how different the band characteristic velocities can be in multiband superconductors, several examples are considered below. Here finding useful illustrations does not require a difficult search in the literature because already the well-known multiband compound MgB_2 provides an instructive example. The tunneling spectra for MgB_2 exhibit the presence of two excitation gaps associated with the σ- and π-band condensates. Based on a number of available first-principle calculations for such an effectively two-band system, one can easily extract the characteristic velocities of the charge carriers. In particular, the averaged band Fermi velocities in the a-b plane can be estimated as [41] $v_{F1}^{(a-b)} = 4.4 \times 10^5$ m/s for the stronger σ band and $v_{F2}^{(a-b)} = 5.35 \times 10^5$ m/s for the weaker π band. As seen, they are not significantly different, giving the ratio $\beta^{(a-b)} = 1.2$. However, the motion of charge carriers in the c direction changes dramatically due to the quasi-2D character of the σ band. In particular, one obtains $v_{F1}^{(c)} = 7 \times 10^4$ m/s, almost an order of magnitude smaller than $v_{F1}^{(a-b)}$, while for the 3D π band the Fermi velocity in the c direction $v_{F2}^{(c)} = 6 \times 10^5$ m/s remains close to $v_{F2}^{(a-b)}$. As a result, the ratio of the band Fermi velocities in the c direction increases by about an order of magnitude as compared to that in the a-b plane, namely, $\beta^{(c)} = 8.7$. Our previous analysis of the deviation rate strongly suggests that this value of β is large enough to have a pronounced disparity between the healing lengths of the σ and π bands. To go into more detail on this point, the band-condensate profiles and the corresponding healing lengths calculated from Eqs. (50) and (52) are shown in Fig. 6 for $\beta = \beta^{(a-b)}$ and $\beta^{(c)}$. Here we utilize the dimensionless coupling constants and DOS's ratio reported for MgB_2 in Ref. [42]: $\lambda_{11} = 2.41$, $\lambda_{22} = 0.78$, $\lambda_{12} = 0.37 \approx 0.15\lambda_{11}$, and $\chi = 1.37$. Of course, one should bear in mind possible uncertainties of the microscopic parameters and limitations of our simplified consideration with 3D spherical band Fermi surfaces. Physically, each band Fermi velocity is averaged over angles in our consideration and, strictly speaking, anisotropy effects are beyond our consideration. However, as our problem is effectively one dimensional, the anisotropy effects can still be captured by changing the ratio of the band Fermi velocities with the orientation of the zero-condensate interface.

The spatial distributions of the band gaps, calculated at $\tau = 0.07$, are shown in Figs. 6(a) and 6(b) for $\beta = \beta^{(a-b)}$ and $\beta^{(c)}$, respectively. Using the dotted horizontal line in both panels, one can estimate that the deviation between the band healing lengths is close to $0.07\xi_{\rm GL}$ in panel (a) while increasing up to $0.3\xi_{\rm GL}$ in panel (b). This agrees with the general trend dictated by Eq. (53). In addition, one can see an important aspect in Fig. 6(b). The point is that the gap associated with band 1 is not a monotonic function of a distance. One can see that Δ_1 rises sharply for $x < 1.3\xi_{\rm GL}$ but then slightly decreases down to its local minimum at $x \approx 2.4\xi_{\rm GL}$. For $x > 2.4\xi_{\rm GL}$ it increases again, slowly approaching the asymptotic value. At the same time Δ_2 exhibits a monotonic increase with x. Thus we find that the band condensates have different healing lengths and, in addition, their spatial profiles are not similar. Based on this observation, one can expect that reducing the deviation between the band healing lengths does not necessarily mean that the system approaches an effectively single-component regime. A mismatch between the band-condensate spatial profiles can still remain, reflecting an essential role of the multiple-condensate structure even for a negligible difference between the band healing lengths. We note that the nonmonotonic behavior of Δ_1 in panel (b) can disappear when higher orders in τ will be included (we are at the edge of the validity domain). However, higher order corrections can hardly remove an important mismatch between the spatial profiles of the band condensates.

In the previous paragraph we have considered how the deviation between the band healing lengths and mismatch between the band-condensate spatial profiles change with β, focusing on the particular values $\beta^{(a-b)}$ and $\beta^{(c)}$ extracted from the first-principle calculations for MgB_2. To gain further insights into the role of β, we note that there is another quantity which depends strongly on the ratio of the band Fermi velocities and can even change its sign, i.e., the deviation of the band healing length from the GL coherence length. As discussed in Sec. II, the leading correction to the GL coherence length is small and positive (at $T < T_c$) in the single-band case. However, this is not correct for multiple bands. In particular, one can see from Fig. 6(d) that for $\beta = \beta^{(c)}$ both healing lengths are smaller than the GL coherence length below T_c. On the contrary, for $\beta = \beta^{(a-b)}$ we have $\xi_i \geqslant \xi_{\rm GL}$; see Fig. 6(c). Furthermore, the leading correction to $\xi_{\rm GL}$ is close to that of the single-band system only for band 1 at $\beta = \beta^{(a-b)}$. In the other cases the absolute value of the quantity $\xi_i - \xi_{\rm GL}$ appears to be much more pronounced. For example, in Fig. 6(c) we have $\xi_2 - \xi_{\rm GL} \approx 0.4\xi_{\rm GL}$ at $\tau = 0.4$, which should be compared to $0.05\xi_{\rm GL}$ obtained previously for the same value of τ in the single-band case; see the discussion after Eq. (23) in Sec. II. By the way, one can see that the deviation between the band healing lengths is not negligible even for $\beta = \beta^{(a-b)} = 1.22$. For example, we obtain $\xi_2 - \xi_1 \approx 0.35\xi_{\rm GL}$ at $\tau = 0.4$, where $\xi_2/\xi_1 \approx 1.3$.

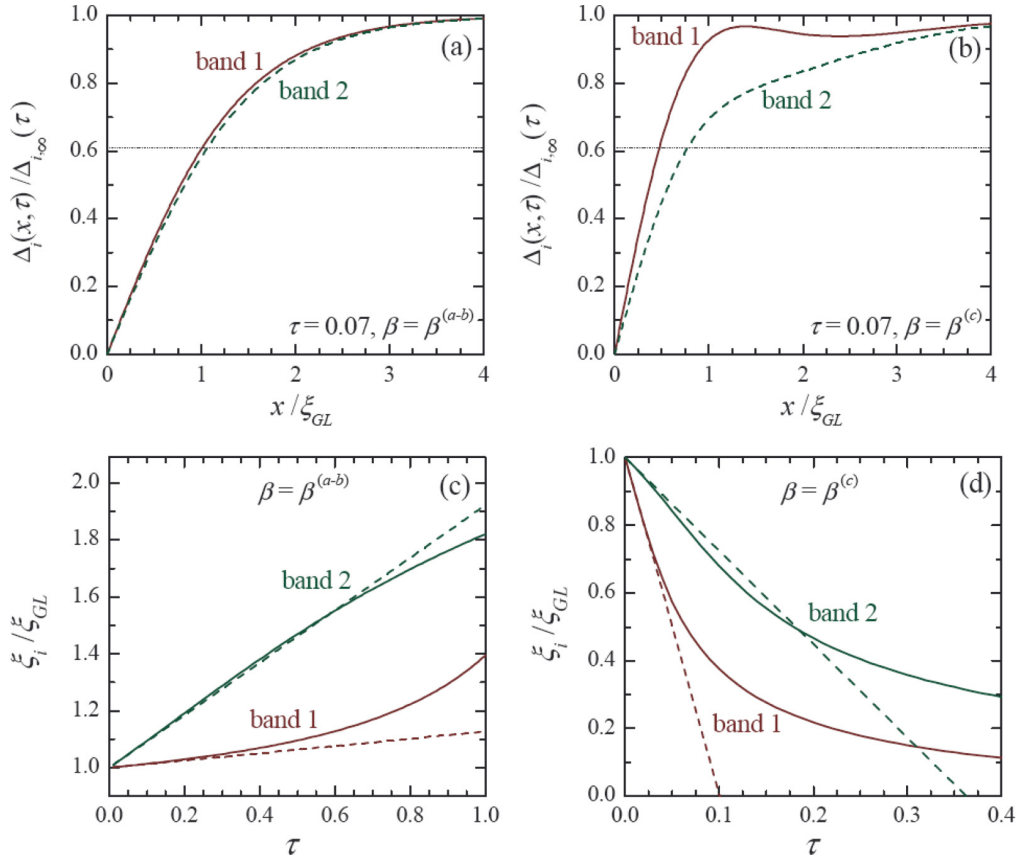

FIG. 6. (a) EGL solution for the band gap $\Delta_i(x,\tau)$ [in units of its asymptotic value $\Delta_{i,\infty}(\tau)$] as a function of the distance from the interface (in units of $\xi_{\rm GL}$) calculated at $\tau = 0.07$ and $\beta = \beta^{(a-b)}$; the solid and dashed curves represent bands 1 and 2, respectively. (b) The same as in panel (a) but for $\beta = \beta^{(c)}$. (c) The relative band healing length $\xi_i/\xi_{\rm GL}$ versus τ at $\beta = \beta^{(a-b)}$: the analytical result of Eq. (52) is given by the dashed line, while the full numerical solution of Eq. (51) is represented by the solid curve. (d) The same as in (c) but now for $\beta = \beta^{(c)}$. The dotted lines in panels (a) and (b) mark $\delta = \tanh(1/\sqrt{2})$ that determines the band healing length according to Eq. (51). The validity domain of the τ expansion can be estimated as $\tau \lesssim \tau^* = 0.4{-}0.5$ for $\beta = \beta^{(a-b)}$ and $\tau \lesssim \tau^* = 0.05{-}0.07$ for $\beta = \beta^{(c)}$; see the discussion in the main text.

One can also learn from Figs. 6(c) and 6(d) that the validity domain of the two-band EGL formalism is strongly dependent on the ratio of the band Fermi velocities. In particular, for $\beta = \beta^{(a-b)}$ the analytical results for the band healing lengths are close to the numerical solutions of Eq. (51) up to $\tau = 0.4{-}0.5$ so that the upper boundary of the validity domain is estimated as $\tau^* = 0.4{-}0.5$. (See the discussion about the validity of the single-band EGL theory in Sec. II.) From Fig. 6(d) we find the considerably smaller value $\tau^* = 0.05{-}0.07$. This shrinking of the validity domain at $\beta = \beta^{(c)}$ is a manifestation of the fact that, for great disparity between the band Fermi velocities, the deviations of the band healing lengths from the GL coherence length (and also from each other) so rapidly increase with τ that higher orders in τ should be incorporated already for $\tau \gtrsim 0.1$.

Continuing our discussion of multiband materials with large differences between the band Fermi velocities, we turn to superconductors with shallow bands, where charge carriers are depleted and have nearly zero velocities [43–46]. Such superconductors recently attracted attention in the context of possible routes to the BCS-BEC superconductivity in solids [44–46]. In particular, it has been found by the ARPES measurements [44] that there exist three contributing bands in iron chalcogenide $FeSe_{0.35}Te_{0.65}$, viz. two shallow hole pockets and one shallow electron pocket. The obtained data suggest that the Fermi energy measured from the band edge in both hole bands can be estimated as 4 meV, whereas for the electron band it is nearly 10 meV. The hole masses are about $3.4m_e$ (m_e is the free electron mass) and $14m_e$. As to the electron effective mass, it is not specified in Ref. [44] but can be estimated as $2.5m_e$ from the results for the electron band in similar compound FeSe [45]. So one can calculate that the ratio of the light-hole Fermi velocity to that of the heavy holes is about 2. The ratio of the electronic band Fermi velocity to that of the light-hole band is also about 2. Thus the maximal ratio of the band Fermi velocities in this system goes up to 4. We note that the recent interest in superconductors with shallow bands and in the related BCS-BEC superconductivity in multiband materials [43–46] makes it possible to expect that new shallow-band superconductors will be fabricated in the near future. Based on the results of the present study, one can expect that the systems with coexisting deep and shallow bands, i.e., with disparate band length scales, will be very promising materials in order to search for superconducting phenomena not intrinsic to single-band systems.

Another useful and very promising example concerns dirty superconductors that can provide additional possibilities to

obtain significantly different spatial scales of the contributing band condensates. In the dirty limit the band healing lengths are determined by the band diffusion coefficients; see, e.g., Ref. [47]. These coefficients can be considerably different. For example, in epitaxial MgB_2 thin films the diffusivities are extracted from the experimental data for the upper critical field [13] as $D_\sigma = 0.23\ \mathrm{cm^2\,s^{-1}}$ for the σ band and $D_\pi = 40\ \mathrm{cm^2\,s^{-1}}$ for the π band. As seen, the diffusion coefficients D_σ and D_π are different by two orders of magnitude (around 170 times). To estimate the low-temperature ratio of the band healing lengths, one can employ the decoupled-band approximation $\xi_i \propto \sqrt{D_i}$ (see, e.g., Ref. [47]), which yields $\xi_\pi/\xi_\sigma \approx 13.2$. As argued in Ref. [13], the presence of the two disparate band length scales is responsible for the formation of broken symmetry vortex structures (like labyrinths of vortices) that have been observed [13] in images of the local stray magnetic fields at the surface of the MgB_2 thin films.

IV. CONCLUSIONS

Concluding, we have analytically calculated the band-dependent corrections to the GL coherence length for the two-band case. Our study has demonstrated that a deviation between the resulting band healing lengths is a product of complex interplay between different tendencies mainly governed by the interband interactions and band Fermi velocities. The interband coupling tends to wash out the disparity of the band spatial scales, while the difference between the band characteristic velocities helps it to sustain. As a result, the band healing lengths can significantly deviate from each other far beyond the regime of nearly decoupled bands.

Our study has been performed for a clean s-wave two-band superconductor within the EGL formalism that goes to one order beyond the standard GL theory in the perturbative expansion of the BCS formalism over the proximity to the critical temperature τ. The advantage of this approach is that it allows for deriving closed analytical results that can be examined in a wide range of the relevant microscopic parameters. In particular, we have obtained analytical expressions for the band gaps in the lowest and next-to-lowest orders in τ for the spatial configuration where the superconducting condensate is suppressed in a half-space. Utilizing these expressions, we have derived the band healing lengths in an explicit form up to the leading correction to the GL coherence length and confirmed the previous results that the band length scales are generally different in the next-to-lowest order in τ. By investigating the deviation between the band healing lengths, we have demonstrated that it is rather sensitive to the interband interactions but also to disparity between the band Fermi velocities. The universal character of the EGL approach allows one to expect qualitatively similar results for systems with an arbitrary number of bands, except for the special case when there is an additional to $U(1)$ symmetry in the system so that the band healing lengths are different even at $T = T_c$; see, e.g., Ref. [48].

The aim of the present study is to demonstrate that disparate band length scales in multiband superconductors can appear far beyond the regime of nearly zero interband couplings. A complete analysis of healing lengths in multiband superconductors, including various pairing symmetries, various numbers of bands, disorder, and anisotropy, is beyond the present work. However, given the complex interplay of the different trends in a relatively simple two-band system with the s-wave pairing and spherical band Fermi surfaces, one can expect that the competition of the band length scales in sophisticated multiband systems is even more tangled and nontrivial.

Finally, it is of importance to stress again that our analytical results on the disparity between the band-dependent corrections to the GL coherence length are relevant for the spatial distribution of the superconducting condensate in the vortex core of multiband materials. Here one should keep in mind that a magnetic field provides an additional coupling between the band supercurrents and, in turn, between the band-condensate spatial profiles. This, of course, deserves additional investigations but, physically, such a magnetic coupling cannot significantly influence the system for large interband couplings. Thus our general qualitative conclusions will not be altered and our findings can motivate experimentalists to look for multiband materials with significantly different band length scales. As argued previously in Refs. [11,20], such materials can have un unusual magnetic response, belonging to the intertype regime governed by the Bogomolnyi self-duality.

ACKNOWLEDGMENTS

T.T.S. and C.C.d.S.S. acknowledge support from the Brazilian Agencies CNPq and FACEPE, under Grants No. APQ-2017-1.05/12 and No. APQ-0198-1.05/14. J.A.A. and A.A.S. are thankful to the Brazilian Agencies CNPq (grant 309374/2016-2) and FACEPE (grant APQ-0936-1.05/15). T.T.S., J.A.A., and A.A.S. thank A. Vagov and A. Perali for useful discussions.

[1] M. V. Milošević and A. Perali, Supercond. Sci. Technol. **28**, 060201 (2015).
[2] E. Babaev, Phys. Rev. Lett. **89**, 067001 (2002).
[3] J. C. Piña, C. C. de Souza Silva, and M. V. Milošević, Phys. Rev. B **86**, 024512 (2012).
[4] S. Z. Lin and L. N. Bulaevskii, Phys. Rev. Lett. **110**, 087003 (2013).
[5] S. Z. Lin and C. Reichhardt, Phys. Rev. B **87**, 100508 (2013).
[6] R. M. da Silva, M. V. Milošević, D. Domínguez, F. M. Peeters, and J. Albino Aguiar, Appl. Phys. Lett. **105**, 232601 (2014).
[7] S. Z. Lin, J. Phys.: Condens. Matter **26**, 493203 (2014).
[8] Y. Tanaka, Phys. Rev. Lett. **88**, 017002 (2001).
[9] Y. Tanaka, J. Phys. Soc. Jpn. **70**, 2844 (2001).
[10] L. Komendová, Yajiang Chen, A. A. Shanenko, M. V. Milošević, and F. M. Peeters, Phys. Rev. Lett. **108**, 207002 (2012).
[11] A. Vagov, A. A. Shanenko, M. V. Milošević, V. M. Axt, V. M. Vinokur, J. Albino Aguiar, and F. M. Peeters, Phys. Rev. B **93**, 174503 (2016).
[12] R. M. da Silva, M. V. Milošević, A. A. Shanenko, F. M. Peeters, and J. Albino Aguiar, Sci. Rep. **5**, 12695 (2015).

[13] P. J. Curran, W. M. Desoky, M. V. Milošević, A. Chaves, J.-B. Laloë, J. S. Moodera, and S. J. Bending, Sci. Rep. **5**, 15569 (2015).
[14] V. Moshchalkov, M. Menghini, T. Nishio, Q. H. Chen, A. V. Silhanek, V. H. Dao, L. F. Chibotaru, N. D. Zhigadlo, and J. Karpinski, Phys. Rev. Lett. **102**, 117001 (2009).
[15] J. Geyer, R. M. Fernandes, V. G. Kogan, and J. Schmalian, Phys. Rev. B **82**, 104521 (2010).
[16] V. G. Kogan and J. Schmalian, Phys. Rev. B **83**, 054515 (2011).
[17] A. A. Shanenko, M. V. Milošević, F. M. Peeters, and A. V. Vagov, Phys. Rev. Lett. **106**, 047005 (2011).
[18] E. B. Bogomolnyi and A. I. Vainstein, Sov. J. Nucl. Phys. **23**, 588 (1976).
[19] E. B. Bogomolnyi, Sov. J. Nucl. Phys. **24**, 449 (1976).
[20] W. Y. Córdoba-Camacho, R. M. da Silva, A. Vagov, A. A. Shanenko, and J. Albino Aguiar, Phys. Rev. B **94**, 054511 (2016).
[21] B. T. Geilikman, R. O. Zaitsev, and V. Z. Kresin, Sov. Phys. Solid State **9**, 642 (1967).
[22] A. Vagov, A. A. Shanenko, M. V. Milošević, V. M. Axt, and F. M. Peeters, Phys. Rev. B **86**, 144514 (2012).
[23] L. Komendová, M. V. Milošević, A. A. Shanenko, and F. M. Peeters, Phys. Rev. B **84**, 064522 (2011).
[24] M. Silaev and E. Babaev, Phys. Rev. B **84**, 094515 (2011).
[25] A. Fente, E. Herrera, I. Guillamon, H. Suderow, S. Mañas-Valero, M. Galbiati, E. Coronado, and V. G. Kogan, Phys. Rev. B **94**, 014517 (2016).
[26] A. Fente, W. R. Meier, T. Kong, V. G. Kogan, S. L. Bud'ko, P. C. Canfield, I. Guillamon, and H. Suderow, Vortices in two-effective-band, stoichiometric high T_c $CaKFe_4As_4$ superconductor, arXiv:1608.00605.
[27] M. Ichioka, V. G. Kogan, and J. Schmalian, Phys. Rev. B **95**, 064512 (2017).
[28] A. V. Vagov, A. A. Shanenko, M. V. Milošević, V. M. Axt, and F. M. Peeters, Phys. Rev. B **85**, 014502 (2012).
[29] A. E. Jacobs, Phys. Rev. Lett. **26**, 629 (1971).
[30] A. E. Jacobs, Phys. Rev. B **4**, 3016 (1971).
[31] A. E. Jacobs, Phys. Rev. B **4**, 3022 (1971).
[32] A. E. Jacobs, Phys. Rev. B **4**, 3029 (1972).
[33] L. Neumann and L. Tewordt, Z. Phys. **189**, 55 (1966).
[34] L. Neumann and L. Tewordt, Z. Phys. **191**, 73 (1966).
[35] C. P. Poole, H. A. Farach, R. J. Creswick, and R. Prozorov, *Superconductivity* (Elsevier, Amsterdam, 2014).
[36] A. A. Shanenko, M. D. Croitoru, and F. M. Peeters, Phys. Rev. B **75**, 014519 (2007).
[37] L. Kramer and W. Pesch, Z. Phys. **269**, 59 (1974).
[38] Y. Chen, A. A. Shanenko, and F. M. Peeters, Phys. Rev. B **89**, 054513 (2014).
[39] A. L. Fetter and J. D. Walecka, *Quantum Theory of Many-Particle Systems* (Dover, New York, 2003).
[40] M. Abramowitz and I. A. Stegun, *Handbook of Mathematical Functions* (Dover, New York, 1972).
[41] A. Brinkman, A. A. Golubov, H. Rogalla, O. V. Dolgov, J. Kortus, Y. Kong, O. Jepsen, and O. K. Andersen, Phys. Rev. B **65**, 180517(R) (2002).
[42] A. A. Golubov, J. Kortus, O. V. Dolgov, O. Jepsen, Y. Kong, O. K. Andersen, B. J. Gibson, K. Ahn, and R. K. Kremer, J. Phys.: Condens. Matter **14**, 1353 (2002).
[43] S. Borisenko, Nat. Mater. **12**, 600 (2013).
[44] Y. Lubashevsky, E. Lahoud, K. Chashka, D. Podolsky, and A. Kanigel, Nat. Phys. **8**, 309 (2012).
[45] S. Kasahara, T. Watashige, T. Hanaguri, Y. Kohsaka, T. Yamashita, Y. Shimoyama, Y. Mizukami, R. Endo, H. Ikeda, K. Aoyama, T. Terashima, S. Uji, T. Wolf, H. von Löhneysenn, T. Shibauchi, and Y. Matsuda, PNAS **111**, 16309 (2014).
[46] K. Okazaki, Y. Ito, Y. Ota, Y. Kotani, T. Shimojima, T. Kiss, S. Watanabe, C.-T. Chen, S. Niitaka, T. Hanaguri, H. Takagi, A. Chainani, and S. Shin, Sci. Rep. **4**, 4109 (2014).
[47] A. Gurevich, Phys. Rev. B **67**, 184515 (2003).
[48] N. V. Orlova, A. A. Shanenko, M. V. Milosevic, F. M. Peeters, A. V. Vagov, and V. M. Axt, Phys. Rev. B **87**, 134510 (2013).

PHYSICAL REVIEW B **99**, 024515 (2019)

Anisotropic superconductors between types I and II

T. T. Saraiva,[1] A. Vagov,[2,3] V. M. Axt,[2] J. Albino Aguiar,[1] and A. A. Shanenko[1]
[1]*Departamento de Física, Universidade Federal de Pernambuco, Av. Prof. Aníbal Fernandes, s/n, 50740-560, Recife - PE, Brazil*
[2]*Institut für Theoretische Physik III, Universität Bayreuth, Bayreuth 95440, Germany*
[3]*ITMO University, St. Petersburg, 197101, Russia*

(Received 15 August 2018; revised manuscript received 30 November 2018; published 28 January 2019)

Self-duality or matching between the magnetic and the condensate coherence lengths is a fundamental property of isotropic superconductors at the critical Bogomolnyi point (B point). The self-dual state of the condensate is infinitely degenerate, which is the core reason for the sharp transition between the superconductivity types in the nearest vicinity of the critical temperature T_c. Below T_c nonlocal interactions in the condensate remove the degeneracy, which leads to the appearance of a finite intertype (IT) domain between types I and II. This domain exhibits the mixed state with exotic field-condensate configurations and nonstandard magnetic response, which cannot be understood within the dichotomy of the conventional superconductivity types. At a first glance, this picture does not apply to an anisotropic system because no spatial matching between the condensate and magnetic field can be generally expected for direction-dependent characteristic lengths. However, contrary to these expectations, here we demonstrate that anisotropic superconductors follow the same scenario of the interchange between types I and II. In anisotropic materials the IT domain is governed by the B point of the effective isotropic model obtained by the appropriate scaling transformation of the initial anisotropic formalism. This transformation depends on the direction of the applied magnetic field, and thus the superconductivity type of strongly anisotropic materials can be dependent on this direction.

DOI: 10.1103/PhysRevB.99.024515

I. INTRODUCTION

Conventional superconductors are traditionally divided into two classes: ideally diamagnetic type-I materials, and type-II superconductors with penetration of a magnetic field in the form of single-quantum vortices arranged in an Abrikosov lattice. The distinction between these types is routinely explained within the Ginzburg-Landau (GL) picture [1–3], where the superconducting magnetic response is fully determined by the GL parameter $\kappa = \lambda/\xi$, with λ and ξ the magnetic and coherence lengths. Type I is realized when $\kappa < \kappa_0 = 1/\sqrt{2}$ and type II occurs for $\kappa > \kappa_0$.

However, as is well known since the 1970s, this classification of superconductivity types does not apply for materials with $\kappa \sim \kappa_0$ [4–18]. The GL picture is valid only in the limit $T \to T_c$ while at $T < T_c$ there is a finite temperature-dependent interval $\kappa^*_{\min} \leqslant \kappa \leqslant \kappa^*_{\max}$ [7,8,10,12,19], where superconductivity cannot be described within the type-I/type-II dichotomy. Materials that belong to this domain in the κ-T plane between types I and II, can be broadly referred to as the intertype (IT) superconductors (see, e.g., recent results for Nb [17,18] and ZrB_{12} [20–22]).

A physical reason for the appearance of the IT superconductivity is the degeneracy of the self-dual condensate-field configurations at the Bogomolnyi point (B point) (κ_0, T_c) [23,24] that separates types I and II. When the degeneracy is removed, e.g., by nonlocal interactions at $T < T_c$, exotic self-dual configurations "escape" their confinement at the B point and shape the mixed state as a finite IT domain [19,25–27]. Note, that this mechanism is much more complex and far-reaching than the type-II/1 concept proposed in earlier works where it was conjectured that the IT superconductivity can be fully understood in terms of nonmonotonic vortex-vortex interaction with long-range attraction and short-range repulsion (see, e.g., Ref. [8]). Recent studies demonstrated that the nonmonotonic pair vortex interaction is only one example of the nonconventional IT properties; others include, e.g., strong many-body (many-vortex) interactions [27,28]. The proximity to the infinitely degenerate B point increases the sensitivity of the superconducting state to external parameters such as temperature, magnetic field, and current, as well as to impurities and system geometry. This sensitivity opens the way for controlled manipulations of the superconducting magnetic properties.

However, until now the relation between the B point and IT superconductivity has been investigated only for isotropic materials. At the same time, most of the real superconductors are anisotropic and in this case the coherence ξ_j and magnetic lengths λ_j $(j = x, y, z)$ are direction dependent and so is the GL parameter $\kappa_j = \lambda_j/\xi_j$. When these lengths have different direction dependences, one can hardly expect to achieve the spatial matching between the condensate and magnetic field, which questions the relevance of the self-dual properties in anisotropic materials. Thus, the scenario of the interchange between superconductivity types worked out for isotropic superconductors (type I-IT-type II) appears to be inapplicable for real anisotropic materials.

The goal of this work is to demonstrate that contrary to these expectations, anisotropic superconductors, even with a high degree of anisotropy, still follow the above scenario of the type interchange. The corresponding IT domain is governed by the B point of an effective isotropic model

obtained by an appropriate scaling transformation of the initially anisotropic formalism. However, this transformation depends on the direction of the applied magnetic field and thus, the superconductivity type of a strongly anisotropic material can depend on the orientation of the system.

II. MODEL AND METHOD

To achieve this goal we consider a single-band s-wave model with an ellipsoidal Fermi surface, as a prototype of anisotropic superconductors. For the sake of clarity, it is also assumed that the magnetic field is directed along one of the principal anisotropic axes. This choice seems to be restrictive but, in fact, our qualitative conclusions do not depend on details of the model and hold in a more general case.

The analysis is done using the extended GL (EGL) formalism [29] that accounts for the leading-order corrections to the GL theory in the perturbative expansion of the microscopic equations with the proximity to the critical temperature $\tau = 1 - T/T_c$ as a small parameter. We briefly recall the main steps of the derivation of this expansion in order to highlight important changes introduced by the anisotropy. First, the condensate contribution to the free energy F is expanded in powers of the order parameter $\Delta(\mathbf{x})$ known to be small near T_c. This yields

$$F = \int d^3\mathbf{x}\left[\frac{\mathbf{B}^2(\mathbf{x})}{8\pi} + \frac{|\Delta(\mathbf{x})|^2}{g} - \sum_{n=0}^{\infty}\frac{1}{n}\int\prod_{j=1}^{2n+1} d^3\mathbf{y}_j\, K_{2n+1}(\mathbf{x}, \{\mathbf{y}\}_{2n+1})\Delta^*(\mathbf{x})\Delta(\mathbf{y}_1)\cdots\Delta^*(\mathbf{y}_{2n})\Delta(\mathbf{y}_{2n+1})\right], \quad (1)$$

where $\mathbf{B}(\mathbf{x})$ is the magnetic field, g denotes the coupling constant, and $\{\mathbf{y}\}_{2n+1} = \{\mathbf{y}_1, \ldots, \mathbf{y}_{2n+1}\}$ stays for the set of spatial coordinates. The integral kernels in Eq. (1) read (m is odd)

$$K_m(\mathbf{x}, \{\mathbf{y}\}_m) = -T\sum_{\omega}\mathcal{G}_{\omega}^{(B)}(\mathbf{x}, \mathbf{y}_1)\bar{\mathcal{G}}_{\omega}^{(B)}(\mathbf{y}_1, \mathbf{y}_2) \times \cdots \mathcal{G}_{\omega}^{(B)}(\mathbf{y}_{m-1}, \mathbf{y}_m)\bar{\mathcal{G}}_{\omega}^{(B)}(\mathbf{y}_m, \mathbf{x}), \quad (2)$$

where ω is the fermionic Matsubara frequency, $\mathcal{G}_{\omega}^{(B)}(\mathbf{x}, \mathbf{y})$ is the Fourier transform of the normal Green's function calculated in the presence of the magnetic field, and $\bar{\mathcal{G}}_{\omega}^{(B)}(\mathbf{x}, \mathbf{y}) = -\mathcal{G}_{-\omega}^{(B)}(\mathbf{y}, \mathbf{x})$. The magnetic-field dependence of $\mathcal{G}_{\omega}^{(B)}$ is taken into account within the standard Peierls approximation sufficient to derive the extended GL theory

$$\mathcal{G}_{\omega}^{(B)}(\mathbf{x}, \mathbf{y}) = \exp\left[\mathbb{i}\,\frac{e}{\hbar c}\int_{\mathbf{y}}^{\mathbf{x}}\mathbf{A}(\mathbf{z})\cdot d\mathbf{z}\right]\mathcal{G}_{\omega}^{(0)}(\mathbf{x}, \mathbf{y}), \quad (3)$$

where the contour integral with the vector potential $\mathbf{A}$ is calculated along the classical trajectory of a charged particle in the magnetic field and the free-particle Green's function at zero field writes as

$$\mathcal{G}_{\omega}^{(0)}(\mathbf{x}, \mathbf{y}) = \int\frac{d^3\mathbf{k}}{(2\pi)^3}\frac{\exp[\mathbb{i}\mathbf{k}\cdot(\mathbf{x}-\mathbf{y})]}{\mathbb{i}\hbar\omega - \xi_{\mathbf{k}}}, \quad (4)$$

where $\xi_{\mathbf{k}} = \varepsilon_{\mathbf{k}} - \mu$ is the single-particle energy measured from the chemical potential. Equations (1)–(4) are valid for an arbitrary single-particle dispersion $\varepsilon_{\mathbf{k}}$. However, analytical results can be obtained only for a limited number of models. One of them is the model of an ellipsoidal Fermi surface, often employed to study anisotropy-related effects. Choosing the principal axes of the ellipsoidal Fermi surface as the coordinate system, one gets $\xi_{\mathbf{k}}$ in the diagonal form as

$$\xi_{\mathbf{k}} = \sum_{j=1}^{3}\frac{\hbar^2k_j^2}{2m_j} - \mu, \quad (5)$$

where m_j is a direction-dependent effective carrier mass.

In the next step of the EGL derivation one substitutes the gradient expansion for the order parameter $\Delta(\mathbf{y}) = \Delta(\mathbf{x}) + [(\mathbf{y}-\mathbf{x})\cdot\nabla]\Delta(\mathbf{x}) + \cdots$ as well as for the field into Eqs. (1)–(3). This allows one to represent nonlocal integrals in Eq. (1) as a series in powers of the order parameter and field, as well as of their spatial derivatives. As the single-particle dispersion is anisotropic, the gradient-dependent contributions to the free energy functional are also anisotropic. However, it is well known that the GL contribution to the free energy can be isotropized for any anisotropic single-particle dispersion by applying a proper scaling transformation [30–32]. In particular, for our choice given by Eq. (5) the spatial coordinates and momenta are scaled as

$$\tilde{x}_j = x_j/\sqrt{\alpha_j}, \quad \tilde{k}_j = \sqrt{\alpha_j}k_j, \quad (6)$$

where

$$\alpha_j = M/m_j, \quad M = \sqrt[3]{m_xm_ym_z}, \quad \alpha_x\alpha_y\alpha_z = 1. \quad (7)$$

This transformation yields the isotropic energy dispersion $\xi_{\tilde{\mathbf{k}}} = \hbar^2\tilde{\mathbf{k}}^2/(2M) - \mu$ with the scaled Fermi wave number $\tilde{k}_F = \sqrt{2\mu M/\hbar^2}$. Further, the anisotropy in the field-dependent contributions to the condensation energy is eliminated by scaling the components of the vector potential and magnetic field as

$$\tilde{A}_j = \sqrt{\alpha_j}A_j, \quad \tilde{B}_j = B_j/\sqrt{\alpha_j}, \quad (8)$$

which obviously preserves the standard relation $\tilde{\nabla}\times\tilde{\mathbf{A}} = \tilde{\mathbf{B}}$ (with the changed gauge). The scaling transformation given by Eqs. (6)–(8) ensures that the GL contribution to the condensate free energy is isotropic but the magnetic-field energy becomes anisotropic [30–32] and writes as $\mathbf{B}^2 = \sum_j\alpha_j\tilde{B}_j^2$. For the case of interest, when the magnetic field is directed along a principal axis, only a single component remains in the field contribution (here it is the z component), i.e., $\mathbf{B}^2 = \alpha_z\tilde{B}_z^2$. Then the factor α_z is eliminated by rescaling the total free energy as $\tilde{f} = f/\alpha_z$ and renormalizing the carrier density of states (DOS) accordingly. As a result, one obtains a fully

isotropic GL functional

$$f = \frac{\mathbf{B}^2}{8\pi} + a|\Delta|^2 + \mathcal{K}|\mathbf{D}\Delta|^2 + \frac{b}{2}|\Delta|^4, \tag{9}$$

where $\mathbf{D} = \boldsymbol{\nabla} - (2\mathbb{i}e/\hbar\,\mathbb{c})\mathbf{A}$ and, from now on, the tilde mark for the scaled quantities is suppressed. The coefficients of this effective isotropic functional are given by the standard expressions

$$a = -N(0)\tau, \quad b = \frac{N(0)}{T_c^2}\frac{7\zeta(3)}{8\pi^2}, \quad \mathcal{K} = \frac{b}{6}\hbar^2 v_F^2, \tag{10}$$

where $\zeta(\cdots)$ is the Riemann zeta function and one uses material parameters of the isotropic "scaled" model such as M and $v_F = \hbar k_F/M$ [see Eq. (7)]. However, a difference with the usual isotropic case is that the DOS is renormalized as $N(0) = N_{\rm in}(0)/\alpha_z$, with $N_{\rm in}(0) = Mk_F/(2\pi\hbar^2)$ being the DOS of the original model.

This scaling has been considered earlier in studies of the mixed state of anisotropic superconductors deep in the type-II regime [30–32]. Notice, however, that this transformation of the originally anisotropic GL formalism leads to an important observation concerning the interchange between superconductivity types I and II: anisotropic materials also have an infinitely degenerate B point that separates types I and II at $T \to T_c$ and unfolds into a finite IT domain below T_c. However, here this point appears in the "scaled" isotropic model. This observation, which has not been discussed previously, implies that the anisotropy does not destroy the isotropic scenario of the type interchange unlike, for example, mechanisms related to finite sample dimensions. The latter eliminate the B-point degeneracy in superconducting films and wires, thereby destroying the sharp transition between types I and II at $T \to T_c$ (see Ref. [25]).

In order to investigate a finite IT domain appearing at $T < T_c$, the leading corrections to the GL contribution are to be retained in the free energy [19]. Such additional contributions are also subject to the transformation defined by Eqs. (6)–(8). However, the final result depends on details of the band structure. The adopted model with an ellipsoidal Fermi surface is special in this regard because it ensures that any term in the expansion of the free energy in powers of the order parameter given by Eq. (1) becomes isotropic under the same transformation. This is seen from the fact that the scaling transformation in Eqs. (6)–(8) reduces the Green's function in Eq. (4) to its isotropic form. Then, the scaled leading corrections to the GL free energy are obtained as

$$\begin{aligned}\delta f = {} & \frac{a\tau}{2}|\Delta|^2 + 2\tau\mathcal{K}|\mathbf{D}\Delta|^2 + \tau b|\Delta|^4 - \frac{c}{3}|\Delta|^6 \\ & - \mathcal{Q}\left(|\mathbf{D}^2\Delta|^2 + \frac{1}{3}\mathrm{rot}\mathbf{B}\cdot\mathbf{i} + \frac{4e^2}{\hbar^2\mathbb{c}^2}\mathbf{B}^2|\Delta|^2\right) \\ & - \frac{\mathcal{L}}{2}[8|\Delta|^2|\mathbf{D}\Delta|^2 + (\Delta^*)^2(\mathbf{D}\Delta)^2 + \Delta^2(\mathbf{D}^*\Delta^*)^2],\end{aligned} \tag{11}$$

where $\mathbf{i} = (e/\hbar\mathbb{c})\mathrm{Im}[\Delta^*\mathbf{D}\Delta]$ is the supercurrent density, the relevant coefficients are

$$c = \frac{N(0)}{T_c^4}\frac{93\zeta(5)}{128\pi^4}, \quad \mathcal{Q} = \frac{c}{30}\hbar^4 v_F^4, \quad \mathcal{L} = \frac{c}{9}\hbar^2 v_F^2, \tag{12}$$

and $N(0)$ is the renormalized DOS introduced in Eq. (10). Notice that the resulting total free energy density $f + \delta f$ coincides with the isotropic Neumann-Tewordt functional [19,33,34].

The choice of the terms contributing to Eq. (11) is dictated by the subsequent τ expansion of the free energy obtained from Eqs. (9)–(12) by substituting $\Delta = \tau^{1/2}(\Delta_0 + \tau\Delta_1)$, $\mathbf{A} = \tau^{1/2}(\mathbf{A}_0 + \tau\mathbf{A}_1)$, and $\mathbf{B} = \tau^{1/2}(\mathbf{B}_0 + \tau\mathbf{B}_1)$ and using the coordinate scaling $\mathbf{x}' = \mathbf{x}\tau^{-1/2}$, which is equivalent to the substitution $\boldsymbol{\nabla}' \to \tau^{1/2}\boldsymbol{\nabla}$. Then, the GL contributions to the free energy are of order τ^2 while the leading corrections are of order τ^3. The obtained τ expansion for the free energy density produces the EGL equations: the GL equations for Δ_0 and $\mathbf{A_0}$ ($\mathbf{B}_0$) and additional equations for Δ_1 and $\mathbf{A}_1$ ($\mathbf{B}_1$). An important advantage of the formalism is that the leading-order corrections to the GL stationary free energy can be expressed only in terms of the solutions of the GL equations (see Ref. [19]).

We complete the discussion of the formalism by briefly dwelling on the validity of the used model with an ellipsoidal Fermi surface. The fact that the leading corrections to the GL theory and, in general, any higher order contributions to the free energy can be converted into the isotropic form by the same scaling transformation is clearly a result of this model. For a more general choice of the single-particle dispersion, the GL contributions can still be isotropized by the above scaling transformation [35]. However, some corrective terms remain anisotropic. In particular, in the leading corrections these are the terms with the fourth-order gradients in Eq. (11) (see the contribution with the coefficient $\mathcal{Q}$). When adopting the dispersion (5), such fourth-order gradient terms are obtained as

$$\begin{aligned}&\sum_{ijnm}\langle k_i k_j k_n k_m\rangle\nabla_i\nabla_j\nabla_n\nabla_m \\ &\qquad \propto \left(\sum_{ij}\langle k_i k_j\rangle\nabla_i\nabla_j\right)\left(\sum_{nm}\langle k_n k_m\rangle\nabla_n\nabla_m\right),\end{aligned} \tag{13}$$

where $\langle k_i k_j k_n k_m\rangle$ and $\langle k_i k_j\rangle$ are the k-averaging integrals of the products $k_i k_j k_n k_m$ and $k_i k_j$ (indices denote the vector components) with the weight given by the product of the Fourier transforms of $\mathcal{G}_\omega^{(0)}(\mathbf{x},\mathbf{y})$ and $\bar{\mathcal{G}}_\omega^{(0)}(\mathbf{x},\mathbf{y})$ (details of the calculation are in Ref. [29]). Equation (13) holds for an ellipsoidal Fermi surface, which yields $\langle k_i k_j k_n k_m\rangle \propto \langle k_i k_j\rangle\langle k_n k_m\rangle$, with a constant proportionality coefficient. When the principal axes of an ellipsoidal Fermi surface form the coordinate system, each factor in the right-hand side of Eq. (13) acquires the diagonal form and is isotropized simultaneously with the GL contribution.

A more general model for the Fermi surface may result in deviations from Eq. (13). Such deviations generate additional anisotropic contributions to the free energy functional that cannot be made isotropic simultaneously with the GL terms. Adopting the model with an ellipsoidal Fermi surface is thus equivalent to neglecting such extra contributions. However, as already mentioned above, only the terms with the coefficient $\mathcal{Q}$ will be affected. The previous investigations in Refs. [19] and [26] have demonstrated that the contribution of these terms to the results for the IT domain is significant only in

multiband materials with one of the contributing bands being shallow, i.e., when the chemical potential μ is close to its edge. However, this case is irrelevant for the current study of single-band materials.

III. SUPERCONDUCTIVITY-TYPE INTERCHANGE AND IT DOMAIN

Utilizing earlier results obtained within the isotropic EGL formalism in Ref. [19], we calculate upper $\kappa^*_{\rm min}$ and lower $\kappa^*_{\rm max}$ boundaries of the IT domain on the κ-T plane, where κ is the GL parameter of the scaled isotropic system. The critical parameters $\kappa^*_{\rm min}$ and $\kappa^*_{\rm max}$ are temperature dependent and defined as follows: at $\kappa > \kappa^*_{\rm min}$ a superconductor can develop a mixed state, while at $\kappa < \kappa^*_{\rm max}$ vortices become attractive at long ranges.

These critical parameters κ^* (and others related to the internal subdivisions in the IT domain) are calculated using the difference ΔG between the Gibbs free energy of a chosen spatially nonuniform field-condensate configuration and of the Meissner state, both calculated at the thermodynamic critical magnetic field H_c [19]. The Gibbs free energy G is obtained from the free energy by subtracting $(\mathbf{H}\cdot\mathbf{B})/4\pi$, with $\mathbf{H} = (0, 0, H_c)$ an external magnetic field.

The calculations are facilitated by performing an additional perturbation expansion of the Gibbs free energy, this time with respect to $\delta\kappa = \kappa - \kappa_0$. Taking into account that $\delta\kappa \sim \tau$, one keeps only the linear contribution in this series expansion. The resulting Gibbs free energy difference (normalized to the sample size L_z in the z direction), obtained from Eq. (11), writes in the dimensionless units as [19]

$$\frac{\Delta G}{\tau^2 L_z} = \tau(\mathcal{A}\mathcal{I} + \mathcal{B}\mathcal{J}) - \sqrt{2}\mathcal{I}\delta\kappa, \tag{14}$$

where for single-band superconductors $\mathcal{A} = -0.407$ and $\mathcal{B} = 0.681$ are universal constants and the integrals

$$\mathcal{I} = \int |\Psi|^2(1-|\Psi|^2)d\mathbf{x}, \quad \mathcal{J} = \int |\Psi|^4(1-|\Psi|^2)d\mathbf{x}, \tag{15}$$

are calculated using a solution Ψ of the self-dual GL equations at κ_0; this solution is normalized as $\Psi(\mathbf{x}\to\infty)\to 1$ and its spatial dependence is given in the units of $\sqrt{2}\lambda$. The absence of the zero-order term in the right-hand side of Eq. (14) is a consequence of the degeneracy of the GL theory at κ_0. One can also see that only the GL contribution $\propto\delta\kappa$ in Eq. (14) depends on the microscopic parameters (via κ), whereas its leading corrections are material independent.

The critical parameters κ^*, that correspond to the appearance/disappearance of a particular field-condensate configuration or a specific property of such a configuration, are found from the equation $\Delta G = 0$ (see details and discussions in Ref. [19]), which resolves as

$$\kappa^* = \kappa_0[1 + \tau(\mathcal{A} + \mathcal{B}\mathcal{J}/\mathcal{I})]. \tag{16}$$

The critical parameter $\kappa^*_{\rm min}$ yields the lower boundary of the IT domain and is defined by the appearance/disappearance of the mixed state. In order to calculate this parameter one considers the limit $\Psi\to 0$ at which $\mathcal{J}/\mathcal{I}\to 0$ and thus $\kappa^*_{\rm min}$ is obtained by substituting $\mathcal{J}/\mathcal{I} = 0$ into Eq. (16). Notice that this result coincides with the one obtained from the more conventional definition for this critical parameter, which follows from the equation $H_c = H_{c2}$, where H_{c2} is the upper critical field. The upper boundary of the IT domain $\kappa^*_{\rm max}$ is related to the sign change of the long-distance asymptote of the vortex-vortex interaction. It is calculated from Eq. (16), using the GL solution for two vortices at the distance R one from another. This solution yields the exact asymptotic result $\mathcal{J}(R)/\mathcal{I}(R)\to 2$ at $R\to\infty$, which is inserted in Eq. (16).

In order to see if a material falls into the type-I, type-II, or IT domains, one needs to compare $\kappa_{\rm min/max}$ with the GL parameter κ of the scaled model given by

$$\kappa = \frac{\hbar\mathbb{c}}{|e|}\sqrt{\frac{b}{32\pi\mathcal{K}^2}}, \tag{17}$$

where b and $\mathcal{K}$ are given by Eq. (10). The B point separating conventional superconductivity types I and II at $T\to T_c$ is determined by the condition $\kappa = \kappa_0$. Returning to the original anisotropic GL model, one obtains the direction-dependent GL parameters as ($j = x, y, z$)

$$\kappa_j = \frac{\hbar\mathbb{c}}{|e|}\sqrt{\frac{b_{\rm in}}{32\pi\mathcal{K}^2_{{\rm in},j}}}, \tag{18}$$

where $b_{\rm in} = b\alpha_z$, and $\mathcal{K}_{{\rm in},j} = \mathcal{K}\alpha_z\alpha_j$ are parameters of the original anisotropic system. Then the relation between the GL parameter of the scaled isotropic model and the direction-dependent GL parameters of the original anisotropic system is

$$\kappa = \sqrt{\kappa_x\kappa_y}. \tag{19}$$

An important consequence of this relation is that the critical B point of the effective isotropic model becomes the critical B line $\kappa_x\kappa_y = \kappa_0^2$ on the plane κ_x-κ_y. Experimentally, κ_j can be changed, e.g., by nitrogen doping (see Ref. [8]). When the B line is crossed, the superconductivity type changes (see the phase diagram in Fig. 1). Below and above this line one has, respectively, types I and II.

One notices that the GL parameter κ in Eq. (17) depends on the field direction, which so far is assumed parallel to the z axis. When the field is directed along the x or y axis, the corresponding superconductivity type may change because the isotropic-model GL parameter becomes $\kappa = \sqrt{\kappa_y\kappa_z}$ or $\kappa = \sqrt{\kappa_x\kappa_z}$, respectively. Thus the value of κ can be strongly dependent on the field direction. To demonstrate this, let us consider the case of strong anisotropy with the effective masses obeying the inequality $m_z \ll m_y \ll m_x$. In this case one obtains $\kappa_z \ll \kappa_y \ll \kappa_x$. It is then easy to see that if $\kappa_y \sim 1$ then $\sqrt{\kappa_z\kappa_y} \ll 1 \ll \sqrt{\kappa_x\kappa_y}$. This implies that when the field is parallel to the x axis, the material belongs to type I; for the field along the z axis it demonstrates a type-II behavior; and when the field is along the y axis, the material is close to the IT regime.

When the temperature is lowered, the B point unfolds into a finite IT interval of κ values. Its boundaries $\kappa_{\rm max/min}(T)$ given by Eq. (16) are material independent and coincide with those obtained for isotropic single-band superconductors [19]. Since the GL parameter κ of the scaled isotropic model is a function of the two direction-dependent GL parameters of the anisotropic model (κ_x and κ_y for the z-directed field),

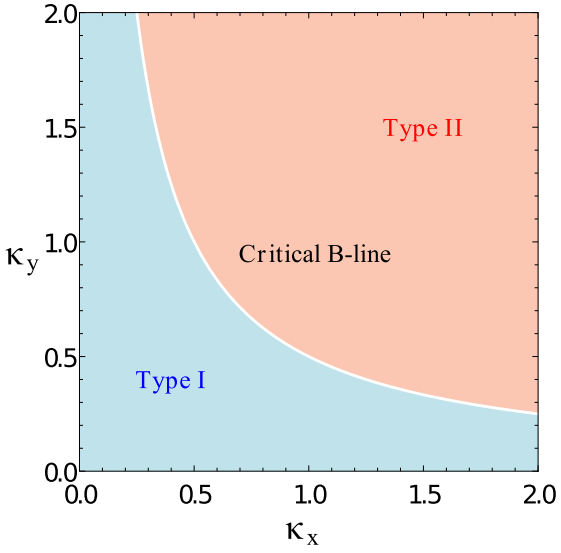

FIG. 1. The phase diagram for superconductivity types in the κ_x-κ_y plane at $T \to T_c$: the blue and red regions correspond to types I and II, respectively, separated by the white critical B line $\kappa_x\kappa_y = \kappa_0^2 = 1/2$.

the boundaries of the IT domain on the κ_x-κ_y plane become temperature-dependent lines, defined by the equations $\kappa^*_{\rm min/max}(T) = \sqrt{\kappa_x\kappa_y}$ (see the phase diagram in Fig. 2). The width of the IT domain increases when the temperature is lowered: in Fig. 2 at $T = 0.5T_c$ it occupies a noticeable part in the phase diagram. Notice that even at these low temperatures the EGL formalism yields quantitatively accurate results, as has been demonstrated in the earlier analysis [19].

IV. CONCLUSIONS

In summary, this work has considered the interchange between superconductivity types I and II in anisotropic superconductors. The analysis is based on the single-band EGL formalism combined with the coordinate-field scaling transformation to isotropize the theory. Calculations have been done for the ellipsoidal Fermi surface in the case when a magnetic field is directed along one of the principal anisotropy axes. We have demonstrated that irrespective of the anisotropy degree, the scenario of the interchange of the types is the same as in isotropic superconductors, being governed by the proximity to the B point at which the field-condensate state is self-dual and infinitely degenerate. Similarly to isotropic materials, the degeneracy is removed at lower temperatures, which opens a finite IT domain between types I and II with unconventional superconducting magnetic properties.

The obtained conclusions are rather counterintuitive because the self-duality property generally is not expected in systems with different direction dependence of the condensate and magnetic lengths. However, here the B point is still present in an effective isotropic model obtained by an appropriate scaling transformation. It has been shown that this transformation and the corresponding GL parameter of the scaled isotropic model strongly vary with the direction of an applied magnetic field so that anisotropic materials can exhibit a qualitatively different magnetic response for different field alignments, which agrees with the experimental observation [36].

We stress that although our results have been obtained for the model with the ellipsoidal Fermi surface, our conclusions hold, at least qualitatively, for more complicated Fermi surfaces. This expectation is based on the fact that contributions neglected in the adopted model can introduce only quantitative corrections to the boundaries of the IT domain but do not alter the physical mechanism behind the interchange of the types. Since we have shown that the mechanism related to the presence of the B point applies to a large class of situations we expect that the type interchange proceeds qualitatively similar in all these cases, in particular, when the field is not directed along one of the principal anisotropy axes. Also, we expect the conclusions hold for materials with many conduction bands as long as the anisotropic contributions, that cannot be made isotropic simultaneously with the GL terms, are marginal, which is typically the case.

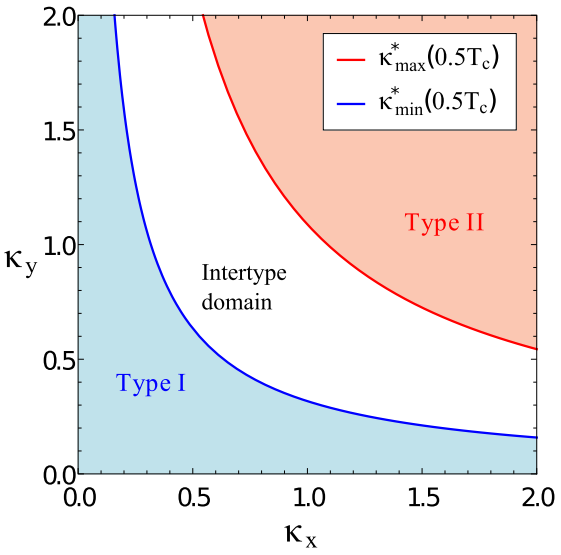

FIG. 2. The phase diagram for superconductivity types in the κ_x-κ_y plane at $T = 0.5T_c$. The blue and red regions correspond to types I and II, respectively, separated by the white region that corresponds to the IT domain $\kappa^*_{\rm min}(T) < \sqrt{\kappa_x\kappa_y} < \kappa^*_{\rm max}(T)$.

ACKNOWLEDGMENTS

This work was supported by the Brazilian agencies Coordenação de Aperfeiçoamento de Pessoal de Nível Superior, CAPES (Grants 223038.003145/2011-00 and 400510/2014-6), Conselho Nacional de Desenvolvimento Científico e Tecnológico, CNPq (Grants 307552/2012-8 and 141911/2012-3), and Fundação de Apoio à Ciência e Tecnologia do Estado de Pernambuco, FACEPE (APQ-0936-1.05/15). A.V. acknowledges the hospitality of the Department of Physics at the Universidade Federal de Pernambuco during his visits in Recife. T.T.S. is grateful to the Institute for Theoretical Physics III at the University of Bayreuth for hospitality during his stay there. A.V. acknowledges support from the Russian Science Foundation under the Project 18-12-00429, used to study connections between anisotropy and nonlocal interactions in superconductors within the EGL formalism.

[1] E. M. Lifshitzand L. P. Pitaevskii, *Statistical Physics*, Part 2, Landau and Lifshitz Course of Theoretical Physics (Pergamon, Oxford, 1980), Vol. 9.
[2] P. G. de Gennes, *Superconductivity of Metals and Alloys* (Benjamin, New York, 1966).
[3] J. B. Ketterson and S. N. Song *Superconductivity* (Cambridge University Press, Cambridge, 1999).
[4] U. Krägeloh, Phys. Lett. A **28**, 657 (1969).
[5] U. Essmann, Physica **55**, 83 (1971).
[6] D. R. Aston, L. W. Dubeck, and F. Rothwarf, Phys. Rev. B **3**, 2231 (1971).
[7] A. E. Jacobs, Phys. Rev. B **4**, 3029 (1971).
[8] J. Auer and H. Ullmaier, Phys. Rev. B **7**, 136 (1973).
[9] U. Klein, J. Low Temp. Phys. **69**, 1 (1987).
[10] H. W. Weber, E. Seidl, M. Botlo, C. Laa, E. Mayerhofer, F. M. Sauerzopf, R. M. Schalk, and H. P. Wiesingerh, Physica C **161**, 272 (1989).
[11] E. H. Brandt, Rep. Prog. Phys. **58**, 1465 (1995).
[12] I. Luk'yanchuk, Phys. Rev. B **63**, 174504 (2001).
[13] M. Laver, E. M. Forgan, S. P. Brown, D. Charalambous, D. Fort, C. Bowell, S. Ramos, R. J. Lycett, D. K. Christen, J. Kohlbrecher, C. D. Dewhurst, and R. Cubitt, Phys. Rev. Lett. **96**, 167002 (2006).
[14] M. Laver, C. J. Bowell, E. M. Forgan, A. B. Abrahamsen, D. Fort, C. D. Dewhurst, S. Mühlbauer, D. K. Christen, J. Kohlbrecher, R. Cubitt, and S. Ramos, Phys. Rev. B **79**, 014518 (2009).
[15] S. Mühlbauer, C. Pfleiderer, P. Böni, M. Laver, E. M. Forgan, D. Fort, U. Keiderling, and G. Behr, Phys. Rev. Lett. **102**, 136408 (2009).
[16] E. H. Brandt and M. P. Das, J. Supercond. Nov. Magn. **24**, 57 (2011).
[17] A. Pautrat and A. Brûlet, J. Phys.: Condens. Matter **26**, 232201 (2014).
[18] T. Reimann, S. Mühlbauer, M. Schulz, B. Betz, A. Kaestner, V. Pipich, P. Böni, and C. Grünzweig, Nat. Commun. **6**, 8813 (2015).
[19] A. Vagov, A. A. Shanenko, M. V. Milošević, V. M. Axt, V. M. Vinokur, J. A. Aguiar, and F. M. Peeters, Phys. Rev. B **93**, 174503 (2016).
[20] Y. Wang, R. Lortz, Y. Paderno, V. Filippov, S. Abe, U. Tutsch, and A. Junod, Phys. Rev. B **72**, 024548 (2005).
[21] J.-Y. Ge, J. Gutierrez, A. Lyashchenko, V. Filipov, J. Li, and V. V. Moshchalkov, Phys. Rev. B **90**, 184511 (2014).
[22] J.-Y. Ge, V. N. Gladilin, N. E. Sluchanko, A. Lyashenko, V. B. Filipov, J. O. Indekeu, and V. V. Moshchalkov, New J. Phys. **19**, 093020 (2017).
[23] E. B. Bogomol'nyi and A. I. Vainstein, Sov. J. Nucl. Phys.-USSR **23**, 588 (1976).
[24] E. B. Bogomol'nyi, Sov. J. Nucl. Phys.-USSR **24**, 449 (1976).
[25] W. Y. Córdoba-Camacho, R. M. da Silva, A. Vagov, A. A. Shanenko, and J. A. Aguiar, Phys. Rev. B **94**, 054511 (2016).
[26] S. Wolf, A. Vagov, A. A. Shanenko, V. M. Axt, A. Perali, and J. A. Aguiar, Phys. Rev. B **95**, 094521 (2017).
[27] S. Wolf, A. Vagov, A. A. Shanenko, V. M. Axt, and J. A. Aguiar, Phys. Rev. B **96**, 144515 (2017).
[28] R. M. da Silva, M. V. Milošević, A. A. Shanenko, F. M. Peeters, and J. A. Aguiar, Sci. Rep. **5**, 12695 (2015).
[29] A. V. Vagov, A. A. Shanenko, M. V. Milošević, V. M. Axt, and F. M. Peeters, Phys. Rev. B **85**, 014502 (2012).
[30] R. A. Klemm and J. R. Clem, Phys. Rev. B **21**, 1868 (1980).
[31] V. G. Kogan and J. R. Clem, Phys Rev. B **24**, 2497 (1981).
[32] G. Blatter, V. B. Geshkenbein, and A. I. Larkin, Phys. Rev. Lett. **68**, 875 (1992).
[33] L. Neumann and L. Tewordt, Z. Phys. **189**, 55 (1966).
[34] L. Neumann and L. Tewordt, Z. Phys. **191**, 73 (1966).
[35] L. P. Gor'kov and T. K. Melik-Barkhudarov, Sov. Phys. JETP **18**, 1031 (1964) [J. Exp. Theoret. Phys. (USSR) **45**, 1493 (1963)].
[36] H. W. Weber, J. F. Sporna, and E. Seidl, Phys. Rev. Lett. **41**, 1502 (1978).

B.2 Publications not directly related to the Thesis

IOP Publishing Superconductor Science and Technology

Supercond. Sci. Technol. **27** (2014) 055002 (12pp) doi:10.1088/0953-2048/27/5/055002

Nucleation of superconductivity in multiply connected superconductor–ferromagnet hybrids

Miguel A Zorro[1], Tiago Saraiva[2] and Clécio C de Souza Silva[1,2]

[1] Programa de Pós-Graduação em Ciência de Materiais, Universidade Federal de Pernambuco, Cidade Universitária, 50670-901, Recife-PE, Brazil

[2] Departamento de Física, Universidade Federal de Pernambuco, Cidade Universitária, 50670-901, Recife-PE, Brazil

E-mail: clecio@df.ufpe.br

Received 3 September 2013, revised 4 December 2013
Accepted for publication 7 January 2014
Published 4 March 2014

Abstract

We investigate theoretically the nucleation of superconductivity in a thin film pierced by ferromagnetic dots. We demonstrate that localized superconductivity near the ferromagnet/superconductor interface is sustained above the second critical field H_{c2} in spite of the deleterious proximity effect of the ferromagnet. This phase is characterized by Little–Parks oscillations similar to those found in perforated films, where surface superconductivity is stabilized by the enhanced properties of the superconductor-vacuum boundary. Here, localization is provided by field compensation induced by the ferromagnet stray field near the ferromagnetic dot. We also show that for an array of such ferromagnetic dots the localized phase around each dot actually percolates through the entire sample, rendering bulk superconductivity at fields considerably higher than H_{c2}.

Keywords: superconductor–ferromagnet hybrids, flux compensation effects, confinement

(Some figures may appear in colour only in the online journal)

1. Introduction

Nanostructured superconductors have been the subject of intense research in recent decades. These materials exhibit a plethora of remarkable phenomena not found in plain films, single crystals or ceramics. For instance, arrays of mesoscopic vortex-pinning sites, such as small open holes (antidots), magnetic inclusions (dots) and blindholes, produce very efficient pinning of vortices, enhancing the critical current of the superconducting material up to values orders of magnitudes higher than those of plain film [1–7]. Moreover, at the so-called matching fields, which correspond to integer (and sometimes fractional) occupation numbers of vortices in the pinning array, the critical currents usually reach even higher values as a consequence of commensurability effects [8–19].

In addition to the superior vortex-pinning properties, multiply connected superconducting films, such as films with antidots, present an enhanced critical field, which is revealed by measurements of the superconductor–normal phase boundary $H^*(T)$. The $H^*(T)$ values measured for a nanostructured film are often considerably higher than those of a co-evaporated plain film, where H^* can be identified as the second critical field, H_{c2} [20]. This is an expected result because the antidots in the film induce a state of surface superconductivity within a distance of the order of the coherence length, $\xi(T)$, which survives at fields considerably higher than H_{c2}. In fact, because measurements in these systems are usually performed at temperatures close to the critical temperature T_c, the width w of superconducting material between consecutive antidots often becomes comparable to or even smaller than $\xi(T)$. In that case, the surface superconductivity state around each antidot coalesces and the whole film becomes superconducting. The corresponding phase boundary is characterized by re-entrances of the superconducting phase at integer and a few rational multiples of the first matching field (H_1, field value corresponding

to one flux quantum per unit cell of the antidot array) because at these field values the vortex lattice becomes commensurate to the pinning array.

In some experiments, it has been observed that the periodic oscillations in the phase boundary at temperatures close to T_c are replaced by aperiodic oscillations at smaller temperatures [21–23]. This is often interpreted as a transition from the collective regime to the so-called single-object regime, where the sheaths of surface superconductivity around each antidot do not overlap because, at that temperature range, $\xi(T)$ becomes considerably smaller than w. In that case, the phase boundary is dominated by Little–Parks-like quantum oscillations with a period that increases when the temperature decreases even further. This can be understood in terms of an effective area where superconductivity resides. As temperature decreases, so does the coherence length and, as a consequence, the effective area of the localized-superconductivity state also decreases. Since in this case the flux distributes through an ever decreasing area, the difference in flux density between consecutive states increases.

Another efficient way to tailor the properties of superconducting (SC) films under a perpendicular field is by exploring the effect of mesoscale inhomogeneous magnetic textures, such as those produced by ferromagnetic (FM) dots [4, 24, 25]. Because both the intensity and direction of the FM dot magnetization can be easily tuned, these SC–FM hybrids provide a high degree of controllability over the properties of the superconductor. In general, these systems produce efficient (and tunable) pinning potentials that prevent vortex motion up to considerably high current densities [4, 26, 27]. Quite often, however, the intensity of the magnetic moments of the dots is high enough to induce vortex–antivortex pairs into the superconductor with profound consequences for its critical behavior [28–30]. For instance, Lange *et al* [24] have shown experimentally that the H–T phase boundary of a thin superconducting Pb/Ge film with a lattice of Co/Pd FM dots deposited on top can have its symmetry axis displaced from $H = 0$ to either positive or negative field values depending on whether the dots are magnetized parallel or antiparallel to an axis normal to the film surface. This was explained as an effect of the compensation of interstitial antivortices induced by the FM dots. A more complete picture of the phenomenon was offered later by Milošević *et al* in the framework of Ginzburg–Landau simulations [31]. Novel strategies for manipulating superconducting properties by exploring vortex–antivortex pairs and their interaction with external fields and currents have been widely investigated over the past decade [32–40].

Most of the theoretical and experimental studies on SC–FM hybrids consider FM dots placed above the superconducting film and electrically isolated from it by an insulating layer, thus avoiding local weakening of superconductivity. An exception can be found in [41], where Marmorkos *et al* studied theoretically giant vortex states around a magnetic dot embedded in the superconducting film. In this last case, however, the study was carried out at zero external field. Another interesting multiply connected superconductor–ferromagnet system has been investigated in [42]. In this case, the authors studied experimentally the phase boundary of a Nb film with embedded ferromagnetic islands. They found field compensation effects similar to those found in [24] and periodic Little–Parks-like oscillations.

In the present work, we investigate the properties of a superconducting film *pierced* by ferromagnetic dots as a function of temperature, dot magnetization, and an additional homogeneous magnetic field. The dots are magnetized perpendicularly to the film plane and actually touch the film, so superconductivity at the SC–FM dot interface is strongly depreciated by the proximity effect. We choose not to follow the usual procedure of inserting an insulating buffer layer because, as it is well known, the superconductor-insulator boundary *per se* induces localized superconductivity at fields higher than H_{c2}. Here we are interested in localized states induced by the inhomogeneous field only. Indeed, we demonstrate via analytical calculations and numerical simulations that, in spite of the depreciative boundary condition, a localized-superconductivity phase can be formed near an FM dot as a result of field compensation induced by the dot stray field. In addition, we show that an array of such FM dots is capable of holding percolated superconductivity at fields considerably higher than H_{c2}.

This paper is organized as follows. In section 2 we present the theoretical framework of our calculations, which are based on the Ginzburg–Landau (GL) theory. The results for the single FM dot case are presented in section 3. First we present analytical results of a simplified model where the flux distribution generated by the FM dot into the film is replaced by a piecewise field profile. This will establish the proof of concept of how the stray field of the FM dots can induce localized superconductivity as well as providing physical insight into the Little–Parks oscillations in this system. Then we present numerical simulation results of the full GL problem that corroborate the analytical predictions. In section 4 we investigate the properties of a square array of such FM dots. Finally, in section 5 we draw our conclusions.

2. Theoretical formalism

We consider an infinite type-II superconducting thin film threaded through by either a single cylindrical magnetic dot of radius a and height h or an array of such dots as depicted in figures 1(a) and (b) respectively. Our calculations rely on the minimization of the Gibbs free energy $\mathcal{G} = \int \mathrm{d}V\, F(\psi, \vec{A})$, where

$$F(\psi, \vec{A}) = |\psi|^2 \left(\frac{1}{2}|\psi|^2 - 1\right) + \frac{1}{1-T}|(-\mathrm{i}\nabla - \vec{A})\psi|^2 + \frac{\kappa^2}{(1-T)^2}\left[|\nabla \times \vec{A}|^2 - 2\vec{H}\cdot(\nabla \times \vec{A})\right] \quad (1)$$

is the Ginzburg–Landau functional. Here, we have expressed physical quantities in the following unit system: (i) T_c (critical temperature) for temperature; (ii) the zero-temperature coherence length $\xi(0) = \sqrt{\hbar^2/4m\alpha(0)T_c}$ for distances; (iii) $\psi_\infty(T) = \sqrt{-\alpha/\beta}$ for the order parameter; and (iv) $H_{c2}(0)\xi(0) = \Phi_0/[2\pi\xi(0)]$ for the vector potential.

Henceforth, we shall restrict ourselves to a superconducting film of thickness d much smaller than the coherence length

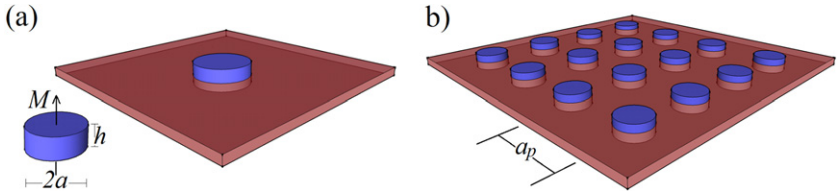

Figure 1. Superconductor–ferromagnetic hybrid sample studied. (a) Single-dot case with radius $a = 7.5\xi(0)$, $h = 10\xi(0)$ and magnetization M out of plane. (b) Dot-array case with $a_p = 60\xi(0)$ the distance between adjacent dots.

(ξ) and the penetration depth (λ). Therefore, the problem is essentially two-dimensional, i.e., variations of the order parameter and the vector potential in the direction perpendicular to the sample can be neglected. Moreover, since in this case $\kappa^* = \lambda^2/(\mathrm{d}\xi) = \kappa\lambda/d \gg 1$, the effect of screening currents can be neglected and the vector potential can be well approximated by $\vec{A} = \vec{A}_0$, where $\vec{A}_0$ is the vector potential of the external field sources in the absence of the superconductor. Accordingly, the problem of minimizing equation (1) is reduced to the search of solutions to the first GL equation,

$$(\mathrm{i}\nabla + \vec{A})^2\psi + (1-T)(|\psi|^2 - 1)\psi = 0. \qquad (2)$$

In particular, in the problem of nucleation of superconductivity, one has $|\psi| \ll 1$ and thus equation (2) can be appropriately linearized. For the single FM dot case, we take advantage of the azimuthal symmetry of the nucleation problem to obtain analytical solutions of the linearized Ginzburg–Landau (LGL) equation following similar nucleation studies performed by other groups [25, 43–46].

In order to find stable solutions beyond the linear approximation, we solve the full non-linear equation (2) numerically. Our procedure is as follows. We start from a given initial configuration of the order parameter and allow for a fictitious time relaxation of the order parameter. This is realized by adding the term $-\eta\partial\psi/\partial t$ to the right-hand side of equation (2) and solving the time-dependent problem by the finite-difference link-variable method until a stationary solution is reached [47–49]. Numerically, we adopt the following criterion for stationarity of the order parameter: $|\psi|^{-1}\Delta|\psi|/h \leq 10^{-8}$, where h is the time step. Although the time evolution towards a stationary regime does not represent a real physical situation[3], the steady state solution is a genuine solution of equation (2).

3. Nucleation around a single magnetic dot

3.1. Analytical results: LGL theory

Here we present analytical results that describe the localized phase of superconductivity for the one-dot case. Our solution has two main assumptions: (i) the nucleation of the superconducting state takes place at $H > H_{c2}(T)$ so we can neglect the non-linear term in equation (2); and (ii) the solution at this field range has azimuthal symmetry, that is, $|\psi|^2$ is invariant under rotations. The last property allows us to write $\psi(\rho,\theta) = f(\rho)\exp(\mathrm{i}L\theta)$ where L is the total vorticity. By substituting this into the linearized version of equation (2), one obtains the following linear equation for the radial function $f(\rho)$:

$$\mathcal{L}f \equiv \left[-\frac{1}{\rho}\frac{\mathrm{d}}{\mathrm{d}\rho}\rho\frac{\mathrm{d}}{\mathrm{d}\rho} + \left(\frac{L}{\rho} - A_\theta\right)^2 - (1-T)\right] f = \Lambda f. \qquad (3)$$

We treat this equation as an eigenvalue problem and search only those solutions corresponding to lowest eigenvalue Λ, which minimizes the free energy.

The vector potential has two contributions: one from the constant external magnetic field, $A^e_\theta(\rho) = H\rho/2$, and the other from the flux density $\vec{B}_{\mathrm{dot}}$ induced by the magnetization $\vec{M}$ of the FM dot. In order to find simple analytical solutions, we follow [50] by choosing a piecewise representation of the z component of the magnetic field profile generated by the dot as illustrated in figure 2. Inside the dot (region I) the field intensity is represented by its mean value $B_{\mathrm{in}} \equiv \frac{1}{\pi a^2}\int_{\rho<a}\vec{B}_{\mathrm{dot}}\cdot\mathrm{d}\vec{a}$. Notice that this equation leads to the relation $B_{\mathrm{in}} = \gamma M$, where γ is a geometrical factor determined by the shape of the dot. The negative flux threading the superconducting region outside the FM dot is represented by a negative uniform field $-B_{\mathrm{out}}$ in the region $a < \rho < b$ (region II). From Gauss law $B_{\mathrm{out}} = \frac{a^2}{a^2-b^2}B_{\mathrm{in}}$. For $\rho > b$ (region III) we assume the field is negligible. These restrictions simplify our vector potential,

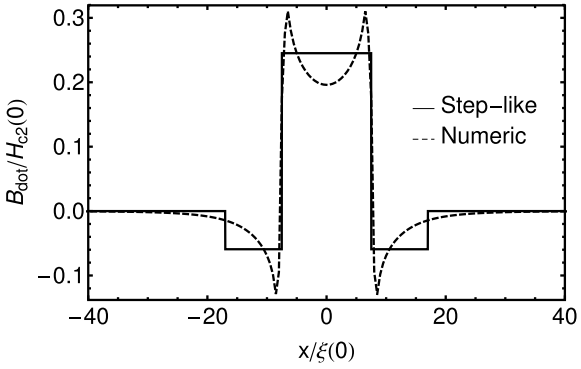

Figure 2. Numeric and step-like field profiles of a dot with $M^z_{\mathrm{dot}} = 0.06H_{c2}(0)$, $a = 7.5\xi(0)$ choosing the thickness of the dot $h = 10\xi(0)$ for the exact profile and the effective range radius $b = 17\xi(0)$ for the approximated profile.

[3] Here, for simplicity, both the scalar potential and time variations of $\vec{A}$ are neglected, thereby ruling out any electric fields by construction. These are essential ingredients in the time-dependent GL theory that allow for investigation of real time-dependent problems in superconducting materials, but they all go to zero when the order parameter reaches a stationary state.

which can now be written in the form [51]

$$A_\theta^{\rm dot}(\rho) = c_1\rho + \frac{c_2}{\rho}, \quad (4)$$

where c_1 is half the field intensity in a given region and c_2 is a constant chosen in such a way as to make the vector potential continuous.

The general solution of equation (3) for each of the above described regions can now be written as

$$f(\rho) = z^{|L'|/2}e^{-z/2}\,[k_1 M(A, B, z) + k_2 U(A, B, z)] \quad (5)$$

where $z = c_1\rho^2$, $L' = L - B_{\rm out}b^2/2$, $M(A, B, z)$ and $U(A, B, z)$ are, respectively, the confluent hypergeometric functions of the first and second kinds (also known as Kummer's functions), with $A = 0.5(1 + |L'| - L') - (1 - T + \Lambda)/4c_1$ and $B = |L'| + 1$. Finally the eigenvalue Λ and coefficients k_1 and k_2 are determined by the transcendental equation that arises from the boundary conditions which are described in more detail in the Appendix.

For a given set of parameters a, b, and γM, describing the flux induced by the FM dot, we can find the phase boundary of the system on the $H \times T$ diagram for different vorticities L by solving the transcendental equation while imposing $\Lambda = 0$, which gives a null free energy. In figure 3 one can see that, when the external field is applied parallel to the dot magnetization, the critical field of the system is higher for the sample with a magnetized dot (red line) than for the plain film (black line). This fact can be seen as a compensation effect, i.e. given a value for the magnetic field $H > H_{c2}$ one can always find a value for M which generates a flux density $B_{\rm dot}$ that diminishes the total field around the dot to a value below H_{c2}, thus allowing superconductivity. The figure also shows oscillations at the critical curve due to vorticity transitions. Similar oscillations were found previously for different systems of superconductors interacting with inhomogeneous electromagnetic fields [52–55].

In order to understand how the system behaves near the transition, we calculate the order parameter and the current density following the method described in the Appendix (formulas (A.12) and (A.13)). Figure 4 shows a few plots of the absolute value of the order parameter $|\psi(\rho)|$ and the superconducting current density $j_\theta(\rho)$ at points slightly displaced from the phase boundary by $10^{-5}T_c$ and indicated in figure 3. Quite generally, the square modulus of the order parameter starts with null value at the border of the dot, increases to a maximum in a distance of the order of $2\xi(T)$ and decreases in a distance of the same order outside of region II. Since $\xi(T) \propto (1 - T/T_c)^{-1/2}$, the typical size of the nucleus tends to decrease when decreasing the temperature. This can be observed in figure 4 except from (d) to (e) where a vorticity state transition takes place causing a redistribution of the current density as discussed below.

The current density profiles over the sample evidence a typical sign inversion at a certain $\rho = \rho^*$. This value can be obtained with the help of equation (A.13) by noticing that the inversion takes place when the superfluid velocity becomes zero. In this case, ρ^* is given by the implicit equation

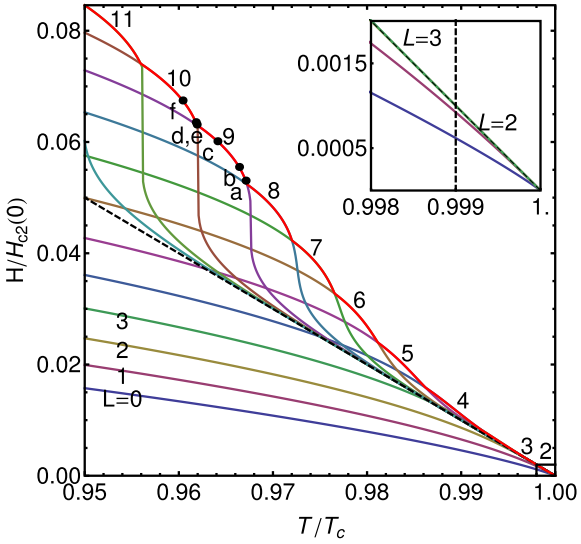

Figure 3. Critical field $H^*(T)$ for $a = 7.5\xi(0)$, $b = 17\xi(0)$ and $M = 0.06H_{c2}(0)$ with a geometrical factor $\gamma \approx 4.1$. In the inset we see that the minimum vorticity of the critical curve is the $L = 2$ state because, differently from all the others, the states $L = 0$ and $L = 1$ are always below the $1 - T$ curve.

$\rho^* A_\theta(\rho^*) = L$. This sign change is indeed expected, since the superconducting current should flow counterclockwise near the FM dot in order to sustain the flux trapped in it whereas somewhat further it should flow clockwise in order to screen the external magnetic field. Depending on whether more current flows clockwise or counterclockwise the total current is positive or negative. In fact, all over the phase boundary, each vorticity transition is followed by a similar redistribution of current density causing a sudden inversion of circulation of the total superconducting current.

The behavior described above is very similar to the current inversions observed in thin superconducting rings (Little–Parks oscillations), where the total current flips sign whenever a new vorticity state takes place. To better illustrate this effect in our system, we present in figure 5 the total supercurrent, I_s, flowing around the FM dot as a function of field in the vicinity of the phase boundary. One can observe that, in contrast to the original Little–Parks effect, where current inversions are periodic, here the magnetic field interval between consecutive L states is not constant. Indeed, as one increases the magnetic field while decreasing the temperature along the phase boundary, the superconducting nucleus becomes more localized. Therefore the trapped flux is obliged to distribute over an ever decreasing area, thus increasing the amount of flux density necessary to stabilize a new flux quantum.

3.2. Numerical results

In order to corroborate the results obtained via the rather simplified model described above and to extend the analysis to fields lower than $H_{c2}(T)$, we numerically integrate the full non-linear problem represented by equation (2) without imposing *a priori* any particular symmetry to the system. To imitate an infinite film, we use periodic boundary conditions

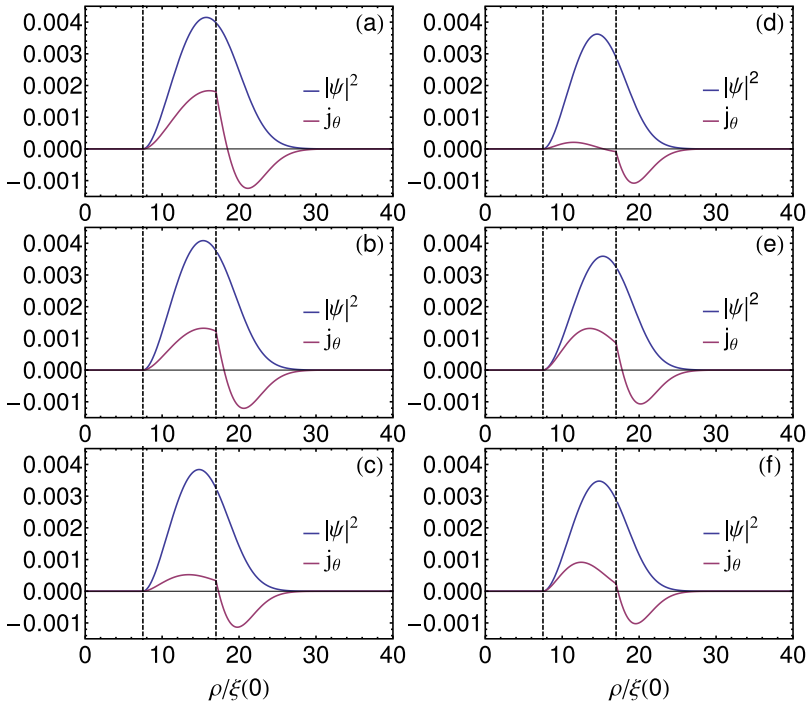

Figure 4. Plots of the Cooper pair density and superconducting current for: (a) $L = 9$, $T \approx 0.967T_c$ and $H \approx 0.053H_{c2}(0)$; (b) $L = 9$, $T \approx 0.966T_c$ and $H \approx 0.0552H_{c2}(0)$; (c) $L = 9$, $T \approx 0.964T_c$ and $H \approx 0.06H_{c2}(0)$; (d) $L = 9$, $T = 0.9619T_c$ and $H \approx 0.063H_{c2}(0)$; (e) $L = 10$, $T = 0.9618T_c$ and $H \approx 0.0632H_{c2}(0)$; (f) $L = 10$, $T \approx 0.96T_c$ and $H \approx 0.067H_{c2}(0)$.

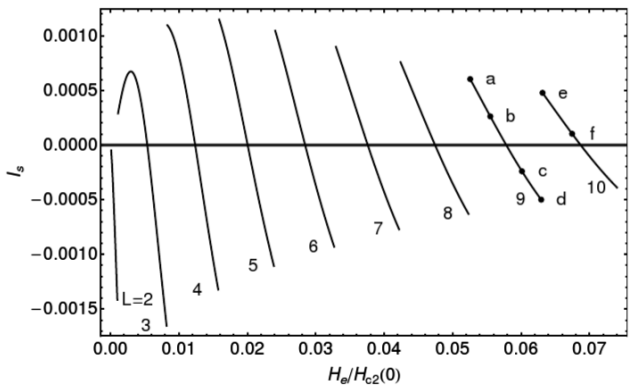

Figure 5. Total superconducting current along the sample as a function of the external magnetic field.

for the order parameter over a square simulation cell. Although strictly speaking this system does not represent the single-dot problem but rather a periodic array of such dots, we choose the side l of the simulation cell much larger than both $\xi(0)$ and the dot radius ($a = 7.5\xi(0)$): $l = 150\xi(0)$. This way, the influence of the periodic boundary conditions on all calculated quantities is negligible in the whole range of parameters except for temperatures very close to T_c ($t \equiv 1 - T/T_c \lesssim 10^{-4}$) (see below).

Equilibrium states of the system are determined by analyzing the mean free energy $G = \mathcal{G}/l^2$ and Cooper pair distribution $|\psi|^2$ as functions of the magnetic field for different dot magnetization values M and temperatures T. For given M and T values we initialize the order parameter as either $\psi = 0$ (corresponding to the normal state) or $\psi = 1$ (Meissner state) everywhere in the superconducting material. For each case the magnetic field is slowly swept up and down while the corresponding stationary configurations of the order parameter are obtained by numerical integration of equation (2) as described in section 2. This procedure often leads to different states for a given magnetic field, which allows us to determine the energy of the lowest lying states, that is, those states closest to the thermodynamic equilibrium [38].

Figure 6 shows isothermal $G \times H$ curves for $T = 0.95T_c$ and different M values. For $M = 0$, the demagnetized FM dot has a minor influence on the superconducting film. However, for $M > 0$, the free energy reaches zero at a field H^* larger than H_{c2} (in units of $H_{c2}(T)$, $H^* = 1.1$ for $M = 0.5$, up to $H^* = 1.6$ for $M = 2$). Moreover, the monotonic behavior of $G(H)$ found for $H < H_{c2}$ is replaced by an oscillatory behavior for $H > H_{c2}$, similarly to what is observed in mesoscopic superconductors. Indeed, as revealed by the absolute value and phase of the order parameter, these trends are direct manifestations of localized superconductivity around the magnetic dot similar to the localized phase described in the previous section.

To illustrate the transition from bulk to localized superconductivity we present in figure 7 plots of $|\psi|^2$ for fields close to and larger than H_{c2} for $T = 0.95$ and $M = 1.5H_{c2}(T)$. For comparison, we also plot $|\psi|^2$ for a few field values for the $M = 0$ case. Whereas for $M = 0$ the sample is completely in the normal state at H_{c2} and above, for the $M = 1.5H_{c2}$ case the bulk of the sample goes to the normal state at H_{c2} while in the region near the FM dot superconductivity remains quite strong, forming a ring of superconducting condensate, similar to the localized state predicted by the analytical model. Interestingly,

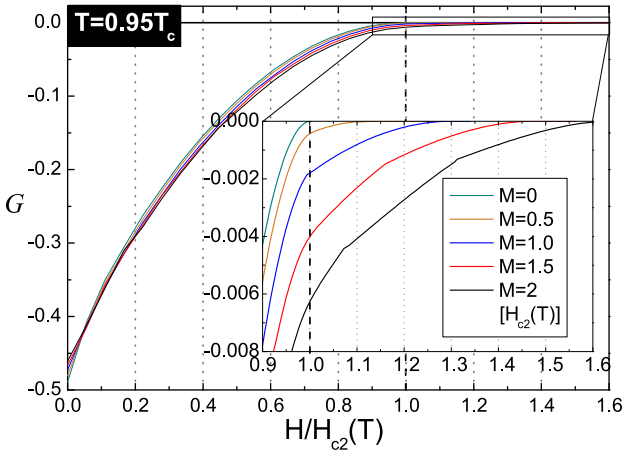

Figure 6. Free energy dependence on the external magnetic field calculated numerically for different values of the dot magnetization M for the single FM dot case.

for fields at and slightly above $H_{c2}(T)$ vortex rings can be identified surround the ring of localized superconductivity. For fields smaller than H_{c2}, the rings gradually change into a triangular lattice. This behavior is similar to the distribution of vortices near a pillar observed via Bitter decoration [56], and can be understood as a compromise between the cylindrical exclusion region imposed by the enhancement of vortex line energy in the pillar and the natural tendency of vortices to form an Abrikosov lattice. In our case vortices are repelled by the negative flux induced by the dot in the vortex-free ring-like region.

In figure 8 we present the superconductor–normal state phase boundary in the H–T plane and the critical vorticity L^* as a function of the external magnetic field calculated numerically for a dot magnetization of $0.06H_{c2}(0)$. L is calculated by counting the number of phase discontinuities encircling the FM dot. The boundary features the same trends predicted by the analytical model discussed in the previous subsection: enhancement of the critical field beyond the $H_{c2}(T)$ line and quantum oscillations associated with vorticity transitions of the flux captured by the FM dot. For comparison, we also present the phase boundary obtained by our analytical model for an FM dot of the same radius and magnetization. It is worth remembering that, in the piecewise approximation of the flux profile induced by the dot, the radius b at which the negative flux distribution is cut off is a free parameter. Therefore, we plot the phase boundary for different values of b. The discrepancy between the numerical and the analytical results is apparent and indeed expected, as the piecewise flux profile is a rather crude representation of the actual profile. However, the main physics behind the localized phase and the quantum oscillations are captured by both models.

Finally, it is worth mentioning that the results shown here have a close similarity to the surface superconductivity phenomena seen in perforated superconducting films. In particular, the Little–Parks-like oscillations observed in the phase boundaries ($T_c(H)$ curves) are typical of doubly connected mesoscopic superconducting systems, with a period that increases with H. However, in contrast to perforated superconductors, the increase of superconductivity near the FM dot does not result from the boundary condition. On the contrary, the specific boundary condition for a superconductor–ferromagnet interface ($\psi = 0$) is highly depreciative of superconductivity, as illustrated in figures 7(a)–(e). Rather, localized superconductivity at fields higher than H_{c2} is sustained by a field compensation effect due to the negative magnetic flux generated by the upward magnetized dot in the close surroundings of the superconductor–FM interface. This kind of localization has been predicted before and experimentally observed in different superconductor–FM hybrids [52, 57, 58]. Here, since the FM dot is embedded in the superconducting film, the magnetic texture exhibits a sharp profile rendering a more efficient localization of the superconducting condensate.

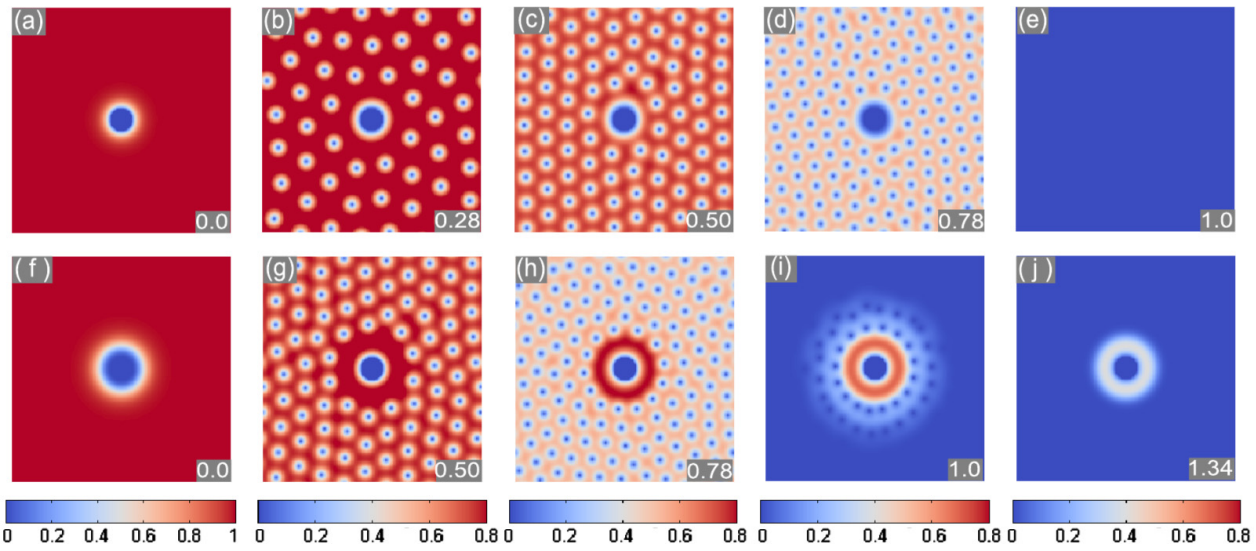

Figure 7. Configurations of $|\psi|^2$ for different values of H (indicated in the bottom-right corner of each panel) for $M = 0$ ((a)–(e)) and $M = 1.5H_{c2}(T)$ ((f)–(j)).

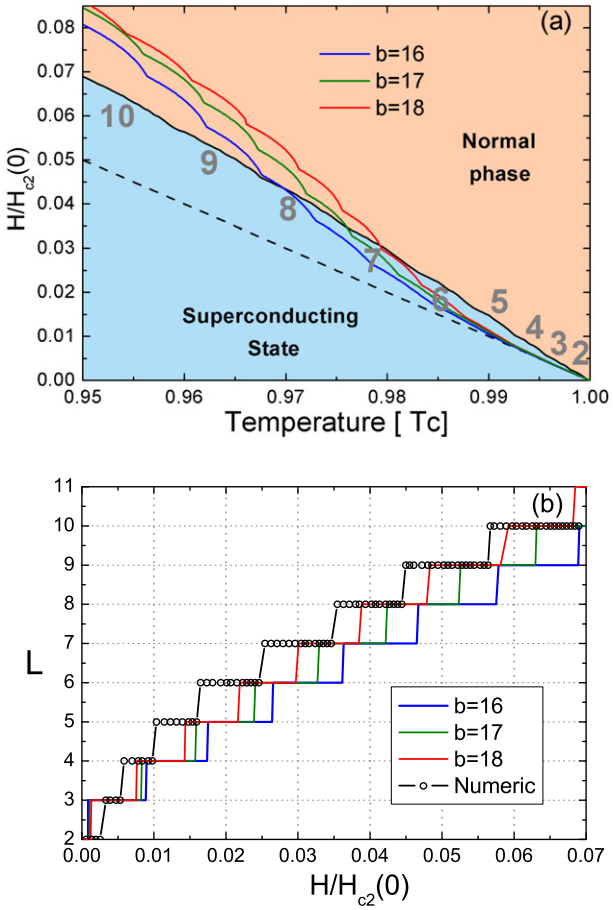

Figure 8. (a) $H(T)$ phase boundary of the single-dot system for $M = 0.06H_{c2}(0)$ obtained by the simulation (black line) and 3 different parameters of the analytical solution (colored lines). (b) The $L(H)$ results for the same case.

A rough schematic illustration of the field compensation effect is shown in figure 9(a). At a field higher than H_{c2} only a small region around the FM dot remains superconducting because there the stray field of the FM dot opposes the applied field H in a way that the local field $h \leq H_{c2}$ in that region, making it more favorable for the nucleation of the superconducting state. However, one has to keep in mind that, since the order parameter has a length ξ to recover from the normal state at the SC–FM boundary, the superconducting nucleus is usually displaced from the region where external field is compensated most efficiently. This can be illustrated by the plots of the actual profiles of the flux density induced by the FM dot and the order parameter shown in figure 9(b) (see also figure 4). Therefore, typically, the nucleus extends over a length about $4\xi(T)$ from the FM dot edge, with a maximum at $\rho \sim a + 2\xi(T)$.

4. Periodic array of magnetic dots

In the previous section we have shown that a single FM dot piercing an infinite superconducting film is capable of stabilizing a localized superconducting state at fields considerably higher than H_{c2}. An important question is whether such localized superconductivity can be upgraded to a bulk superconducting phase of enhanced critical field that percolates throughout the entire film. A possible way to accomplish that is by, for instance, introducing not one but many FM dots placed in a way that the localized phases around each of them couple to one another. To test this idea, we solved equation (2) for a superconducting film with a square array of threading FM dots. The calculations were carried out following the same numerical procedure described in the previous sections. This time, we take a simulation cell of area $240\xi(0) \times 240\xi(0)$ with periodic boundary conditions comprising 16 identical FM dots of radius $7.5\xi(0)$ arranged in a 4×4 array of periodicity $60\xi(0)$. This choice of parameters leads to a width $w = 45\xi(0)$ of superconducting material between neighboring FM dots. For a typical temperature $T = 0.98T_c$, this gives $w = 6.4\xi(T)$, which, based on the results of the previous section, is enough space for a ring-like superconducting nucleus to form around each FM dot near the phase boundary.

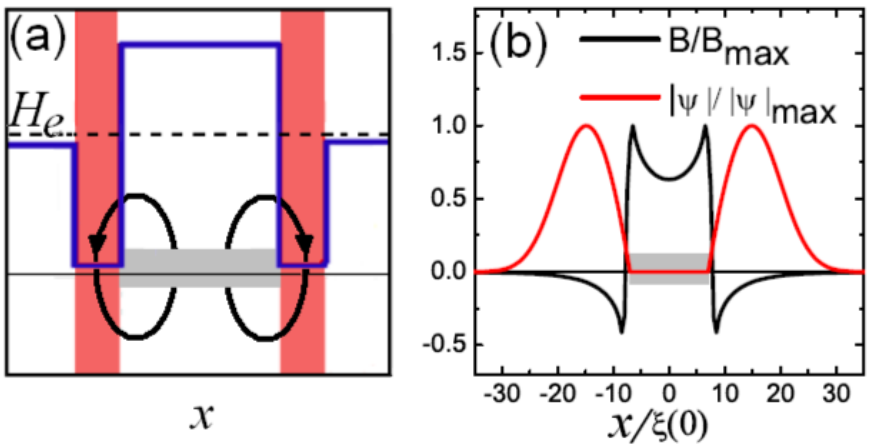

Figure 9. (a) Schematic illustration of the field compensation effect in the SC–FM hybrid. The black dashed horizontal line indicates the applied field H_e. The black loops show the orientation of the flux density generated by the dot. The blue line shows the total magnetic field, with the minima helping the superconducting domains in the SC–FM hybrid, shown in red. (b) The actual profile of the flux density induced by the FM dot and the numerically calculated Cooper pair distribution for $M = 0.06H_{c2}(0)$, $H = 0.054H_{c2}(0)$ and $T = 0.96T_c$.

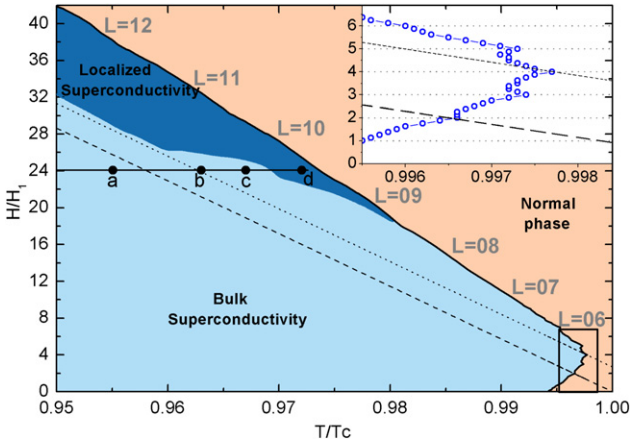

Figure 10. Phase Diagram of the periodic array of FM dots. The dashed line shows the $H_{c2}(T)$ frontier of a plain film, and the dotted line depicts the displaced second critical field $H'_{c2}(T)$ explained in the text.

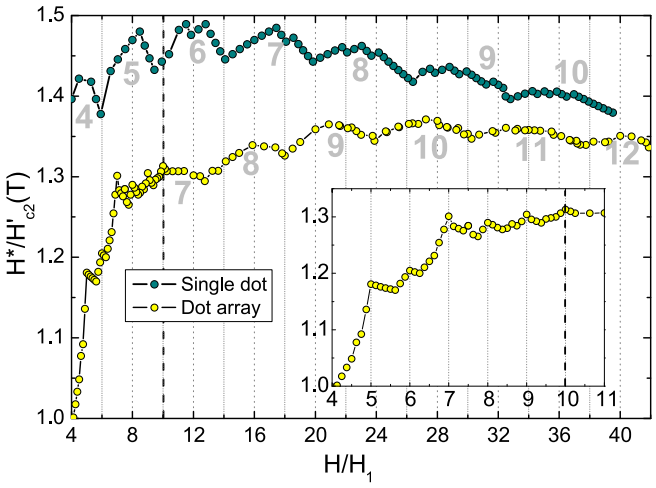

Figure 11. The critical field as a function of the applied field normalized by H_1 for the single-dot and dot-array systems. For convenience we normalized the single-dot critical field by $H_{c2}(T)$ and the multi-dot by $H'_{c2}(T)$.

The results for a magnetization $M = 0.06H_{c2}(0)$ are summarized in the diagram depicted in figure 10. For convenience, here we express H in units of the first matching field, $H_1 = \Phi_0/l^2$, which is the field value corresponding to one flux quantum per unit cell area of the FM dot array. This diagram reveals a few remarkable properties. First, the maximum critical temperature is obtained at a finite positive magnetic field value rather than at $H = 0$. This is a result of the well-known field-induced superconductivity effect demonstrated experimentally [24, 59] and theoretically [31] in superconducting films with a periodic array of magnetic dots on top. This phenomenon results from the ability of the FM dots to induce antivortices in the interstitial region. Therefore, a non-negligible positive value of the external magnetic field (which we shall call the compensation field, H_{comp}) is necessary in order to compensate this negative flux. Usually, H_{comp} is a multiple of the matching field H_1, which is a result of the fact that each FM dot generates an integer number of antivortices in the interstitial region [60]. Here we found $H_{comp} = 4H_1$. For $H = H_{comp}$, all antivortices are removed from the sample thus enhancing $T_c(H)$ to a maximum value. The overall effect is a displacement of the whole diagram $4H_1$ upwards. On the other hand, the boundary between the superconductor and the FM dots induces poorer superconductivity nearby, thus inducing a slight reduction of the maximum critical temperature down to $0.998T_c$. As a guide to the eye, we plot in figure 10 the modified second critical field $H'_{c2}(T)$, which we define as the boundary of bulk superconductivity one would expect after displacing the H–T diagram $4H_1$ upwards and $0.002T_c$ leftwards. For comparison, we also show the plain $H_{c2}(T)$ line (dashes). It becomes clear that the effect of the FM dots is more than a mere translation of the phase diagram (see below).

Another interesting trend observed in the phase boundary shown in figure 10 is the presence of both periodic matching features for $H \lesssim 10H_1$ (see the inset) and aperiodic oscillations for $H \gtrsim 10H_1$. As usual, these distinct behaviors can be better identified by plotting the upper critical field (at which the entire sample goes to the normal state) H^* as a function of H (figure 11). Here we normalize H^* by H'_{c2} in order to quantify the enhancement of the critical field with respect to the $H'_{c2}(T)$ line. For comparison, we also present the $H^*(H)$ line for the single-dot case.

A change of behavior and enhancement of the critical field similar to those presented in figure 11 has been observed experimentally only in superconducting films with a periodic array of antidots [22, 23, 61]. The different behaviors have been interpreted as a change between two well defined regimes, as follows. (i) The collective regime, taking place at high T and low H, is characterized by cusps in $T_c(H)$ at multiples (and sometimes fractional multiples) of the first matching field. In this regime, superconductivity is distributed throughout the entire film and the matching features are essentially collective (non-local) phenomena, similar to the periodic oscillations of wire networks. (ii) The single-object regime, taking place at low temperatures and high fields, is characterized by localization of superconductivity at thin sheaths surrounding the antidots. In this case, the sample behaves effectively as an array of uncoupled superconducting loops embedded in a film in the normal state. The relevant length scale determining which of the regimes will dominate is $\xi(T)$. Roughly speaking, the collective regime dominates when $\xi(T) \gtrsim w$, with w the width of superconducting material between consecutive antidots.

Here, as evidenced by the configurations of the Cooper pair density, indeed the phase boundary for $H \gtrsim 10H_1$ is characterized by strong enhancement of superconductivity at rings encircling the FM dots, similar to the single FM dot case studied in the previous section. Therefore, one could say that this field region corresponds to a single-object regime, with uncoupled loops of superconducting state. However, a closer look into the Cooper pair distribution reveals that, at least for fields up to $\sim 20H_1$, these superconducting loops are in fact coupled to each other by 'necks' of non-negligible density of Cooper pairs. Figure 12 illustrates the evolution of the order parameter as one approaches the phase boundary by increasing the temperature at a fixed external field $H = 24H_1$. Even in the point closest to the boundary one can clearly

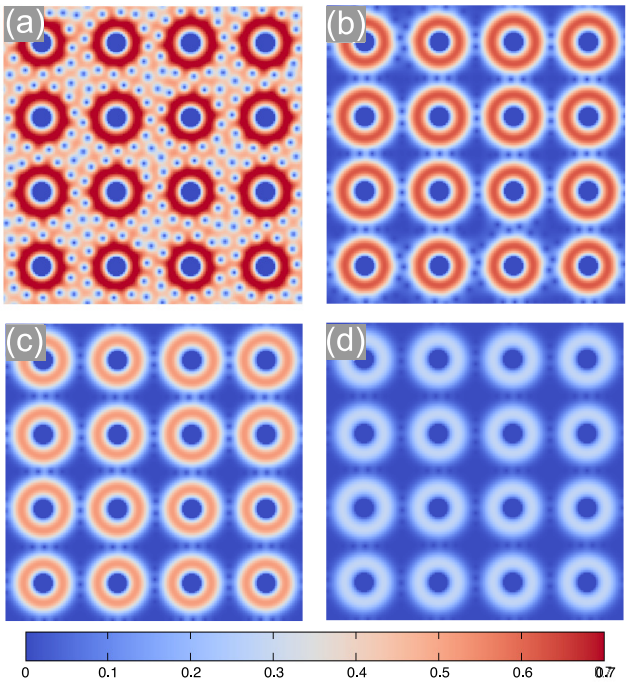

Figure 12. Configurations of $|\psi|^2$ for $M = 0.06H_{c2}(0)$ and $H = 24H_1$ for different values of temperature. (a) $T = 0.955T_c$, (b) $T = 0.963T_c$, (c) $T = 0.967T_c$, (d) $T = 0.972T_c$. These values are marked on the H–T phase diagram to see the evolution of the localized regime.

identify individual vortices in between neighboring rings of localized superconductivity, indicating non-negligible density of Cooper pairs at those regions. This means that, even in the otherwise localized regime, superconductivity percolates across the whole sample and, therefore, the material is capable of sustaining a non-negligible macroscopic supercurrent density. For that reason, the bulk-superconductivity phase is effectively stretched up to fields considerably larger than H'_{c2} in a wide temperature range.

In order to establish which region of the H–T diagram can safely be taken as bulk superconductivity, in the sense described above, and which one may be considered as a phase of localized superconductivity at uncoupled regions, we adopt the following criterion: the system is assumed to be in the bulk-superconductivity state when the maximum value of the order parameter $|\psi|$ along each neck cross-section line (see figure 12) is larger than 0.1. This guarantees that all necks have a considerable number of Cooper pairs bridging the superconducting loops. In contrast, the normal state is reached when the mean value of $|\psi|$ in the entire sample is zero within the numerical accuracy of our calculations. These criteria define the localized-superconductivity and bulk-superconductivity regions depicted in figure 10.

Recently, the existence of compensation effects as well as the Little–Parks-like oscillations in a similar multiply connected superconductor–ferromagnet system has been demonstrated experimentally by Haindl *et al* [42]. However, in their case, the typical width of superconducting material confined in between neighboring ferromagnetic islands is smaller than $\xi(T)$, in a way that the localized states probably coalesce in a wire network state. Accordingly, the oscillations they observe in the phase boundary are essentially periodic.

5. Conclusion

In summary, we have demonstrated by analytical calculations within the linearized GL theory and numerical simulations of the non-linear GL equation that a superconducting film with a cavity filled by a ferromagnetic dot is capable of sustaining a localized superconducting phase at fields considerably larger than H_{c2}. This phase is induced by a field compensation effect due to the negative flux generated into the superconductor by the dot, which is magnetized off plane. In several aspects it resembles the surface superconductivity regime around a mesoscopic empty cavity. For instance, the resulting superconductor–normal phase boundary presents aperiodic Little–Parks-like quantum oscillations associated with an integer value of the total vorticity trapped by the cavity. Here, however, the phase boundary can be easily manipulated by controlling the magnetic state of the dot.

We also analyzed the effect of an array of such ferromagnetic dots. In this case, we have found a transition from periodic, collective oscillations to aperiodic, Little–Parks-like oscillations in the phase boundary, similar to the transition between the so-called collective and single-object regimes of perforated superconducting films observed experimentally. To our knowledge, the transition between these regimes has never been investigated theoretically before, either in films with antidots or with ferromagnetic dots. Nevertheless both regimes have been addressed separately within the framework of the Ginzburg–Landau theory. Here, our Ginzburg–Landau simulations allowed us to access the Cooper pair distribution (from the phase boundary down to deep inside the bulk-superconductivity state) and conclude that, at least for moderate fields, what is called a single-object regime is in fact a phase where the superconducting loops are connected by bridges of non-negligible superconductivity. Therefore, the otherwise localized state percolates across the whole sample even in regions near the part of the phase boundary dominated by quantum oscillations.

Acknowledgments

We would like to thank S. Haindl for useful discussions. This work was supported by the Brazilian science agencies CAPES, CNPq and FACEPE, and the FACEPE/CNPq-PRONEX program, under Grant No. APQ-0589-1.05/08.

Appendix. Details of the analytical solution

Here we give the details of the analytical solution of the LGL equation presented in section 3.1. The linearized GL equation,

$$[(-i\vec{\nabla} - \vec{A})^2 - (1 - T)]\psi = 0, \qquad (A.1)$$

may be solved by performing the following separation of variables: $\psi(\rho, \theta) = f(\rho)\exp(iL\theta)$ (where L is the vorticity and we impose the rotation symmetry around the dot). This

procedure makes the equation depend only on ρ and now we have a linear second order ordinary differential equation

$$\mathcal{L}f \equiv \left[-\frac{1}{\rho}\frac{\mathrm{d}}{\mathrm{d}\rho}\rho\frac{\mathrm{d}}{\mathrm{d}\rho} + \left(\frac{L}{\rho} - A_\theta\right)^2 - (1-T)\right] f = 0 \tag{A.2}$$

where the vector potential is given by the following piecewise function:

$$A_\theta(\rho) = \begin{cases} \dfrac{B_{\mathrm{in}} + H}{2}\rho, & \text{if } \rho \le a, \\ \dfrac{H - B_{\mathrm{out}}}{2}\rho + \dfrac{B_{\mathrm{out}}b^2}{2\rho}, & \text{if } a \le \rho \le b, \\ \dfrac{H\rho}{2}, & \text{if } b \le \rho. \end{cases} \tag{A.3}$$

The simplified model of the field profile as a step-like function gives us a vector potential of the form $A_\theta(\rho) = c_1\rho + c_2/\rho$ (where c_1 is twice the local field and c_2 can be used to make the vector potential continuous) and we can transform the equation above by performing the following change of variable

$$f(\rho) = (c_1\rho^2)^{|L'|/2}\mathrm{e}^{-c_1\rho^2/2}w(\rho), \tag{A.4}$$

and obtain the Kummer's equation for the new function $w(z)$, defining $z = c_1\rho^2$

$$z\frac{\mathrm{d}^2w}{\mathrm{d}z^2} + (B - z)\frac{\mathrm{d}w}{\mathrm{d}z} - Aw = 0, \tag{A.5}$$

where

$$A \equiv 0.5(1 + |L'| - L') - (1 - T + \Lambda)/4c_1 \qquad B \equiv |L'| + 1 \tag{A.6}$$

and the general solution for $w(z)$ is a linear combination of the Kummer's functions $M(A, B, z)$ and $U(A, B, z)$. Now we have the general solution for $f(\rho)$

$$f(\rho) = \begin{cases} 0, & \text{if } \rho \le a, \\ k_1 f_{21}(\rho) + k_2 f_{22}(\rho), & \text{if } a \le \rho \le b, \\ k_3 f_{31}(\rho) + k_4 f_{32}(\rho), & \text{if } \rho \ge b \end{cases} \tag{A.7}$$

where in f_{ij}, i denotes the spatial domain (2 for $a \le \rho \le b$ or 3 for $\rho \ge b$) and j determines whether the Kummer's function is of the first ($j = 1$), M, or the second ($j = 2$), U, kind. Here we describe the boundary conditions for our problem. To account for the proximity effect at the superconductor/ferromagnet interface, we take $f = 0$ at $\rho = a$. At $\rho = b$ we assume that the order parameter and its derivative are continuous. Since we are looking for solutions localized near the FM dot, we take $|\psi|^2 \to 0$ for $\rho \to \infty$. The fact that the term $(z)^{|L'|/2}M(A, B, z)$ dominates over $\mathrm{e}^{-z/2}$ and diverges for $z \to \infty$ requires that $k_{13} = 0$ in region III as was done in [21]. To summarize, our boundary conditions are

$$\begin{aligned} f(a) &= 0 \\ f(b^-) &= f(b^+) \\ f'(b^-) &= f'(b^+) \\ f(\rho \to \infty) &= 0 \end{aligned} \tag{A.8}$$

and we see that $f_{31}(\rho \to \infty) \to \infty \Rightarrow k_3 = 0$ so we make $k_4 \neq 0$ to exclude trivial solutions. Now we define $\tilde{f}(\rho) = f(\rho)/k_4$ and with the second and third boundary conditions we obtain

$$\frac{k_1}{k_4} = \frac{\tilde{f}'_{222}f_{312} - \tilde{f}'_{312}\tilde{f}_{222}}{\tilde{f}'_{222}\tilde{f}_{212} - \tilde{f}'_{212}\tilde{f}_{222}}\tilde{f}_{211} \tag{A.9}$$

$$\frac{k_2}{k_4} = \frac{\tilde{f}'_{312}\tilde{f}_{212} - \tilde{f}'_{212}\tilde{f}_{312}}{\tilde{f}'_{222}\tilde{f}_{212} - \tilde{f}'_{212}\tilde{f}_{222}}\tilde{f}_{221}. \tag{A.10}$$

The first boundary condition results in a transcendental equation for Λ

$$\tilde{f}_{211}\left(\tilde{f}'_{222}\tilde{f}_{322} - \tilde{f}_{222}\tilde{f}'_{322}\right) - \tilde{f}_{221}\left(\tilde{f}'_{212}\tilde{f}_{322} - \tilde{f}_{212}\tilde{f}'_{322}\right) = 0 \tag{A.11}$$

where the third index of the notation $\tilde{f}_{ijk}$ means that the function is being evaluated at the radius a ($k = 1$) or b ($k = 2$). We also have to make sure the solutions have the value $\tilde{f}_{212}\tilde{f}'_{222} - \tilde{f}_{222}\tilde{f}'_{212} \neq 0$ to avoid divergence on the order parameter. Finally we impose that k_4 is a constant that minimizes the free energy for the obtained $\tilde{f}$ function. With this procedure we find [62]

$$\psi(\rho, \theta) = (-\Lambda\beta_A)^{1/2}\tilde{f}(\rho)\exp(\mathrm{i}L\theta) \tag{A.12}$$

$$j_\theta(\rho) = \Lambda\beta_A\left[\frac{L}{\rho} - A_\theta(\rho)\right]\tilde{f}(\rho)^2 \tag{A.13}$$

$$F = -\frac{\Lambda^2}{V\beta_A} \tag{A.14}$$

where $\langle\cdots\rangle$ means average over the superconducting film and $\beta_A = \langle f^4\rangle/\langle f^2\rangle^2$ is the Abrikosov parameter (which is independent of k_4). Notice that the term $\frac{L}{\rho} - A_\theta(\rho)$ is the only one that changes sign. Therefore, we can straightforwardly find the radii values where the current becomes null using the expression for the vector potential (equation (A.3)).

References

[1] Fiory A T, Hebard A F and Somekh S 1978 Critical currents associated with the interaction of commensurate fluxline sublattices in a perforated Al film *Appl. Phys. Lett.* **32** 73–5
[2] Moshchalkov V V, Baert M, Metlushko V V, Rosseel E, Van Bael M J, Temst K, Jonckheere R and Bruynseraede Y 1996 Magnetization of multiple-quanta vortex lattices *Phys. Rev.* B **54** 7385–93
[3] Martín J I, Vélez M, Nogués J and Schuller I K 1997 Flux pinning in a superconductor by an array of submicrometer magnetic dots *Phys. Rev. Lett.* **79** 1929–32
[4] Morgan D J and Ketterson J B 1998 Asymmetric flux pinning in a regular array of magnetic dipoles *Phys. Rev. Lett.* **80** 3614–7
[5] Van Bael M J, Lange M, Raedts S, Moshchalkov V V, Grigorenko A N and Bending S J 2003 Local visualization of asymmetric flux pinning by magnetic dots with perpendicular magnetization *Phys. Rev.* B **68** 014509
[6] Silhanek A V, Raedts S, Lange M and Moshchalkov V V 2003 Field-dependent vortex pinning strength in a periodic array of antidots *Phys. Rev.* B **67** 064502

[7] Raedts S, Silhanek A V, Van Bael M J and Moshchalkov V V 2004 Flux-pinning properties of superconducting films with arrays of blind holes *Phys. Rev.* B **70** 024509
[8] Metlushko V *et al* 1999 Interstitial flux phases in a superconducting niobium film with a square lattice of artificial pinning centers *Phys. Rev.* B **60** R12585–8
[9] Velez M, Jaque D, Martín J I, Montero M I, Schuller I K and Vicent J L 2002 Vortex lattice channeling effects in Nb films induced by anisotropic arrays of mesoscopic pinning centers *Phys. Rev.* B **65** 104511
[10] Misko V, Savel'ev S and Nori F 2005 Critical currents in quasiperiodic pinning arrays: chains and penrose lattices *Phys. Rev. Lett.* **95** 177007
[11] Kemmler M, Gürlich C, Sterck A, Pöhler H, Neuhaus M, Siegel M, Kleiner R and Koelle D 2006 Commensurability effects in superconducting Nb films with quasiperiodic pinning arrays *Phys. Rev. Lett.* **97** 147003
[12] Berdiyorov G R, Milošević M V and Peeters F M 2006 Novel commensurability effects in superconducting films with antidot arrays *Phys. Rev. Lett.* **96** 207001
[13] Berdiyorov G R, Milošević M V and Peeters F M 2006 Vortex configurations and critical parameters in superconducting thin films containing antidot arrays: nonlinear Ginzburg–Landau theory *Phys. Rev.* B **74** 174512
[14] Berdiyorov G R, Milošević M V and Peeters F M 2006 Superconducting films with antidot arrays: novel behavior of the critical current *Europhys. Lett.* **74** 493
[15] Berdiyorov G R, Milošević M V and Peeters F M 2009 Composite vortex ordering in superconducting films with arrays of blind holes *New J. Phys.* **11** 013025
[16] Misko V R and Nori F 2012 Magnetic flux pinning in superconductors with hyperbolic-tessellation arrays of pinning sites *Phys. Rev.* B **85** 184506
[17] Libál A, Olson Reichhardt C J and Reichhardt C 2009 Creating artificial ice states using vortices in nanostructured superconductors *Phys. Rev. Lett.* **102** 237004
[18] Latimer M L, Berdiyorov G R, Xiao Z L, Peeters F M and Kwok W K 2013 Realization of artificial ice systems for magnetic vortices in a superconducting moge thin film with patterned nanostructures *Phys. Rev. Lett.* **111** 067001
[19] Ray D, Olson Reichhardt C J, Jankó B and Reichhardt C 2013 Strongly enhanced pinning of magnetic vortices in type-II superconductors by conformal crystal arrays *Phys. Rev. Lett.* **110** 267001
[20] Silhanek A V, Van Look L, Jonckheere R, Zhu B Y, Raedts S and Moshchalkov V V 2005 Enhanced vortex pinning by a composite antidot lattice in a superconducting Pb film *Phys. Rev.* B **72** 014507
[21] Bezryadin A and Pannetier B 1995 Nucleation of superconductivity in a thin film with a lattice of circular holes *J. Low Temp. Phys.* **98** 251–68
[22] Rosseel E, Puig T, Baert M, Van Bael M J, Moshchalkov V V and Bruynseraede Y 1997 Upper critical field of Pb films with an antidot lattice *Physica* C **282–287** 1567–8
[23] Van de Vondel J, de Souza Silva C C and Moshchalkov V V 2007 Diode effects in the surface superconductivity regime *Europhys. Lett.* **80** 17006
[24] Lange M, Van Bael M J, Bruynseraede Y and Moshchalkov V V 2003 Nanoengineered magnetic-field-induced superconductivity *Phys. Rev. Lett.* **90** 197006
[25] Aladyshkin A Y, Ryzhov D A, Samokhvalov A V, Savinov D A, Mel'nikov A S and Moshchalkov V V 2007 Localized superconductivity and Little-Parks effect in superconductor/ferromagnet hybrids *Phys. Rev.* B **75** 184519
[26] Karapetrov G, Milošević M V, Iavarone M, Fedor J, Belkin A, Novosad V and Peeters F M 2009 Transverse instabilities of multiple vortex chains in magnetically coupled $NbSe_2$/permalloy superconductor/ferromagnet bilayers *Phys. Rev.* B **80** 180506
[27] Silhanek A V, Gillijns W, Moshchalkov V V, Metlushko V and Ilic B 2006 Tunable pinning in superconducting films with magnetic microloops *Appl. Phys. Lett.* **89** 182505
[28] Milošević M V and Peeters F M 2004 Vortex–antivortex lattices in superconducting films with magnetic pinning arrays *Phys. Rev. Lett.* **93** 267006
[29] Neal J S, Milošević M V, Bending S J, Potenza A, San E L and Marrows C H 2007 Competing symmetries and broken bonds in superconducting vortex–antivortex molecular crystals *Phys. Rev. Lett.* **99** 127001
[30] Iavarone M, Scarfato A, Bobba F, Longobardi M, Karapetrov G, Novosad V, Yefremenko V, Giubileo F and Cucolo A M 2011 Imaging the spontaneous formation of vortex–antivortex pairs in planar superconductor/ferromagnet hybrid structures *Phys. Rev.* B **84** 024506
[31] Milošević M V and Peeters F M 2005 Field-enhanced critical parameters in magnetically nanostructured superconductors *Europhys. Lett.* **70** 670–6
[32] Milošević M V, Berdiyorov G R and Peeters F M 2005 Mesoscopic field and current compensator based on a hybrid superconductor–ferromagnet structure *Phys. Rev. Lett.* **95** 7004–8
[33] Milošević M V and Peeters F M 2006 Vortex–antivortex nucleation in superconducting films with arrays of in-plane dipoles *Physica* C **437/438** 208–12
[34] de Souza Silva C C, Silhanek A V, Van de Vondel J, Gillijns W, Metlushko V, Ilic B and Moshchalkov V V 2007 Dipole-induced vortex ratchets in superconducting films with arrays of micromagnets *Phys. Rev. Lett.* **98** 117005
[35] Lima C L S and de Souza Silva C C 2009 Dynamics of vortex–antivortex matter in nanostructured ferromagnet–superconductor bilayers *Phys. Rev.* B **80** 054514
[36] Van de Vondel J, Silhanek A V, Metlushko V, Vavassori P, Ilic B and Moshchalkov V V 2009 Self-organized mode-locking effect in superconductor/ferromagnet hybrids *Phys. Rev.* B **79** 054527
[37] Gladilin V N, Tempere J, Devreese J T, Gillijns W and Moshchalkov V V 2009 Vortex–antivortex pair generation by an in-plane magnetic dipole on a superconducting film *Phys. Rev.* B **80** 054503
[38] Pina J C, Zorro M A and de Souza Silva C C 2010 Vortex–antivortex states in nanostructured superconductor ferromagnet hybrids *Physica* C **470** 762–5
[39] Kapra A V, Misko V R, Vodolazov D Y and Peeters F M 2011 The guidance of vortex–antivortex pairs by in-plane magnetic dipoles in a superconducting finite-size film *Supercond. Sci. Technol.* **24** 024014
[40] Milošević M V, Peeters F M and Janko B 2011 Vortex manipulation in superconducting films with tunable magnetic topology *Supercond. Sci. Technol.* **24** 024001
[41] Marmorkos I K, Matulis A and Peeters F M 1996 Vortex structure around a magnetic dot in planar superconductors *Phys. Rev.* B **53** 2677–85
[42] Haindl S, Thersleff T, Shapoval T, Lai Y W, McCord J, Schultz L and Holzapfel B 2011 Advanced Nb/FePt $L1_0$ hybrid thin films *Supercond. Sci. Technol.* **24** 024002

[43] Buisson O, Gandit P, Rammal R, Wang Y Y and Pannetier B 1990 Magnetization oscillations of a superconducting disk *Phys. Lett.* A **150** 36–42
[44] Moshchalkov V V, Qiu X G and Bruyndoncx V 1997 Paramagnetic meissner effect from the self-consistent solution of the Ginzburg–Landau equations *Phys. Rev.* B **55** 11793–801
[45] Schweigert V A and Peeters F M 1999 Influence of the confinement geometry on surface superconductivity *Phys. Rev.* B **60** 3084–7
[46] Pogosov W V 2002 Vortex phases in mesoscopic cylinders with suppressed surface superconductivity *Phys. Rev.* B **65** 224511
[47] Kato R, Enomoto Y and Maekawa S 1991 Computer simulations of dynamics of flux lines in type-II superconductors *Phys. Rev.* B **44** 6916–20
[48] Kato R, Enomoto Y and Maekawa S 1993 Effects of the surface boundary on the magnetization process in type-II superconductors *Phys. Rev.* B **47** 8016–24
[49] Milošević M V and Geurts R 2010 The Ginzburg–Landau theory in application *Physica* C **470** 791–5
[50] Milošević M V, Yampolskii S V and Peeters F M 2002 Vortex structure of thin mesoscopic disks in the presence of an inhomogeneous magnetic field *Phys. Rev.* B **66** 024515
[51] Jackson D 1998 *Classical Electrodynamics* 3rd edn (New York: Wiley)
[52] Aladyshkin A Y, Buzdin A I, Fraerman A A, Mel'nikov A S, Ryzhov D A and Sokolov A V 2003 Domain-wall superconductivity in hybrid superconductor–ferromagnet structures *Phys. Rev.* B **68** 184508
[53] Gomes R R, de Oliveira I G and Doria M M 2012 Little-Parks oscillations near a persistent current loop *Phys. Rev.* B **85** 144512
[54] Gillijns W, Aladyshkin A Y, Lange M, Van Bael M J and Moshchalkov V V 2005 Domain-wall guided nucleation of superconductivity in hybrid ferromagnet–superconductor–ferromagnet layered structures *Phys. Rev. Lett.* **95** 227003
[55] Milošević M V and Peeters F M 2005 Vortex–antivortex nucleation in magnetically nanotextured superconductors: magnetic-field-driven and thermal scenarios *Phys. Rev. Lett.* **94** 227001
[56] Berdiyorov G R, Misko V R, Milošević M V, Escoffier W, Grigorieva I V and Peeters F M 2008 Pillars as antipinning centers in superconducting films *Phys. Rev.* B **77** 024526
[57] Buzdin A I and Mel'nikov A S 2003 Domain wall superconductivity in ferromagnetic superconductors *Phys. Rev.* B **67** 020503
[58] Yang Z, Lange M, Volodin A, Szymczak R and Moshchalkov V V 2004 Domain-wall superconductivity in superconductor–ferromagnet hybrids *Nature Mater.* **3** 793
[59] Gillijns W, Milošević M V, Silhanek A V, Moshchalkov V V and Peeters F M 2007 Influence of magnet size on magnetically engineered field-induced superconductivity *Phys. Rev.* B **76** 184516
[60] Silhanek A V, Gillijns W, Milošević M V, Volodin A, Moshchalkov V V and Peeters F M 2007 Optimization of superconducting critical parameters by tuning the size and magnetization of arrays of magnetic dots *Phys. Rev.* B **76** 100502
[61] Bezryadin A, Ovchinnikov Y N and Pannetier B 1996 Nucleation of vortices inside open and blind microholes *Phys. Rev.* B **53** 8553–60
[62] Yampolskii S V and Peeters F M 2000 Vortex structure of thin mesoscopic disks with enhanced surface superconductivity *Phys. Rev.* B **62** 9663–74

Deformation of loops in 2D packing of flexible rods

T. A. Sobral,[1,*] V. H. de Holanda,[2] F. C. B. Leal,[2] and T. T. Saraiva[2]

[1] *Departamento de Física, Universidade Federal do Ceará, 60451-970, Fortaleza, Brazil*
[2] *Departamento de Física, Universidade Federal de Pernambuco, 50670-901, Recife, Brazil*

(Dated: April 6, 2018)

The injection of a long piece of flexible rod into a two-dimensional domain yields a complex pattern commonly studied through elasticity theory, packing analysis, and fractal geometries. The loop is an one-vertex entity which naturally emerges in this system. Each loop has elastic features whose function in 2D packing has not yet been discussed. In this Letter we point out how the shape of a given loop in the complex structure allows to estimate local deformations and forces. First, we build sets of symmetric free loops and performed compression experiments. Then, tight packing configurations are analyzed by using image processing. We found that the dimensions of the loops, confined or not, obey the same dependence on the deformation. The result is consistent with a simple model based on 2D elastic theory for filaments, where the rod adopts the shape of Euler's elasticas between contact points. The force and stored energy is obtained from numerical equations. In an additional experiment, we obtain that the compression force for deformed loops corroborates the theoretical findings.

The injection of filaments into cavities is a basic problem involving elasticity and self-exclusion. These are two themes of great importance in nature, with wide range of influence from polymeric packing [1, 2] to DNA packaging in viral capsids [3–5]. In this Letter, we focus on the two-dimensional confinement, which has been studied both experimentally and theoretically [6–10]. In a typical 2D confinement as show in Fig. 1(a), the formation of self-contact points divides the area of the cavity in cells with variable number of vertexes. "Loop" is the term used to designate single-vertex cells [11], as those highlighted in Fig. 1(b). The identification of loops allows to identify the points of higher curvatures [12] and helps to determine the morphology of the complex pattern [6]. In addition, the number of loops gives the jamming length and the dynamic state of the system [13, 14]. Despite these intrinsic relevance, the shape of the conforming loop has been little studied. Here, we report a set of three experiments and a model that describes the deformations of the loop. The main objective is identifying physical quantities in the complex confined system by analyzing the shape of a single loop.

We built elastic loops from rods and ribbons and compared them with loops in the packing of a single filament into circular and rectangular cavities. We observed that, under compression, the dimensions of the loops vary according to the same curve irrespective of confinement. From this result we propose how to infer local information in complex patterns from simple analysis of shape and size of loops. The theoretical description follows the elastic model for filaments [15–17], and allows us to determine the shape of the loops, as well as the force and stored energy.

The objective of the first experiment is determining the mechanical response of a single loop under compression. The loops were constructed by bending a piece of rod in order to merge the ends into a vertex point. A bent rod

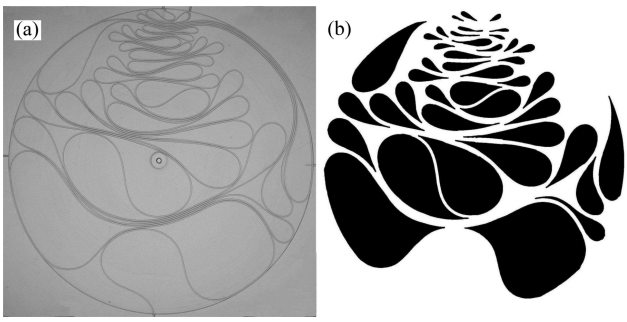

FIG. 1. (a) The packing of a 1 mm thick nylon fishing line into a circular cavity with diameter of 200 mm. (b) The loops (in black) are closed domains with one vertex.

leaves the planar configuration when the ends are close to each other [17, 18], then transparent parallel plates are used to constraint it. The rods used are either nylon fishing lines of 0.80 mm of diameter or polymeric tubes of 5.0(2.5) mm of outer(inner) diameter. The constraint plates are made of acrylic with a thickness of 1.0 cm. We also construct planar loops from ribbons with width 1.0 cm, and made of either A4 paper or transparent Mylar sheets. An interesting point is that loops made from ribbons with large width are naturally planar [19], and have the advantage of eliminating friction effects due to contact with parallel plates.

The initial conformation is denominated "free loop". The perimeter $\lambda = \lambda_0$ is defined when the flexible rod or ribbon is straight, and was chosen randomly in an interval $\lambda_0 = \{97 - 366\}$ mm. The loops are large in order to avoid plasticity effects. The height h of the loop is defined along its symmetric axis as the distance from the vertex to the top of the bulge. Perpendicularly, the largest width of the loop is w [Fig. 2(a)]. Both h and w are measured with a digital caliper. The initial ratios $h_0/\lambda_0 = (0.424 \pm 0.007)$ and $w_0/\lambda_0 = (0.210 \pm 0.008)$

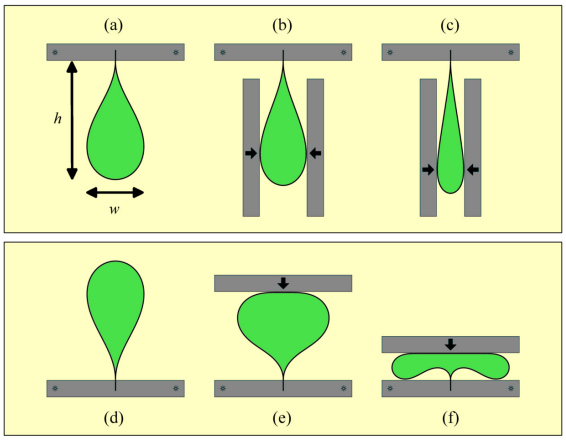

FIG. 2. Superior view of deformed loops: (a-c) compressing sideways by imposing smaller widths, and (d-f) compressing along the symmetric axis by imposing smaller heights.

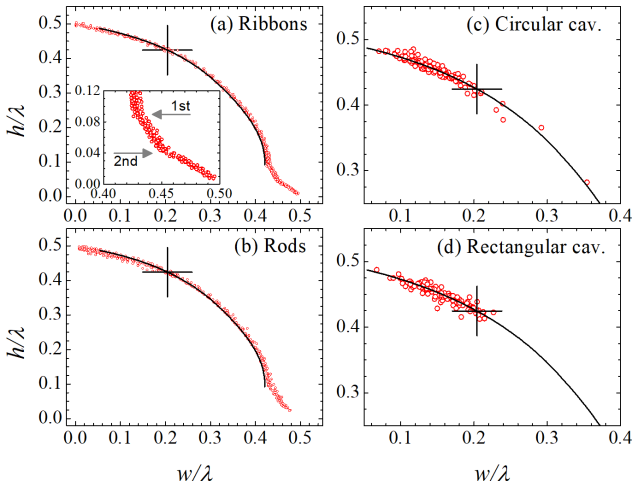

FIG. 3. The $h \times w$ diagram for deformed loops made of (a) ribbons, and (b) fishing lines. With image processing, loops are obtained from (c) the packing of a nylon fishing line into circular cavities, and (d) the packing of a tubular rod into rectangular cavities. The big cross indicates the sizes of the free loop. The solid line is obtained from the theoretical reasoning. See text for more details.

are essentially the same irrespective the type or material. For rods, we measured the dimensions h_0 and w_0 from the neutral axis.

The experiment consists of compressing the loop along two perpendicular axis (Fig. 2). In the first part, the loop is compressed between two parallel aluminum plates, requiring w to decrease as illustrated in Fig. 2(a-c). Care is taken in order to preserve the loop as symmetric as possible. The system responds by increasing the height h. The compressing continues until the physical limit $w \to 0$ which leads to $h \to \lambda/2$. During this process, the contact points between the loop and the compression plates move downwards as indicated by small arrows in Fig. 2(b-c). In the second part of the experiment, the loop is compressed between two parallel aluminum plates, requiring h to decrease as illustrated in Fig. 2(d-f). In this case, the system responds by increasing w. The compressing continues until the physical limit $h \to 0$ which leads to $w \to \lambda/2$. The experiment is performed horizontally over a table without gravitational effects.

The results of the experiment illustrated in Fig. 2 is shown in Fig. 3(a-b) as a $h \times w$ diagram, normalized by λ. The diagram is identical for loops built from ribbons (Fig. 3a) and rods (Fig. 3b), and agrees with the theoretical description (solid line) based on Euler's elastica which we discuss afterwards. The values for the free loop are indicated by a big cross. Since compressing w leads to higher h, the graph in Fig. 3(a-b) must be read from the cross to the left. On the other hand, compressing h leads to higher w, and the graph in Fig. 3(a-b) must be read from the cross to the right. Therefore, the range of the data shown in the Fig. 3(a-b) covers the entire physical domain, from values of dimensions for the free loop to completely crushed shapes.

The free loop has an anisotropic shape and its response to compression is different depending on the load axis. While the reduction in w leads to an increase in h until the physical limit $h \to \lambda/2$, a reduction in h leads to an increase in w until a limited value, $w \to w_m = (0.429 \pm 0.005)\lambda$. If the compression continues beyond this point, the curve follows towards the physical limit $w \to \lambda/2$ with two discontinuities in its slope [see inset in Fig. 3(a)]. The first discontinuity, at $h = (0.089 \pm 0.002)\lambda$, is due to the emergence of new contact points between the loop and the plates as shown in Fig. 2(f). The second discontinuity, at $h = (0.042 \pm 0.002)\lambda$, is due to the emergence of two self-contact points which divides the loop into three shapes: one curved triangle between two small loops.

In order to study the problem of 2D confining, the flexible rod can be split at the contact points into pieces that are treatable numerically with Euler's equation [10, 20]. The problem is complex due to the fractal distribution of contact points [12]. It has been discussed whether self-contacts define arcs of propagating forces across the structure [6, 12]. Here, on the other hand, we focus on the shape of the loops as a guide to access both qualitative and quantitative information about local deformations and energy. The second experiment consists in the two-dimensional injection of thin rods into planar slender cavities. The objective is to analyze how the loops, which are naturally formed in the confinement, behave in light of the $w \times h$ diagram. This experiment is also divided in two parts. In the first one, nylon fishing lines with a diameter of 1.0 mm are injected into circular cavities with 201 mm in diameter as shown in Fig. 1(a). In the second part of the experiment, polymeric tubular rods with

50 mm in diameter are injected into rectangular cavities of 400×200 mm^2 as illustrated in Fig. 4(a). All injections are performed manually into a dry cavity, free of lubricants, in a rate about 1 cm/s. The injection stops when the system jams due to the rigidity around the injection channel.

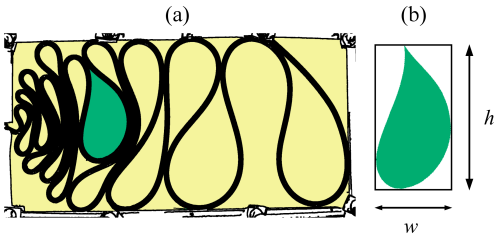

FIG. 4. (a) Digital image of the tight packed flexible tube of 50 mm in diameter inside a rectangular cavity of 200 × 400 mm^2. (b) Each loop is framed inside a rectangle which defines h and w (see text for details).

The particular conformation presented in Fig. 4(a) is chosen as a representative case where we can briefly discuss the role of the elasticity, self-exclusion, and friction with the cavity. The first loops that formed are pushed away from the injection channel, shown in the right region of Fig. 4(a). These loops are larger, and requires low values for the injection force in the early stages. Observe that the shape of the loops are prevented from changing due to the contacts with the cavity and friction. The rod has small self-contact regions, and the stacked loops transmit the force through the system by compressing each other. The geometric pattern and local rigidity are then governed by the elasticity of the loops. On the other hand, the last loops are close to the injection channel, see left region of Fig. 4(a). The injection force in this stage is higher, which reduces the perimeter of the loops and limits them to occupy the periphery of the pattern, without contacting the cavity. The rod has large self-contact regions that transmit the force through the system. In the case shown in Fig. 4(a) the loops are compressed by neighbors in a configuration that resembles Fig. 2(a-c). In a cavity of generic shape, however, we expect that the loops can interact also as in Fig. 2(d-f). For example, there are differences between patterns generated from circular and rectangular cavities [Compare Fig. 1(a) and Fig. 4(a)].

In order to construct a $h \times w$ diagram for loops inside cavities, we need to measure its dimensions non-invasively. We can select the loops by image processing [Fig. 4(a)]. However, the loops interact in a complicated manner and assume non-symmetric shapes, so that we need to revise the definitions of h and w. We focus here on the reading of the geometric pattern by prioritizing simple definitions. First, the selected loop is inscribed into a rectangle. Rotating the loop will change the aspect ratio of the frame. The chosen angle is that which maximizes the height of the frame, as shown in Fig. 4(b). This dimension is identified as h or w accordingly to the position of the tip and the bulge of the loop. Following this procedure, all symmetrical loops illustrated in Fig. 2 maintain their dimensions. The points at the edge of the loop are interpolated by a curve that allows us to measure the dimensions h, w, and λ with the same units. Such method is repeated for each loop in the image. The result is shown in Fig. 3(c) for loops inside circular cavities, and in Fig. 3(d) for loops inside rectangular cavities.

The main result in Fig. 3 is that the loops obtained from injection of rods (c and d) present the same behavior as the loops outside the cavities (a and b). However, the data from packed loops distribute themselves majoritarily in the left side of the diagram, instead of spreading over the whole diagram. This is in agreement with the fact that the loops are aligned perpendicular to the injection channel. The injection force then acts to compress the loops laterally, reducing both their perimeter and width. However, Fig. 3(c) shows that few loops are also longitudinally compressed in circular cavities. In this cavity rotation and slippage are more accessible than in the rectangular one. In the general sense, this confirms that the way at which the loops populate the diagram depends on the shape and size of the cavity.

Let us begin our reasoning by considering the free loop. Between contact points, the vector force is fixed along the arc length s of the rod, $\vec{F}(s) = P\hat{i}$. Therefore, the shape is governed by infinitesimal torques $d\Gamma(s) = F \sin\theta \, ds$, where θ is the angle between $d\vec{s}$ and the direction of the force $\vec{F}$. The torque is related to the local curvature, $\Gamma(s) = -\mu \frac{d\theta}{ds}$, where μ is the bending rigidity. We can write

$$\frac{d^2\theta}{d\hat{s}^2} = -\sin\theta, \tag{1}$$

where the hat over q means $\hat{q} \equiv q\sqrt{F/\mu}$. The coordinates are given by integration of $d\hat{x}(\hat{s})/d\hat{s} = \cos\theta$ and $d\hat{y}(\hat{s})/d\hat{s} = \sin\theta$. The general solutions are obtained in terms of elliptic integrals and elliptic functions, and the overall shape is determined by the elliptic parameter p [16]. The free loop corresponds to the elastica with a self-contact point, at $\hat{s} = \hat{s}^*$, in which the following conditions hold

$$\hat{x}(\hat{s}^*) = \hat{x}(0) \quad \text{and} \quad \frac{d\hat{x}(\hat{s})}{d\hat{s}}\Big|_{\hat{s}=\hat{s}^*} = 0. \tag{2}$$

The outcome is a numeric equation for p whose solution is $p^* = 0.731183$ [16]. We determine λ, h, and w by computing the vertex point and the points of maximum. We find $h_0/\lambda = 0.424308$ and $w_0/\lambda = 0.204214$, irrespective of the bending rigidity. These values are in agreement with the experimental finding, then we can state that the self-touching elastica describes quite well the shape of the free loop.

Our model for a general symmetric loop requires attention to points where an external force acts to deform the loop. We assume here that the lateral compression of the loop is equivalent to a longitudinal stretching. In this manner, all compression in Fig. 2 can be described by the application of a single normal force $\vec{N} = N\hat{j}$ at the middle point of the loop. The loop is thus composed of mirrored elasticas. The total force becomes $\vec{F} = P\hat{i} + N\hat{j}$ and the reference line of the elasticas changes from the horizontal to an oblique direction, whose angle is $\gamma_0 \equiv \tan^{-1}(N/P)$. Eq. 1 remains valid, but the contour conditions (Eq. 2) are adapted for rotated coordinates. Then, we obtain a numeric equation for p whose solution now depends on the angle γ_0. Figs. 5(a-f) show how two symmetrical elasticas merge in order to compose the deformed loop. Fig. 5(g) shows how the self-touching condition changes the elliptic parameter as a function of the angle γ_0.

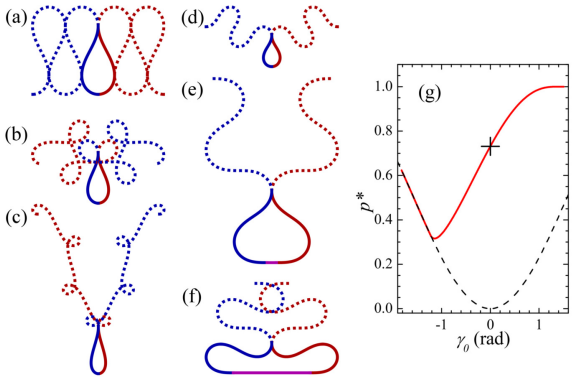

FIG. 5. The symmetric loop is composed of two elasticas (a-f) rotated respectively by $\gamma_0 = \{0, 0.60, 1.20, -0.55, -1.27, -1.82\}$ rad. (g) p^* dependence with the compression force through γ_0. The dashed line corresponds to $\dot{\gamma}_0 = 0$ case. See text for details.

The free loop corresponds to $\gamma_0 = 0$ and it is illustrated in Fig. 5(a). In the stretching case $\gamma_0 > 0$, the elliptic parameter increases [Fig. 5(g)] and the elasticas have pieces that cross each other, as shown in Fig. 5(b-c). In the compressing case $\gamma_0 < 0$, the elliptic parameter decreases [Fig. 5(g)] and the elasticas have no crossing points, as shown in Fig. 5(d-f). The dashed line in Fig. 5(g) shows where the contact point in the bulge has null curvature, and corresponds to $p^* = \sin^2(\gamma_0/2)$. Because the compressing plate does not allow convex curvature, the contact region becomes a straight line which extends itself between two inflectional points. From this simple model, we can determine the lengths λ, h and w, as shown by solid lines in Fig. 3.

The agreement between the theoretical curve and the experimental data (Fig. 3) shows the relevance of this purely elastic model. Furthermore, we can calculate the force associated with a given shape, $F = \mu(\hat{s}/s)^2$. The result for the force is shown in Fig. 6 and (inset) the energy cost of deformation $\Delta E = W = \int \vec{N}\cdot d\vec{h}$. Big crosses in Fig. 6 indicate the values for the initial condition.

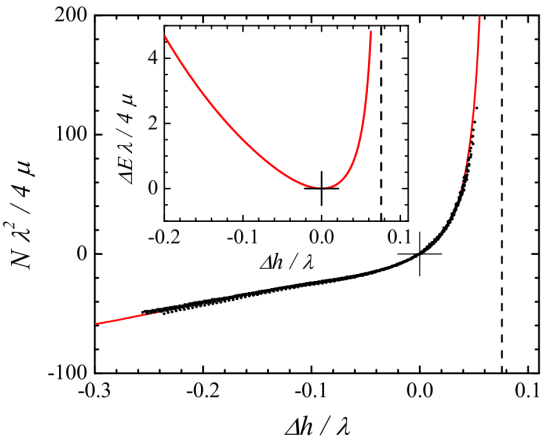

FIG. 6. The force N and (inset) the stored energy E as functions of the deformation $\Delta h/\lambda$ for purely elastic loops. Black points corresponds to experimental data. Dashed lines indicate the physical limit of deformation. See text for details.

In a third experiment, a dynamometer is attached to the vertex of the loop in order to measure the compression force N as function of deformations Δh. The stretching part was implemented by fixing the bulge with a metallic hook. Fig. 6 shows the experimental data as black points, with instrumental precision of 1 cN, space steps of 2 mm, and using 10 different ribbons of Mylar sheets. Due to asymmetry, the force is greater when the loop is stretched than when it is compressed by a same extension. The dashed line in Fig. 6 shows the limit of null curvature, where $h = \lambda/2$, and force and energy diverge because small radius of curvature. The agreement between model and experiment allows us to estimate both the force and stored energy for loops inside complex patterns. We hope that such results open up new possibilities for application of statistical techniques to 2D confining of flexible rods.

We acknowledge Professor Eduardo O. Dias from UFPE for fruitful discussions. The present work was supported by CNPq, Conselho Nacional de Desenvolvimento Científico e Tecnológico, Brazil (numbers 157218/2012-0, 141813/2016-4, and 152053/2016-6).

* tsobral@fisica.ufc.br

[1] P. J. Flory, *Principles of polymer chemistry* (Cornell University Press, 1953).
[2] P.-G. De Gennes, *Scaling concepts in polymer physics* (Cornell university press, 1979).
[3] N. Stoop, J. Najafi, F. K. Wittel, M. Habibi, and H. J. Herrmann, Phys. Rev. Lett. **106**, 214102 (2011).

[4] R. Vetter, F. K. Wittel, and H. J. Herrmann, Nature communications **5** (2014).
[5] V. H. de Holanda and M. A. F. Gomes, Phys. Rev. E **94**, 062406 (2016).
[6] N. Stoop, F. K. Wittel, and H. J. Herrmann, Phys. Rev. Lett. **101**, 094101 (2008).
[7] Y. C. Lin, Y. W. Lin, and T. M. Hong, Phys. Rev. E **78**, 067101 (2008).
[8] C. C. Donato, M. A. F. Gomes, and R. E. de Souza, Phys. Rev. E **67**, 026110 (2003).
[9] L. Boué and E. Katzav, EPL (Europhysics Letters) **80**, 54002 (2007).
[10] S. Deboeuf, M. Adda-Bedia, and A. Boudaoud, EPL (Europhysics Letters) **85**, 24002 (2009).
[11] C. C. Donato, M. A. F. Gomes, and R. E. de Souza, Phys. Rev. E **66**, 015102 (2002).
[12] C. C. Donato and M. A. F. Gomes, Phys. Rev. E **75**, 066113 (2007).
[13] T. A. Sobral and M. A. F. Gomes, Journal of Physics D: Applied Physics **48**, 335305 (2015).
[14] T. A. Sobral and M. A. F. Gomes, Phys. Rev. E **95**, 022312 (2017).
[15] L. D. Landau and E. M. Lifshitz, *Theory of Elasticity* (Pergamon Press, 1986).
[16] M. Nizette and A. Goriely, Journal of Mathematical Physics **40**, 2830 (1999).
[17] V. G. A. Goss, G. H. M. van der Heijden, J. M. T. Thompson, and S. Neukirch, Experimental Mechanics **45**, 101 (2005).
[18] F. Bosi, D. Misseroni, F. Dal Corso, and D. Bigoni, Proceedings of the Royal Society of London A: Mathematical, Physical and Engineering Sciences **471** (2015).
[19] Y. Morigaki, H. Wada, and Y. Tanaka, Phys. Rev. Lett. **117**, 198003 (2016).
[20] L. Boué, M. Adda-Bedia, A. Boudaoud, D. Cassani, Y. Couder, A. Eddi, and M. Trejo, Phys. Rev. Lett. **97**, 166104 (2006).
[21] S. Deboeuf, E. Katzav, A. Boudaoud, D. Bonn, and M. Adda-Bedia, Phys. Rev. Lett. **110**, 104301 (2013).